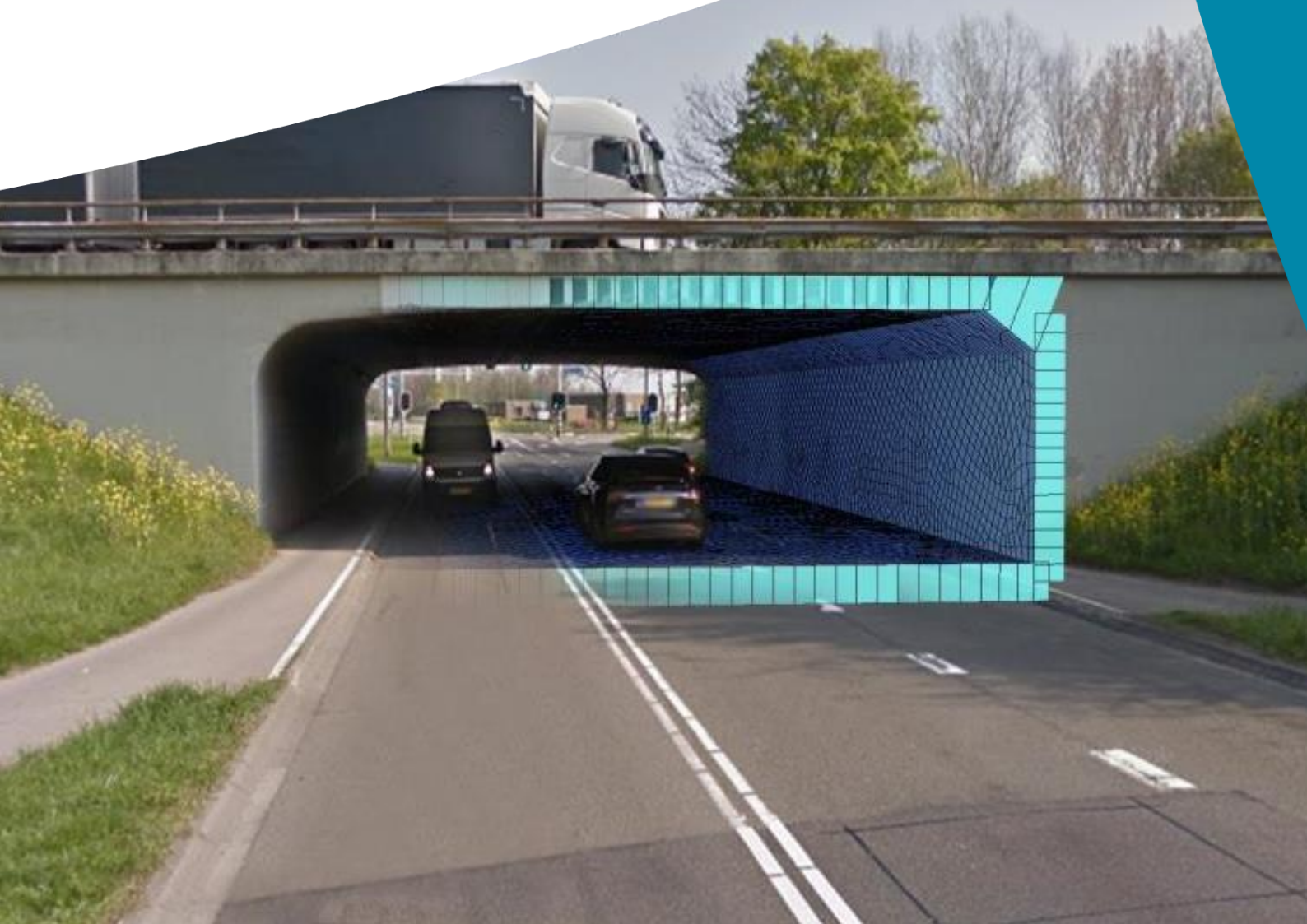# Automated Structural Assessment of existing reinforced concrete underpasses

D.H.J.M. Jilissen

Automated Structural Assessment of existing reinforced concrete underpasses

by

D.H.J.M. Jilissen

in partial fulfilment of the requirements for the degree of

Master of Science
in Civil Engineering

at the Delft University of Technology,
to be defended publicly on January 20, 2021 at 15:30.

This thesis is confidential and cannot be made public until January 20, 2024.

An electronic version of this thesis is available at http://repository.tudelft.nl/.

Preface

The present report is the result of the research into an automated assessment of existing reinforced concrete underpasses and culverts in the Netherlands. I conducted this research as the final part of the Master Structural Engineering with specialization in Concrete Structures at the Faculty of Civil Engineering and Geosciences of the Delft University of Technology. This research was realized in collaboration with the engineering and consultancy firm Royal HaskoningDHV. From February 2020 to December 2020 I worked on the research and writing of the thesis.

The main goal of this graduation research is to investigate how a consistent approach and an improvement of efficiency can be achieved for the assessment of existing reinforced concrete underpasses and culverts in the Netherlands by automating the structural assessment. For this, answers are given to questions such as what do these structures look like, when were they built, how do you model the load effect, what is the current capacity, which parameters are important and which can be neglected or standardized and are there typical structures with problems.

The first month of the research was carried out at Royal HaskoningDHV's Rotterdam office location, but from March 2020 I mostly worked from my student room in Delft due to the impact of COVID-19 in the Netherlands. Despite primarily working from home because of this pandemic, I would like to express my thanks for the pleasant cooperation with the T&P Infrastructure Rotterdam advisory group. In particular, my thanks go to Mr. R.P.H. Vergoossen for both professional supervision and support of the graduation process.

The graduation research was supervised from the Delft University of Technology by Mr Y. Yang, Ms E.O.L. Lantsoght and Mr. M.A.N. Hendriks, whom I would like to thank for the interest in my research and for giving good advice.

I hope you enjoy reading this thesis report.

Danny Jilissen
Delft, January 2021

Abstract

Much of the Dutch infrastructure was built in the 1960s and 1970s and includes an estimated 55.000 bridges and viaducts. These aging structures have reached the end of their designed service life or will reach it in the short term. It is estimated that 15% of these structures have a box-shaped cross-section as being reinforced concrete underpasses and culverts. Replacing all these structures in the short term is not practical and financially feasible. In order to preserve these structures, it must be demonstrated based on a structural assessment that the structural safety is guaranteed. So many assessments will be performed by different engineers which is a time-consuming process and results in a non-consistent assessment where unnecessary disapproval occurs which in turn leads to unnecessary costs and loss of time. The aim of this thesis is to set up a structured consistent automated method with which unnecessary disapproval and unjustified approval is avoided, a necessary efficiency improvement is achieved and structures where structural safety is at risk can be identified. To this end the following research question has been formulated: *"How can the structural assessment of existing reinforced concrete underpasses be automated to provide a quick and cost-efficient generic method which prevents unnecessary disapproval and unjustified approval, which ultimately makes it possible to build structured knowledge of the existing underpasses?"*

In order to answer the research question, quantitative research has been conducted in which numerical data from parameter studies is collected and analysed to investigate relationships between the studied variables, find patterns and generalize results. First a data analysis of existing underpasses and culverts in the Netherlands was carried out, after which the modeling of the load effect and the capacity of existing reinforced concrete structures was investigated. An automated analytical model was created for the first step to determine the load effect. The determination of the capacity of existing concrete structures was investigated arithmetically. As a second step to determine the load effect, a model refinement was performed by automating a 3D FEM plate model. Structures from the database were assessed with both the analytical model and the 3D FEM model and a sensitivity analysis was performed based on theoretical structures within the boundaries derived from the data analysis.

This research shows that a model refinement from an analytical model to a 3D FEM plate model results in a reduction of the calculated governing bending moment of approximately 18% and a decrease in the calculated unity check (UC) for shear with about 5% while shear is governing for two-thirds of the underpasses and culverts studied. For structures prior to the *Gewapend Beton Voorschriften* (GBV) 1962 bending is usually the governing failure mechanism, for structures from the GBV 1962 era shear force is clearly the governing failure mechanism and after the GBV 1962 shear force is still the governing failure mechanism for many underpasses, but bending is also more often found as governing failure mechanism. The analytical model in this research uses the Guyon-Massonnet method for the distribution of traffic load to determine the bending moment and a method developed in this study as an extension of method 7.3-7 from CEB-*fib* model code 2010 to determine the shear force as a result of the tandem system load. For the determination of the shear capacity a distinction is made between the analytical model and the 3D FEM plate model. For the analytical model formula 6.2a from *Richtlijnen Bestaande Kunstwerken* (RBK) and formula 6.2b according to the Eurocode (EC) has been used with the addition of the plate factor k_p from the RBK because, based on the arithmetic research, it is expected that with formula 6.2b from the RBK the shear capacity is overestimated. Initially the analytical model with the method based on 7.3-7 from (CEB-fib, 2010) resulted in an average increase of the calculated shear force of 16%. Additional research has shown that comparable UCs with an average deviation of 5% in favour of the 3D FEM plate model are obtained when a limited vertical load distribution for the method 7.3-7 of CEB-fib in the analytical model and formula 6.2.b according to RBK for the 3D FEM plate model is calculated, whereby it can be concluded that vertical load distribution under a certain angle, as prescribed by EC, gives good results for bending but not for shear with method 7.3-7 from (CEB-fib, 2010) and that the shear capacity for the 3D FEM plate model

can be determined according to formulas 6.2.a and 6.2.b from RBK. It turned out that special attention must be paid in the assessment of these structures to the anchoring of the reinforcement in the section at the end of the haunch and at the face of the support, as this has proved to be critical in several cases. From both the assessment of structures from the database and the sensitivity analysis, it appears that structures from local authorities with an unknown design concrete strength class, which data analysis has shown to be common, are often disapproved based on shear. The differences found in the load effect calculated with the analytical model or the 3D FEM plate model means that the analytical model is an efficient first step for assessing existing reinforced concrete underpasses and culverts, especially for large batches, since the analytical model is about ten times as fast as the 3D FEM plate model. The 3D FEM plate model allows to assess structures with an intersection angle smaller than 80_{gon} and in view of the reduction in the calculated UCs, it offers the possibility to still approve an underpass or culvert if it is disapproved by the analytical model based on the governing UC.

The conclusion is therefore that it is the most efficient method to first assess the large batches with the analytical model and that the 3D FEM plate model for structures with an intersection angle smaller than 80_{gon} and structures that are disapproved with the analytical model offers added value in terms of a lower UC. From the comparison with the 3D FEM plate model it is concluded that the method as an extension of method 7.3-7 from (CEB-fib, 2010) results in too optimistic values for the occurring shear force as a result of the tandem system load due to an overestimation of the vertical load distribution.

This research shows that an automated structural assessment in which an analytical model is combined with a script-based FEM analysis leads to an Automated Structural Assessment Tool of added value on the classic approach of assessing existing concrete underpasses and culverts by significantly improving efficiency and therefore to realize a cost-efficient method. Further research into the vertical distribution of local loads through soil and asphalt layers on reinforced concrete slabs must demonstrate to what extent vertical load distribution can be taken into account for the determination of the occurring shear force of local loads with the method based on 7.3-7 from (CEB-fib, 2010) and that therefore an increased shear capacity in terms of a higher plate factor k_p for the calculated shear force with a linear elastic FEM model may be used.

Content

Appendices

Table of Tables

Table of Figures

Abbreviations

Abbreviation	Explanation
ASA	**Automated Structural Assessment**
CC	**Consequence Class** in which a structure is classified according to EC0, whereby the severity of the consequences of failure of the structure is decisive for determining the class. In the EC, a distinction is made between CC1, CC2 and CC3, where CC3 is the class for structures with the highest severity of the consequences of failure.
CUR	**CUR**-recommendations are publications in which agreements between parties in the Dutch construction industry are recorded. CUR with a number refers to a specific recommendation, like CUR124 refers to CUR-recommendation *"Constructieve veiligheid bestaande bruggen en viaducten van decentrale overheden"*.
EC	**Eurocodes** are the European series of (58) codes for testing the structural safety of structures in the built environment. EC with a number refers to the part of the series, like EC2 refers to Eurocode part 2 concrete structures.
FEM	The **Finite Element Method** is a numerical method for solving partial differential equations in boundary value problems. In the FEM, a structure is divided into many simpler parts, called finite elements, for which a system of algebraic equations is obtained that models the entire problem.
GBV	***"Gewapend Beton Voorschriften"*** is a series of old Dutch concrete design codes with, among other things, former concrete strength classes and steel grades. GBV followed by a year refers to a specific code released in that year, like the GBV 1962.
LM	**Load Model** from Eurocode, Load Model 1 defines global traffic load on bridges (NEN-EN 1991-2)
NEN	***"NEderlandse Norm"*** guides and stimulates the development of standards in the Netherlands. In addition, NEN manages and publishes the standards applicable in the Netherlands, including the European Eurocodes, which are referred to as NEN-EN. NEN-EN 199 with an added number stands for the relevant Eurocode, for example NEN-EN 1990 refers to Eurocode 0 basis for structural design.
ODE	An **Ordinary Differential Equation** is an equation that contains one or more functions of one independent variable and the derivatives of those functions.
RBK	***"Richtlijnen Bestaande Kunstwerken"*** is a technical document from RWS with additional requirements and advice for assessing the structural safety of an existing Dutch structure during reconstruction, use and disapproval.
RC	**Reinforced concrete** is a widely used building material consisting of concrete and steel reinforcement bars.
RHDHV	Engineering and consultancy firm **Royal HaskoningDHV**
ROK	***"Richtlijnen Ontwerp Kunstwerken"*** is a technical document from RWS with additional generic requirements that the design and implementation of a new structure to be built must meet. The ROK also applies to new parts of existing structures, when these parts are replaced, or to widening when structures are expanded.
RWS	***"Rijkswaterstaat"*** is the executive agency of the Ministry of Infrastructure and Water Management in the Netherlands. The organization manages and develops the main roads, main waterways and main water systems on behalf of the ministry.
SLS	**Serviceability Limit State** is the limit state for use, which means that a (concrete) structure must be usable for the intended function for the designed service life. Excessive deflection, excessive cracking or other aspects that lead to durability problems in the use phase are checked in the SLS.
TS	**Tandem system** from load model 1 of Eurocode (NEN-EN 1991-2) representing a heavy vehicle
UDL	**Uniformly distributed load** from load model 1 of Eurocode (NEN-EN 1991-2)
UC	**Unity Check** defined as the load effect (E) divided by the capacity (R). A unity check is approved if $E/R \leq 1,0$.
ULS	**Ultimate Limit State** is the limit state where the strength and stability of a structure is checked for design loads.

VB	**_"Voorschriften Beton"_** is an old Dutch concrete design code first released in 1974 (VB 74), replacing the GBV 1962, and later revised in 1984 as the VB 74/84.
VBB	**_"Voorschriften Beton – Bruggen – Constructieve eisen en rekenmethoden"_** is a former Dutch standard which succeeded the VOSB 1963 in 1995 and contains requirements for the load-bearing capacity and deformations that bridge structures made of reinforced or prestressed concrete must comply. The standard also contains the determination methods, but also load models, on the basis of which it can be tested whether the requirements are met.
VBC	**_"Voorschriften Beton – Constructieve eisen en rekenmethoden"_** is the predecessor of Eurocode 2 and succeeds the VB 74/84 in 1990 and has been revised once leading to the VBC 1995.
VOSB	**_"Voorschriften voor het Ontwerp van Stalen Bruggen"_** is a series of old Dutch design codes for steel bridges with, among other things, former design loads for bridges. VOSB followed by a year refers to a specific code released in that year, like the VOSB 1933 which is the first VOSB.

List of symbols

This list of symbols shows the symbols used in this thesis, which are based on the Eurocode with additions from NEN series and RBK. The symbols are divided into Latin symbols and Greek symbols.

Latin symbols

Symbol	Explanation
a_v	distance from the face of the load plane to the face of the support
A_c	area of the concrete cross-section. For a rectangular cross-section, this is the product of the width and height of the slab or beam.
A_s	area of the reinforcement steel in tension
$A_{sl,red}$	cross-sectional area of reinforcement steel reduced in proportion to the anchoring
b	element width
b_w	effective slab width
c	concrete cover
C	Eurocode concrete class (notation: $Cf_{ck}/f_{ck,cube}$, like C35/45)
d	effective height of the cross-section
e	edge distance
E	load effect
EI	bending stiffness
E_c	calculation value of the elasticity modulus of concrete (Young's modulus)
E_f	fictitious elasticity modulus (NEN-EN 1992-1-1 Dutch National Annex Table NB.1)
E_s	calculation value of the elasticity modulus of reinforcing steel (Young's modulus)
f_{bd}	design value of the ultimate bond stress
f_{ck}	characteristic cylinder compressive concrete strength
$f_{ck,cube}$	characteristic cube compressive concrete strength
f_{cm}	mean cylinder compressive concrete strength
f_{cd}	design cylinder compressive concrete strength
f_{ctm}	mean tensile concrete strength
$f_{ctk,0,05}$	5% fractile tensile concrete strength
f_{ctd}	design tensile concrete strength
f_{yk}	characteristic yield strength of reinforcing steel
f_{yd}	design yield strength of reinforcing steel
F	concentrated load
h	structural height of an element
I	moment of inertia of the total concrete slab cross-section
k	modulus of subgrade reaction
k_p	plate factor for massive slabs (in RBK also called k_{cap}; $k_p = k_{cap}$)
K_r	rotational spring stiffness
l_{bd}	design value of the required anchorage length
$l_{bd,provided}$	provided anchorage length
$l_{b,min}$	minimum anchorage length for bars in tension
L	length in span direction
M	bending moment
M_{Ed}	design value of the calculated bending moment
M_{Rd}	design value of the bending moment resistance
N	axial load
N_{obs}	number of heavy trucks per year per lane
q	distributed load
R	resistance

Symbol	Explanation
V	shear force
V_{Ed}	design value of the calculated shear force
V_{Rd}	design value of the shear force resistance
$V_{Rd,c}$	design value of the shear force resistance without shear reinforcement
V_{TS}	design value of the calculated shear force due to the TS load(s)
w	displacement; $w_z(x,y)$ means displacement in z-direction related to x, and y
x_u	is the height of the concrete compressive zone in ULS
z	internal lever arm of the cross-sectional forces

Greek symbols

Symbol	Explanation
α_e	ratio between E-moduli of steel and concrete; $\alpha_e = E_s/E_{cm}$
α_n	utilisation ratio of axial loading
α_{trend}	correction factor reduced trend
β	reduction factor for loads within $2d$ from its support for the determination of V_{Ed}
γ_c	partial safety factor for concrete
γ_s	partial safety factor for reinforcement steel
$\gamma_{Gj,sup}$	load factor for permanent loads
$\gamma_{Q,1}$	load factor for dominant load (in this thesis traffic loading)
ε_c	strain of concrete
ε_{cu}	ultimate compressive strain in the concrete
ε_s	strain of reinforcement steel
θ	angle of the concrete compressive strut
κ	curvature
ν	Poisson's ratio (transverse contraction coefficient)
ν_{min}	minimal shear stress capacity of concrete without shear reinforcement (based on bending)
ρ	reinforcement ratio
ρ_l	reinforcement ratio for the main reinforcement
σ_{cp}	compressive stress in the concrete as a result of a normal force or prestress
τ	shear stress due to torsion
φ	rotation, coefficient of internal friction
Ψ	correction factor for a reference period shorter than 100 years
$\emptyset$	diameter of reinforcement bar

1

Introduction

1.1   Context

An underpass or underbridge is basically a tunnel of small dimensions in length and width, due to the limited dimensions these structures are classified as a bridge or a viaduct instead of a tunnel. Most of these structures are made with reinforced concrete and have been constructed since the 1930s. These underpasses may have a function as culvert, bicycle or pedestrian underpass or as an underpass for mixed road traffic where a complete roadway is passed through an underpass under another road.

It is estimated that there are about 55000 bridges and viaducts in the Netherlands of which the majority is managed and owned by local and regional authorities. Based on (Rijkswaterstaat, 2008) it is estimated that about 15%, which is approximately 8000, of the existing structures in The Netherlands are box shaped structures. The actual number of structures with a box shaped construction may be higher because objects with a span of less than 3,5 m have not been included in the research by Rijkswaterstaat, while culverts and bicycle underpasses may well have a span of less than 3,5 m.

Existing reinforced concrete underpasses vary in year of construction ranging from the 1930s to recently completed projects. It is generally known that a large part of the Dutch infrastructure was built in the 1960s and 1970s. According to (CROW-CUR, 2019) most of these ageing structures have reached, or will soon reach, the end of their designed service life, which may be a reason to doubt structural safety. In addition, the regulations, calculation methods and material properties have changed considerably over time, which may also be a reason to doubt the structural safety of an existing structure. Furthermore, the road layout on top of the underpass may have changed over time, or the owner wants to make changes, which can cause drastic changes in the loads to be applied on the structure which will also change the structural safety of a construction.

It is not practical and financially feasible to replace all these structures in the short term, according to (CROW-CUR, 2019) just measures to keep all these structures safe and sound are expected to cost billions of euros over the coming years. Besides, closing traffic lanes or roads leads to traffic disruption which results in social costs. However, because the owners of civil structures in the Netherlands are legally obliged to guarantee structural safety, the structural safety of existing objects must be validated in case of doubt in order to be able to maintain them. This validation takes place based on a structural analysis of the existing structure. Comprehensive, this means that many verification calculations will have to be made in the future to confirm that an existing construction meets the applicable requirements.

1.2   Problem description

Many structural assessments of existing RC structures must be made in the near future, which will be performed by different engineers. Since there is no structured approach for performing such verification, this undoubtedly results in an unstructured approach using different methods resulting in incomparable results from a time-consuming process. Even when the same level of modeling and software is used it does not necessarily lead to the same results meaning that the engineer can make a big difference, which is called the "engineers' factor" and is the general point towards automation.

In (Blaauwendraad, 2010) nineteen structural engineers who attended a continuing education course were asked to calculate bending moments and design the reinforcement for a receding wall. The moment peaks and the associated required reinforcement obtained by these participants differ by a factor two up to four, even when using the same software.

In (Rijkswaterstaat, 2008) different engineering firms were asked to classify constructions owned by Rijkswaterstaat based on unity checks obtained from structural analysis. Again a big scatter can be found varying from 2% to 55% of the structures assessed classified as unsafe for actual use, depending on the engineering firm has assessed. According to (Rijkswaterstaat, 2008) only 3,3% of the 151 box-shaped structures that was assessed was classified as safe against brittle failure without any restrictions for use. Knowing that there is a big scatter in results obtained by different firms, one may wonder if in reality more structures should be classified as safe without any restrictions for use.

These two studies substantiate the statement that different structural engineers may come to very different results. The problem is that based on these two studies it is expected that for a significant number of cases a structure can disapproved based on structural safety while in reality the required level of safety is met, which leads to unnecessary disapproval. In some cases, a second opinion is requested by the client in the event of disapproval, which in turn leads to unnecessary costs and loss of time.

In addition to accuracy and consistency, there is another general problem in the Netherlands for assessing existing structures in the infrastructure. There is, based on (van der Ploeg, 2018), a demand for more efficiency because of shortage of engineers to assess all the existing structures, the capacity for a more traditional approach is no longer available, and is rather costly, and there is therefore a need for automation.

1.3 Goal of research

1.3.1 Aim of the thesis

The aim of this thesis is to achieve the following four points for the structural assessment of existing reinforced concrete underpasses:

1. Deliver a consistent method with well-documented underlying assumptions.
2. Avoid unnecessary disapproval and unjustified approval.
3. Provide a quick and (cost)-efficient structural analysis.
4. Identify underpasses where structural safety is at risk.

In case different calculation methods are used in the structural analysis, mutual results for different structures cannot be compared. However, if the same method is always used, mutual results of different calculations can rightly be compared. In this way the structures where structural safety is most likely to be at risk can be identified and one can build on knowledge of existing underpasses in the Netherlands.
Ultimately, recommendations can be given in prioritization within the asset management of the assessment of existing reinforced concrete underpasses in the Netherlands based on the standardized method for calculating the structural safety.

1.3.2 Research questions

In order to achieve a good objective, it is important to know what is to be investigated and what steps are required for this. What will be investigated will be clearly formulated on the basis of the main question.

"How can the structural assessment of existing reinforced concrete underpasses be automated to provide a quick and cost-efficient generic method which prevents unnecessary disapproval and unjustified approval, which ultimately makes it possible to build structured knowledge of the existing underpasses?"

The main question is then divided into sub-questions. Each sub-question covers an important part of answering the main question.

Phase 2: Definition

    2.1. *"Which types of underpass constructions exist in the Netherlands and in which number do they occur?"*

    2.2. *"How did the underpass constructions structurally develop over time under different design codes?"*

    2.3. *"What typical construction types of underpasses are worth to be automated?"*

Phase 3: Design

    3.1. *"Which parameters significantly influence the structural behaviour of the underpass and must be taken into account during calculations and which parameters can be neglected or standardized?"*

    3.2. *"Which checks have to be performed by the automated structural assessment of existing reinforced concrete underpasses?"*

    3.3. *"Which forms of modeling can be included in the automated structural assessment tool as a possible calculation method and when are they applied?*

Phase 4: Identification

    4.1. *"Which typical underpasses do not fulfil the requirements stated in the standards and guidelines and why are the requirements not met?"*

1.3.3 Objective

The solution is sought in an automated structural analysis tool that can analyse these structures, chose an appropriate calculation method and finally gives an automatically generated report based on basic input parameters. In this way a standard approach is achieved and scatter in results due to user input can be prevented. In addition, the calculation can be easily adjusted, something that normally takes a lot of manhours. In this way a large batch of underpasses can be assessed in a very limited time.
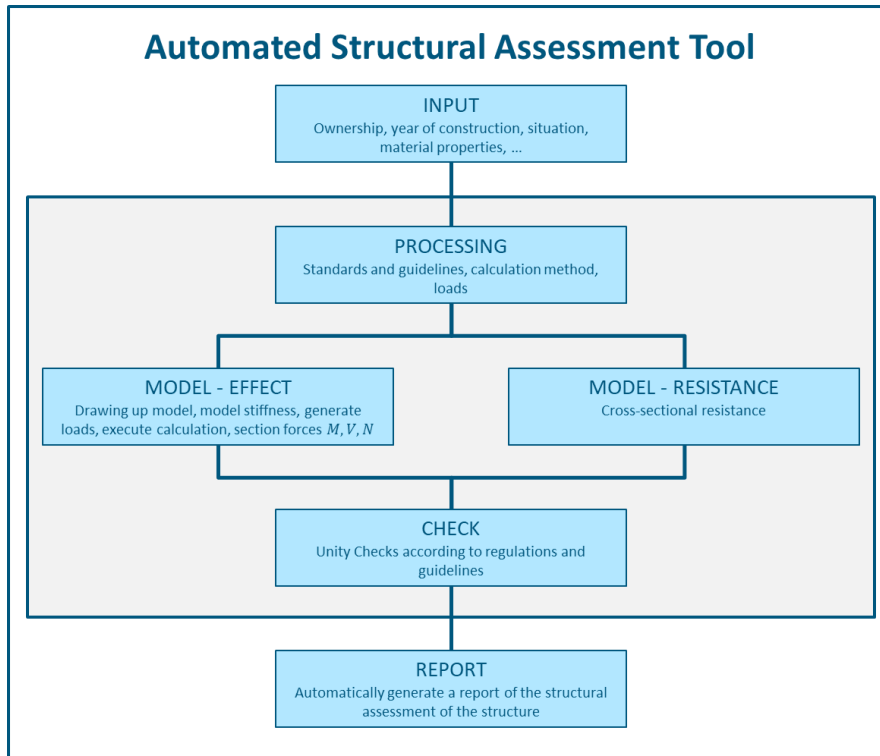
Figure 1 Basic flowchart of Automated Structural Assessment Tool

1.4 Scope

This research focuses on the assessment of existing reinforced concrete underpasses in the Netherlands. These underpasses vary in function from culvert, pedestrian or bicycle tunnel to an underpass for a complete road with mixed traffic. These concrete objects occur in the Netherlands with a construction year from the early 20th century.

Three main types of construction are distinguished for underpasses in this research, presented in Table 1.

Table 1 Overview of main construction types within thesis scope

Main construction type	Foundation
Closed single-cell box	On grade / pile foundation
Single span portal	On grade / pile foundation
Concrete deck	On sheet piles

A1) Closed box, on grade

A2) Closed box, on pile foundation

B1) Portal, on grade

B2) Portal, on pile foundation

D) Concrete deck with sheet piles
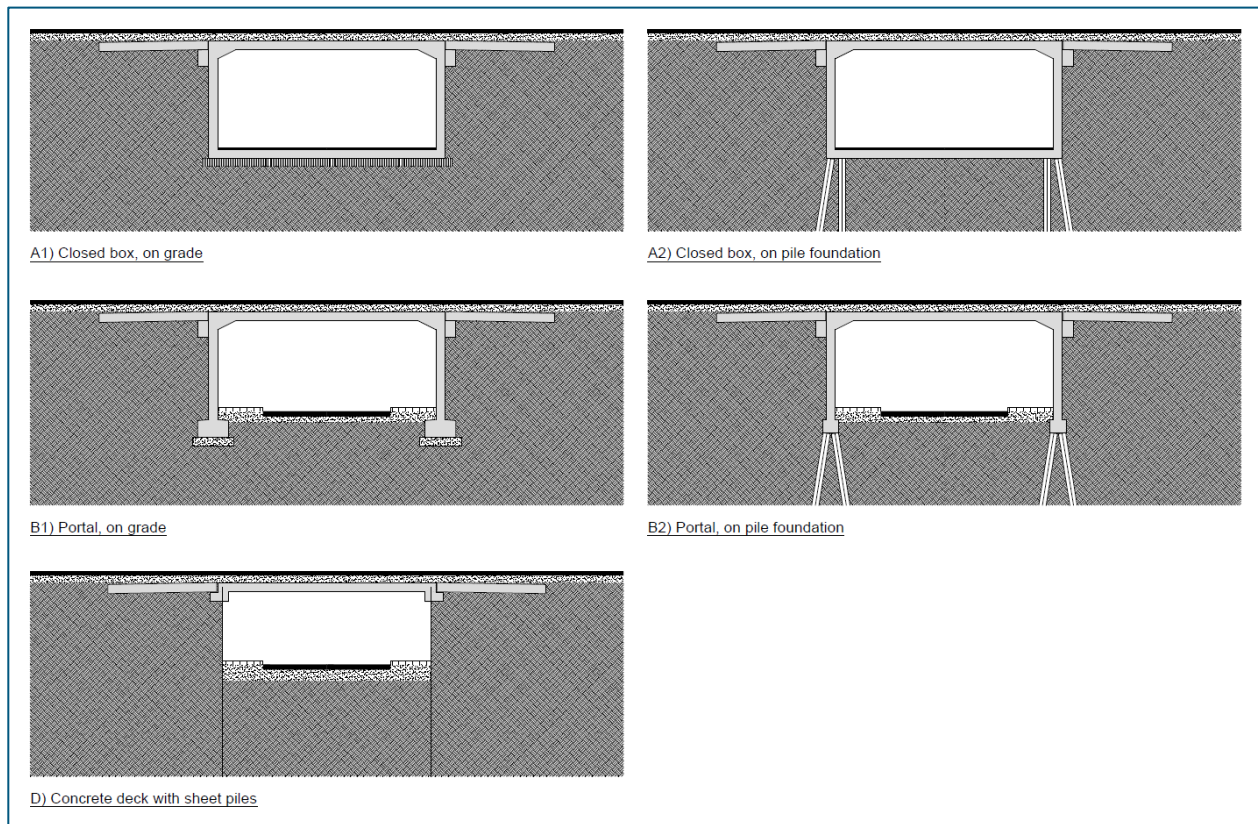
Figure 2 Sketch representation of objects within the scope as stated in Table 1.

The research is limited to single span underpasses because the mechanical behaviour, mainly of the deck, is therefore comparable in all cases. Although a concrete deck on steel sheet piles seems to be a completely different construction, it has been included because a simple model can be made similar to the concrete box.

The structural analysis of the assessment is limited to the superstructure of a construction, this is in line with the approach as prescribed in RBK in case there is no reason to doubt the soundness of the substructure. The geometry of the construction is further limited to solid slabs, meaning no holes in the slabs. In the past, in addition to ribbed reinforcement bars, smooth bars were also used, which is why constructions with both reinforcement profile types are placed within the scope of the research. The deck slab is actually always only equipped with longitudinal and transverse reinforcement, without the application of shear reinforcement. Therefore, this research is focussed on elements without shear reinforcement.

When assessing structural safety only the ULS verification must be considered. Legally no requirements are stated regarding SLS verification, meaning that in the assessment the design requirements for serviceability do not have to be met.

1.4.1 Excluded in advance

In addition to describing what falls within the scope of the research, this section describes which specific cases are anyway placed outside the scope of the study.

This research focuses only on underpasses for which the upper section is driven by road traffic, railway bridges and aqueducts are excluded due to different loading.

This research focuses on reinforced concrete structures with a solid cross-section with the same concrete quality, which means that prefab girders with an infill deck fall outside the scope. For sake of simplicity are structures with prestressing in the span direction in the decks not included in the research. This research is limited to single span underpasses, which means that multi-box or multi-span portals are outside the scope of the research due to a different mechanical behaviour of these types of structures.

In order to be allowed to assess a construction only on the superstructure, there may be no doubt about the structural safety of the substructure. This means that objects with structural damage to the substructure or uneven settlements fall outside the scope of this research because in these cases there is reason to doubt the structural safety of the substructure.

Quantitatively not much can be said about risk at this stage of the study, therefore an extensive risk analysis is outside the scope of this research.

1.5 Research strategy

The research has been subdivided into five phases starting with the plan of approach, which is briefly explained in this chapter.

In the definition phase, a preliminary study, described in chapter 2, is being carried out in which a literature review and a data analysis of existing reinforced concrete underpasses in the Netherlands are carried out. In addition, knowledge of standards and guidelines for assessing existing structures is gathered during this phase, but this is not reported.

In the design phase, the longest running phase in the research, the automated structural assessment tool for reinforced concrete underpasses is developed and validated. To this end various modeling methods are investigated, and a sensitivity analysis of different parameters is performed.

As soon as the tool is available, the research moves to the identification phase, in which the tool is used to look at the distribution of the results of structural assessments and it is investigated whether structures with certain properties structurally do not meet the set requirements. This allows identification of underpasses where structural safety is at risk.

In the finalization phase recommendations are given in prioritization within the asset management of the assessment of existing reinforced concrete underpasses in the Netherlands based on the standardized method for calculating the structural safety. This last phase also includes making improvements to the graphical user interface and the automatically generated assessment report.

An overview of the thesis outline and a flowchart of the research strategy are shown in Figure 3 and Figure 4 respectively.

Phase 1: Plan of Approach	Phase 2: Definition	Phase 3: Design	Phase 4: Identification	Phase 5: Finalization
• Context & problem description • Goal of the thesis • Scope • Research strategy	• Literature review • Data analysis	• Develop ASA tool including different modeling methods • Sensitivity analysis • Validation	• Investigate distribution of results • Identify underpasses where structural safety is at risk	• Recommendations • Improve GUI • Automatically generated report

Figure 3 Overview of thesis outline

Phase 1:
Plan of Approach

Plan of Approach
Plan of Approach with defined goal, scope and research strategy

Phase 2:
Definition

Literature review
Current state of knowledge of automated assessment
Current way of modeling

Geometry
Data analysis of underpasses in NL and typical construction designs, dimensions, materials, etc.

Standards & Guidelines
Required knowledge of standards and guidelines for the assessment of existing concrete underpasses.

Phase 3:
Design

Automated Structural Assessment Tool

Analytical Model
Drawing up model based on ODE

validate

Finite Element Model 1
Model using 1D beam elements in 2D frame model

validate

Finite Element Model 2
Model using 2D shell elements in 3D space model

Sensitivity analysis
Investigate sensitivity of parameters and decision making between models

Model Resistance
Modeling of the cross-sectional resistance

Validation
Validate calculation methods by recalculating closed projects

Phase 4:
Identification

Analyse
Investigate distribution of results and identify underpasses where structural safety is at risk based on UC

Phase 5:
Finalization

Improve GUI
Making the ASA tool more user-friendly

Recommendations
Prioritize underpasses where structural safety is at risk based on UC

Automated Report
Realizing an automatically generated report

Figure 4 Flowchart of research strategy

2
Preliminary study

The preliminary study is divided into two parts. First, the research is placed within the existing knowledge by means of a literature review addressing a gap in the current knowledge. Subsequently, information about existing RC underpasses in the Netherlands and the structural assessment methods are analysed.

2.1   Literature review

Several researches have been conducted into making advanced models that best describes the behaviour of one specific construction, like in the thesis by (Uysal, 2017) and the series by (Burns, 2006), (Abolmaali & Garg, 2008a; 2008b), (Garg & Abolmaali, 2009) and (Garg, Abolmaali, & Fernandez, 2007), published in the Journal of Bridge Engineering of ASCE, but little research has been conducted into simple or advanced models to assess a whole set of constructions of the same type. A more extensive analysis of the literature can be found in Appendix A1.

Automated assessment
From January 1983 to March 1990, research, reported in (Coleman, Harrison, & Woodson, 1990), has been carried out to develop a standard procedure for determining the structural capacity of reinforced concrete box-shaped culverts in airfield pavements under aircraft loads for the US Army Corps of Engineers. The reason this research was conducted is that many assessments are performed on regular basis to check whether the pavement meets the required structural capacity for traffic loads of that time and the anticipated loads of the future. Just like in this research the goal was a method to be able to rapidly evaluate the structural capacity of a box-shaped structure. Two alternatives have emerged in this study, one being a FEA model developed in 1980 and the other method used design rules from standard ACI-318 dating from 1963. The FEA model provided powerful modeling capabilities and a good level of detail when used properly by the engineer. Nevertheless, this alternative was not chosen because it was too complicated and too asked much computing power at the time. The model based on design rules was simple, straightforward and user-friendly and therefore more suitable as standard method. Nowadays there is of course much more computing power than in the 1980's, but it is important to consider computing time, simplicity and user-friendliness to achieve a tool suitable for practice and prevent errors by the user.

In (Uysal, 2017) can be read that the province of Zuid Holland uses a simple analytical model to assess existing RC underpasses and culverts. This is not yet an automated assessment, only a generic model for the load effects, but it does show that there is a demand for a generic method.

Modelling
Depending on the purpose, there are various models that can be used to describe the structural behaviour of a box-shaped structure. In (Uysal, 2017) the province of Zuid Holland uses a simply supported beam with rotational springs, representing the connection of the deck with the walls, which almost completely clamps the beam. This analytical model, shown in Figure 5, is simple, fast and easy to use and check.
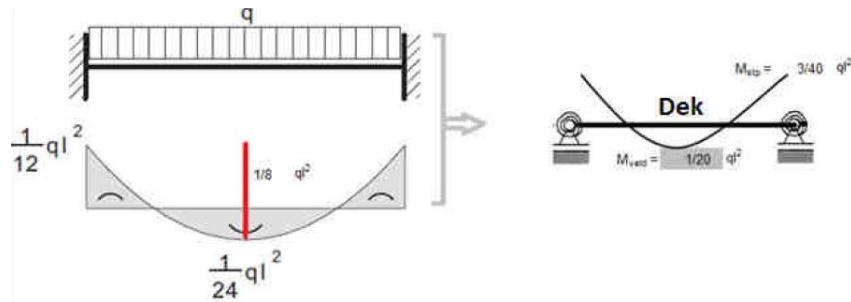
Figure 5 Model of province of Zuid Holland (source: (Uysal, 2017))

The province estimates that the deck is almost completely clamped by its walls, resulting in $\frac{1}{20} \cdot q \cdot L^2$ for the sagging moment and $\frac{3}{40} \cdot q \cdot L^2$ for the hogging moment which together is $\frac{1}{8} \cdot q \cdot L^2$ again. From (Uysal, 2017) however it can be concluded that the deck will behave less like a clamped beam, which means that the sagging moment at midspan is assumed to be too small and the hogging moment at the support is overestimated. Note that this has no influence on the shear force distribution since the bending moment line is only shifted and not changed shape. With this simple model the effects due to self-weight, vertical ground and water loads, the weight of asphalt and LM1 or LM2 can be captured. The UDL and TS of LM1 must be distributed and translated to a representative uniform load in kN/m.

A model that goes one step further is a 2D framework with 1D beam elements, which Uysal used to check the analytical model of the province of Zuid Holland. In his research he used two models, shown in Figure 6, to receive the normative sagging and hogging bending moment. Uysal has also noted that the model that accounts for the haunch overestimates the hogging moment. The model captures the effect of self-weight, vertical and horizontal ground and water loads, foundation type and stiffness, the weight of asphalt and LM1 or LM2. The UDL and TS of LM1 must be distributed and translated to a representative uniform load in kN/m.
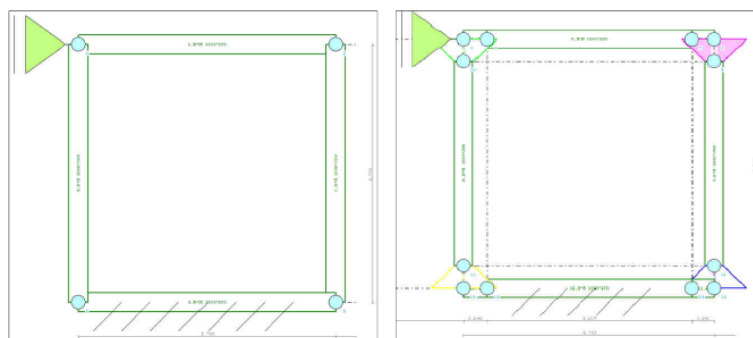
Figure 6 2D framework models used in (Uysal, 2017), left: max. sagging moment, right: max. hogging moment

In case a new model is constantly being made for every specific case, which is more the classic method, a transition is quickly made to non-linear FEA when the behaviour must be described as precisely as possible, this is reflected in (Uysal, 2017) and (Garg & Abolmaali, 2009). The 2D model of Uysal, which makes use of 2D elements, turns out not to be able to accurately predict the behaviour of a box-shaped structure loaded by a wheel load while Abolmaali describes the behaviour of several objects loaded similarly to the objects in (Uysal, 2017) with a 3D model with both 2D and 3D elements very well. Uysal decided to not make a 3D model since the structure was build up with small precast elements with a limited length. Furthermore, he expected that a more advanced model would not give much better results, it would take much longer to run and would be more difficult to model. However, he did not investigate that but only assumed it. In this research, however, many structures that were built in-situ have much bigger dimensions, which probably

benefits from a larger 3D model because of load distribution. The disadvantage of these models, however, is that much information about material properties and the layout of the structure and its reinforcement is required, which is often not available. On top of that, the computation time of such models is so long, and the process can diverge, that it is unlikely that these non-linear FEA models are workable for the structural assessment of a whole set of structures.

Based on this information a more advanced variant of an analytical model consisting of a simply supported beam with springs and linear FEA models with 2D frames consisting of 1D beam elements could be considered. To achieve a better understanding of the distribution of concentrated loads 3D FEA models could be made. The strategy to start with a safe hypothesis, modelling method, at the beginning of the research and to apply refinements when more accuracy is needed is in line with the Levels of Approximation (LoA) approach of (CEB-fib, 2010).

Sensitivity
Some research has already been conducted into the sensitivity of various parameters to the forces in box-shaped structures.
In (Coleman, Harrison, & Woodson, 1990) a small sensitivity analysis was performed which showed that box-shaped culverts are relatively insensitive to variations in the lateral earth pressure coefficient k. This is consistent with the test results from (Garg, Abolmaali, & Fernandez, 2007) which have shown that the presence of soil pressure on the wall has no significant influence on the failure capacity when loaded with a wheel load, which was governing for the tested culverts.

The influence of the internal water level in a culvert has also been investigated in (Coleman, Harrison, & Woodson, 1990). It showed that the internal water level has a negative effect on the bending moment in the midspan of the wall and the deck, but the effect drops below 10% when the live loads are present which ensures that the internal water level has relatively little influence due to the much larger live load.
The model of the province of Zuid-Holland for the assessment of box-shaped structures in (Uysal, 2017) turned out to be too much of a clamped beam, but no further investigation has been performed. However, the stiffness ratio between the walls and the deck largely determines the moment distribution in the deck and will therefore have to be investigated further.

According to (Uysal, 2017) the reinforcement configuration appears to have a major impact on the failure load, which means that much of the construction data must be known for reliable analysis. This ties in with the story in (Cullington, Daly, & Hill, 1996) where it appears that the anchoring length of the tension reinforcement in the deck has a major influence on the capacity of the structure. They also observed in 1996 evidence of shear enhancement despite the short anchorage at shear spans of d and $2d$. The shear capacity where the load is placed within a distance $2d$ from the support seemed to be significantly higher, which is in accordance with the current norm in NEN-EN 1992-1-1, in which loads within a distance $2d$ from the face of the support may be lowered by a factor β. However, this is only valid under the condition that the longitudinal reinforcement is fully anchored at the support.

Meanwhile (Abolmaali & Garg, 2008) suggests that the critical location of the wheel load was at a distance d from the tip of the haunch, resulting in shear failure, where d is the effective height of the bottom reinforcement at midspan in the top slab. The difference is the presence of a haunch, which locally increases the shear capacity significantly by increasing the cross-sectional height.
Results from (Uysal, 2017) show that LM1 from EC is governing over LM2 from EC, both for bending moment and shear. Which makes sense for structures with a relative long span since the total load from LM1 is bigger than the total load of LM2. For structures with a relative short span however LM2 may be governing.

Other comments

The calculated shear capacity in literature was almost always much lower than the actual, tested, capacity, which shows that it is still difficult to fully predict shear failure. Remarkable, however, was the large variation between test results in both (Cullington, Daly, & Hill, 1996), (Uysal, 2017) and (Abolmaali & Garg, 2008), varying from differences of 7% to as much as a factor of 2 for the same tests.

The test results from (Uysal, 2017), (Garg, Abolmaali, & Fernandez, 2007) and (Abolmaali & Garg, 2008) may be used at a later stage to verify the ASA tool and to provide insight into the reserves for a number of specific constructions.

An alternative approach for assessing existing RC structures, especially if the reinforcement layout is unknown, is studied in (Harrewijn, 2019), in which the minimum capacity is estimated based on old design codes using Reversed Engineering.

2.2   Underpass constructions in the Netherlands

The Netherlands has many underpasses that realize a grade-separated crossing, of which box-shaped reinforced concrete underpasses were built from the early 20th century. These constructions are built to allow a small waterway or cycle path to pass under a road or to allow a road from a lower network to pass under a road from a higher network. Typically, the span is limited to about 15m resulting in the box-shaped cross-section, larger spans are only realized with prestressed concrete. The width of the deck, the length of the underpass, varies from about 5m, when the object is situated in a bicycle path, up to 100m in case the structure is situated in a highway and thus strongly depends on the situation in which the construction is located. All these different situations also mean that structures are managed by different authorities, like municipalities, provinces and Rijkswaterstaat, and that they were built in the past on behalf of various clients with different regulations and site controls.

Most underpasses are constructed on site, up to a length of approximately 15m the underpass will be poured in one go, longer underpasses will be constructed in several sections with joints. With the emergence of the prefab industry in the 1970s more and more culverts and bicycle underpasses are being realized with prefab elements. Nowadays almost all culverts and bicycle underpasses are constructed with prefab elements. Larger traffic underpasses often cannot be made with prefab elements due to transport limitations. In order to cause as little inconvenience to traffic as possible, in the case of highways, the underpass is often made next to the road and then retracted during the night in a weekend.

Figure 7 Example of a box-shaped reinforced concrete underpass situated in the A27 near Utrecht constructed in 1970 (from RHDHV)

Figure 8 shows a typical cross-section of an underpass structure with several important parameters.
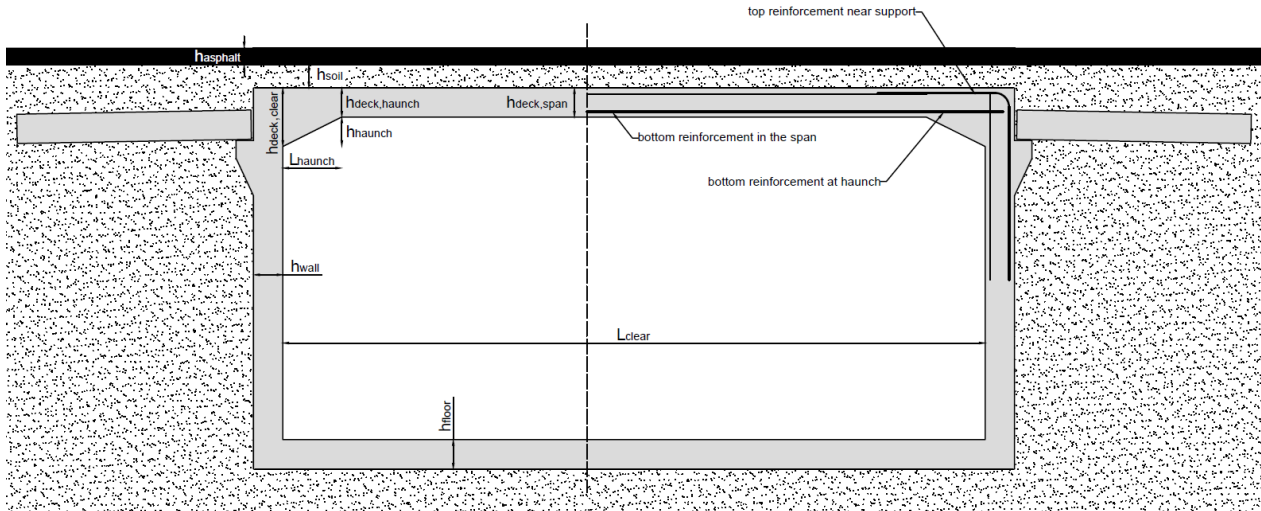
Figure 8 Overview of a typical cross-section with several important parameters. Note that not all reinforcement is drawn.

2.2.1   Estimation of number of underpasses in the Netherlands

Underpasses and culverts are situated both in the main road network and the lower network systems. The main roads in the Netherlands are owned by Rijkswaterstaat, the others by local authorities like provinces or municipalities. In order to further emphasize the importance of this study, an attempt has been made to estimate the total number of structures within the scope of the research.

Rijkswaterstaat
Based on (Rijkswaterstaat, 2020), RWS manages a total of approximately 6.600 structures, which is approximately 12% of the estimated total number of structures in the Netherlands.
The basic information of structures managed by Rijkswaterstaat is public and available via the DISK GeoWeb website. DISK is the data information system for structures of Rijkswaterstaat including bridges, tunnels, aqueducts, ecoducts, viaducts, culverts, lacks and weirs. Rijkswaterstaat makes a distinction between underpasses, for traffic, and culverts, for waterways. The number of underpasses and culverts, per foundation year, originate from the DISK GeoWeb website (Rijkswaterstaat, 2020). The total number of underpasses and culverts owned by Rijkswaterstaat and the percentage to the total number of structures owned by Rijkswaterstaat are presented in Table 2.

Table 2 Number of structures owned by Rijkswaterstaat (Source: data collected from DISK)

Category	Number of structures	Percentage of RWS total
Underpasses	591	9%
Culverts	730	11%
Combined total	1321	20%

The percentage for underpasses corresponds to the share found in (Rijkswaterstaat, Eindrapportage beoordeling kunstwerken, 2008) in which 1.200 structures of Rijkswaterstaat were investigated. In this research culverts were excluded.
The combined total of 20% of all structures owned by Rijkswaterstaat, which is a significant amount of more than 1300 structures, are within the scope of the thesis project supporting its relevance. The year of construction of underpasses and culverts which are now owned by Rijkswaterstaat are graphically presented in Figure 9.
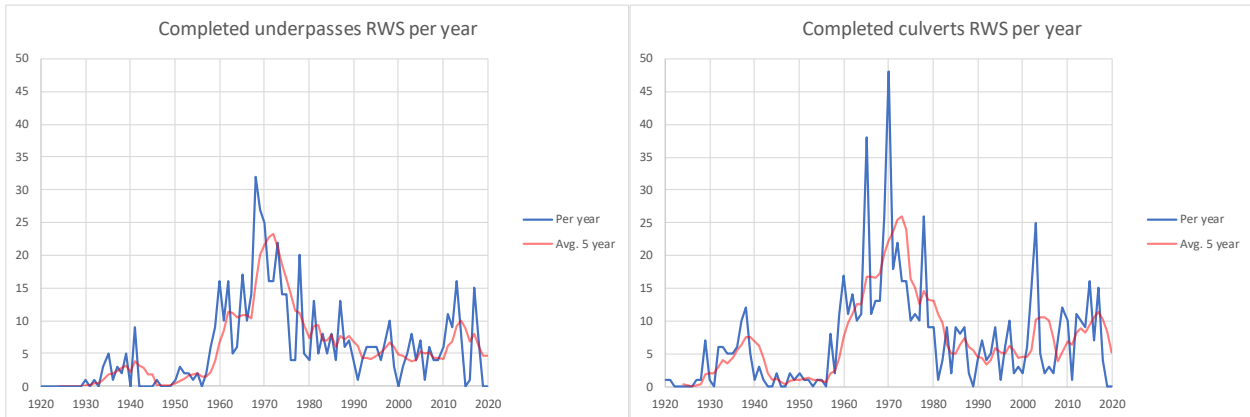
Figure 9 Distribution of completed underpasses (left) and culverts (right) owned by RWS over the years (source: produced from data obtained from DISK)

The combined data of underpasses and culverts that are managed by Rijkswaterstaat is shown in Figure 10.
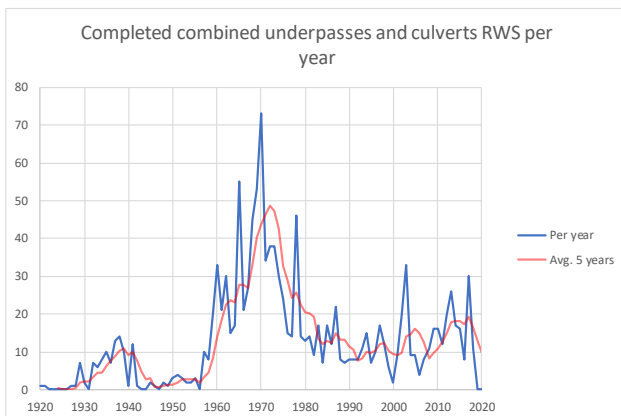
Figure 10 Combined distribution of completed underpasses and culverts owned by RWS over the years (source: produced from data obtained from DISK)

In general, the charts of underpasses and culverts match. The differences that are visual are that there are more old culverts, constructed before 1950, compared to underpasses and that the construction peaks of the graph which represents culverts is higher, which corresponds to the data of Table 2 that Rijkswaterstaat has more culverts than underpasses.

Comments to development of finished constructions over time:
- The oldest structure, a culvert, owned by Rijkswaterstaat dates from 1920. The main reason that Rijkswaterstaat does not own older structures is that it manages the structures in the main road and water ways, which was not constructed yet.
- The eldest structures, before 1950, were previously in an area access road but later on upscaled to a highway, the structures in these roads remained and became later on part in the highway system. From the graphs it is clear that this phenomenon primarily occurs with culverts.
- During World War II (1940-1945) the number of constructed structures declined drastically, which is not unexpected. But for several years after the war still almost no underpasses and culverts were completed, the construction of the infrastructure was almost completely stopped, since the government first focused on the reconstruction of housing.

- In the 1960s the construction of a highway system in the Netherlands started. The big wave of construction from late 1960s to early 1970s corresponds to the vast number of kilometres of highway constructed in this period. The reasons for the fast decline in the early 1970s are, according to (Vergoossen R. , 2019) based on a newspaper article from April 25th 1972, the lack of sufficient money and the change in view of environmental conservation and public transport.

Local authorities

Very little is known about the number and type of structures in the management of local authorities. In (CROW-CUR, 2019) it is estimated that there are about 55.000 bridges and viaducts in the Netherlands, which means that after deduction of 6.600 RWS structures, there must be about 48.400 structures in the management of local authorities. It is very likely that many culverts are not included in this estimate, while it is expected that there are many culverts in the infrastructure of local authorities since regional and local roads frequently cross small waterways. On the other hand, roads and waterways crossing the highway system are owned by Rijkswaterstaat. Which means that the majority of underpasses and culverts owned by local authorities are bicycle underpasses and culverts not crossing a highway.

In the end it is still an estimate, some aspects argue for a larger share while others suggest a smaller share. That is why the percentages of Rijkswaterstaat are used to estimate the number of underpasses (9%) and culverts (11%) in the management of local authorities, resulting in approximately 4.300 underpasses and 5.300 culverts owned by the local authorities. The combined total of underpasses and culverts owned or managed by local authorities is therefore estimated at 9.600 structures.

2.2.2   Reasons for assessment

If there is any doubt about the structural safety of a structure, the object must be assessed. During the lifetime of an existing RC underpass, various reasons for doubts about the structural safety may arise for carrying out a structural assessment.

Structural damage

One reason for assessing a structure is if there is significant damage to the structure. Examples include cracking, corrosion of the reinforcement steel, deformations, settlements or collision damage. A structural assessment must then reveal whether any structural measures are necessary to maintain the structure.

Reconstruction or renovation

In case of a reconstruction or renovation with structural consequences of the structure, an assessment is also necessary. Overlay with a new asphalt layer or the installation of a noise barrier, which increases the characteristic permanent load compared to the design, are examples of this.

Change of function

A frequently occurring reason, according to (Gijsbers, Dieteren, & van der Veen, 2012), for a structural assessment is a change in the function of the structure. An example is the increase in the characteristic traffic load compared to the design. In such cases too, there may be doubts about the structural safety.

End of design life

When the end of the intended life is near, a structural assessment is often carried out to see whether the structure can be used for a short or longer period. The structural assessment is carried out because it must be verified that the structural requirements are also met during extended use.

New insights into the behaviour of the construction or construction parts can also be a reason to doubt the constructional safety, as a result of which a new assessment is carried out. This was also seen in (Rijkswaterstaat, 2008) with regard to the shear capacity of concrete bridges.

2.3 Development of design codes

This section provides a brief overview of the development of the design codes. No extensive analysis is shown here, as this has been widely written in other research and various Cement articles. A general consideration of the development of concrete design codes is described in (Gijsbers, 2012) and (Gijsbers, Dieteren, & van der Veen, 2012). The development of the calculated shear capacity according to Dutch design codes is described in a series of three articles in (Vergoossen, 2008, April; 2008, May; 2008, July).

2.3.1 Concrete design codes

GBV series
The first design code for concrete dates from 1912, namely the GBV 1912, and was a handy booklet with a limited content of approximately 20 pages. A limited revision followed a few years later, the GBV 1918, which was then followed by the GBV 1930. The size of the GBV 1930 was relatively much larger, the division was still the same with the chapters 'General provisions', 'Materials', 'Execution' and 'Construction'. A decade later, the GBV 1940 follows, in which the new chapters 'Allowable stresses', 'Site controls' and 'Deviations' have been added. With the chapter 'deviations' the designer was given the opportunity to deviate from the allowable stresses under certain conditions, so that the designer is given more freedom for special and complicated constructions in order not to hinder the technique of reinforced concrete in its development. Ten years later the GBV 1950 follows. Apart from the addition of a chapter on 'mushroom floors', based on an American code, little has changed in the code.
Then follows the last code in the GBV series, the GBV 1962. The code is considerably more extensive and has changed a lot compared to its predecessor. The main reason for this is the rapid development of concrete technology after World War II. Much research preceded the creation of the GBV 1962. Briefly, the chapter 'Execution and construction' was split into two separate chapters, the chapter 'site controls' disappeared, parts of which were included under 'materials', the chapter 'allowable stresses' was expanded with 'deflection and crack width' and the chapters 'Crack method' and 'Test loading' were added. The crack method made it possible for the first time to perform a ULS check. Altogether, the GBV 1962 is a considerable overhaul.

VB series
The GBV series was replaced by the VB series, which was published in separate volumes between 1974 and 1983 but was called VB 1974. In 1984 this series, including interim revisions, was re-released in bundled form as VB 1974/1984. With a completely new structure and more than 500 pages, it was again considerably larger than the latest code from the GBV series. Even more than with the GBV 1962, the results of research were used in drawing up the VB series.
With the advent of the VB series, the system of allowable stresses came to an end and a capacity check based on ULS verification was used. Increased confidence in knowledge and quality control led to a reduction of the safety factor from 1,8, from the crack method of the GBV 1962, to 1,7. The shear capacity was made dependent on the concrete strength class, which depends on the cube compressive strength, and was now also determined with an effective cross-section. The assigned shear capacity of a cross-section decreased significantly with this new approach. The main reason for this was that structures were increasingly constructed with high-quality reinforcing steel (QR40, FeB 400), compared to the old soft reinforcing steel (QR22), which meant that less longitudinal reinforcement $A_{s,l}$ was used because the design was mainly based on the bending moment capacity. However, less longitudinal reinforcement $A_{s,l}$ also means a decrease in the shear capacity of the cross-section. Therefore, on the basis of the codes it is expected that for structures constructed with soft reinforcement steel bending moment will be predominantly governing and that the first structures designed with high-strength steel with relatively little longitudinal reinforcement $A_{s,l}$ shear capacity will be governing.

The VBC's

In the 1980s the demand for uniformity and national policy grew, which led to the development of the national Building Decree, *Bouwbesluit*. Uniformity found its way into the Building Decree in the form of the demand for uniform performance requirements and uniform determination methods for testing these requirements. The VBC 1990 was the first code in the VBC series and succeeded the VB 1974/1984. The VBC had a completely new set-up which had to ensure uniformity in comparison with the previous series of design codes. With the VBC the partial safety factors for loads and materials were also introduced, which are based on probabilistic analyses. The idea behind these different safety factors is that the same safety margin is maintained in the design for different load situations and different materials. The calculation of the shear force capacity was changed again. The limit value for the nominal shear stress without shear reinforcement was further reduced. Where in the VB 74/84 $\tau_d \leq 0,5\,f_b$ could be maintained, in the VBC that was reduced to $\tau_d \leq 0,4\,f_b$, which reduced the shear capacity in the calculation even further. But in addition to this lower limit, a "luxury formula" was also introduced with which a higher τ_d-value could be calculated for some situations. In addition to the tensile strength f_b of the concrete, this "luxury formula" was dependent on a height effect k_h, a slenderness factor k_λ and the percentage of tensile reinforcement in the longitudinal direction ω_0.

The VBC was revised once leading to the VBC 1995 which did not introduce any significant changes. The responsible standards committee decided not to issue any new revisions after the VBC 1995, pending the Eurocodes that are in effect from April 1, 2012 to the present day.

An overview of all successive RC design codes before the introduction of the EC in 2012 is shown in Figure 11.

Figure 11 Overview of RC design codes before the introduction of the EC in 2012

The critical reader may have noted that so far little attention has been paid to changes in the calculation rules for bending moment capacity. This is because a good model has been available for bending for a long time. The assumption that straight sections remain straight, known as the "needle principle" describes reality very well. In addition, the failure behaviour in bending failure can be predicted much better than in shear force, this is because, in contrast to bending, shear force has a brittle failure behaviour. The calculation models for shear force capacity have changed considerably over the years with the different design codes and even to this day there is not one unambiguous model available.

Materials

In the past 100 years, both concrete and reinforcing steel have undergone great development.

In the first GBVs there was no question of concrete classes. From the GBV 1940 a distinction was only made between whether or not a site control would be executed for which structures with site control could be subdivided into two classes which depended on the measured cubic compressive strength of the concrete. The concrete with site control was expected to have a higher concrete strength due to better quality control. Only from the GBV 1962 an actual division into concrete classes, with the designation with K-values, was made. As of the VB series, concrete was designated with B-values, which continued in the VBC series. With the effect of a new design code, more and stronger mixtures became available. The development of the strength of concrete mixes is shown in Figure 12.

As with concrete, there were no different types of reinforcing steel in the first GBVs. Different classes, based on strength, are mentioned for the first time in the GBV 1940, but really different classes of reinforcement steel would only have been used from the GBV 1950, of which an overview is given in (Latour, 1958). Previously, only soft steel was used, which has a relatively low tensile strength. In addition to the strength

of the steel, there was also a development in the shape or profile of the bars. In the past, many experiments have been done with the profile of reinforcing bars, as a result of which there have been many variants in reinforcing steel profile types, as can be read in (Gantvoort, 1964). A clear distinction is made between smooth and ribbed reinforcing steel. In general, the soft steel, class QR24 or less, was smooth and the stronger steel, above class QR 24, ribbed. Reinforcing steel with high strengths, which was already technically available in the GBV 1940, is ribbed in order to shorten the required anchorage length to transfer the high forces to the concrete. Figure 12 shows that high strength reinforcing steel was available before the revision of the calculation method for shear force capacity in the VB 1974 design code.
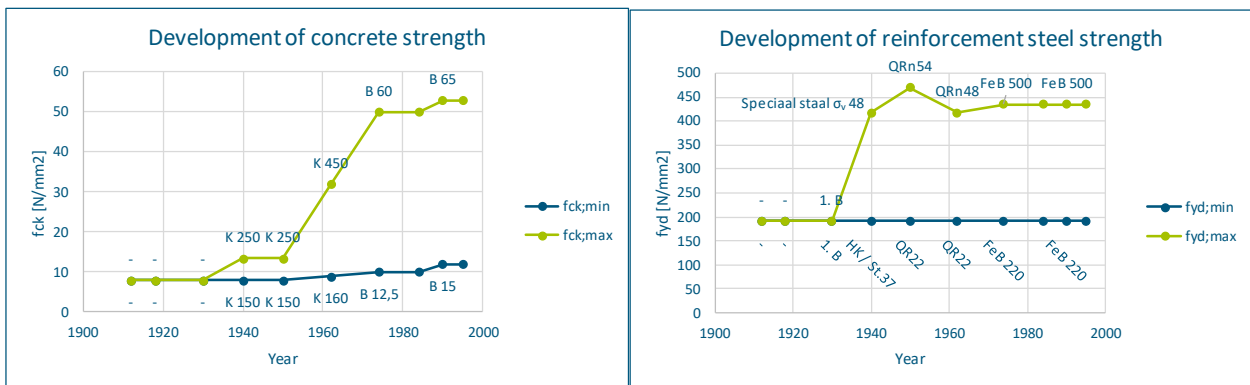
Figure 12 Development of concrete (left) and reinforcement steel (right) strength, based on RBK Table 2.2 and 2.6

The application of high-strength steel, above class QR24, was somewhat behind the availability, because it was still too expensive in the beginning. The application of high-strength steel developed mainly in the 1960s where in the 1970s almost only QR40 was used.

The NEN8702, which is based on the older RBK, gives an overview of concrete and reinforcement steel classes which were used in the past with corresponding design value for the strength in accordance with EC. The concrete and reinforcement steel classes are based on table 2.2 and 2.6 of RBK respectively, which can be found in Appendix A2.

2.3.2 Design traffic load

The concrete design codes do not give design traffic loads for concrete bridges, these load models originate from the steel bridge design codes called VOSB. The first VOSB originates from 1933, which was already revised in 1938 but without changes of the design traffic load. Both VOSB 1933 and 1938 make a distinction into four classes of road bridges, whose classifications according to description are shown in Table 3. Class D disappeared with the arrival of the VOSB 1963, the other classes were retained, although classes A, B and C were now designated 60, 45 and 30 respectively. After the VOSB series, a separate code for concrete bridges, the VBB 1995, was introduced in 1995, which also used classes 60, 45 and 30. With the arrival of the EC in 2012, the principle of load classes disappeared.

Table 3 Overview of traffic classes according to VOSB 1933 and VOSB 1938.

Class	Description
Class A / 60	Bridges in the main roads, where traffic diversion is excluded
Class B / 45	Bridges in the main roads, when it is possible to guide a very heavy vehicle, if only exceptionally, along a (by) road with bridges built to class A.
Class C / 30	Bridges not intended for very heavy vehicles
Class D	Bridges intended for light vehicles only

Since the first design traffic load in the VOSB 1933 to the EC today, a distinction is made for traffic loads on bridges between uniformly distributed loads (UDL) and concentrated loads. The concentrated load is a representation of the heaviest expected vehicle and consists of multiple axles with wheel loads in what is called the design truck, later tandem system (TS). Contrary to the class division, a few things have certainly changed in the design traffic loads over time. An overview of the traffic loads per standard and class is shown in Table 4.

Table 4 Overview of design traffic load

Design code	Class	UDL [kN/m²]	TS
VOSB 1933 / 1938	A	4	3 x 200 kN [v]
	B	4	1 x 200 kN + 2 x 100 kN
	C	3,5	2 x 100 kN
	D	3	2 x 50 kN
VOSB 1963 / VBB 1995	60	4[i]	3 x 200 kN [vi]
	45	3[ii]	3 x 150 kN
	30	2[iii]	3 x 100 kN
EC 2012	N.A.	9[iv]	2 x 300 kN

i with a maximum of 12 kN/m[1] per lane.
ii with a maximum of 9 kN/m[1] per lane.
iii with a maximum of 6 kN/m[1] per lane.
iv characteristic value for lane 1 of LM1 in EC, for other lanes or remaining area UDL = 2,5 kN/m².
v choice of 1 x 100%, 2 x 90% or 3 x 80% TS.
vi choice of 1 x 100% or 2 x 80% TS

Although the traffic intensity has increased tremendously since 1933 and more and more heavy trucks are driving on the roads, the load effect of these heavy trucks has generally not increased when looking at the design traffic loads. However, in the old design codes a *"stootcoefficient"*, Dynamic Amplification Factor (DAF), had to be taken into account, which is not the case the case for EC since it is incorporated in the representative loads. In the EC, a DAF up to 1,3, or 1,15 for good asphalt, must be used at expansion joints for fatigue and LM2, but because underpasses and culverts do not have expansion joints, according to NEN-EN 1991-2 art. 4.3.3 (3) and art. 4.6.1 (6), it is not necessary to use the DAF. On top of that, the safety in the old design codes was provided by an allowable stress, which is approximately a factor of 1,7 to 1,8 lower than the characteristic material strength, which in the design resulted in much more material use compared to the method of partial safety factors used in the EC. Indirectly, a higher safety factor was applied, also to permanent loads.

2.4   Data analysis

It is of importance to have an understanding about what kind of construction types are present in the Netherlands and how old these structures are. In addition, it is important to know how many there are and between what the underpass facilitates an intersection. Based on the information found lower and upper bounds of parameters of the structure can be set which in turn can be used to perform assessments on theoretical underpasses and generating data. Another reason for this analysis is to investigate if typical changes in the underpass constructions can be found in relation with different codes used for their design, answering sub-question 2.2. Note that an extensive analysis, with graphical representation of the data, can be found in Appendix A3.

2.4.1   Starting Points

Predefined scope

For this analysis, only existing underpasses with a concrete main loadbearing structure of the type box, portal or concrete plate on sheet piles were searched. It concerns both underpasses in the main road network, owned by Rijkswaterstaat, and underpasses that are not part of the main road network which are owned by a province or municipality. Existing RC underpasses from the early twentieth to the early twenty-first century are being sought. The idea behind this is that structures designed with the first concrete standard, the GBV 1912, up to the latest standard before the introduction of the EC, the VBC 1995, are included. The predefined scope for this data analysis is described in more detail in section 1.4.

Available data

The basic information about Rijkswaterstaat structures, which is publicly available on the DISK GeoWeb website, does not provide enough information for assessing a structure. The data concerning the underpasses itself comes from structural assessments of existing underpasses already carried out by RHDHV as well as some other parties and is available, for employees, on the online database of RHDHV.

2.4.2   Evaluation used data

The available documents of a total of 64 structures were examined. Documents include DISK reports, reports of structural assessments, calculations, shape drawings and reinforcement drawings.

Procedure stocktaking

To make an inventory of the required data, the available drawings were first examined. If the drawings present do not provide sufficient usable data, any available calculations will be inspected. In addition, data from inspection reports have been examined, but these mainly contain brief information regarding the geometry of the structure and the layout of the reinforcement.

Sequence in case of conflicting information:
1. Shape drawings
2. Reinforcement drawings
3. Calculations
4. DISK report
5. Inspection reports

The reason why DISK and inspection reports which contain actual measured dimensions are at the bottom of the list is because these measurements can contain errors and may include defects to a structure. Therefore, they do not give a good value for the dimensions keeping in mind that these objects represent a much larger group of objects in the same category.

The underpasses and culverts are further categorized by the road or waterway they are situated in or cross, as shown in Table 5.

Table 5 Overview of crossing categories. Explanation of terms used can be found in Appendix A3.

Situated in	Crossing
Highway	Highway (ramp/exit)
	Area access road
	Byroad
	Cycling path
	Waterway
Area access road	Byroad
	Cycling path
	Waterway
Byroad	Cycling path
	Waterway

Availability of data

The number of objects included in the database is limited, 64 different structures are investigated and added. Most of the data for these objects was available.

- Of the structures in the "Byroad – Box" category, about 14% of the structures have no or insufficient data;
- Of the structures in the "Cycling path – Box" category, about 20% of the structures have no or insufficient data;
- Of the structures in the "Culvert – Box" category, about 25% of the structures have no or insufficient data;
- Of the structures in the "Byroad – Portal" category, about 29% of the structures have no or insufficient data;
- On average, about 19% of the structures studied have no or insufficient data.

Sufficient data was available for 82% of the structures owned by Rijkswaterstaat. At 75%, that percentage was slightly lower at the local authorities, consisting of municipalities and provinces. However, it is expected that the percentage of municipalities and provinces that have sufficient data for structural analysis of their bridges and viaducts will actually be a lot lower. In (Mulder, 2015), a survey was conducted among more than 400 municipalities in the Netherlands, of which barely 30% responded, into the existing bridges and viaducts. The responses received showed that the construction year was not even known for 15% of the constructions. In addition, it is remarkable that almost 75% of the municipality did not answer, the reasons for this may vary, but it suggests that the availability of information is even lower for this group.

Usability of data

The starting point is that all available information from RDHV's online database is used, including drawings, calculations and reports. If the data is incomplete or missing, the object is nevertheless added, either with an "unknown" entry for the unknown parameters.
It has been found that the material properties of concrete and steel usually can be obtained from the shape and reinforcement drawings, if they are available and readable.

2.4.3 General findings based on available data

Distribution of data

The distribution of the structures in the data set, shown in Figure 13, is reasonably in line with the spread seen in the number of completed structures per year which are now managed by Rijkswaterstaat, which is presented in Figure 10 repeated on this page.
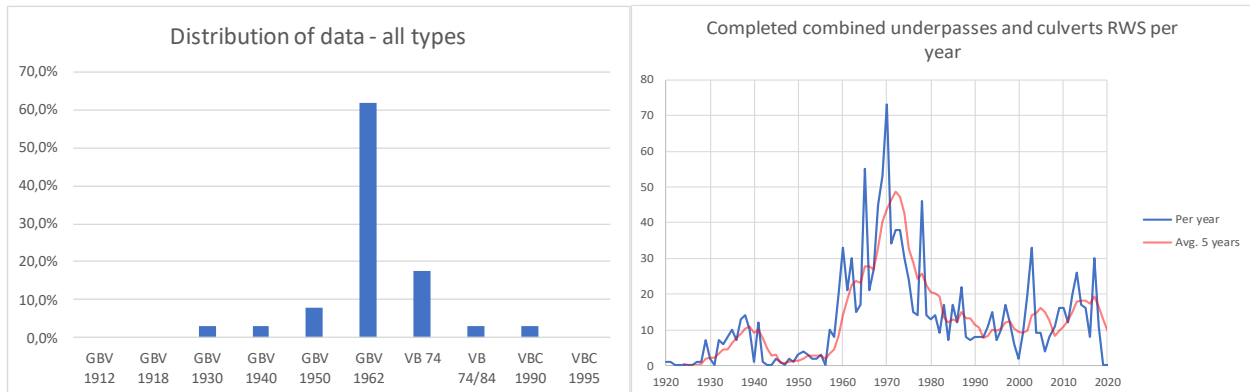
Figure 13 Distribution of data within the studied structures (left) and completed underpasses and culverts by RWS per year (right)

More than 60% of the available data for underpasses is designed according to the GBV 1962. This is as expected, knowing that a wave of infrastructure construction took place in the late 1960s to early 1970s, shown in Figure 10. In addition, Rijkswaterstaat had a research carried out in (Rijkswaterstaat, 2007) and (Rijkswaterstaat, 2008) that focused on structures designed according to the GBV 1962 because this standard introduced a change in cross-section capacity that was later expected to cause problems with the shear force capacity.

Structures from the first half of the 1960s, which are a significant number according to Figure 10, will have been designed according to the GBV 1950 because the design of these structures was often made before the new code went into effect. However, fewer structures were found than the number of structures from this period in Rijkswaterstaat's management would suggest. It is believed that the reason for this is that most assessments carried out in recent years are for structures designed according to the GBV 1962, since it was believed to cause problems.

The fact that hardly any constructions have been found dating from before the introduction of the GBV 1950 can be explained from the data of Rijkswaterstaat that there are simply not many structures from that time. The underlying road network, which is managed by the local authorities, is a lot older and is expected to have more structures from the period before 1950, however no old projects with structures from this period have been found.

Very few structures have been found which are designed according to VB 74/84 or later design codes, while there is a significant number of structures from this period in the database from Rijkswaterstaat.

The main reason is that for structures before 1974, before the VB 74, there was a change in codes related to the shear force capacity and therefore all structures of RWS had to be assessed. Structures designed according to the VB 74 or later design codes only had to be assessed in case of damage or change in loads or structure. Another general logical explanation is found in the fact that no assessments are yet being carried out for these structures, because they have not reached the end of their designed service life yet. However, it is expected that assessments will also have to be carried out for these structures in the near future.

Underpasses and culverts

Within the dataset, 70% of the structures appear to be managed by RWS. This is contradictory to the number of objects that RWS manages compared to the local authorities, which are estimated to have eight times as many.

The data shows that 81% of the investigated structures are of the box-shaped construction type, as described in section 1.4, the distribution of construction types is shown in Figure 14. The vast majority of the structures, over 70%, are founded on grade, as can be seen in Figure 14. If only box-shaped structures are considered, even 80% has a foundation on grade.
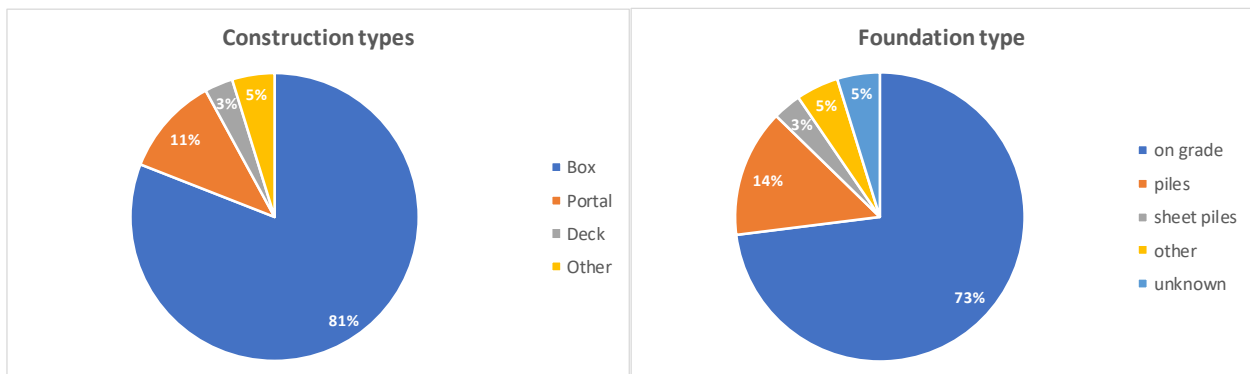
Figure 14 Distribution of construction types (left) and foundation types (right)

The fact that this percentage is high can be justified by the fact that the box cross-section has a floor through which the load is spread on the subsoil, if the subsoil directly under the structure allows these kinds of loads. This means that in most situations no foundation piles are required which otherwise transfer high concentrated loads. This is probably also a reason why so many box cross-sections have been used to avoid the need for an expensive pile foundation.

About the same percentage as can be seen in road categories under management, namely that about 70% of the objects are located in a highway. It is striking that the other objects are almost exclusively located in an area access road, while it is expected that many culverts are in the lower byroad network.

Figure 15 shows the distribution of what is crossed, the type of the underlying network. The fact that the share of byroads is so high is due to the large share of objects of RWS, as a rule a highway, which intersects grade-separated with other roads. The share of culverts, and thus waterways, will in practice be larger than shown in Figure 15. Many assessments of RWS as part of the research reported in (Rijkswaterstaat, 2008), where a minimum span of 3,5m was applied, so that most culverts fell outside the scope. It is also expected that the local authorities will have many culverts for which few assessments have been performed.
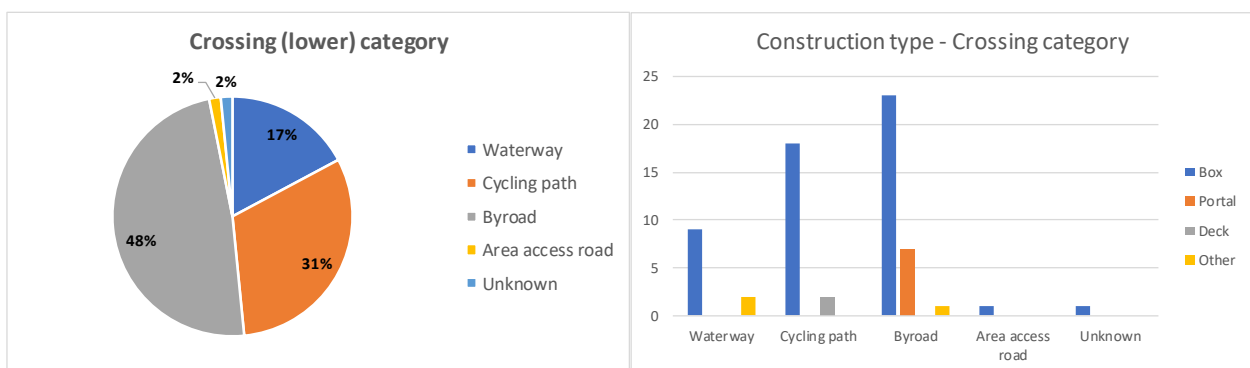
Figure 15 Distribution of crossing category (left) and construction type per crossing category (right)

From Figure 15 it is clearly visual that the box-shaped construction type is dominating. The concrete deck on sheet piles does not seem to occur often, it is therefore unlikely to occur often in future assessments of existing structures. Portal structures in the dataset only occur where a byroad crosses some other road, where the span is relatively large, therefore it seems unlikely that portal structures occur where waterways or cycling paths cross another road.

Load classes
As can be seen from section 2.3.2, the Netherlands, unlike many other countries, already had a load model at an early stage with a 60-ton truck that was used in the design calculations for the main road network. This now has its advantages. Figure 16 shows that approximately two-thirds of the structures investigated were designed with a 60-ton truck, namely class A/60.
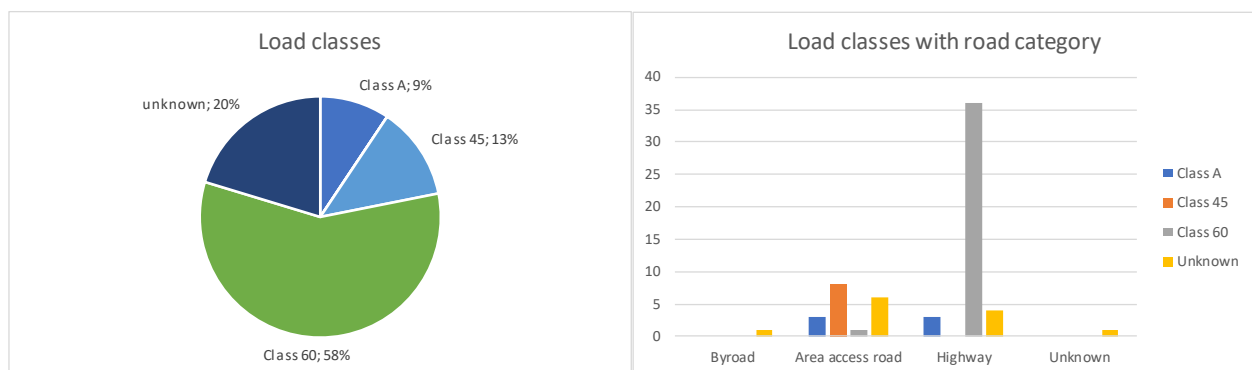
Figure 16 Distribution of load classes (left) and load classes with road category (right)

Figure 16 shows that the large share of Class 60 is almost entirely in the highway category. Namely, of the examined structures in a highway, 86% were designed according to Class 60, the rest were designed according to the older Class A or was unknown. No lighter load classes have been found for structures in a highway. Based on this data, it is therefore unlikely that a structure was designed according to a lighter load class and is currently still in a highway. It seems that data on structures in a highway are usually known, only in 7% of the investigated cases the load class was unknown. Structures situated in an area access road are usually designed according to Class 45, however there is much more spread in load classes compared to structures in a highway. Relatively speaking, data on structures in an area access road are often not known regarding load class, namely in 33% of the cases examined. The overall percentage for unknown load class is expected to increase as more local government objects are added to the dataset, because they have stored the data much less well in the past.

2.4.4 Findings of box-shaped structures

Because more than 80% of the structures investigated are of the box-shaped type, a further analysis is carried out for this construction type. In total, it concerns 52 objects with a box-shaped cross-section, 83% of which are considered complete. The information about an object is considered complete if the reinforcement configuration is known so that an assessment can be performed.
It may not come as a surprise that the year of construction of box-shaped structures is concentrated around 1969, just like the RWS data. The angle between the road across and through the underpass is called the intersection angle. The angle of intersection is in 75% of the investigated cases within the range from 80gon (≈72°) to 100gon (90°), which is according to RBK a requirement if a construction is modelled with beam elements. The minimum angle of intersection found is 53,2gon, which is 47,9 degrees, and 100gon is naturally the largest angle.

Geometry

The general analysis, described in paragraph 2.4.3, shows that underpasses are used at different intersections with different road or waterway types, this is reflected in the large spread of span length. Within the box-shaped structures the span, the distance in the clear, varies from 1,44m, for a small culvert, all the way up to 13,0m for the crossing between an area access road and a highway. Data clusters in span length based on intersecting category, like culverts, bicycle underpass or underpass for mixed road traffic, have not been found. The data is fairly evenly distributed, where the culvert has an average of 4,0m, a bicycle underpass 5,0m and a traffic underpass 8,0m. With a mixed traffic underpass, the spread in span, from 4,0m to 13,0m, is very large.

The total width of the deck, popularly the length of the underpass, varies with the function of the road in which the construction is situated. An underpass in a highway is, of course, longer than one under a local road. In the available data, the length of the underpasses varies from about 10 to 90 meters. Because of the load distribution, it is interesting to know what the joint to joint distance from the deck is. All data falls within a range of 4,8 to 28,2 meters for the joint distance, with a few exceptions with smaller and higher values. On average, the joint-to-joint distance is 16,8m.

For the thickness of the deck, three sections are considered, at midspan, at the junction of the haunch and in the clear with the wall. In general, the deck between the two haunches is equally thick everywhere, the thickness in the clear of the wall is in most cases significantly bigger. In 79% of the box-shaped structures examined, a haunch was present to make the deck thicker near the wall. Of the remaining part, 15% had a constant height, a parabolic course hardly occurs at 4%. In the remaining 2% of the cases, the course was unknown or unclear. An overview of the distribution in deck thicknesses is given in Table 6.

Table 6 Overview of distribution of deck thickness in different sections.

Section	Min [mm]	Q2 [mm]	Q3 [mm]	Max [mm]	Median [mm]	Mean [mm]
$h_{deck,midspan}$	300[i]	350	578	750	410	452
$h_{deck,haunch}$	300[i]	350	585	775	420	463
$h_{deck,clear}$	340	550	870	1100[ii]	700	724

i one in dataset with 170mm but marked as outlier.
ii one in dataset with 1450mm but marked as outlier and is a slightly different cross-section.

The relationship between span length and the thickness of the deck, shown in Figure 17, is approximately linear from a span of 4m. For smaller spans, the thickness of the deck is not reduced for practicality.
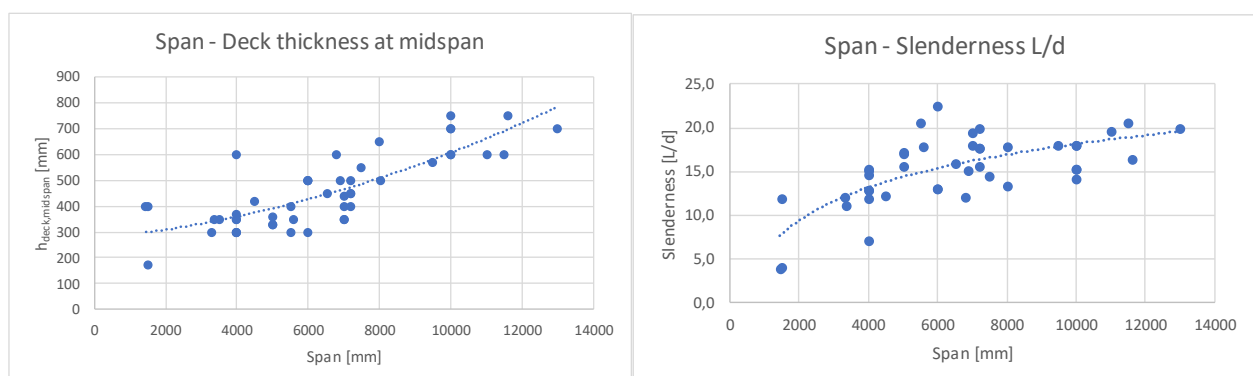
Figure 17 Ratio between span and deck thickness (left) and ratio between span and slenderness L/d (right)

For the box-shaped structures an average slenderness, which is defined as L_{clear}/d, of 15,3 is found and of all objects examined, the slenderness of the middle 50% of the structures falls within the range of 13,0 to 17,9. Low slenderness is found in structures with a relatively small span, like culverts or small bicycle underpasses, where the deck cannot be made slimmer due to practical considerations. The lowest slenderness found for an underpass for mixed traffic is 13,3. The higher slenderness ratios primarily occur with relatively large spans, where a road for mixed traffic crosses a highway for example. The correlation is shown in Figure 17. No clear correlation has been found between slenderness and load class.

The internal height of the box also shows that this construction type has been used in various situations. Two clear groups can be seen in the data, one group includes culverts and bicycle underpasses and the group has an average internal height of 2,6 m and the other group are the crossings between two roads where the box has an average internal height of approximately 4,5 m. The ratio between width and height of the box cross-section can also be divided into two clear groups based on internal height, shown in Figure 18. The span, or width of the box, over height ratio varies from 1,1 to 3,0.
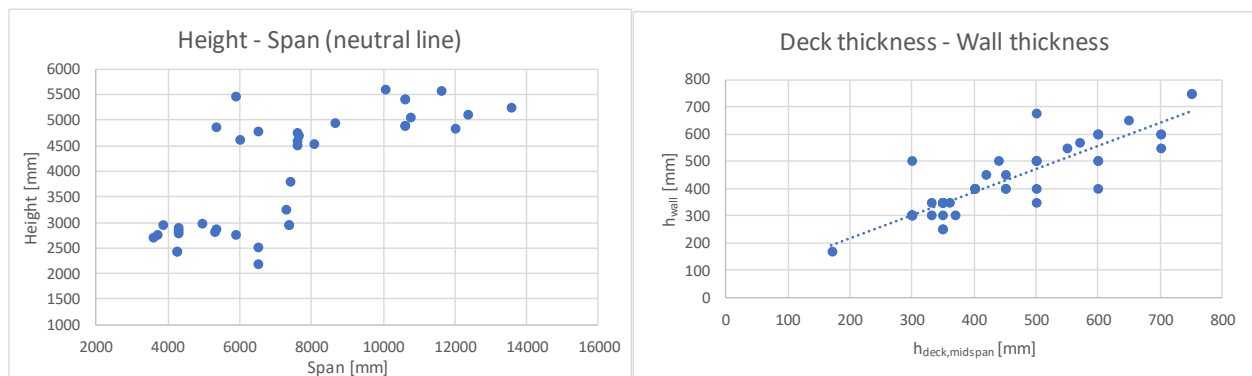
Figure 18 Correlation between height and span of neutral line (left) and correlation between deck and wall thickness (right)

The thickness of the floor, walls and deck varies and just like the slenderness these thicknesses are strongly correlated with the span of the structure. An overview of the distribution in thicknesses is given in Table 7.

Table 7 Overview of distribution of wall and floor thickness.

Element	Min [mm]	Q2 [mm]	Q3 [mm]	Max [mm]	Median [mm]	Mean [mm]
h_{wall}	250[i]	300	538	750	400	434
h_{floor}	300	350	600	800	500	484

i one in dataset with 170mm but marked as outlier.

A clear correlation has been found between the thickness of the deck and the thickness of the wall, where the trend is, with a few exceptions, that these thicknesses follow each other, as shown in Figure 18. Based on these data, it is unlikely that large differences exist between the thickness of the deck and the thickness of the walls, which also makes sense from a mechanics point of view.

Concrete

The concrete class was unknown in more than half (55%) of the investigated box-shaped structures. In case the concrete class is known, the most common class is GBV 1962 K300 (29%). Thereafter, and from a later period as well, B 30 (10%) from the VB series. Together these options cover 94% of the investigated cases. The total distribution of concrete classes of the examined data of box-type structures is shown in Figure 19. In case a structure was built by RWS before 1976 the RBK states that a concrete class C35/45 according to the EC may be used, even if the concrete class is unknown. This is based on a large-scale research reported in (Rijkswaterstaat, 2008) into structures built under the GBV standard series. A higher strength

than the concrete classes in the old standards results from the continuous hydration of the concrete, which has increased its strength. Based on the data, this will have a significant positive effect for most structures. This does not apply to structures of local authorities. Due to a greater spread in the tested samples, a C16/20 must be maintained according to CUR124 if the concrete strength class is unknown. This is significantly lower and is expected to have a major impact on the calculated shear capacity. The available data concerning concrete class is plotted within the development of concrete strength in Figure 19.
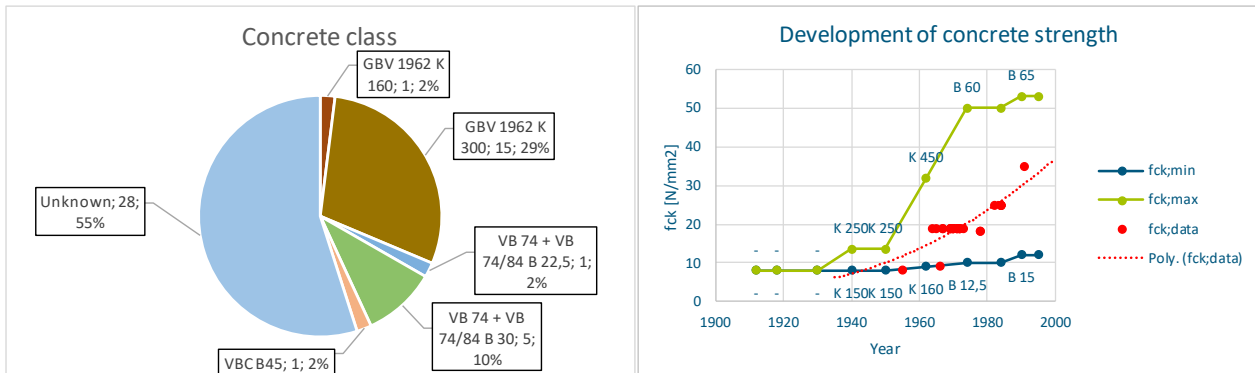
Figure 19 Distribution of concrete classes (left) and available data within development of concrete strength from RBK (right)

Reinforcement

Most of the investigated structures (60%) have an orthogonal reinforcement mesh, which can be explained by the large number of structures with a 100gon or almost 100gon intersection angle. Reinforcement parallel to the road occurs in 21% of the structures studied, the other 19% is unknown. For structures with an intersection angle greater than 80gon it is very likely that the reinforcement mesh is orthogonal because this applies to 83% of the investigated cases, however this percentage is too small to assume the mesh for an intersection angle greater than 80gon as orthogonal. For the structures with main reinforcement parallel to the road, no specific correlation was found with the year of construction other than that they occur from 1950 to 1984, under different standards from the GBV 1940 up to and including the VB 74.

It can be seen that the most used steel classes come from the design codes from around 1970, which can be explained by the fact that most structures have a year of construction around 1970. Most common is GBV 1962 QR40 (33%), after that FeB 400 HW, HWL (29%) from the VB series and thereafter 27% is unknown. These are by far the largest categories, covering 89% of the investigated structures. Contrary to what the design codes suggest, little variation can be found in the different reinforcing steel qualities in practice. Remarkable is the low proportion of soft steel found in the data. Eight different steel grades were found in the study, the distribution is shown in Figure 20.
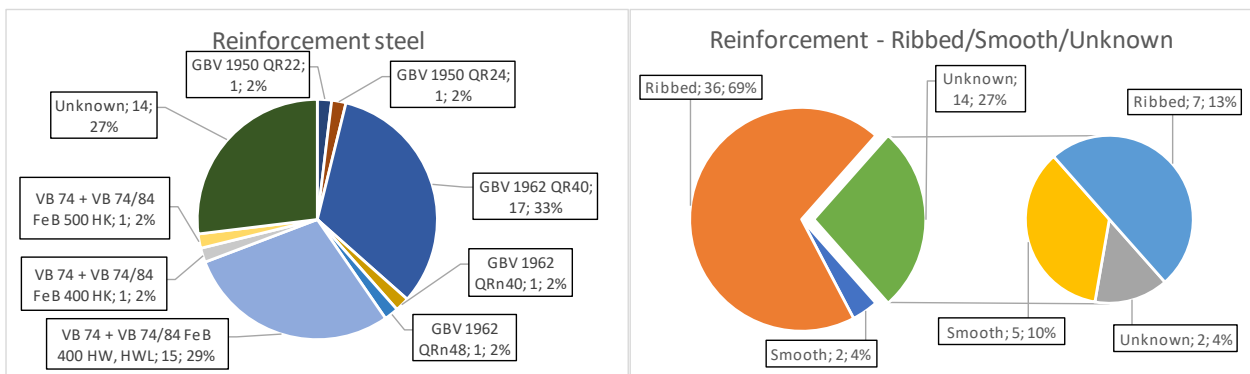
Figure 20 Distribution of reinforcement steel classes (left) and reinforcement profile type (right)

Purely based on the reinforcing steel used, 69% is ribbed, only 4% is smooth and the profile of 27% is unknown. But based on the year of construction, with the used design code, and guidelines from RBK the proportion unknown can be made smaller. The unknown group of 27% is then subdivided in 13% ribbed, 10% smooth and 4% unknown. Combined, this results in 82% ribbed steel, 14% smooth steel, and only 4% is unknown. The distribution of ribbed or smooth steel is graphically represented in Figure 20.

Many different bar diameters have been used in the past, ranging from 12 mm to 32 mm. The most common diameters are 16mm (20%), 25mm (15%), 20mm and 12mm (14%) but relatively a large scatter has been found including some diameters that are no longer used today. This concerns the diameters 14, 18, 19, 22, 24 and 28. At the connection between the deck and the wall, smaller diameters occur relatively more often, because there are several layers there, which result in the same total cross-sectional area.

Compared to the other parameters, the spread in concrete cover is small with 71% of the data points falling within the range 25mm to 30mm. The minimum and maximum found are 20 mm and 40 mm, respectively.
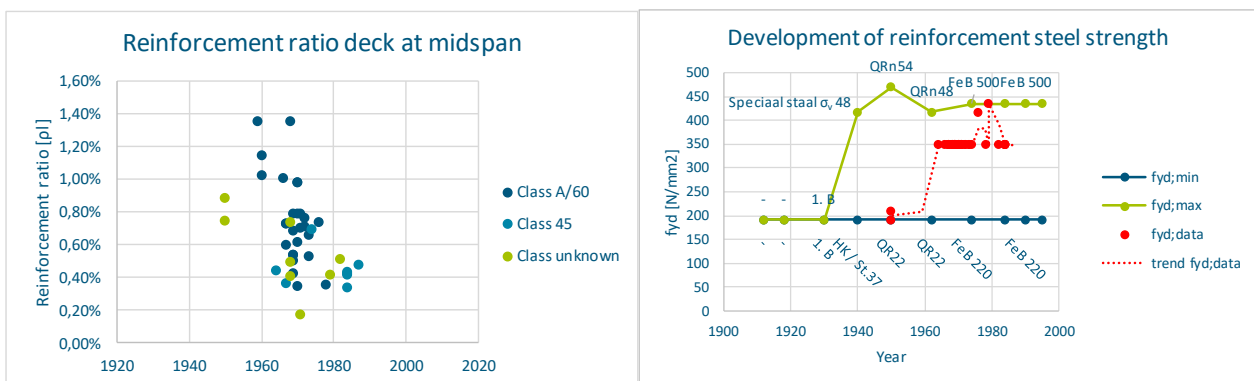
Figure 21 Reinforcement ratio of the deck at midspan (left) and the data compared to the development of reinforcement steel (right)

The reinforcement ratios found vary widely, even for structures designed according to the same load class, as shown in Figure 21. Because almost all structures are designed with QR40 or FeB400, no clear relationship was found between the reinforcement ratio and the reinforcement steel used. There are no clear causes why higher or lower ratios have been used. It is clear, however, that structures designed according to load class 45 have, on average, a significantly lower reinforcement ratio. The data shows that there is generally slightly, on average 7%, more area of reinforcement (mm²) at midspan of the deck than at the connection with the wall. Because most cross-sections (79%) are executed with a haunch, the reinforcement ratio in the clear is on average considerably lower. The fact that higher strength reinforcing steel became financially attractive in the 1960s is reflected in the data shown in Figure 21. The suspicion that high-strength steel was already frequently used before the introduction of VB 74 is consistent with the data.

2.5   Discussion

In the literature review no linear elastic 3D model with plate elements was encountered. Such a model has been found several times in completed projects of RHDHV. A 3D FEM model with plate elements is certainly interesting to investigate in relation with the distribution of traffic loads on bridge decks, because it is expected to play a significant role.

One point that can be discussed is whether the data obtained from RHDHV is a good reflection of the actual underpass constructions in the Netherlands. The objects in the dataset are almost all from old assessments, not only performed by RHDHV, for which design drawings are available. In (Bleijenberg, Maljars, Polder, Steenbergen, & Vervuurt, 2017), the Netherlands Organization for Applied Scientific Research (TNO) reports that archives of old bridges are often incomplete. One can therefore wonder whether there is a structural difference between structures whose drawings have been preserved or whether it is purely coincidental. However, the widespread in the data suggests the latter. Another point that can be discussed regarding the data used is that it is concentrated around 1969. It gives a good picture for objects from that period, but a less good picture for structures that were built later and need to be assessed in the future.

Section 2.2.1 describes that local authorities are expected to manage more than eight times as many underpasses and culverts than RWS. It is therefore remarkable that the number of structures in the dataset that are managed by the local authorities is only 30%. According to (Mulder, 2015), this can be blamed on poor policy in which too little has been invested in maintenance and the limited availability of information of structures from local authorities. An explanation from a different angle could be that, unlike RWS, the provinces and municipalities are less likely to find their way to RHDHV.

It should be noted that over the years RWS has also transferred the management of a significant number of structures to the local authorities. This usually concerns constructions that are no longer situated in the national highways but are therefore designed according to load class A/60 and often built with site control. This affects the calculated capacity of the structure in an assessment. No lower load classes than class A/60 were found for structures in a national highway, on which it can be concluded that, based on the data, a lower load class in a national highway is not common. It cannot be excluded because old structures which used to be in a lower road network, and designed to a lower load class, are now situated in a national highway because the road was once upgraded to a national highway.

Regarding the development of the design code, because of the data mainly from GBV 1962 to VB74, no clear connection with the new insight into shear capacity can be seen in the data. A high-quality steel, QR40 or FeB400, has been used in all constructions from that period and there is no clear jump in the reinforcement ratio. There seems to be a downward trend in the data which can be explained as coincidence by the objects included in the dataset. The group of data points that have a relatively lower reinforcement percentage around the 1980s are mainly bicycle underpasses, which are relatively small and situated in roads which may be designed according to load class B or 45. What is striking is the large scatter in the reinforcement ratio ρ_l. An explanation for this could be that both the old and the new design code were used within this period. In addition, it may be that the "engineers' factor" was already present at the time, especially in periods of transition from old to new design codes with new calculation methods and materials.

3

Load effect with analytical model

This chapter examines the load effects based on an analytical model. The research starts with a basic analytical model with the Guyon-Massonnet method. In addition, the stiffness relationships and their influence on the moment distribution between different elements of the structure based on the fictitious stiffness modulus E_f are investigated. Finally, an analytical method for the in-plane shear distribution of the TS load in a RC slab is investigated.

3.1   Introduction

Assessment of a civil structure must be executed conform *Bouwbesluit 2012*, which refers to the Eurocode, NEN8700 and NEN8701. The Eurocode provides principles for the structural design, the load models and rules regarding the calculation of concrete structures. The NEN8700, which provides additional rules for existing structures, may be used for assessing existing structures that are at least 15 years old. The NEN8701 is an elaboration of the guidelines from NEN8700 which refers to the loads on the structure. This code is based on the Eurocode NEN-EN 1991 and must be read in conjunction with it. Loads may be reduced in relation with the remaining service life in case it is less than the design service life. On top of that RBK and CUR124 are used, which supply additional guidelines and requirements for the assessment of existing civil structures owned by RWS and local authorities respectively. For the assessment of existing structures applies that during the residual service life it should be safe and usable. In addition to the standard assessment levels provided in NEN8700, 'new construction', 'reconstruction' and 'disapproval', RBK provides an extra assessment level 'usage' to fill the gap between reconstruction and disapproval. However, the usage level is only classified in CC3 for RWS structures. Most assessments of existing structures will take place at the reconstruction level for the local authorities, and for structures of RWS the usage level will in many cases be applied, unless a reconstruction takes place, then reconstruction level will also be applied. A remaining service life of 30 years is recommended for both levels, a project specific longer remaining service life can be agreed.

The structural safety of existing structures is determined in an assessment based on a ULS verification calculation. As a first step, an analytical model has been made, this model is relatively quick, simple to validate and provides insight into the structural behaviour. In addition, this simplified model can be used for the different construction types as described in section 1.4.

For a detailed description and interpretation of the current standards, guidelines and regulations, reference is made to Appendix B1. The full background of the complete analytical model, as described in this chapter, can be found in Appendix B2.

3.2   Analytical Model

For the modelling of the superstructure of concrete bridges, a distinction is made between the types of plates, beams, boxes and tubes. Underpasses and culverts are box structures, while its deck can be seen as a plate. Due to the ratio of dimensions of subparts in combination with the fact that the walls are horizontally elastically supported by soil it is that in general the deck of the underpass box-shaped structure is the most critical part. This is supported by the dimensions, design calculations and assessments found in the data analysis as described in chapter 2. Therefore, only the deck is modelled as a simply supported beam which represents a strip of the deck of 1m. The connection with the walls is accounted for by adding rotational springs at the supports, which stiffness depends on the stiffness of the walls.

The vertical load on the deck is divided into dead loads and live loads. For this model, the vertical dead load consists of self-weight of the deck, load from soil cover and the asphalt layer on top of the deck. LM1 from EC has been applied for the variable traffic load. LM1 consists of a UDL and a TS. The concentrated load of TS is spread through the asphalt and any existing soil cover. A TS consists of two axles, each with two wheels. In the direction of travel, the distance between the wheels is only 0,80m, the centre-to-centre distance is 1,20m. Based on the data analysis of chapter 2 together with the minimum asphalt thickness according to ROK of 120 mm, the load planes of the wheels almost always overlap, creating a combined load plane. In case the load planes of the wheels do not overlap, the gap is so small that a combined load plane is still assumed accepting a negligible error. A schematization of the model with an overview of the applied loads is shown in Figure 22.
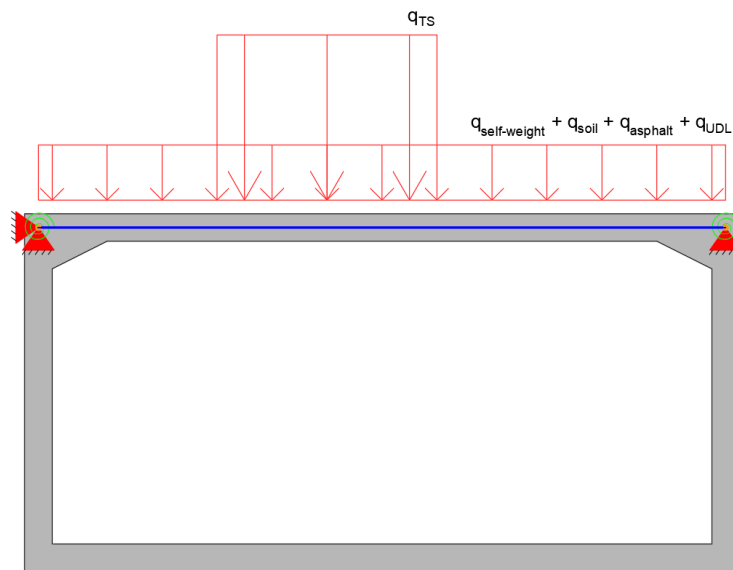
Figure 22 Schematization of the analytical model with the applied loads

3.2.1 Ordinary Differential Equation based parametric equations

A simply supported beam can be described with the Euler-Bernoulli beam theory. This theory only includes bending of the beam, so shear deformation is not accounted for, but since the deck of underpasses is relatively slender the error will be negligible. The classical displacement method is used to find the ODEs for the basic load cases, the model of this method is shown in Figure 23.
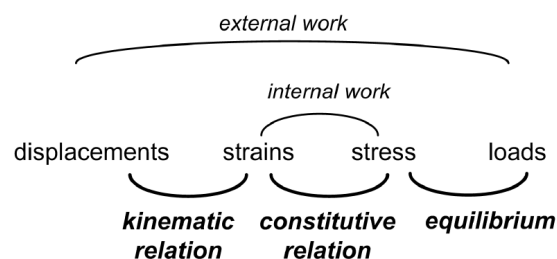
Figure 23 Classical displacement method (from: (Welleman, 2017))

In order to find the ODEs first, the kinematic relations are formulated from which the constitutive relations are drawn up and finally the equilibrium conditions are formulated. These relations and conditions result in the ODEs.

It is generally known that for the Euler-Bernoulli theory the following applies:

- Kinematic relation: $\varphi = -\frac{dw}{dx}; \kappa = \frac{d\varphi}{dx};$ (3.1)
- Constitutive relation: $M = EI \cdot \kappa;$ (3.2)
- Equilibrium: $\frac{dV}{dx} = -q; \frac{dM}{dx} = V;$ (3.3)
- ODE: $EI \cdot \left(\frac{d^4w}{dx^4}\right) = q$ (3.4)

The general solution to this single ODE is:

$$w = \frac{q \cdot x^4}{24 \cdot EI} + \frac{C1 \cdot x^3}{6} + \frac{C2 \cdot x^2}{2} + C3 \cdot x + C4$$ (3.5)

The presence of TS creates a discontinuity in the load, whereby the beam has to be split at the edge of TS. This means that a system of three 4th order ODEs must be drawn up for which twelve boundary or matching conditions must be formulated in order to find the integration constants and solve the problem. Boundary and matching conditions are equations which say something about the displacement, rotation, moment or shear force at a certain point. To speed up the process, MAPLE software is used for the mathematical calculations to determine all solutions.

The advantage of approaching the problem with ODEs is that equations are obtained with which the moment and the shear force can be calculated for each cross-section. In addition, the critical location of TS on the deck can be determined for bending moment or shear force in a particular section. The formulas for shear force, bending moment and the critical location of TS for a particular cross-section are then exported to Excel resulting in a parametric calculation model. The basic model with the parameters is shown in Figure 24.
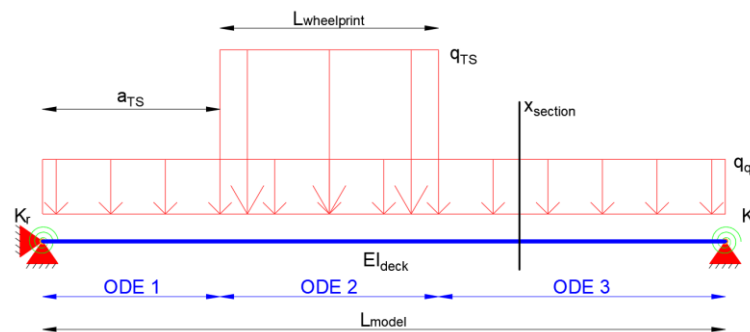
Figure 24 Overview parameters of ODE-based analytical model

Guyon-Massonnet

With a strip model, a representative load for the traffic load from LM1 must be drawn up, as the strip is only 1m wide, which means that load distribution must be taken into account. Load distribution of LM1 at a distribution angle, for concrete 45 degrees, would result in too conservative values, therefore the method of Guyon-Massonnet is used. In this method, a 4th order differential equation (3.6) describes the orthotropic slab behaviour with as input the geometry, elastic modulus of the concrete, flexural stiffness θ (3.7) and torsional stiffness α (3.8) of the slab. The method assumes that the slab is deformed as a half-sine wave. Within RHDHV, this method is available in a verified Excel sheet prepared by R.P.H. Vergoossen, to which only minor changes have been made. The main change for the realization of this module is the automation of finding the critical output point in transverse direction for the representative UDL and TS loads. For the background of the Guyon-Massonnet method and the way in which the normative representative loads are determined, reference is made to Appendix B2.

$$\rho_{xx} \frac{\partial^4 w}{\partial x^4} + \left(2\alpha\sqrt{\rho_{xx}\rho_{yy}}\right)\frac{\partial^4 w}{\partial x^2 \partial y^2} + \rho_{yy}\frac{\partial^4 w}{\partial y^4} = \rho(x,y) \tag{3.6}$$

$$\text{Flexural stiffness } \theta = \frac{b}{l}\sqrt[4]{\rho_{xx}/\rho_{yy}} \tag{3.7}$$

$$\text{Torsional stiffness } \alpha = \frac{\gamma_{xy}+\gamma_{yx}+\nu\rho_{xx}+\nu\rho_{yy}}{2\sqrt{\rho_{xx}\rho_{yy}}} \tag{3.8}$$

The Guyon-Massonnet method is limited to the transverse load distribution of bending moment, making this method not applicable for the determination of shear force due to TS. For this, a graphical method is developed within this research which is based on the model according to fib model code 2010 7.3-7, which is covered in section 3.4.

3.2.2 Control sections

The occurring section forces moment (M) and shear force (V) are determined in sections of the structure. Which sections have to be checked, and at which section force, depends on the shape of the moment and shear force line. A section is made at the locations of a global or local maximum of a section force. In addition, sections are checked where the capacity of the cross-section abruptly decreases in combination with a relatively large section force present. The general shape of the shear force and the moment line is shown in Figure 25, which also lists the section forces to be checked.
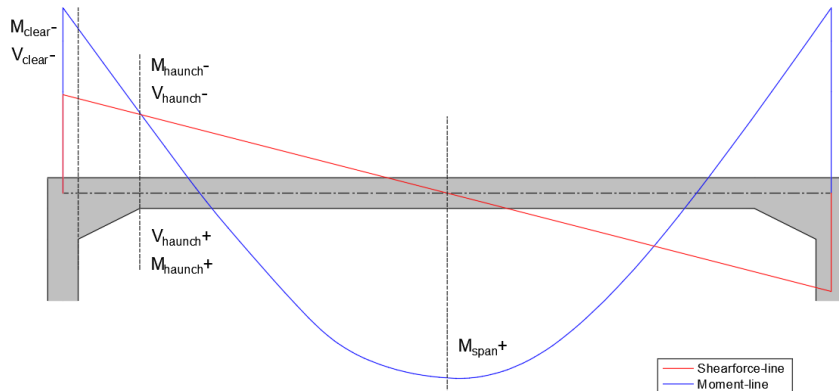
Figure 25 General shear force- and moment-line with sections and section forces to be checked

The most obvious sections that are checked are the maximum sagging moment in the span M^+_{span} and the shear force and the hogging moment in the section in the clear of the wall, V^-_{clear} and M^-_{clear} respectively, because the global maxima of the section forces occur there. However, the maximum sagging moment does not necessarily have to occur exactly in the middle of the span because it depends on the location of TS, hence the name span instead of midspan. If a haunch is present, which often appears to be the case from the data analysis in chapter 2, the deck thickness near the wall varies from the thickness at the connection of the haunch $h_{deck,haunch}$ to the thickness at the clear with the wall $h_{deck,clear}$ over a length of the haunch L_{haunch}. At the end of the haunch, the cross-section is significantly smaller than in the clear of the wall, which is expected to have a significant influence on both the bending moment resistance M_{Rd} and the shear resistance V_{Rd}, while the section forces are still relatively high. That is why the shear force and moment are also checked for this section. A distinction is made between a positive bending moment M^+ and a negative bending moment M^- because the lower and upper reinforcement respectively then function as tensile reinforcement $A_{s,l}$ and must be used to determine the capacity of the section concerned. This is because it can occur in the presence of long haunches that a positive moment occurs in the section of the haunch depending on the location of TS. In other words, for a correct determination of V_{Rdc} the question is whether

the upper or lower reinforcement is active and it is therefore important to know the moment line and the location of the moment zero point. The ODE-based method is extremely suitable for this, since a fully parametric equation for the moment line is known.

3.2.3   Determination of section forces

Before section forces are calculated, the loads are first multiplied by the correct load factors. The load factors are automatically calculated based on assessment level, consequence class, reference period, remaining service life and the number of heavy trucks per year per lane N_{obs}. This takes into account the reduction factors α_Q and α_q and the correction factors Ψ and α_{trend} from NEN8701 for traffic loads of LM1 for a reference period shorter than 100 years and a trend reduction compared to the year 2060 respectively. All the section forces are calculated using both combination 6.10a and 6.10b from NEN-EN 1990, the maximum values between the two are automatically taken per load case. Appendix B2 explains the determination of load and combination factors in detail.

Bending
The location of TS is important for determining the maximum section forces in a certain section. This is quite simple for the maximum sagging moment in the span, namely in the middle of the span where at the same time the global maximum of the sagging moment is located. For the other two sections, determining the maximum section forces is somewhat more complicated.

For the calculation of the longitudinal reinforcement the moment-line should be shifted by a distance $a_l = d$ in the unfavourable direction, based on the so-called shift rule from NEN-EN 1992-1-1 section 9.2.1.3. The reason for this is that due to the occurrence of shear cracks, the tensile reinforcement only becomes active over a distance d, when the usual 45° for this crack for non-prestressed concrete is maintained. In this method the shifting of the moment line takes place by requesting the moment of the relevant ODE at a distance d of the specific section in the unfavourable direction, the principle is shown in Figure 26. The maximum sagging moment in the span is therefore relatively simple because it concerns a global maximum and does not need to be shifted.
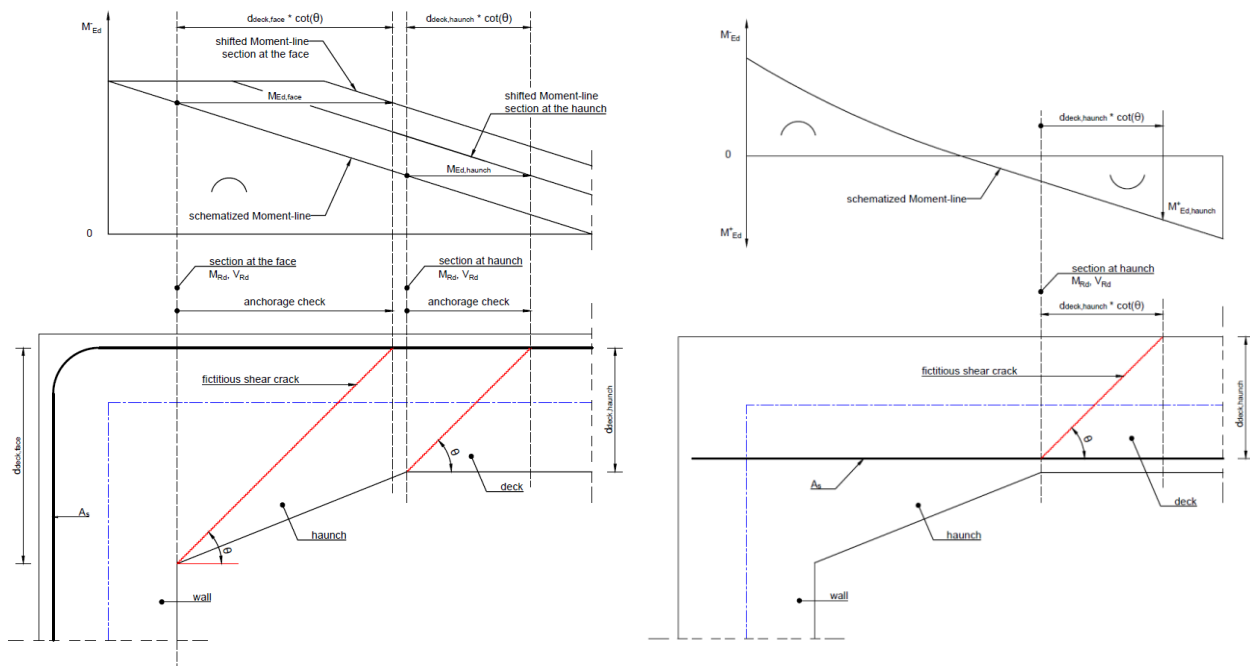
Figure 26 Shifting the Moment-line for a negative moment (left) and a positive bending moment at the haunch (right)

The hogging moment for the section in the clear $M_{Ed,clear}^-$ is read at the support since shifting over a distance $a_l = d_{deck,clear}$ in the negative direction would lead to a point out of model for most cases, therefore the global maximum at the support is taken, as shown in Figure 26. Based on the available data, the probability that $d_{deck,clear}$ is less than half the wall thickness, meaning a smaller shift of the moment-line resulting in a lower hogging moment, is so small that this assumption is accepted.

The location of the TS for the maximum hogging and sagging moment in the sections in the clear and at the end of the haunch is determined by solving the ODE and analytically maximizing the moment in the relevant section plus a distance of the relevant d in the unfavourable direction. The critical location of TS for a maximum sagging or hogging moment in a certain section is determined by differentiating M, from the relevant ODE, with respect to a, the distance from the model support to the edge of the load plane of TS, and solving the found equation equal to zero. The equation for the slope of the moment line is defined as $\frac{\partial M}{\partial a}$, where M is a fully parametric equation. The critical distance a for the specific bending moment at the relevant section is found by solving $\frac{\partial M}{\partial a} = 0$, in which x is defined as the distance from the support to the relevant section. This is further elaborated in Appendix B2.

For all sections, both the sagging moment and the hogging moment are determined, this is necessary to be able to redistribute the bending moment later if necessary. If reinforcement with ductility class B has been used, redistribution according to RBK 5.5 (105) is allowed up to 20% and takes place within a load case. In addition, the shear force per load case is calculated for verification and a load case with TS on $2d + 0,5\,h_{wall} - 0,5\,h_{deck}$ where the shear force at a distance d from the clear is calculated to later compare with the results of the method, for determining the shear force as a result of TS in an RC slab, described in section 3.4.

Shear
The shear force due to the distributed loads, being the self-weight, the weight of soil and asphalt and the UDL from LM1, is determined with the formulas for shear effect obtained from ODEs based on the Euler-Bernoulli beam theory. The characteristic value for the q-load as a result of the UDL load is calculated with the Guyon-Massonnet method. The shear force as a result of TS is determined with a separately developed method which is described in section 3.4.

The shear force is checked in the section in the clear of the wall and at the end of the haunch. Because calculations are made with a so-called oblique section, the various load cases are read at other sections due to the difference in the point of application of the load for determining the shear force in the observed section. The uniform load as a result of own weight acts on the neutral line of the deck while the load as a result of soil cover, asphalt and UDL acts on the top of the deck, shown in Figure 27. The reason for the displacement of the load with respect to the considered section has to do with the load transfer, which takes place via the compressive strut at an angle θ.

In the section in the clear, the extra height by the possible presence of a haunch is ignored. The question is whether the compressive strut from the connection of the haunch to the wall runs at 45° through the haunch and through the deck, especially in the case that the length-height ratio of the haunch is 1:1 and therefore also makes an angle of 45°. The choice to use only the height of the deck at the connection of the haunch results in slightly higher values of the shear force because the locations of V_{Ed} to be considered are less far from the section in the clear and is therefore slightly conservative but safe.
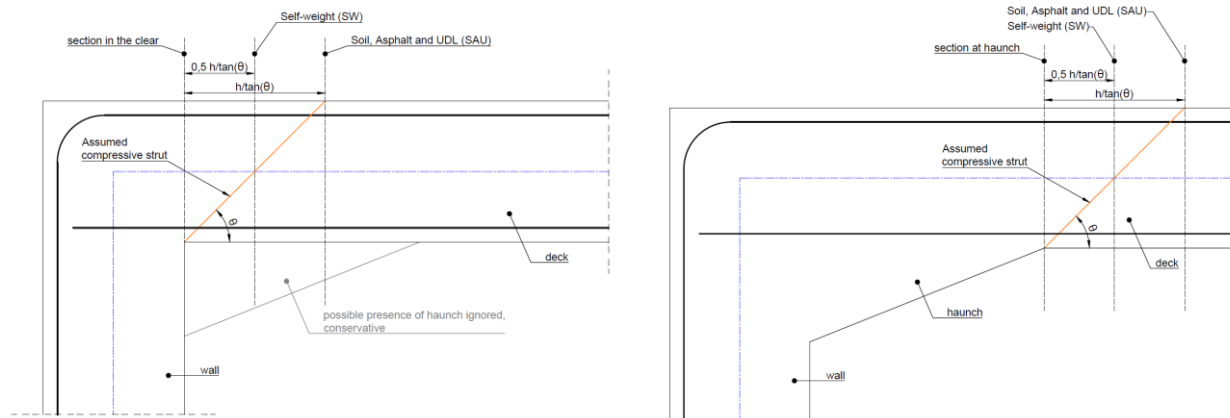
Figure 27 Point of application of load for determination of V_{Ed} in section in the clear (left) and section at the haunch (right)

For standard non-prestressed concrete structures, an angle $\theta = 45°$ is used for the compressive strut. However, the horizontal soil pressure against the walls creates a normal force in the deck, which can be seen as a kind of prestressing σ_{cp}. In NEN 8702 6.2 (3) it is stated that $\theta = 45°$ for elements with $\sigma_{cp} = 0\ MPa$ and $\theta = 30°$ may be used for elements with $\sigma_{cp} \geq 5\ MPa$, for which it applies that intermediate values of σ_{cp} are interpolated linearly may be used to determine θ. A smaller angle θ, making the compressive strut less steep, has the advantage that the resultant in vertical direction, the shear force, becomes smaller, which in this case is expressed by the location to determine the occurring shear force being further away from the section under consideration, so that a lower value is taken into account. The effect of this proposed guideline from the draft version of NEN 8702 on the shear force to be considered has been investigated. Calculations show that even in the most favourable scenarios for constructions with a large soil cover, of approximately 5m, a large construction height, of approximately 7m, and with a minimum deck thickness of 300 mm the influence is still negligible at less than 1% reduction of V_{Ed}. For an angle $\theta = 30°$ an advantage of about 6% would be achieved over $\theta = 45°$. However, the horizontal soil pressure on the wall does not provide enough normal stress σ_{cp} in the deck to achieve this.

3.2.4 Representative cross-sections

For the further sensitivity analysis of various parameters, 3 types of constructions have been set up based on the data analysis in chapter 2. The three types are based on three categories of spans with corresponding dimensions. The first category mainly represents culverts and bicycle underpasses, categories II and III respectively represent small to large underpasses for mixed traffic. An overview of the main dimensions used is shown in *Table 8*. Within these categories, an established parameter can be varied for research.

Table 8 Main parameters of representative theoretical cross-sections

		Cat I	Cat II	Cat III
L	[m]	3,5	7,0	13,0
$h_{deck,span}$	[mm]	300	450	750
$h_{internal}$	[m]	2,0	4,5	5,0
$deck\!:\!wall\!:\!floor\ thickness\ ratio$		1:1:1	1:1:1	1:1:1

3.3 Fictional stiffness

The bending moment distribution in the deck structure between the two supportive walls depends on the stiffness ratio between both elements. When an element becomes stiffer relative to the other element, it will draw more bending moment to it. The stiffness of the material is incorporated in the determination of the rotational stiffness. By changing the rotational stiffness of the supports, the model can change between a simply supported beam and a clamped beam. The associated sagging and hogging bending moments change drastically. The stiffness ratio between the wall and the deck of the box cross-section has an influence on the rotational stiffness and thus an influence on the moment development. Because a large axial force acts on the wall, it is expected to react significantly stiffer than the deck, so that the ratio $E_{wall}/E_{deck} > 1$ is expected.

EC 2 provides a method to determine the stiffness based on the nominal stiffness, which takes into account the effects of cracking, non-linear material properties and creep on the overall behaviour. However, according to the Dutch national annex, it is not allowed to use the nominal stiffness method because it often leads to incorrect, underestimated stiffnesses. Alternatively, the stiffness for rectangular cross-sections may be determined with the fictitious elastic modulus E_f. The fictitious E-modulus E_f is based on the slope of the M-N-κ diagram between the origin and the point $M = 0,8\, M_{Rd}$, which means that a load of 80% of failure load is assumed, $M_{Ed} = 0,8\, M_{Rd}$, with occurring normal force N_{Ed}. A so-called E-heavy cross-section, with reinforcement, and the bi-linear stress (σ) - strain (ε) diagram is assumed. At $0,8\, M_{Rd}$ the reinforcement is still in the linear elastic branch, while the concrete compression zone is usually no longer. If the load is substantially lower or higher, the calculated stiffness E_f is therefore not correct. Calculations for the structures in the dataset however show that the load does not deviate substantially from 80% failure load with an average UC of $UC_{avg} = 0,85$. The flexural stiffness EI of the deck and the wall is determined by the moment of inertia I of the E-heavy cross-section. The construction height h, the amount of reinforcement ρ in the deck and the wall and the occurring moment M_{Ed} and normal force N_{Ed} are the influencing parameters. At low section forces the concrete is still uncracked and the flexural stiffness EI is relatively high, at the moment of crack formation the flexural stiffness of the concrete decreases. In the fictional modulus of elasticity it is assumed that the moment of inertia I is constant, $\frac{1}{12}\, b\, h^3$ for rectangular cross-sections, which means that the E_f changes to realize the decrease in flexural stiffness EI for cracked cross-sections.

3.3.1 Influence of stiffness ratio on moment distribution

To demonstrate the importance of the stiffness ratio between the wall and the deck, research was conducted into the influence of the stiffness ratio on the distribution between sagging and hogging bending moment of the deck structure. For this the analytical calculation model with distribution of traffic load according to the Guyon-Massonnet method is used. For the calculation of E_f it is assumed that the stiffness is constant over the whole height of the wall and the full length of the deck. In reality, the stiffness increases towards the connection between the deck and the wall by the presence of a haunch or a local increase in reinforcement ratio in the connection between the two slabs. This effect is neglected because the moment distribution is determined by the rotational stiffness which is calculated with the bending stiffness of the wall for which the predominant section, the mid-section, is decisive.

Moment ratios $M_{Ed;clear}/M_{Ed;span}$ between 0,45 and 1,35 were found for the examined structures of Category I to III. Within these cases, increases in this ratio have been found between 17% and 61% in case the stiffness ratio changed from 1,0 to 2,0. However, these values are extremes found in limit cases, which are unrealistic. When one is limited to the results of the more realistic geometries, the ratio $M_{Ed;clear}/M_{Ed;span}$ ranges from 0,7 to 1,35 and within a case this ratio increases between 23% and 44% in case the stiffness

ratio $E_{f;wall} / E_{f;deck}$ changed form 1,0 to 2,0, shown in Figure 28. Values of the same order of magnitude were found when going from a ratio of 1,0 to 0,5.
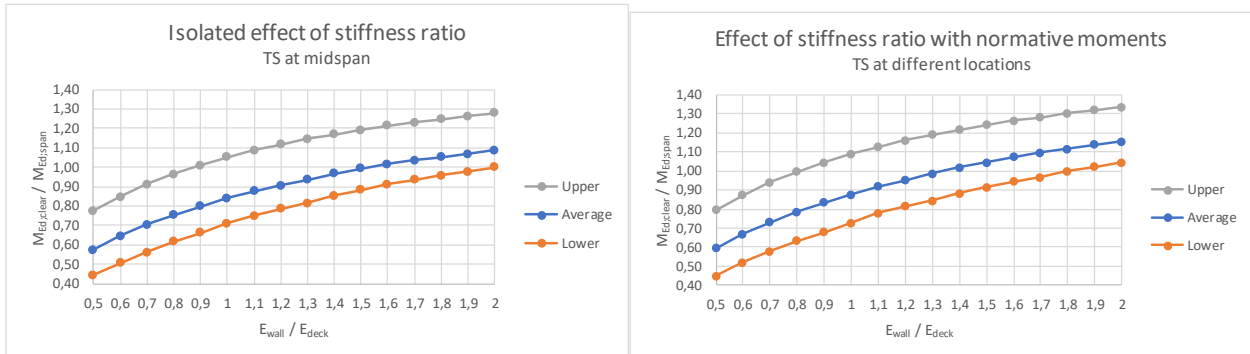
Figure 28 Effect of stiffness ratio on bending moment ratio between hogging and sagging bending moment.

Table 9 shows the percentage change in the ratio between the hogging moment and the sagging moment, from which the relevance becomes more clear.

Table 9 Relative influence of stiffness ratio E_{wall}/E_{deck} to moment distribution $M_{Ed,clear}/M_{Ed,span}$

	$\dfrac{E_{wall}}{E_{deck}}$	$\dfrac{M_{Ed,clear}}{M_{Ed,span}}$	$\dfrac{E_{wall}}{E_{deck}}$	$\dfrac{M_{Ed,clear}}{M_{Ed,span}}$	$\dfrac{E_{wall}}{E_{deck}}$	$\dfrac{M_{Ed,clear}}{M_{Ed,span}}$	$\dfrac{E_{wall}}{E_{deck}}$	$\dfrac{M_{Ed,clear}}{M_{Ed,span}}$	$\dfrac{E_{wall}}{E_{deck}}$	$\dfrac{M_{Ed,clear}}{M_{Ed,span}}$	$\dfrac{E_{wall}}{E_{deck}}$	$\dfrac{M_{Ed,clear}}{M_{Ed,span}}$
Cat I		-38%		-7%		0,73		+7%		+26%		+44%
Cat II	0,5	-32%	0,9	-5%	1,0	0,88	1,1	+5%	1,5	+19%	2,0	+32%
Cat III		-27%		-4%		1,09		+3%		+14%		+23%

Larger spans seem to have a proportionately greater share of hogging moment than sagging moment. With shorter spans, however, the ratio between the moments increases considerably faster than with longer spans. Larger spans are less sensitive to changes in the stiffness ratio between the deck and the wall in relation to the moment distribution. Changing the stiffness ratio between the deck and the wall changes the critical location of TS for the maximum hogging bending moment. By increasing the ratio $E_{f;wall} / E_{f;deck}$ from 1,0 to 2,0 the critical location of TS moves towards the support. A change between 4% and 9% has been observed for the location in the main cases, where the largest relative change of the critical location of TS has been observed in Case I. As the moment distribution for the main cases changes significantly, when changing the ratio $E_{f,wall}/E_{f,deck}$ between 0,5 and 2,0, the sensitivity of the stiffness ratio is further investigated.

3.3.2 Stiffness ratio sensitivity

Since it appears that the change in stiffness ratio between the walls and the underpass deck has a significant influence on the moment distribution between hogging and sagging bending moment, the sensitivity of this stiffness ratio is investigated. The calculation, approximation, of the material stiffness is based on NEN-EN 1992-1-1 NA Table NB-1 *Fictieve elasticiteitsmodulus E_f*. The background to this calculation is shown in Appendix B2.

The stiffness ratio is determined by the difference in two main parameters, namely the utilisation ratio of axial loading α_n and the reinforcement ratio ρ, which are defined as follows:

$$\alpha_n = N_{Ed}/N_{Rd} \tag{3.9}$$
$$\rho = (A_{s,t} + A_{s,c})/A_c \tag{3.10}$$

A difference in stiffness could be caused by a difference in concrete quality, however it is very unlikely that the deck and the wall are not made with the same concrete quality and is therefore not included. If the same concrete quality for the wall and deck is assumed, a difference in utilization ratio α_n will mainly be caused by a difference in thickness of the wall compared to the thickness of the deck. The reinforcement ratio does have an influence, but it is very limited compared to the concrete cross section when it comes to a change in α_n. The reinforcement ratio has however a direct influence on the determination of E_f and thus on the stiffness ratio between the wall and the deck. A higher reinforcement ratio immediately results in a higher stiffness, which means that the stiffness ratio can change quickly if the reinforcement configuration of the deck and wall differs. The normal force on the wall is caused by a combination of the deck's self-weight, permanent load from soil and asphalt and traffic load. Even though traffic load is a variable load, it is nevertheless included in the calculation of the stiffness of the wall, because the critical situation for the underpass is considered, which includes traffic load on the deck.

A normal force in the deck is caused by horizontal soil pressure which acts on the structure. This is considerably less than the vertical load on the wall and in most cases this will always be the situation. The main reason for this is that the traffic load is primarily transferred on the wall, which means that the traffic load does not cause additional soil pressure. Only in cases with a large soil cover and a limited deck width can traffic load be transferred via surrounding soil. In addition, the horizontal soil pressure is calculated as neutral soil pressure with $k_{0;soil} = 1 - \sin(\varphi_{soil}) = 0,5$, so that the horizontal soil pressure will always be lower than the vertical soil pressure.

Calculations have shown that it is very unlikely for the utilization ratio of the wall $\alpha_{n,wall}$ to exceed 0,1. An upper limit for the stiffness ratio E_{wall}/E_{deck}, shown in Figure 29, is found if it is assumed that the reinforcement ratio of the wall and the deck are the same and the deck has no normal force acting on it $\alpha_{n,deck} = 0$. It is an upper limit because a normal force, which is neglected, acts on the deck from horizontal soil load which will decrease the stiffness ratio E_{wall}/E_{deck}. In addition, given the moment distribution of the wall compared with the deck, the reinforcement ratio in the wall will be lower rather than higher than the deck. The section of the wall at the connection with the deck may have a higher reinforcement ratio if the reinforcement of the deck is bent in the wall and the wall is less thick. However, this reinforcement will not continue through the entire wall, but only the anchorage length.
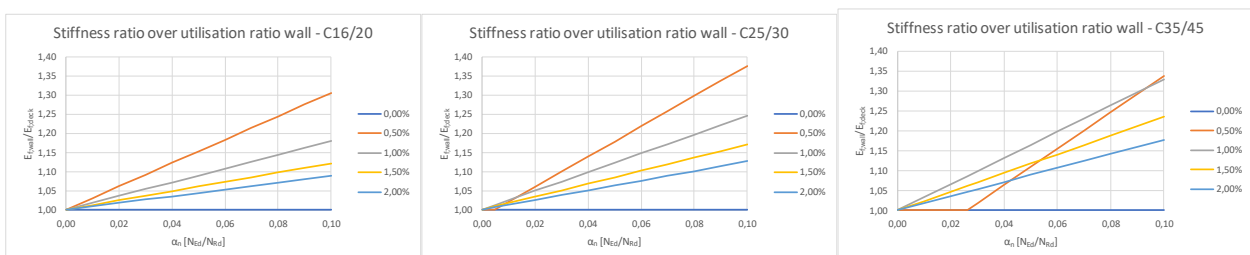
Figure 29 Potential stiffness ratio for different reinforcement ratios and concrete classes, for equal wall and deck

Based on the results from the theoretical analysis of the formulas applied on the deck and wall there is a potential ratio between the stiffness of the wall and the deck up to $E_{f,wall}/E_{f,deck} \approx 1,35$, which would mean a change in the moment ratio $M_{Ed,clear}/M_{Ed,span}$ of approximately +15%. Figure 29 also shows that the influence of the concrete strength class on the stiffness ratio is limited, while the reinforcement ratio has a significant influence.

Because the stiffness ratio potentially has a significant influence on the distribution of the bending moment between the span and the support, further research has been carried out based on the theoretical structures Cat I to III, which are further divided into two variants. A variant VTS with an upper limit of the slenderness

whereby a maximum shear force is obtained with little soil cover, and a variant VSW with a lower limit value for the slenderness so that maximum shear force is obtained with a large soil cover in connection with the high self-weight. The calculations were performed with the analytical model including the method from paragraph 3.4 for the determination of V_{TS}. Figure 29 shows that, based on the formulas, the biggest stiffness difference is achieved with a reinforcement ratio ρ_l between 0,50% and 1,00%. It should be noted that it concerns the combined reinforcement ratio of both the compression reinforcement and the tension reinforcement. In Figure 21 (left) from the data analysis described in paragraph 2.4, it appears that for the tension reinforcement in most cases a ratio $\rho_{l,t}$ of 0,35% to 0,80% is already present. In line with the sensitivity and the data analysis, a reinforcement ratio of 0,50% and 1,00%, for both the deck and the wall, in combination with different concrete strength classes has been investigated. In addition, it was investigated what the influence is of a reduced reinforcement ratio in the wall compared to the deck. The fictitious E-modulus of the wall and the deck are calculated with a separate developed module, *"Fictieve elasticiteitsmodulus"*, which also takes into account a normal force in the deck as a result of horizontal soil pressure.
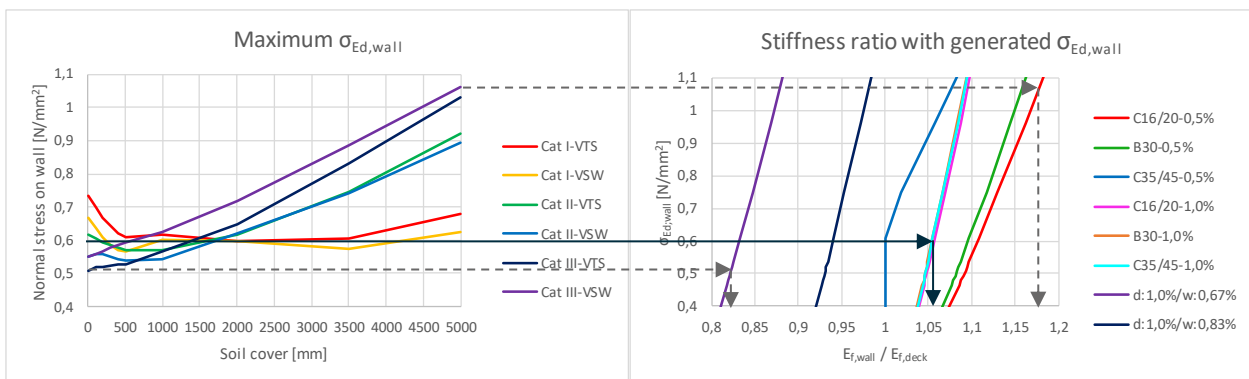
Figure 30 Lower and upper bound for $\sigma_{Ed,wall}$ (left) and the required normal stress $\sigma_{Ed,wall}$ for stiffness ratio $E_{f,wall}/E_{f,deck}$ (right). Graphs of 1,0% reinforcement ratio overlap.

At low reinforcement ratios, the concrete strength class still has a clear influence on the stiffness ratio, this is because for higher concrete strength classes the lower limit for E_f is not exceeded for both the wall and the deck, so that the ratio remains 1,0 with an increasing normal stress in the wall. At a higher reinforcement ratio, for example 1,0% in Figure 30, the concrete strength class no longer has a significant influence. For reinforcement ratios between 0,5% and 1,0% the stiffness ratio varies between 1,0 and 1,18, assuming equal reinforcement ratios for the wall and the deck, and is therefore limited. However, the ratio in reinforcement ratios of the wall in relation to the deck has a significant influence, with the ratio going just the other way, less than 1,0. In case the wall has substantially less reinforcement than the deck, the stiffness ratio becomes negative, which means that the sagging bending moment in the span actually increases. The lower limit from Figure 30, where the wall has 33% less reinforcement than the deck, results in a 9% shift from the hogging moment to the sagging moment. The soil next to the wall, which in principle is a bedding, is not included in the determination of the stiffness of the wall but has an increasing significance on the actual stiffness by a decreasing bending stiffness of the wall. The upper limit of the stiffness ratio, based on a large span Cat III structure with a very large soil cover in combination with a low concrete strength and a low reinforcement ratio, is approximately 1,18, resulting in an 11% shift from the sagging moment to the hogging moment.

3.3.3 Maintained stiffness

The situations where $\rho_{deck} = \rho_{wall}$ would suggest that a stiffness ratio of 1,0 to 1,1 should be maintained, which results in a shift of the moment line from 0% to 7% to the hogging moment. In case the wall has less reinforcement than the deck, which occurs regularly, based on the fictitious elastic modulus method, the stiffness ratio would quickly drop below 1,0, resulting in an increase up to 9% of the sagging moment in the span. However, the method is based on the M, N, κ-diagram and does not take into account the presence of soil next to the wall for determining the stiffness of the wall. The soil next to the walls increases the stiffness of the wall if the wall has a relatively low bending stiffness, after all if the wall were infinitely stiff, it does not matter whether or not soil presses against the wall, a reaction will only occur from the soil if the wall deforms. Applying the fictitious elastic modulus method does mean that additional information, more input parameters, with regard to the compression and tensile reinforcement in the wall and the compression reinforcement in the deck are required. This data is not always available, takes extra time to collect if it is available and increases the risk of errors. Since the positive influence is limited, the negative influence is limited by the presence of soil and applying the fictitious elasticity method requires extra data, a stiffness ratio $E_{wall}/E_{deck} = 1,0$ is used as standard. The influence of the soil next to the walls and under the floor is further investigated with a framework model, to be read in paragraph 5.1.

If the moment in the span is not satisfactory and additional data are known, the module can still be used to determine E_f. Especially structures with a low concrete strength class, for example from local authorities which means that C16/20 may be used, in combination with an equally low reinforcement ratio for the wall and the deck $\rho_{wall} = \rho_{deck}$ of around 0,50%, have a chance of a favourable effect of the stiffness ratio $E_{f,wall}/E_{f,deck}$.

3.4 Shear force in a RC slab due to TS load

With Guyon-Massonnet, the transverse distribution of TS, which are local loads, cannot be properly approximated. In (CEB-fib, 2010) figure 7.3-7 a method is prescribed which is used as a basis for the method developed in this research for the determination of the occurring shear force near the support in the RC deck as a result of TS.

3.4.1 Basic graphical model

The shear force as a result of TS from LM1 is calculated based on the method described in CEB-fib model code 2010 7.3-7, whereby the distribution of the shear force per TS is worked out graphically. Different embodiments of this method can be found in different publications, among which the method is described in (Lantsoght, 2012) and (CEB-fib, 2010). In the first mentioned publication, the load is placed at a distance $2,5d$ from the support and spread to the centre of the support, while in the latter publication the load is placed at a distance $2d$, which matches with the reduction factor β for loads within $2d$ of the support, and the load is distributed to a control section some distance away from the support. Calculations, comparing the different calculated shear force values due to TS, have shown that the method described in (CEB-fib, 2010) results in somewhat more conservative values. To ensure that the calculation is not too optimistic, the method as in (CEB-fib, 2010) is used for further development in this study. The horizontal distribution, in plane of the slab, of the TS load takes place from the rear of the load plane, also called wheel print. The basic method used is shown in Figure 31.
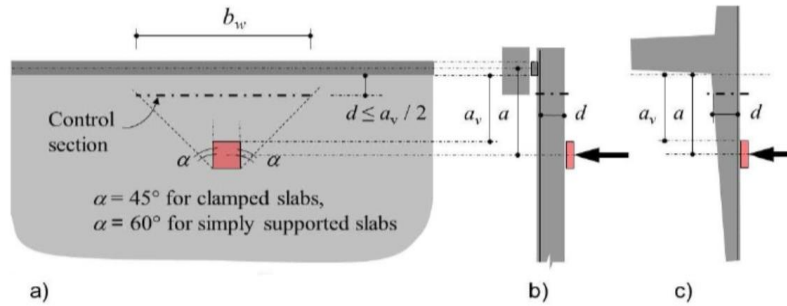
Figure 7.3-7: Location and length of the control section, bw, for the determination of the shear resistance of slabs with point loads located near a support-line; (b) simple edge support; (c) clamped edge support

Figure 31 Method used from CEB-fib Model Code 2010 Figure 7.3-7

It is not inconceivable that effective width b_w will overlap, since an axle of TS has two wheels. Overlapping of the effective widths b_w of two wheel prints of a single axle is considered as in (CEB-fib, 2010), which describes that in case b_w of two wheel prints from a single axle overlap each other at the control section the load and effective width may be merged and distributed evenly over the combined width b_w. This is graphically displayed in Figure 32.
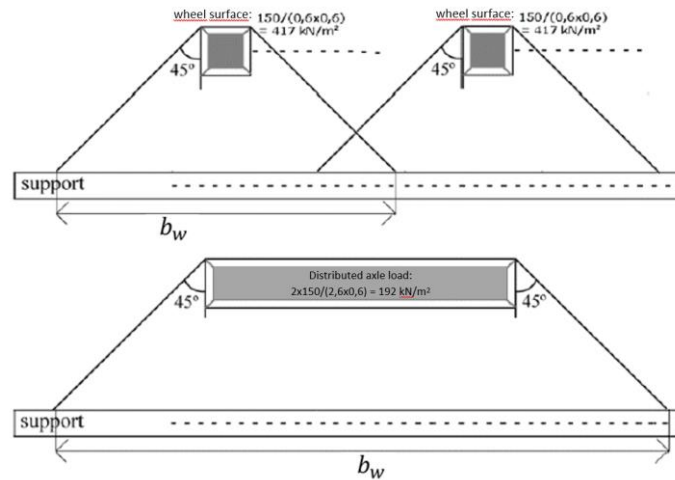
Figure 32 Overlap of b_w from wheels on one axle (source: CEB-fib model code 2010)

3.4.2 Extension to bridge deck

The basic graphical model as described in paragraph 3.4.1 has been further developed to be applied to the deck of a culvert or underpass structures. In contrast to bending, the load is distributed to the top of the concrete deck to determine the occurring shear force. This means that the wheel loads are first spread vertically due to the presence of asphalt and a possibly present soil or filling layer. Depending on the thickness of these layers and whether or not the effective width b_w overlaps, various load planes are possible, resulting in different load situations. A distinction is made in four different cases based on the vertical distribution of the TS load. In total, four situations are conceivable based on formulas for overlap of wheel print in driving direction, overlap of wheel print in width and overlap of effective width. These cases are shown in Table 10.

Table 10 Different cases bases on load plane of TS

Case	Overlap in driving direction	Overlap in TS width	Overlap of effective width
Case I	✖	✖	✖
Case II	✖	✖	✔
Case III	✔	✖	✔
Case IV	✔	✔	✔

A calculation, provided in Appendix B2, with the most unfavourable values, partly based on the data analysis in chapter 2, shows that Case I practically does not occur due to vertical load distribution in combination with horizontal distribution in the slab. This is confirmed by the general statement in (Lantsoght, 2012) and is therefore not further elaborated in this research. For Cases II to IV, a distinction is made between two load situations per case. A situation called "Middle", shown in Figure 34, in which the TSs are placed in such a way that a maximum shear force is created in the plate, usually in lane 2. In the other situation, called "Edge", the TSs are placed such that a maximum shear force takes place at the edge. In total, six situations have been worked out. The basis for each case is the same, the separate cases are mainly made to make automation easier. The complete background can be found in Appendix B2.

According to the *fib* method presented in Figure 31, the control section should be at a distance $d \leq a_v/2$. Because a_v, the distance from the face of the load plane to the face of the support, is set at $2d$ for maximum shear force, the control section, represented in Figure 34 by the black dash-dot-dash line, is kept at a distance d from the clear of the wall.

Load distribution takes place from the rear of the wheel prints in accordance with (CEB-fib, 2010) and (Lantsoght, 2012) for Case II. For Case III and IV, distribution of the front axle takes place from the wheel print centre between axle 1 and axle 2, distribution of the rear axle takes place from the rear of the wheel print just like in Case II. This is made visual in Figure 33. If only distribution from the centre of the load plane would be used, a jump in the shear force to be taken into account would arise between Case II and III, which in reality does not take place. Besides, the distribution from the centre of the load surface is not in line with (CEB-fib, 2010) and (Lantsoght, 2012), what would lead to unnecessarily conservative values.
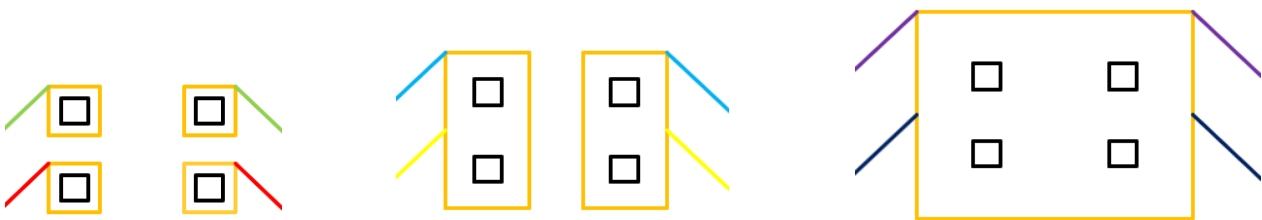
Figure 33 Load plane of Case II (left), Case III (middle) and Case IV (Right)

TS(s) are placed on the basis of the lane layout, the heaviest loaded lane with TS1, is placed at the minimum edge distance from the deck so that the heaviest TS load can distribute as little as possible. In addition, lanes 2 and 3 may be placed. All TS(s) are placed in the centre of the lane. Basically, TSs are always placed as close as possible, at a distance $2d$, to the control section in order to achieve minimum spread width b_w. However, TS2 and TS3 are placed in such a way that a certain overlap of the effective widths with the effective width of TS1 is created. For situation "Middle" this overlap strip has a minimum width of $4d$ and is usually located in the overlap between lane 1 and 2. The width of $4d$ of the overlap strip corresponds to RBK requirement 6.2.1 (10) that the calculation value of the shear force V_{Ed} must be determined by averaging over a width of $4d$ when calculating slabs using 2D slab modeling. For situation "Edge" however this overlap strip is with a width of $2d$ inwards from the edge of the deck.

An increase in the vertical load distribution or placing TS1 further from the control section by an increase in the effective height d of the deck provides a larger effective width b_w of TS1. As a result, TS2 and TS3 may need to be moved further away from the control section to create an overlap of $4d$. However, this shift of TS stops when the centre of TS is halfway through the span because then the maximum distribution of that TS has been reached, recognizable by the "envelope" that arises as shown by TS3 in Figure 34. The load distribution in plane of the slab takes place by bending, if TS were to be placed further it would be closer to the other support point, resulting in a smaller effective width b_w. This means that the overlap strip can be smaller than $4d$ due to a limited span length. This is typical for culverts and underpasses, but for normal bridges with relatively larger spans this does not occur.

The occurring shear force due to an axle of TS is described in (CEB-fib, 2010) as an average shear force per meter of line support, which is obtained by dividing the total axle load by the corresponding effective width b_w. Contrary to the method prescribed in *fib*, however, it can happen that a TS is placed halfway through the span. This means that the part of the load that is transferred to the other, not considered support, cannot be neglected. This is taken into account when determining the design value of the shear force by only taking into account the load part of an axle that also goes to the considered line support. For TS2 and TS3, it is also taken into account whether the overlap of $4d$, or $2d$ for edge loading, is realized. If this is not the case, the average load of the TS in question is multiplied by the percentage of overlap that is realized in relation to the desired overlap of $4d$ for load case "Middle" or $2d$ for load case "Edge".

	Tandem system 1		Tandem system 2		Tandem system 3	
Effective width 1st axle	**4,71**	m	**5,42**	m	**8,37**	m
Effective width 2nd axle	**5,91**	m	**7,82**	m	**8,37**	m
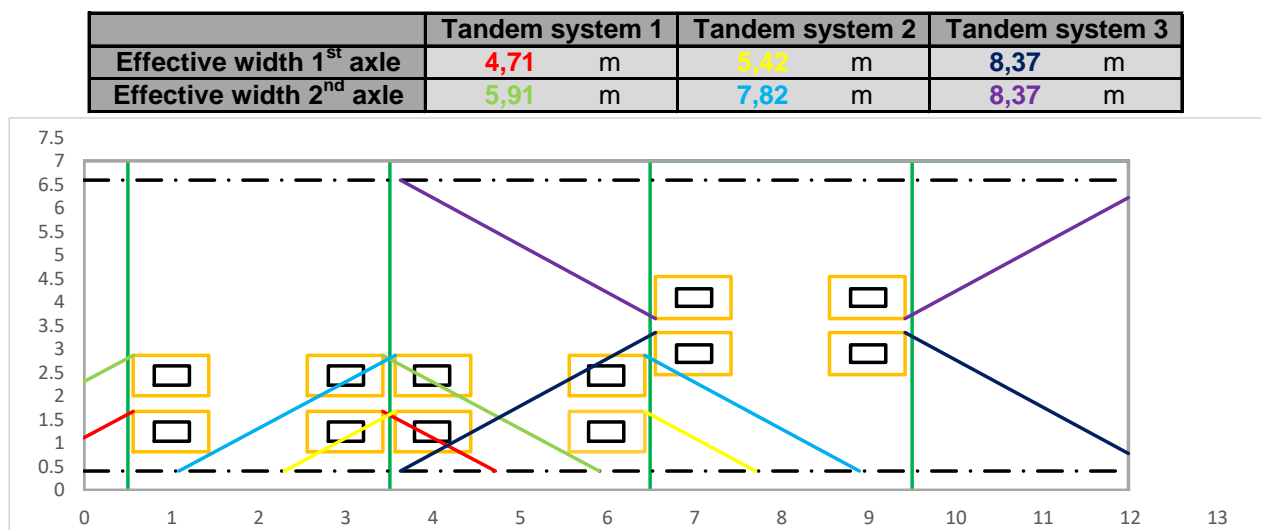
Figure 34 Example of visualization of effective widths per axle per TS of Case II load situation "Middle" (part of output from module). The part between the red and dark blue line is the critical strip with, in this particular case, a width of $4d = 1,62m$.

In (CEB-fib, 2010) a distinction is made between a hinged and a clamped line support. For a hinged line support, a horizontal distribution angle of 60 degrees may be maintained, for a clamped line support this is only 45 degrees. A larger distribution angle results in larger effective widths and therefore a lower calculation value of the shear force. Both from the literature in chapter 2 and from calculations earlier in this chapter it is known that the deck is not completely clamped by the wall. The question then is whether it is possible to deviate from 45 degrees to an intermediate value. The difference between a horizontal distribution angle of 45 and 60 degrees has been calculated with the developed method and, for the most practical cases, turns out to be a reduction of the shear force to be taken into account of about 15% to 20%. But of course, it is not a hinged support either. If the angle is assumed halfway between the two at 52,5 degrees, the advantage is only 5% to 10%. However, the publication does not state that intermediate values may be interpolated. Above all, the method recommended in (CEB-fib, 2010) is based on extensive research. The clamped variant, shown in Figure 31 c), from that study is in reality also not completely clamped either, but the model

has been calibrated based on tests. That is why it has been decided to use 45 degrees for the horizontal distribution angle, just like in the example of (CEB-fib, 2010), which results in somewhat conservative and safer values. Later in this research a model refinement is done by making a 3D FEM model with plate elements as an extra step in the determination of the load effects for structures that do not comply with the analytical model.

A clamped line support, with a horizontal distribution angle of 45 degrees, in combination with the relatively short spans of culverts and underpasses ensures that the load case "Middle" is practically always governing. For the load case "Edge" the span is usually too short and the distribution angle too small to create an overlap, which can be seen in Figure 35, making this load case not governing. For normal bridges with a hinged support, and thus a horizontal distribution angle of 60 degrees, and a relatively long span, the load case "Edge" is often the governing load case. The fact that more load distribution occurs as the support moves more towards a hinged support, is also apparent from calculations made with various 2D FEM models with 2D plate elements.

	Tandem system 1		Tandem system 2		Tandem system 3	
Effective width 1st axle	**4,71**	m	**8,73**	m	**8,37**	m
Effective width 2nd axle	**5,91**	m	**8,73**	m	**8,37**	m
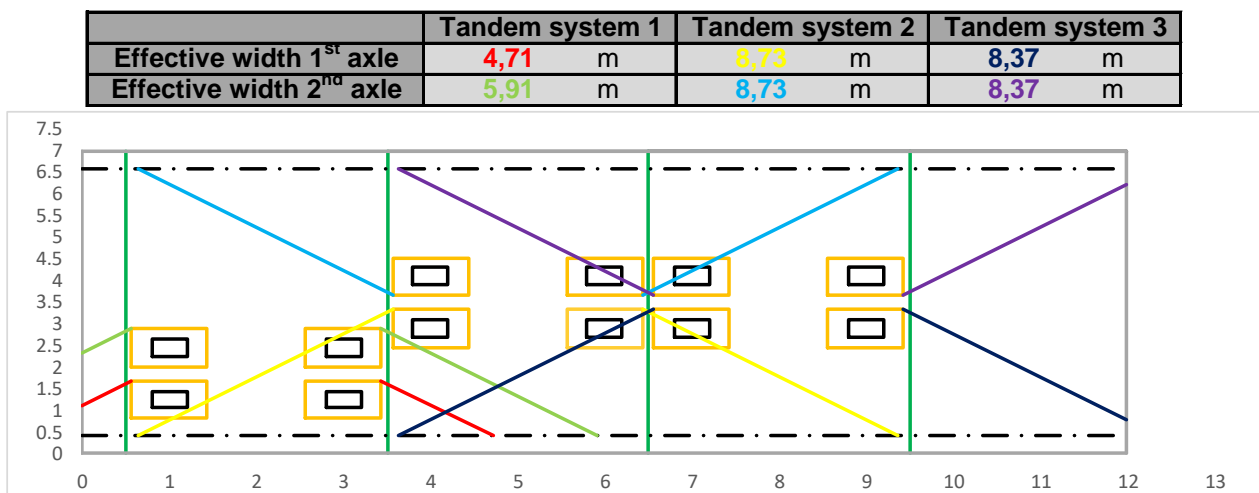
Figure 35 Example of visualization of effective widths per axle per TS of Case II load situation "Edge" (part of output from module). Overlap of TS2 with 0,18m < 0,81m (2d) due to span length. TS3 has no influence due to limited span length.

A full example of this method can be found in Appendix B2. This method is fully parametrically automated in a separate module which can be controlled later by the ASA Tool. Because this method is made in a separate module, it is also available separately for other projects.

3.4.3 Shear effect compared

The shear force due to TS calculated with the developed method based on (CEB-fib, 2010) is compared in this paragraph with the calculated shear force according to the Guyon-Massonnet method in the beam model and a 2D FEM plate model calculated in SOFiSTiK. In the analytical model, the Guyon-Massonnet method is used to determine the load distribution for the occurring moment, with this load the shear force due to TS in the section at a distance d from the face of the support was also determined for control purposes. The 2D FEM model consists of a single slab which has a line support with rotational springs at the location of the walls. These rotational springs are calculated by SOFiSTiK based on the height, thickness and end clamping of the wall, but fully correspond to the calculated rotational stiffness as in the analytical model. To obtain as close as possible matching results, a section is created at the same distance from the face of the wall as the control section in the fib method. The TSs are placed in the same locations as in the fib method, the load distribution to the top of the concrete slab is also included so that there is no difference on the load side. Because the magnitude of the shear force to be taken into account V_{TS} is strongly dependent on the soil cover and with a varying soil cover the various cases from the fib method are analysed,

the shear force to be taken into account as a result of TS is investigated for varying soil cover. The relatively simple 2D FEM model is shown in Figure 36. 2D quadrilateral elements with a regular mesh with an element size of half the slab thickness were used. The possible presence of haunches is, just as in the analytical model, not included in the calculation of the load effect.
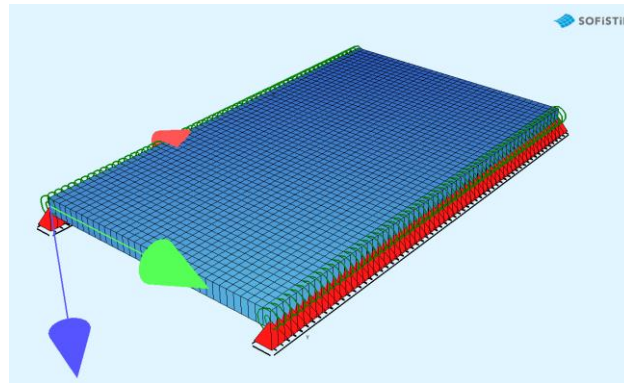
Figure 36 Used 2D FEM plate model from SOFiSTiK consisting of quadrilateral elements with a mesh size of half the slab thickness, rotational springs represent the supportive walls.

It can reasonably be expected that the influence of TS in relation to the soil cover depends on the length of the span, therefore the research is carried out on the structures described in paragraph 3.2.4, CAT I to CAT III with a clear-span of 3,5m to 13m. The results of the three investigated methods are shown in Figure 37, mutual results from CAT I to CAT III should not be compared with each other because more parameters than just the clear-span have been adjusted.

a)

b)

c)

d)
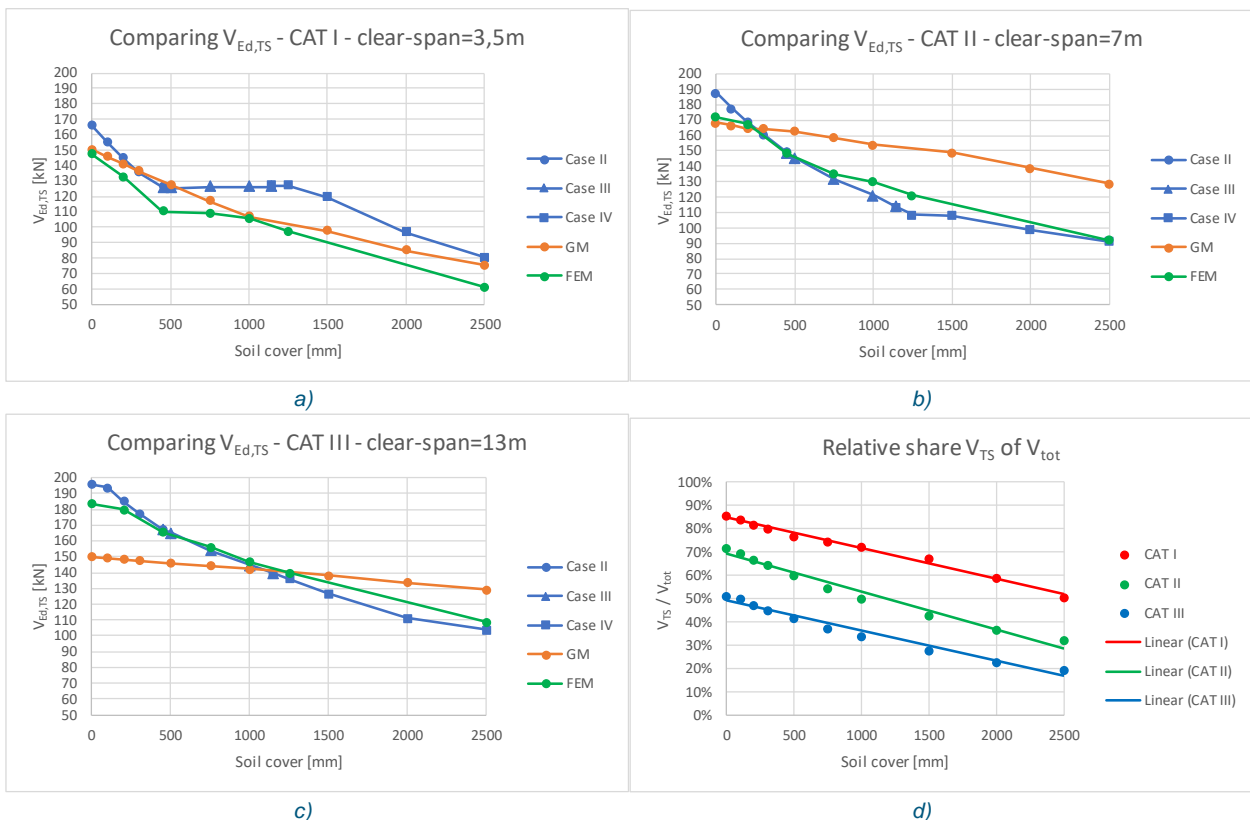
Figure 37 Comparison of calculation results for V_{TS} according to Guyon-Massonnet, the developed method based on fib and a 2D FEM plate model for CAT I (a), CAT II (b) and CAT III (c) structures and the share of $V_{TS,fib}$ in the total calculated shear force (d).

In general, based on the investigated structures, the method developed based on (CEB-fib, 2010) seems to correspond reasonably with the results from the FEM model and at least describes the behaviour better compared to the Guyon-Massonnet method, especially with medium to large spans. For structures with very little or no soil coverage, the fib method overestimates the shear force due to TS by about 10%. For structures with a medium to large span, the method may underestimate the shear force as a result of TS by up to 10%. The largest relative deviation of 10% occurs with the CAT II structure with 1250mm soil cover, Figure 37 *d)* shows that V_{TS} in that situation accounts for approximately 50% of the total occurring shear force, which means that, assuming the uniformly distributed load is correctly assumed, the underestimation of the total occurring shear force is only 5%.

The response of CAT I, shown in Figure 37 *a)*, seems rather remarkable where a kind of plateau is created between 500mm and 1000mm soil coverage. In the case of a limited span with an increasing soil cover, the load plane becomes larger, so that TS may be placed further back until TS reaches the limit point, as described in paragraph 3.4.2. This means that when adding soil the overlap strip becomes smaller than $4d$, which means that the load would increase. However, this effect is counteracted by an increase in b_w, due to larger vertical load distribution through the increased soil layer, which in turn reduces the calculated shear force. In this case, the two effects are almost in equilibrium, creating a plateau.

It was expected that Guyon-Massonnet will result in higher values for the shear force since transverse load distribution is not properly accounted for. However, in some situations Guyon-Massonnet results in lower values. Guyon-Massonnet assumes a deformed slab in sinusoidal shape, whereby the load must be reasonably in the centre of the slab. In this case the load is at $2d$ from the face of the support, so the slab will not deform as a half-sine. In addition, the analytical model always assumes one distributed load, while with small coverage this is not always the case, then there should be two distributed loads on the span, this can also ensure that Guyon-Massonnet for small coverage is more favourable. However, the latter effect is not the case with CAT III due to the large height of the deck, with CAT I and CAT II this is the case, but the difference in the shear force to be maintained is not significant.

For the load distribution in the horizontal plane of the slab, an angle of 45° has been used based on the (CEB-fib, 2010) recommendation for clamped slabs. Because the deck is not completely clamped by the wall, the angle of 45° could be adjusted to an interpolation between 45° and 60° in proportion to the clamping. The plate model with springs has been compared with a plate with a simply supported edge and a fully clamped edge, which indeed shows that more distribution occurs if an edge is simply supported and thus yields lower maxima. Figure 37 shows, however, that for CAT II and CAT III more distribution, by maintaining a larger angle, leads to unrealistic values compared to the FEM model. Even though the deck is not completely clamped, but is modelled with rotational springs, it is better to maintain the in-plane distribution angle for a clamped slab. The method as in (CEB-fib, 2010) is based on extensive research by (Muttoni, Rodrigues, & Burdet, 2006), a clamped slab in that study is also not fully clamped in practice, but monolithically connected, which may explain why a distribution according to a clamped slab is the most similar.

3.5   Discussion

Under a bending moment, oblique cracks occur when ribbed reinforcement bars are used due to the anchoring of the tension reinforcement in the concrete. Due to these oblique cracks it is necessary to determine the bending moment in a section under the angle of the "virtual crack", which is 45° for RC, which means that the moment line must be shifted. If plain reinforcement bars were infinitely smooth, these cracks would run vertically through the deck and the moment line would not have to be shifted in the negative direction, which is favourable. The problem, however, is that bars are not infinitely smooth and it is not known to what extent the angle of the cracks decreases compared to ribbed steel, which is why it is currently not permitted by regulations to do this differently for plain bars and an angle of 45° must still be maintained. However, it is debatable whether maintaining a 45° angle for plain bars is not too conservative. The unfavourable effect of plain reinforcement bars on the anchoring is, for example, included in the RBK in formula 8.4.2 (2) by an extra parameter $\eta_3 = 0,5$, which basically means that it is assumed that plain bars have 50% less bond than ribbed reinforcement bars.

Paragraph 3.3 shows that the assumed fictitious elastic modulus E_f for the walls and the deck, and thus the ratio in stiffness, can have a major influence when a skewed ratio is assumed. The stiffness ratio determines the moment distribution and thus the maximum hogging moment near the supportive wall and the sagging moment in the span. RBK allows up to 20% redistribution of bending moment, when reinforcement with ductility class B is applied, while the engineer can further redistribute the bending moment by adjusting the stiffness ratio between the walls and the deck as long as the sum of the moment capacities at the support and in the span is larger than the sum of the occurring hogging and sagging bending moment. It is possible to choose, also in the ASA Tool, to use the calculated fictitious elastic modulus, but such a method is not mandatory. On the other hand, when assessing an existing structure, as opposed to a new construction, an NLFEA may be used, in which redistribution of more than 20% occurs since it continues to theoretical failure. By putting it that way, assuming a E_f-ratio equal to $E_{f,wall}/E_{f,deck} = 1,0$ combined with a maximum redistribution of bending moment of 20% may still result in conservative, but correctly according RBK recommendations, results.

Method CEB-fib model code 2010 7.3-7 is intended for determining the shear force in slabs loaded with concentrated loads near a line support, without the influence of a second line support at the other end of the slab. The influence of the second support is however present for structures with a limited span. Regarding the comparison with the FEM model it should be noted that the FEM model is a linear elastic analysis which means that it does not take into account the non-linear behaviour due to cracks at the ULS. The results of CAT I deviate in value from the values found in the FEM model, because not enough calculations have been made with changes in individual parameters, it cannot be ruled out whether the second support is the only influence factor. In structures with a large soil cover the TSs are often far from, not close to, the line support, especially TS3, which raises the question whether the method is still applicable or not. First of all, FEM models show that the occurring shear force as a result of TS decreases drastically with load distribution due to large soil coverage and that the shear force effect as a result of TS becomes more limited compared to the occurring shear force due to the weight of the soil layer, in addition an error in the calculated distribution of TS becomes relatively smaller and smaller as the thickness of the soil layer increases, so that a small error in the determination of the shear force due to TS is negligible with large soil cover. It may happen that based on the total width of the roadway 3 TSs should be used, but that based on the joint-to-joint-distance TS3 is not modelled in the method for determining the shear force due to TS. In this situation TS3 would be partially on the considered segment but this load is not accounted for. However, it has been found that the extra load in the critical strip due to TS3 is, with approximately 5%, very limited with respect to the total shear force due to the other TSs and therefore the error that occurs by omitting TS3 is accepted in this particular situation. Although the calculated results with the developed method for determining V_{TS} show no major deviations on the negative side, an underestimation of the occurring shear

force, it cannot be guaranteed based on the available results that this always applies to every possible variant.

3.6 Conclusion

Solving the set of 4th order ODEs based on the Euler-Bernoulli beam theory offers the possibility to set up a complete parametric analytic model. The idealization of the structures considered does not change, so that the ODEs only need to be solved once, resulting in fully parametric equations for the bending moment and shear force. Due to its speed, this method has proven to be particularly suitable for determining the load effect of a large set of structures.

In theory, a large difference in stiffness, expressed in the calculated fictive stiffness modulus E_f, between the walls and the deck can have a significant influence on the moment distribution between the sagging moment in the span and the hogging moment at the face of the wall. With a calculated ratio $E_{f,wall}/E_{f,deck} = 2,0$, a shift of about 30% takes place from the sagging moment to the hogging moment. However, calculations show that such stiffness ratios will not occur often in practice, for which it has been concluded that the same E-modulus can be used as standard for the walls and the deck. In some cases this assumption may be conservative, resulting in an overestimation of the sagging moment in the span, in those situations it may still be useful to determine the fictitious elastic modulus E_f of the deck and the walls to obtain a more realistic moment distribution.

The extension of the method for determining shear force near supports from (CEB-fib, 2010) to the deck of an underpass, culvert or slab bridge, based on a check with a 2D FEM plate model, yields more realistic values than the shear force calculated according to the Guyon-Massonnet method. In general, depending on the span, a calculation of the occurring shear force as a result of TS according to Guyon-Massonnet leads to an underestimation of the shear force with small soil coverage, less than approximately 200mm, and an overestimation of the shear force with larger soil covers of approximately 500mm. Later in this research, a 3D FEM model with plate elements will be automated with which this theorem can be further investigated.

4
Load bearing capacity of existing structures

This chapter discusses the load bearing capacity of existing RC structures. The capacity of a structure is determined based on the cross-sectional capacity, of which the determination of the shear capacity of existing structures is further investigated. Special attention is paid to the anchoring of reinforcement and its influence on the calculated capacity. The preliminary study, described in chapter 2, shows that the material properties of many structures are unknown, the importance of these data is investigated. Finally, the results of the analytical model are examined, both for structures from the database and the results of a sensitivity analysis.

4.1 Cross-sectional resistance compared

The load bearing capacity of a concrete structure is determined in the critical cross-sections where the occurring bending moment or shear force is at a global or local maximum or where the capacity of the structure is relatively low. The sections which are checked are described in paragraph 3.2.2. These sections are selected based on the section forces occurring in the deck in combination with the expected capacity in the relevant section.

A model has been available for determining the bending moment capacity of a concrete section for years that closely approximates reality. The model assumes moment and force equilibrium where the tensile force is fully absorbed by the reinforcing steel and the compressive force is absorbed in a compression zone in the concrete. This theory rests on the "needle principle" which means that cross-sections remain straight. This theory is confirmed by many 3- and 4-point bending tests. Bending is generally not a brittle failure mechanism and therefore the tests are easy to control. For the determination of the moment capacity, reference is made to Appendix C1, later in this chapter in paragraph 4.2 the influence of the anchoring of reinforcement is discussed.

Not everything is still known for determining the shear capacity of a concrete cross-section, which is reflected in the design codes as there is still no single unambiguous model which fully and correctly describes the shear capacity of a concrete cross-section.

4.1.1 Determination of the shear capacity

For the shear capacity of existing structures, NEN8700 does not provide additional information with respect to EC with regard to determining the calculated capacity of a structure, so the formulas from EC are used. For RWS constructions, the RBK provides adapted formulas with an increased calculated capacity. The CUR124, for objects of local authorities, refers to the NEN8700 and therefore does not provide an adjusted calculation method compared to EC. Both EC and RBK use two formulas, a lower limit formula (6.2.b), also called v_{min}-formula, and a long (6.2.a), or luxury, formula including the longitudinal tension reinforcement ρ_l. Because the long formula has no lower limit, which prevents zero capacity for 0% longitudinal reinforcement, the lower limit formula is added. The idea behind this lower limit formula is that a cross-section fails at moment instead of shear force based on minimal reinforcement ratio for moment capacity. The difference between formulas from EC and RBK lies in the fact that RBK takes into account a plate factor k_p and k_{cap} and has added the yield strength of the tensile reinforcement f_{yk} arithmetically.

The background of k_p and k_{cap}, which are applied in the v_{min}-formula and the luxury formula, lies in the determination of the shear capacity formulas which are based on beam tests. In the case of a beam, a small local deviation in the concrete can cause premature shear failure. This is reflected in the large scatter in the

shear capacity found in 3- and 4-point bending tests, resulting in a low calculation value because the 5% lower limit is adhered to. In the case of slabs, several beams would be placed one behind the other and a small local deviation in the material has less effect due to redistribution or spreading. After all, when a weaker beam is surrounded by stiffer, sturdier beams, the weak beam will suffer less, which means that it will be less loaded. besides, the bending theory is only pure for point loads with point supports, while plates are usually supported in line and the loads in a 3- and 4-point bending test are also not pure point loads. With a value of $k_p^{\frac{3}{2}} = 1,31$ the plate factor provides a significant increase in the calculated shear force capacity.

The v_{min}-formula from EC is calibrated on tests with reinforcing steel FeB 500 with a yield strength of $f_{yk} = 500 \, N/mm^2$. This yield strength is not included in the formula in the EC because it is assumed that FeB 500 reinforcing steel is always used. In section 2.3.1 can be read that many different qualities were available in the past. From (Lantsoght, 2012), elaborated in Appendix C1, it appears that v_{min} increases in capacity, the size of the factor, when a lower yield strength of the reinforcement is applied. It is therefore that in RBK it was decided to add the steel quality in terms of the yield strength f_{yk} in the v_{min}-formula so that an increased capacity is found for lower steel qualities. The idea behind this is that the v_{min}-formula is a lower bound formula, the cross-section would fail due to bending moment instead of shear force. In the case of a low tensile strength, a relatively large amount of reinforcement, expressed in mm^2, is laid in a cross-section which is favourable for the shear force capacity since it is determined by the reinforcement area A_s with respect to the concrete in a cross-section A_c, the reinforcement percentage ρ_l. Table 11 shows the influence of a lower f_{yk} for the constant factor in the v_{min}-formula.

Table 11 Influence of lower f_{yk} for shear capacity of v_{min} formula for common steel grades

Reinforcement steel	Yield strength $f_{yk} \, [N/mm^2]$	Constant in v_{min}-formula EC	Capacity advantage [%]
EC FeB 500	500	0,035	Calibrated formula
VB 74 + VB 74/84 FeB 400	400	0,039	11%
GBV 1962 QR40	400	0,039	11%
GBV 1962 QR24	240	0,050	43%
GBV 1962 QR22	220	0,052	49%

Note that when f_{yk} is taken from the constant factor in the v_{min}-formula, there is still a difference of the constant factor between EC and RBK. The difference in the constant factor in the formula for v_{min}, 0,83 for RBK and 0,77 for EC, can be traced to the assumption made for the internal lever arm z. RBK makes an estimate for z with $z = 0,95 \, h$, while EC estimates this with $z = 0,90 \, h$. This difference in internal lever arm leads to the difference in the constant factor in the formula for v_{min} where RBK calculates an 8% higher capacity.

When performing various test calculations, it was striking that in many cases the lower limit formula delivered a larger shear capacity than the luxury formula. This has led to doubts whether the formula for v_{min} as prescribed by the RBK is not too optimistic resulting in an overestimation of the shear capacity. This doubt arose on the basis of a combination of factors. By applying the Guyon-Massonnet method in combination with the newly developed method for shear force distribution, described in paragraph 3.4, more load distribution occurs on the effect side, resulting in a lower design value of the load in a cross-section under consideration. At the same time, an increase in capacity takes place by maintaining a higher concrete strength C35/45, the plate factor k_p and increased v_{min} at lower steel grades than FeB 500. Combining all these effects raises doubts as to the correctness and safety of their application. It is interesting that the

NEN8702, which provides additional rules for existing concrete structures, and the new EC 2020 are in development and that there is a deviation from the current EC and the RBK regarding whether or not to include the plate factor and increase the capacity for lower steel grades. In the draft version of the NEN8702 one can read that it is decided to apply the plate factor and not to increase the shear capacity based on v_{min} for steel grades lower than FeB 500. In the draft version of EC 2020 it is the other way around, where the f_{yk} is applied in the v_{min} formula, but the plate factor k_p is not. Variations in whether to include both factors and the relationship to the luxury formula have been investigated. The most important variants from this study are the EC variant, as the lower limit, the RBK variant as the upper limit, a variant that takes the plate factor k_p into account on the EC formula, comparable to NEN8702 and a variant according to the RBK formula where only the effect for lower steel grades has been applied meaning $k_p = 1,0$. An overview of the investigated formulas is shown in Table 12.

Table 12 Overview of investigated main variants for formulas of shear capacity

	6.2.a – Shear failure	6.2.b – Transition to flexure
EC	$V_{Rd,c} = \left(0,12 \, k \, (100 \, \rho_l \, f_{ck})^{\frac{1}{3}} + k_1 \, \sigma_{cp}\right) b_w \, d$	$V_{Rd,c} = \left(v_{min} + k_1 \, \sigma_{cp}\right) b_w \, d$ $v_{min} = 0,035 \, k^{\frac{3}{2}} f_{ck}^{\frac{1}{2}}$
RBK	$V_{Rd,c} = \left(0,12 \, k_{cap} \, k \, (100 \, \rho_l \, f_{ck})^{\frac{1}{3}} + k_1 \, \sigma_{cp}\right) b_{wgem} \, d$	$V_{Rd,c} = \left(v_{min} + k_1 \, \sigma_{cp}\right) b_w \, d$ $v_{min} = 0,83 \, k_p^{\frac{3}{2}} k^{\frac{3}{2}} f_{ck}^{\frac{1}{2}} / f_{yk}^{\frac{1}{2}}$
EC + k_p	$V_{Rd,c} = \left(0,12 \, k_{cap} \, k \, (100 \, \rho_l \, f_{ck})^{\frac{1}{3}} + k_1 \, \sigma_{cp}\right) b_{wgem} \, d$	$V_{Rd,c} = \left(v_{min} + k_1 \, \sigma_{cp}\right) b_w \, d$ $v_{min} = 0,035 \, k_p^{\frac{3}{2}} k^{\frac{3}{2}} f_{ck}^{\frac{1}{2}}$
RBK - k_p	$V_{Rd,c} = \left(0,12 \, k_{cap} \, k \, (100 \, \rho_l \, f_{ck})^{\frac{1}{3}} + k_1 \, \sigma_{cp}\right) b_{wgem} \, d$	$V_{Rd,c} = \left(v_{min} + k_1 \, \sigma_{cp}\right) b_w \, d$ $v_{min} = 0,83 \, k^{\frac{3}{2}} f_{ck}^{\frac{1}{2}} / f_{yk}^{\frac{1}{2}}$

Comparing calculation methods

Research into the different variants for the calculation of the shear force capacity has been done based on the longitudinal reinforcement ratio ρ_l, the plate factor k_p and the decoupling of the steel grade in the v_{min}-formula. The other parameters have no influence relative to each other because they are integrated in the same way. For each variant, capacities were calculated with variation in parameters. These capacities are plotted against each other and made clear in Figure 38, reference is made to the RBK v_{min}-formula.
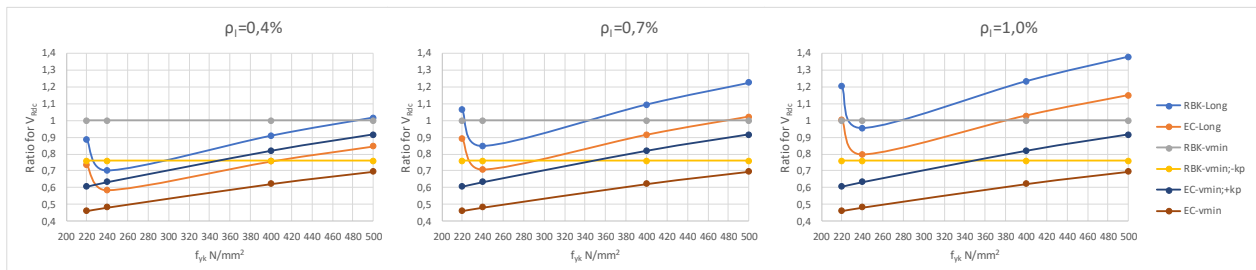
Figure 38 Overview of shear capacities of different calculation methods with reference RBK v_{min} formula as 1,0.

When looking purely at the RBK formulas, it is remarkable that for lower, but practical, reinforcement ratios formula 6.2.b gives a significant higher capacity than formula 6.2.a, meaning that based on RBK formulas the cross-section should fail by bending moment while for EC formula 6.2.a is larger than 6.2.b. Calculations show that for a reinforcement ratio $\rho_l < 0,53\%$, RBK formula 6.2b is always decisive with respect to the

luxury formula. This picture therefore corresponds with the test calculations, since a large part of the structures in the available data have such a reinforcement ratio.

Looking at the two variants of the v_{min}-formula, it can be seen that there is indeed a significant difference, especially from a practical point of view. Because the variant $RBK_{v_{min}-k_p}$ only has a plate factor of 1,0, it is constant at 0,76 in relation to the original RBK v_{min}-formula regardless of reinforcement ratio or steel grade. The EC variant including plate factor does not depend on f_{yk} and therefore changes relative to the original RBK v_{min}-formula. For a FeB 500 steel grade, which is the standard nowadays, the variant is only 8% lower than the original RBK formula because EC assumes a lower constant factor in the v_{min}-formula. A QR40 or FeB 400 according to EC with plate factor k_p loses, with a factor of 0,82 compared to the original RBK v_{min}-formula but gains 8% compared to the variant $RBK_{v_{min}-k_p}$. Lower steel grades lose compared to $RBK_{v_{min}-k_p}$ due to the effect of f_{yk}. For example, a QR24 is 0,64 compared to the original RBK formula, which is 16% lower than the $RBK_{v_{min}-k_p}$ variant. Since the lower limit formula is independent of the reinforcement ratio, the two variants always intersect at 345 N/mm².

For both variant $EC_{v_{min}+k_p}$ and variant $RBK_{v_{min}-k_p}$ it actually applies that for the most practical reinforcement ratios, 0,40% and higher, the luxury formula provides a larger capacity, so it does not matter what is held. Only for the low steel grade QR24 there is a small difference at 0,40% reinforcement ratio or lower. However, QR24 steel grade has hardly been found in the data, although this does not mean that it does not occur.

A conscious choice
The RBK considers both the plate factor and the influence of the steel grade and thus gives the highest capacity. The NEN8702 uses a v_{min}-formula as in EC with the addition of the plate factor k_p. In the new EC, of which a draft version is currently available for comment, a formula has been chosen in which the effect of the steel grade is included but an increased capacity for plates in the form of a plate factor is omitted. The current EC does not include either effect and therefore provides the lowest calculated shear capacity.

The current formulas are calibrated on tests with FeB 500, the arithmetic replacement of FeB 500 to lower strengths, resulting in a higher shear capacity, does not really have to correspond one to one. In theory, especially for QR 22 and QR 24, a very large increase in the capacity could be booked, of which the question is whether this will work completely in practice, because the shear force capacity depends on many factors that cannot always be isolated. After all, no specific tests have been done that support this theory. Because an automated analysis is set up in this study, some conservatism is safe, therefore the beneficial effect of a lower f_{yk} on the shear force capacity is not taken into account.

The doubts about the correctness and safety of the application of the plate factor k_p or k_{cap} due to improved load distribution on the effect side in combination with an increase in the capacity side as result of this plate factor is unjustified. Even if the load distribution on the effect side were fully utilized, the plate effect on the capacity side is still there. It is important to understand that this are two separate effects, which means that the same effect is not benefited twice. That is why the plate factor k_p or k_{cap} is taken into account for determining the shear capacity of a concrete cross-section. This means that the choice is made to use the EC v_{min}-formula with addition of the plate factor k_p, which is in line with NEN 8702. For the luxury formula, the RBK formula is simply used.

Influence on UC of available data

The influence of the different formulas for $V_{Rd,c}$ on the UCs of the structures calculated with the analytical model was investigated. All constructions are calculated with the different variations on the shear force formulas as shown in Table 12. An overview of the calculation results for the different calculation variants for determining the shear force capacity is shown in Table 13.

Table 13 Overview of calculation results for the different calculation methods for determining the shear force capacity of 6.2b, it is assumed that reinforcement is fully anchored.

	RBK		$\mathbf{RBK_{v_{min}-k_p}}$		$\mathbf{EC_{v_{min}+k_p}}$		EC	
U.C. < 1,0								
Number of objects	33		33		33		33	
Objects U.C. < 1,0	28	85%	26	79%	26	79%	16	48%
U.C. > 1,0								
Objects U.C. > 1,0	5	15%	7	21%	7	21%	17	52%
Failure due to shear	2	40%	4	57%	4	57%	15	88%
Failure due to bending	3	60%	3	43%	3	43%	2	12%
Governing - General								
Shear governing	18	55%	22	67%	21	64%	29	88%
Bending governing	15	45%	11	33%	12	36%	4	12%
Governing - Sections								
VEd;haunch+	5	15%	5	15%	5	15%	5	15%
VEd;haunch-	9	27%	11	33%	11	33%	15	45%
VEd;clear	4	12%	6	18%	5	15%	9	27%
MEd;midspan	13	39%	11	33%	10	30%	4	12%
MEd;haunch+	0	0%	0	0%	0	0%	0	0%
MEd;haunch-	0	0%	0	0%	0	0%	0	0%
MEd;clear	2	6%	0	0%	2	6%	0	0%

To determine the shear capacity, taking into account the present longitudinal reinforcement by ρ_l, formula 6.2a from RBK is used without adjustments, so including the k_{cap} factor. Note that for k_{cap} applies that $k_{cap} = k_p$. Formula 6.2b has been adapted to the version from the EC with the addition of k_p from RBK, indicated by $EC_{v_{min}+k_p}$ in table 13.

A clear difference between RBK and EC can be seen by the large difference in the number of structures with a UC<1,0 according to both calculation methods. If the EC were to be maintained, more than half of the structures would not comply based on the calculation, while with the RBK 85% of the structures would comply, an increase of 87%. When looking at what is governing for a structure, it can be seen that any additional failure case at EC is due to shear force. A difference is also clearly visible in the general consideration. RBK is approximately a fifty-fifty distribution between moment and shear while EC is clearly dominated by shear failure, which can also be seen from the critical sections. The EC is almost always normative for shear force in the section with the haunch, while RBK is almost as often normative for moment in the span. For the variants, which lie between EC and RBK, an image such as RBK applies in which both shear force and bending moment may be governing. It can be concluded that it is most likely that the shear force in the haunch under a negative moment, or less likely under a positive moment, or the sagging moment in the span is governing. In the event that, after redistributing the moment, a structure still disapproved based on the sagging moment in the span while there is still unused capacity in the clear, it can be checked whether the stiffness ratio between the deck and the wall must be adjusted using the method of E_f as described in paragraph 3.3.

The differences between the variant according to RBK without plate factor k_p in the lower limit formula 6.2b and the variant according to EC with plate factor k_p are small. The difference would have been larger if the dataset was dominated by structures with QR22 or QR24 reinforcement instead of QR40 and FeB 400,

because the beneficial effect of k_p is smaller than the beneficial effect of a low f_{yk} from the RBK formula as shown in Figure 38. Due to the predominance of QR40 and FeB400, the choice for $EC_{v_{min}+k_p}$ ensures that some structures drop from a UC>1,0 to a UC<1,0. At the same time, there are some structures where the steel quality is unknown, which means that a low steel grade must be maintained, resulting in a lower capacity because the low tensile strength f_{yk} is not taken advantage of leading to a UC>1,0. Ultimately, it doesn't matter much compared to each other, as shown in Table 13. It should also be kept in mind that the calculated shear capacity according to formula 6.2b means that bending moment should be governing for the considered cross-section.

The conservative attitude towards formula 6.2b of RBK leads to a 7% decrease in structures with a UC<1,0 due to the reduced shear capacity. The increase of constructions with a UC>1,0 is limited because formula 6.2a, which has not been changed, is now governing in most cases.

4.2 Anchorage of reinforcement

Reinforcement bars must be anchored in such a way that the bonding forces can be safely transferred to the concrete to avoid longitudinal cracks or spalling. This has been less taken into account in the past, which means that the reinforcement cross-section may need to be theoretically reduced to prevent cracking or spalling of the concrete or slipping of the reinforcement bar.

In case the reinforcement is not fully anchored, the cross-sectional area of the present reinforcement must be reduced in proportion to the anchoring, for which the following applies:

$$A_{sl,red} = \frac{l_{bd,provided}}{l_{bd}} A_{sl} \qquad (4.1)$$

Where,

$l_{bd,provided}$	is the provided anchorage length
l_{bd}	is the design value of the required anchorage length
A_{sl}	is the area of the tension reinforcement present in the considered cross-section
$A_{sl,red}$	is the area of the tension reinforcement present taking into account the available anchorage length

The reduction of the cross-sectional area of the reinforcement that can be used for calculation has a direct influence on both the moment and shear capacity. Since the mean UC calculated with the analytical model on the assumption that all reinforcement is fully anchored is $UC_{avg} = 0,85$ in combination with the direct influence on the design value of the capacity, the anchoring of reinforcing bars has been further investigated.

The determination of the required and available anchorage length is elaborated in Appendix C1.

4.2.1 Required anchorage length

The anchorage length of a bar to be considered fully anchored is calculated based on NEN-EN 1992-1-1 section 8.4 with additions from RBK. The design value of the required anchorage length l_{bd} is calculated in three steps. The ultimate bond stress f_{bd} is determined first, the ultimate bond capacity must be sufficient to prevent anchor failure. For the application of plain reinforcement steel, the factor η_3 is introduced from RBK into the formula for f_{bd}, which is the coefficient on bar profiling, for which applies that for ribbed reinforcement steel $\eta_3 = 1,0$ and plain reinforcement steel $\eta_3 = 0,5$. The less good bond of plain reinforcement bars therefore results in a reduction of the design value of the ultimate bond stress f_{bd} of 50%. The second step is calculating the basic anchorage length $l_{b,rqd}$ which is the required anchorage length for a full anchorage of the maximum allowable force, $A_s \sigma_{sd}$, for a straight bar assuming a constant bonding stress f_{bd}. Finally, the design value of the anchorage length l_{bd} is determined with a lower limit

value $l_{bd,min}$. The design value of the anchorage length l_{bd} takes into account the effect of the shape of the reinforcement bar (α_1), the effect of concrete cover (α_2), the effect of confinement by transverse reinforcement (α_3), the effect of confinement by welded transverse reinforcement (α_4) and the effect of confinement by transverse pressure p in the ULS along l_{bd} (α_5). For anchoring a bar, a distinction is made between anchoring with a straight bar end and a bar end other than straight. A bar end other than straight is, for example, when a bar is bent from the deck into the wall, this concerns the shape of the bar and is taken into account by α_1. Because it rarely occurs that shear reinforcement is present in the investigated structures, it is assumed that no transverse reinforcement is present, which means that $\alpha_3 = 1,0$ and α_4 is fixed by EC2 at $\alpha_4 = 0,7$.

The required anchoring length can vary widely from approximately 150mm to more than 1,5m, which is strongly dependent on bar diameter and concrete strength class, while the data analysis from chapter 2 shows that bar diameters from 12mm to 32mm have been used in a reasonably even distribution and that the concrete strength class is often unknown, resulting in the use of the widely separated class C35/45 for RWS constructions and C16/20 for constructions of local authorities. But also the bar shape, straight or bent, and the ratio of the concrete cover to the centre-to-centre distance of the bars have a significant influence on the required anchorage length, this is for bars with a diameter of 16mm and 25mm, the most common diameters from the data analysis from section 2.4, shown in Figure 39.
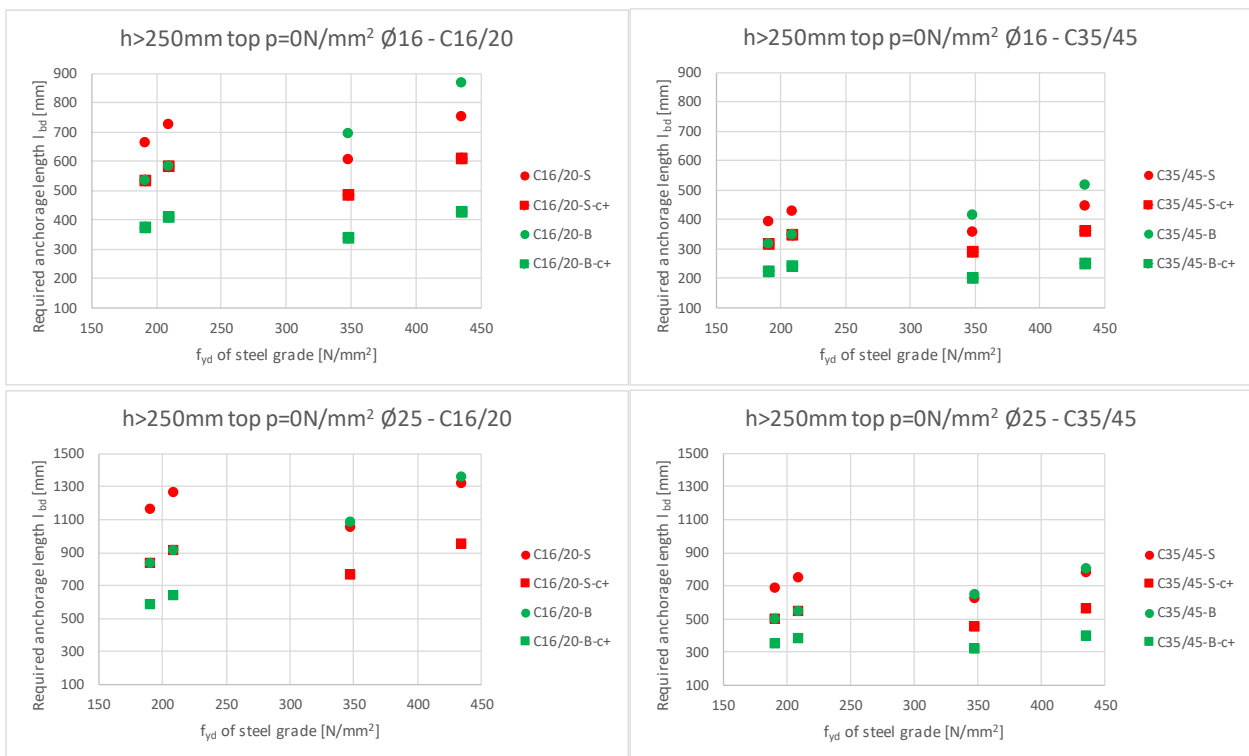
Figure 39 Required anchorage length l_{bd} for different concrete class, steel grade, straight or bent and with increased concrete cover for element height larger than 250mm with reinforcement bar at the top of the cross-section and a transverse pressure $p = 0\ N/mm^2$. Red data point: Straight; Green data point: Bent; Dot data point: $c_d = 30mm$; Square data point: $c_d = s \gg 30mm$. Overlap of green dots and red squares: limit of $\alpha_2\,\alpha_3\,\alpha_5 \geq 0,7$ is reached (=0,7).

With only one exception, in all the situations studied, shown with the data points in Figure 39, the required anchorage length l_{bd} is reduced by 41% when C35/45 is applied compared to C16/20. The exception is at the lower limit of the required anchorage length where $l_{b,min}$ becomes normative over l_{bd} with only, but still significant, a reduction of 22%. The advantage for RWS structures is that in the original design often a lower concrete strength class was taken, for example K300 from the GBV 1962, but that a C35/45 may now be

used in the assessment, which means that the required anchoring length is significantly reduced. Plain reinforcement bars, as expected, have a significantly longer anchorage length required. In case of anchoring with a straight bar end, the difference with ribbed steel is 50%. When anchoring with bent bars, the difference is smaller because RBK assumes a larger effect of bent bars for plain steel than ribbed steel, processed in α_1, resulting in a difference of approximately 30% between plain and ribbed bars. Bending of plain reinforcement bars provides a significant reduction of l_{bd}, based on additional formulas for plain reinforcement bars from RBK. Ribbed steel has a better bond with the concrete, but therefore requires more coverage to transfer the full absorbable force from the bar to the concrete. Ribbed steel does not benefit from an anchoring with bent bar end under normal coverage, like $c_d = 30mm$, on the contrary l_{bd} becomes 0% to 30% larger depending on bar diameter where a smaller bar diameter experiences a relatively larger increase in l_{bd} than a larger bar diameter, this is a no linear effect. A concrete cover much larger than normal edge coverage allow greater force to be transferred to the concrete and corrugated steel also benefits from the bended bar end. Plain reinforcement bars benefit quite quickly from the effect of a bent bar end, with normal coverage a reduction of up to 30% of l_{bd} depending on bar diameter where larger diameter leads to greater reduction as long as the concrete cover is larger than the bar diameter. If the coverage on the relevant member is sufficient, a bended bar end will always yield a reduction of 30% compared to anchoring with a straight member, unless the lower limit of $l_{b,min}$ is reached. In old codes it was prescribed that bars in tension, which most reinforcement bars are, should always be provided with a hook. The coverage has a large influence on the required anchorage length l_{bd}, because the force has to be transferred from the reinforcing bar to the concrete. The required anchorage length of the bar depends on the ratio between the concrete cover around the bar and the bar diameter. The difference between a normal edge coverage, like $c_d = 30mm$, and the upper limit value for reduction, which is already achieved for most practical centre-to-centre distances of the bars, varies between 19% and 51% for the examined cases. It is therefore recommended to assume minimal concrete coverage because the negative effect of a small coverage of the anchorage is much greater than the positive effect of a large coverage on both the moment and shear capacity.

A transverse pressure p along the anchorage length has a positive effect on the anchorage, reducing the required anchorage length l_{bd}. Reinforcement bars from the bottom layer of the deck, which act as tension reinforcement under a positive bending moment in the section at the end of the haunch, which are anchored straight in the re-entrant corner to the wall could benefit from this due to the presence of a relatively large normal stress. It is very unlikely that the bottom reinforcement from the deck has been bent into the wall. The graphs in Figure 40 show the effect of a transverse pressure for different bar diameters with steel grade QR24 and QR40 or FeB400. The effect of a transverse pressure is limited on small bars like diameter 12mm but becomes more significant as the diameter of the bar increases.
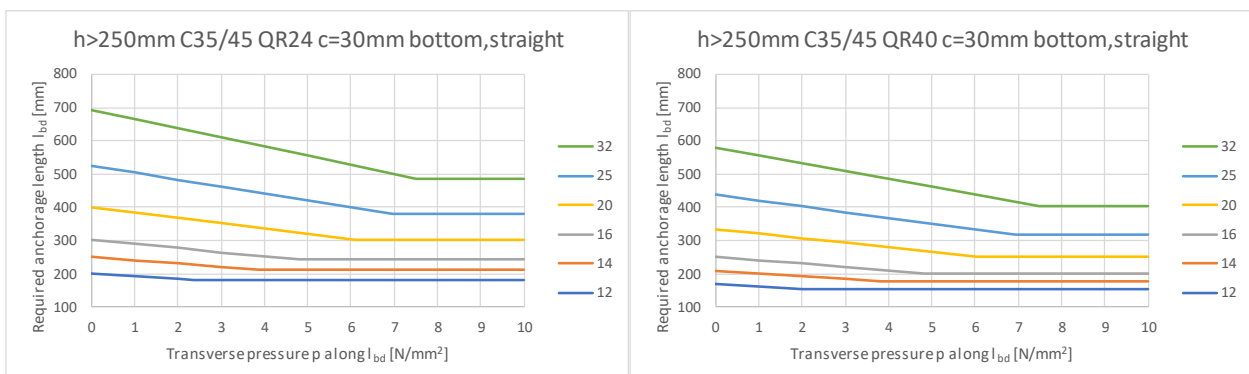
Figure 40 Effect of transverse pressure on the required anchorage length l_{bd} for bottom reinforcement bar with straight anchoring of steel grade QR24 plain bars (left) and QR40 or FeB 400 ribbed bars (right)

There is a lot of potential to be gained, shown in Table 14, which depends on the bar diameter used but is constant for different concrete strength classes and steel grades including plain or ribbed reinforcement bars.

Table 14 Potential reduction of anchorage length l_{bd} for different bar diameters, independent of concrete strength and steel grade including plain and ribbed reinforcement bars

Bar diameter	Ø12	Ø14	Ø16	Ø20	Ø25	Ø32
Potential reduction of l_b	-10%	-16%	-19%	-24%	-28%	-30%

Based on the study of the mean normal force in the wall from section 3.3.2, it appears however that it is unlikely that σ_{cp} will exceed 1,1 N/mm². It can then be seen from Figure 40 that the gain, in the form of a shorter required anchorage length, is limited by the presence of a stress perpendicular to the bar axis. Since the influence is limited and to build in some form of conservatism and safety, the influence by transverse pressure is neglected meaning $p = 0 \, N/mm^2$. The effect of the coverage (α_2) on the relevant bar in the part that is anchored in the wall is also so large that the effect of any normal force (α_5) no longer has any added value due to the limits $0{,}7 \leq \alpha_2 \, \alpha_3 \, \alpha_5 \leq 1{,}0$. But because an average has to be taken and the bar is in many cases anchored in the wall for less than half the anchoring length, it was chosen for safety and simplicity to start from the concrete cover on the reinforcement in the section halfway the length of the haunch, which means that the beneficial effect of the larger coverage on the bar is included to a limited extent.

4.2.2 Provided anchorage length

The provided anchorage length $l_{bd;prov}$ depends on specific details of the reinforcement layout and the cross-section with corresponding bending moment. In total, the anchoring of the tension reinforcement is checked for three situations. In the section of the clear of the wall, the top reinforcement is checked under the assumption that only a hogging moment occurs in that section. In the section at the end of the haunch, both the top and bottom reinforcement is checked because there both a sagging and hogging bending moment can occur. It is assumed that the bottom reinforcement in the span is fully anchored at the section of the maximum sagging moment in the span, because the bottom reinforcement usually extends into the wall and can therefore be assumed as fully anchored.

The anchoring of the top reinforcement in the deck, under a hogging moment, is checked from both the section in the clear and the section in the haunch, shown on the left and right respectively in Figure 41.
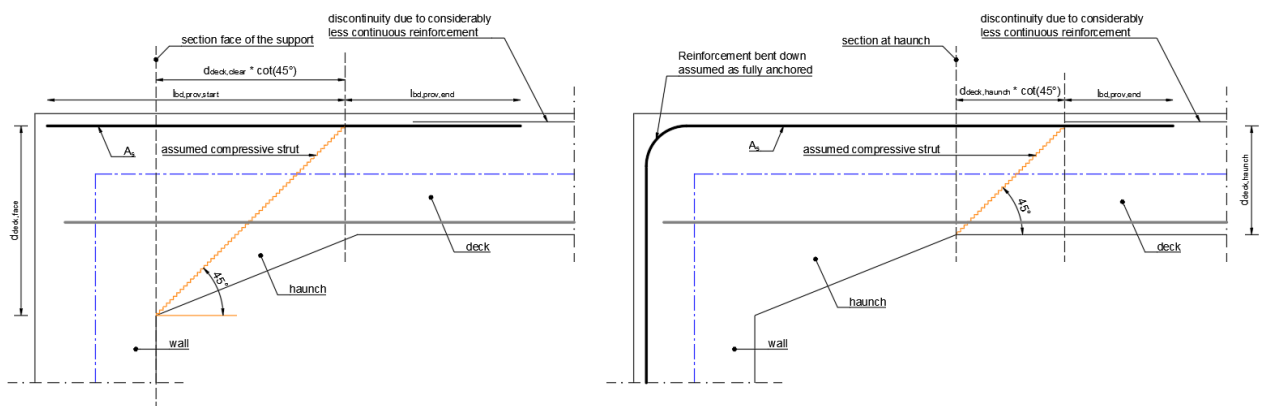
Figure 41 Schematics of determining the provided anchorage length of the top reinforcement in section in the clear (left) and section at the haunch (right)

The anchoring of the top reinforcement under a hogging moment, the schematization of which is shown in Figure 41 for both the section in the clear and the section at the end of the haunch, is in most cases only

checked at the bar end in the deck, called end with $l_{bd,prov,end}$. If the top reinforcement is bent into the wall then it is assumed that the reinforcement at that bar end is fully anchored in the wall, called start with $l_{bd,prov,start}$. In many cases, it actually concerns the vertical reinforcement of the wall which has been bent into the deck, this was done from the practical point of view that the deck was poured later than the wall. The top reinforcement for the hogging moment must be anchored in the deck, referred to as the end of the bar, because the continuous top reinforcement in the deck is substantially less, like from a bar diameter 20 to a bar diameter 12, which creates a discontinuity. If the bar is not bent from the wall into the deck and therefore has a straight bar end, which is very unlikely but shown left in Figure 41, the anchoring at the start is also checked. To check the anchoring of the top reinforcement, only the length of the relevant bar beyond the clear $L_{p,clear}$ and whether or not the reinforcement is bent into the wall is required, the other parameters are automatically determined based on assumptions. Due to the effect of oblique cracks, the anchorage must be checked at a distance equal to $d \cot (\theta)$, where θ is the angle of the compressive strut for which the standard value of $\theta = 45°$ for reinforced concrete is used in accordance with EC2.

It is usually not expected that a sagging bending moment, which results in tension at the bottom, can occur in the section of the haunch, but certainly for long haunches this does occur. The anchoring of the bottom reinforcement is defined as the explanation in Figure 42. It is assumed that the bar end is fully anchored in the span because the bar extends sufficiently far. In the available data it did not occur that the lower reinforcement of the deck is bent into the wall, therefore it is unlikely to occur in practice and a straight bar end is assumed. The length of the bar beyond the face of the wall is almost never indicated on old reinforcement drawings and this length is also difficult to measure in practice. An estimation formula is used which determines the reasonable maximum length, so that no user input is required. The possible error is limited, since in practice this bar usually extends beyond the face of the wall.
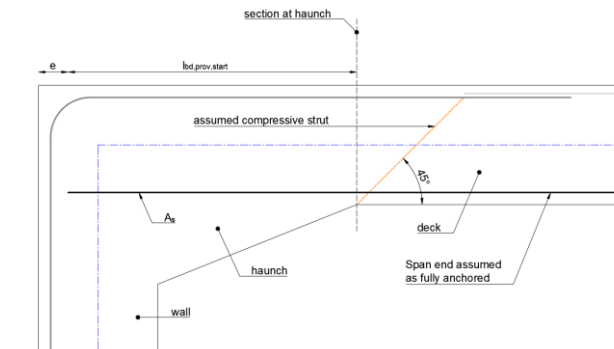
Figure 42 Schematics of determining the provided anchorage length of the bottom reinforcement in the section at the haunch

There is practically no more anchoring available than determined with this method, in case this check does not comply, it will certainly not comply. If the calculation shows that it is fully anchored, there is reason to believe that it is, where a deviation remains limited.

4.2.3 Influence of anchorage

Based on available reinforcement drawings, an estimate has been made of the length of the top reinforcement in the deck beyond the face of the wall, so that the anchoring of the reinforcement in the deck can be determined. Of the 33 structures, for which sufficient data is available and have an intersection angle greater than or equal to 80gon so that the analytical model can be used, it was possible to determine the anchoring of the reinforcement for 27 structures. In the other 18% of the structures, clear reinforcement drawings which provide detailed information necessary for determining the available anchorage length were missing. The check of the anchoring of the reinforcement of a structure offers more reliability of the outcome of the assessment compared with the assumption that it is fully anchored, however it requires more sensitive input which is not always available.

Several tests like (Muttoni, Rupf, & Ruiz, 2013) and (Olesen, Sozen, & Siess, 1965) show that shear cracks near the support occur at an angle of less than $\theta = 45°$, the size of the angle which according to the current EC may be maintained for RC slabs without shear reinforcement, but tends more towards $\theta \cong 30°$. For the anchoring of reinforcement bars, a smaller angle θ has a negative effect because the reinforcement becomes anchored over a smaller length $l_{bd,prov}$ since the distance $d \cot(\theta)$, the distance from where a bar can be anchored due to oblique cracks, increases with a decreasing θ. When calculating with an angle of 45 degrees and cracks do occur at an angle of 30 degrees, the anchoring of the top reinforcement of the deck takes place at the location of these shear cracks. However, a reinforcement bar cannot be properly anchored in a shear crack and can therefore be seen as dangerous. The influence of assuming more horizontal shear cracks, meaning changing the recommended angle from $\theta = 45°$ to $\theta = 30°$, on the UC of the structures in the dataset has been further investigated.
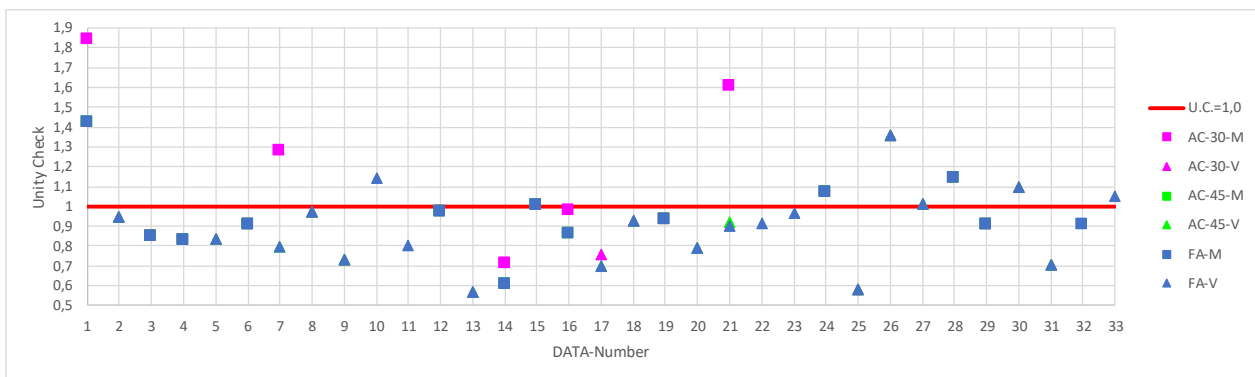
Figure 43 Unity Checks for analysed structures out of available data calculated with the Analytical Model. Results show data assuming Fully Anchorage (FA) with shear (V) or bending moment (M) governing, Anchorage Checked (AC) with $\theta = 45°$ and $\theta = 30°$. If no increased UC is obtained, the data points overlap showing only the data of Fully Anchorage.

Figure 43 shows that the practical influence of the anchorage length on the available data is small when an angle $\theta = 45°$ is used for the compressive strut and the oblique cracks. In only a single case (4%) the reinforcement is not fully anchored and as a result a higher UC is obtained, as can be seen by data number 21 in Figure 43. When it is assumed that $\theta = 30°$ the influence of the anchoring of reinforcement on the UC becomes greater. The number of structures for which the reinforcement is no longer fully anchored due to a smaller angle θ is significant, with $\theta = 30°$ 22% of the reinforcement of the structures under investigation is not fully anchored. More significant is the increase in UC for structures of which the reinforcement is no longer fully anchored, on average the UC for these structures increases by 35%. Structures for which bending moment is decisive under the assumption that the reinforcement is fully anchored are more likely to experience an increase in UC as a result of limited anchoring. What is also striking is that the proportion of structures where shear force is governing decreases when reinforcement turns out not to be fully anchored because bending moment becomes governing. What can be seen in the data is that a limited

anchoring mainly has a negative influence on the bending moment capacity. For the structures with data numbers 7 and 21, the influence of a limited anchoring at $\theta = 30°$ is relatively very large and the capacity becomes insufficient, meaning the UC becomes larger than 1,0. The typical problem with these structures is that the bent reinforcement from the wall does not extend far enough into the deck, so when assuming an angle of $\theta = 30°$ the bended reinforcement is not anchored and it can only be assumed that a force can be transferred to the continuous top reinforcement, which is usually substantially less in cross section. As an example the detail of reinforcement in the connection between the wall and the deck of structure with data number 21 is shown in Figure 44, in this case the top reinforcement changes from $\emptyset 25 - 200$ to $\emptyset 16 - 200$ which is almost a factor 2,5 in A_s.

	Bent reinforcement from wall into deck
	Continuous top reinforcement deck
	Assumed shear crack with $\theta = 45°$
	Assumed shear crack with $\theta = 30°$
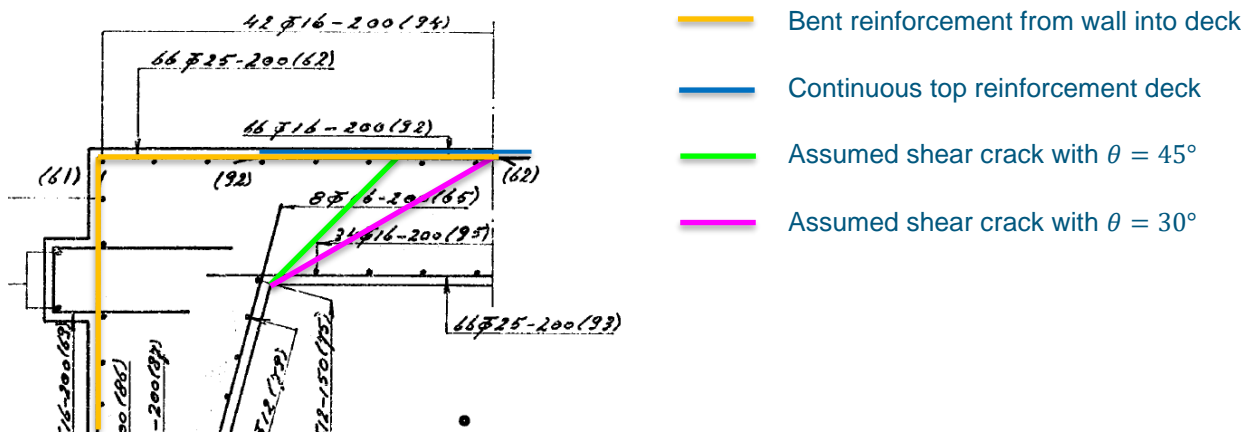
Figure 44 Detail of reinforcement in connection between wall and deck of structure DATA-021

4.3 Importance of material research

Concrete strength class

Table 13 of the previous paragraph shows that for the chosen calculation method, 6.2a according to RBK and 6.2b according to EC with the addition of the plate factor k_p, shear force is governing in almost two thirds of the investigated cases. The concrete strength class, which is included in both 6.2a and 6.2b, has a direct influence on the shear force capacity. The data analysis, described in chapter 2, shows that the concrete strength class is unknown for more than half of the structures studied. In general, the lowest concrete strength class from the design code with which a structure is designed must be used for the calculation. The data analysis also shows that the concrete strength class, on average a K300 or B30, is significantly above the minimum values from the design codes when strength class is known.

At the end of 2006, Rijkswaterstaat decided to make an inventory, published in (Rijkswaterstaat, 2007), of whether and which structures it manages built before 1976 have an increased risk regarding no longer meeting the requirements concerning brittle failure behaviour, including shear failure, which concluded that about 1.200 structures had an increased risk. To this end, project "*Dwarskrachtproblematiek Betonnen Kunstwerken*", reported in (Rijkswaterstaat, 2008), was set up in which the structures concerned were assessed to determine the extent and nature of the increased risk. Within this large-scale study, the concrete strength of the existing structures built before 1976 was investigated. For concrete slab constructions a strength of C35/45 appears to be exceeded only with a chance of 10%, which is accepted, resulting in a regulation in RBK. According to RBK 3.1.2 (10) 2. for structures built before 1976, a concrete strength class C35/45 may be used for slabs, boxes and tunnels, which is related to this research. The compressive strength of C35/45 is higher with $f_{ck} = 35 \, N/mm^2$ than that of the often used K300 with the EC-based value of $f_{ck} = 19 \, N/mm^2$, which leads to a difference factor 1,22 in $V_{Rd,c}$ 6.2a and 1,36 in $V_{Rd,c}$ 6.2b. The positive influence on the shear capacity can therefore make the difference for many structures. The higher concrete

strengths which are now found from tests than the original calculation value, based on 28 days, is due to ongoing hydration, which further increases the strength. A similar study of the concrete compressive strength has also been carried out among structures managed by local authorities. Due to a large spread in the results obtained, in combination with a higher percentage of structures for which no information is known, the concrete strength class to be used for a structure of the local authorities may only be a C16/20 if the concrete strength class is unknown as stated in CUR 124 section 6.2.This means that in many cases the calculated shear force capacity for structures of local authorities is relatively low. If two exact the same structures were assessed, one based on RWS management and the other from local authorities, then in the case of a K300 concrete the calculated shear capacity for a structure under the management of a local authority would have 26% lower calculated shear capacity than the same structure in the management of RWS, purely because of the concrete compressive strength that can be taken into account. When the concrete class is unknown, the calculated shear capacity is even 32% lower for the same structure.

The effect of the concrete strength class to be used is also visible in the results, shown in Table 15, of the calculated structures from the dataset. For structures owned by local authorities, based on the available data, shear force is relatively more often governing, which leads to more frequent disapproval, UC>1,0, of a structure. However, this statement has limited reliability because it is based on a limited amount of data. To reinforce this statement, two assessments were made for Cat II-based structures, once according to RBK and once according to CUR124, varying in span and soil cover. The results of the calculations comparing RBK with CUR124 based on UC of theoretical structures is shown in Figure 45.

Table 15 Overview of calculation results of 33 objects from dataset, calculated with the analytical model

		Structures owned by RWS		Structures owned by local authorities	
Number of structures in dataset		25		8	
U.C. > 1,0	Total	3	12%	4	50%
	Shear	1	33%	3	75%
	Bending	2	67%	1	25%
Governing shear		14	56%	5	63%
Governing bending		11	44%	3	37%
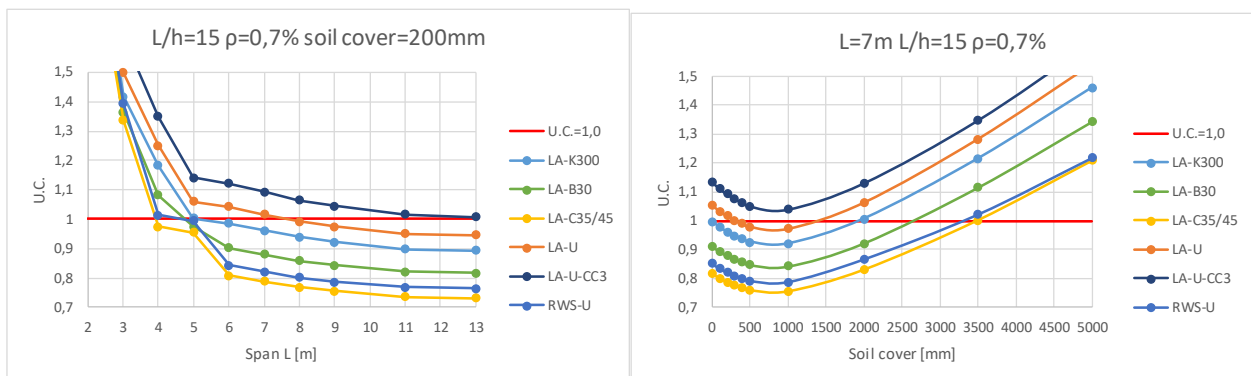
Figure 45 Comparing UC of same Cat II-based structures calculated for RWS and local authorities with different concrete quality

In the left-hand graph of Figure 45 the UC of a theoretical structure is plotted for different span lengths, whereby the difference in ownership between RWS and local authorities is made clear. For RWS, the assessment level 'use' and CC3 was used, for local authorities, assessment level reconstruction and CC2 were used. The load factors were therefore assessed in favour of structures for local authorities. For small spans the UC in this graph increases quickly above 1,0, this is because the fixed slenderness creates

unrealistic thin decks. In practice, for most constructions a lower limit of approximately 300mm applies to the thickness of the deck, which in this graph would mean a cut-off at a span length of approximately 5m. It should also be noted that the same haunch, with length and thickness of 300mm, was used for all spans, this ensured with RWS data that bending moment was decisive for short spans, hence the plateau where redistribution ensures equal U.C. At local authorities, shear force remained the norm due to low concrete strength. According to the RWS assessment, the UC is around 0,8 for the examined structure with spans from 6m onwards, while the UC remains critical around 1,0 according to local authorities' assessment. In the right-hand graph of Figure 45 the UC of a theoretical structure is plotted for different soil cover thicknesses. The graphs are the same in shape, mainly shifted, for both cases the UC initially decreases by increasing the soil coverage after which a tipping point is reached, in this specific case around 800mm soil cover, after which the UC increases again. The decrease in small coverages is due to the load distribution of TS from LM1, at a certain point the extra distribution due to soil no longer outweighs the added weight on the deck and the UC goes up again. The effect of different assessment is significant again, for these variations most structures for RWS would suffice, while the same structures would not suffice for local authorities in case of an unknown concrete strength class. A large variation in the test results was found in the investigation of the concrete compressive strength among structures of local authorities, therefore there is a good chance that a higher concrete compressive strength than C16/20 will be found by testing of the concrete of an individual structure owned by local authorities. The data analysis from paragraph 2.4 shows that K300 under the GBV 1962 and B30 under the VB 74 were often used. Figure 45 shows that the UC decreases significantly if tests show that a higher quality than C16/20 is present. Research into the compressive strength, and thus the strength class, of the concrete of a specific structure owned by local authorities offers serious possibilities if initial calculations show that the structure does not comply with shear force in case the concrete strength class is unknown.

Paragraph 4.2.1 shows that the concrete strength class also has a significant influence on the required anchoring length l_{bd}, regardless of which steel grade is used. Although it appears from paragraph 4.2.3 that 96% of the structures analysed have fully anchored reinforcement, in practice it may occur that the reinforcement is not fully anchored, which means that a reduced capacity must be used for calculating, which may result in disapproval of a structure. If the concrete strength class for such a construction is unknown, an investigation into the concrete strength class offers an opportunity to take into account a better anchoring of the reinforcement, which increases the calculated capacity and the construction may be approved.

Steel grade

The data analysis in paragraph 2.4 shows that, in contrast to the concrete strength class, the steel grade is often, for 73% of the investigated structures, known. In case the steel grade is unknown, it is in practice much more difficult to find out the steel grade than the concrete strength class. When the steel grade is unknown, this only has a direct negative effect on the moment capacity, because it has been decided not to adopt the favourable effect on the lower limit formula for the shear force capacity, formula 6.2b, through the arithmetic release of the tensile strength f_{yk} from RBK, of which the background is described in section 4.1.1. If the steel grade is unknown, the lowest steel grade according to the original design code must be assumed. These low strengths as QR22 and QR24 not only have a significantly lower yield strength f_{yk}, but are also designed as plain reinforcement which usually requires a longer anchorage length l_{bd} for full anchoring than the stronger but ribbed QR40 and FeB400 steel grades, as can be seen in Figure 39 from paragraph 4.2.1. If, due to a longer required anchorage length l_{bd}, the reinforcement cannot be considered as fully anchored, this has an indirect negative effect on both the moment and shear force capacity because a reduced cross-sectional area of the reinforcement steel $A_{s,red}$ must be used in the strength calculation. QR32 is the first steel grade after QR24 for which it can be assumed that it is designed as ribbed steel. The steel grade may be difficult to determine, but it is relatively easy to determine whether the reinforcement used contains plain or ribbed steel. If research shows that the steel used is ribbed, a QR32 can be assumed.

The data analysis from paragraph 2.4 shows that 82% of the structures investigated had ribbed reinforcing steel and from paragraph 4.2.3 it appears that in 96% of the investigated cases the reinforcement could be considered as fully anchored.
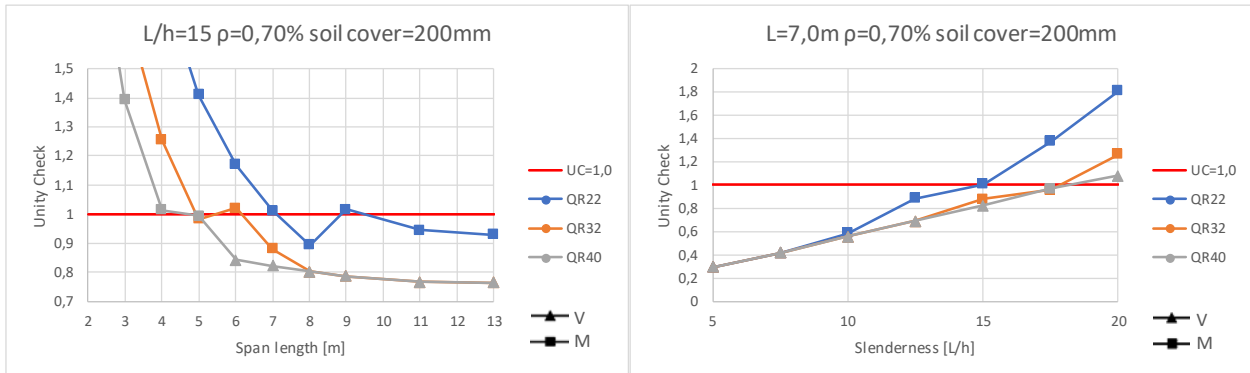
Figure 46 Comparing UC of same Cat II-based structures calculated as RWS-Usage-CC3 with different steel grades with fully anchored reinforcement (graphs partly overlap)

Figure 46 shows that for the same reinforcement ratio it makes no difference whether QR22 or QR40 is used as long as shear force is governing. The steel grade therefore has no direct influence on the shear capacity, which is also evident from the formulas. A higher steel grade with the same reinforcement ratio for the tension reinforcement does have a significantly higher moment capacity. As can also be seen from paragraph 4.4.1, bending moment is generally governing for low steel grades, like QR22 and QR24, and both shear force and bending moment can be governing for higher steel grades. When the reinforcement layout is known but the steel grade is unknown, so a comparison with the same reinforcement ratio, the steel grade has a significant influence where determining whether plain or ribbed reinforcement steel is used can be of great advantage. However, from the data analysis it appears that it is not often the case that the steel grade is unknown while the reinforcement layout is known. In case the steel grade is unknown, it can in principle be deduced based on the calculated UC for bending moment whether QR24 or QR40 has been used.

4.4 Results of analytical model

4.4.1 Parameter studies

Failure mechanism with ribbed or plain reinforcement bars

Based on the literature, it is expected that the applied steel grade, where mainly the use of plain or ribbed reinforcing steel, is to a large extent decisive for the governing failure mechanism bending moment (M) or shear force (V). To investigate this, the influence of steel grade QR40 or FeB400 compared to QR24 on the governing UC is examined for the three defined structure groups, Cat I to Cat III with clear-spans of 3,5m, 7,0m and 13,0m respectively, with changing slenderness of which the results are shown in Figure 47 to Figure 49. A relatively limited soil cover of 200 mm is used in the analysis because it is expected that bending moment will be governing for large soil covers due to limited load distribution of TS and a large proportion of UDL as a result of the dead weight of the soil.
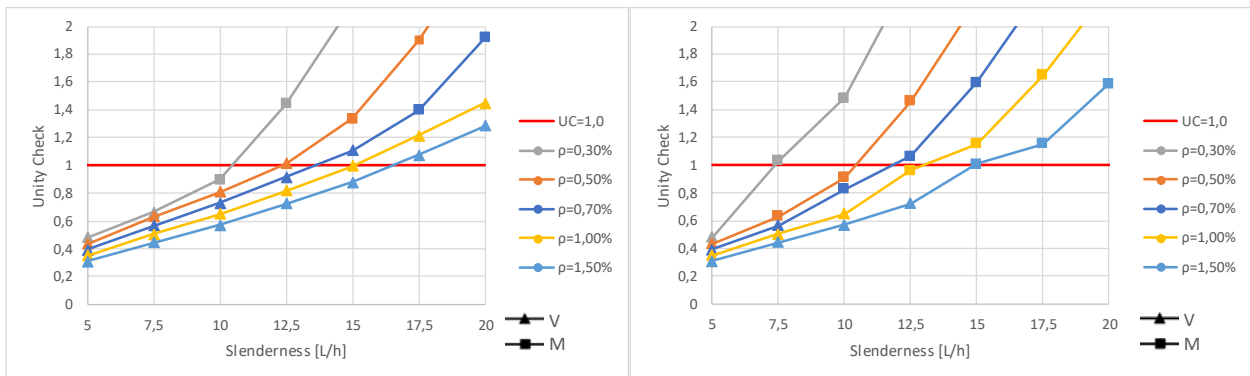
Figure 47 Sensitivity of slenderness and reinforcement ratio for RWS Cat I (L=3,5m) structures with 200 mm soil cover, C35/45 concrete and QR40 / FeB400 (left) and QR24 (right) reinforcement
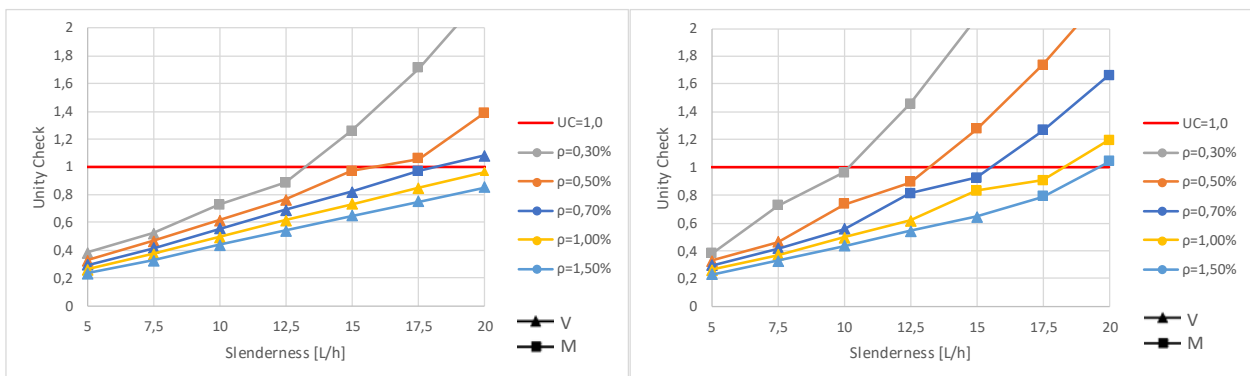
Figure 48 Sensitivity of slenderness and reinforcement ratio for RWS Cat II (L=7m) structures with 200 mm soil cover, C35/45 concrete and QR40 / FeB400 (left) and QR24 (right) reinforcement
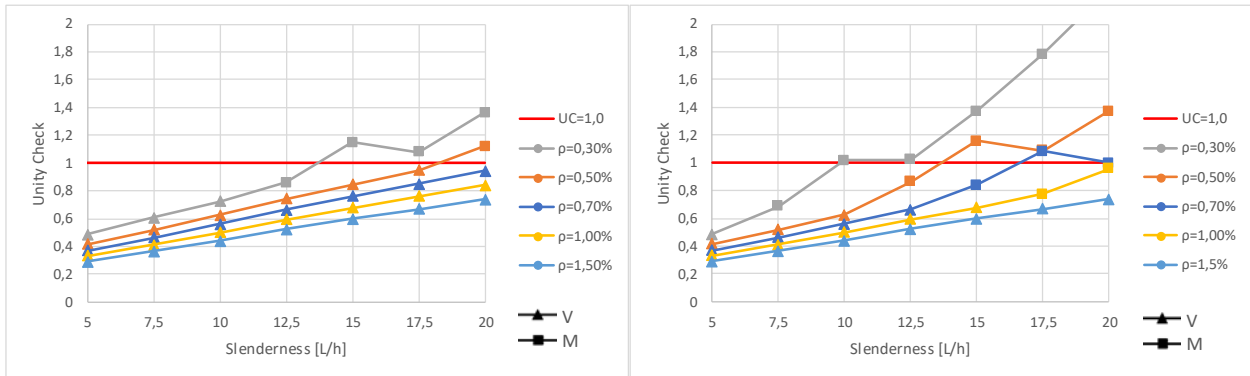
Figure 49 Sensitivity of slenderness and reinforcement ratio for RWS Cat III (L=13m) structures with 200 mm soil cover, C35/45 concrete and QR40 / FeB400 (left) and QR24 (right) reinforcement

With the same reinforcement percentage ρ_l, a lower steel grade does not result in a lower UC if shear force is governing. As soon as bending moment becomes governing, the lines for the UC for QR24 in Figure 47 to Figure 49 increases faster than for QR40 or FeB400. A relatively low tensile strength of QR24 provides a higher UC than higher steel grades in case of bending, since the moment capacity is determined by the moment equilibrium between tension in the reinforcement and pressure in the compression zone of the concrete. As shown in Figure 47 to Figure 49, generally bending moment is governing for soft steels such as QR22 and QR24. If bending moment becomes governing for an increase in slenderness, a kink in the line can be seen in Figure 47 to Figure 49, this kink is caused by redistribution of the bending moment at the moment the reinforcement starts to yield. The bending moment is redistributed up to 20% so that the UC can be more favourable after redistribution.

However, in the past structures were mainly designed based on bending moment, so when a higher steel grade was used, much less steel was used to absorb the tensile force resulting from the calculated bending moment. Figure 50 shows the UC for the same construction with different steel grades but with different reinforcement ratios based on the same tensile strength per meter width of the slab.
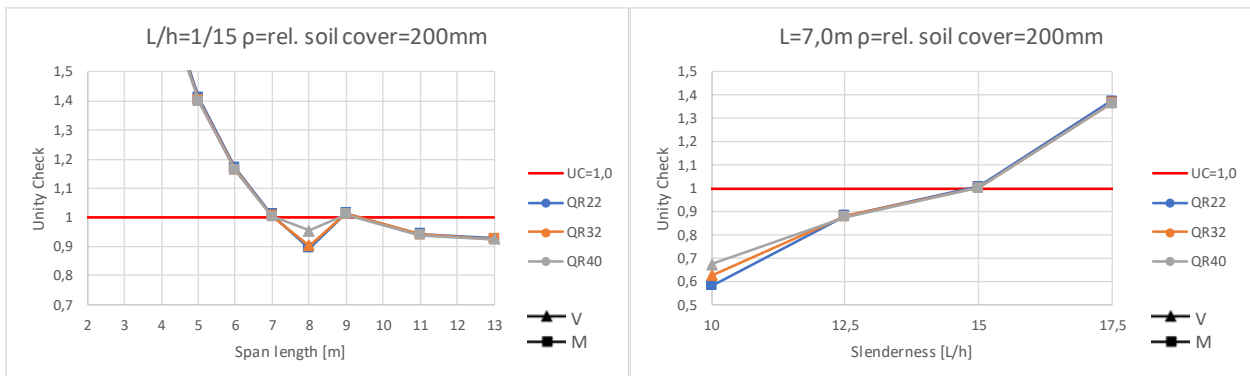
Figure 50 Comparison of the UC with different steel grades with same tensile strength per meter width of the slab for Cat. II based structure owned by RWS with C35/45 concrete. Lines partially overlap.

Figure 50 shows that it indeed occurs that when a higher steel grade with the same moment capacity is used, a higher UC for the shear capacity is found due to a limited proportion of reinforcement steel ρ_l.

Failure mechanism with small or large soil cover
As was shown in paragraph 3.4.3 by Figure 37 d), the TS has a large share in the load effect of the deck of an underpass or culvert with limited soil cover and is therefore decisive for the section forces that occur. As can be seen from paragraph 3.4, a larger effective width b_w for TS as a result of larger soil cover results in

a significant decrease in the shear force to be accounted for. At the same time, more deadload is added to the deck when a thicker soil layer on top of the deck is applied. The influence of the soil cover on the governing UC and mechanism has been further investigated for the structure categories with clear-spans of 3,5, 7,0 and 13 meters as defined in section 3.2.4, the results of which are shown in Figure 51 and Figure 52.
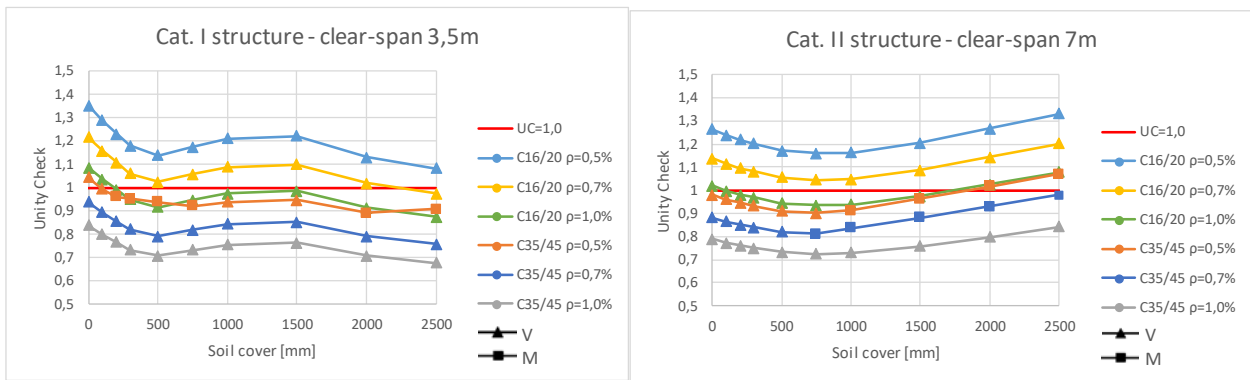
Figure 51 Influence of soil cover for RWS Cat. I (left) and RWS Cat. II (right) structures with QR40 / FeB400 reinforcement
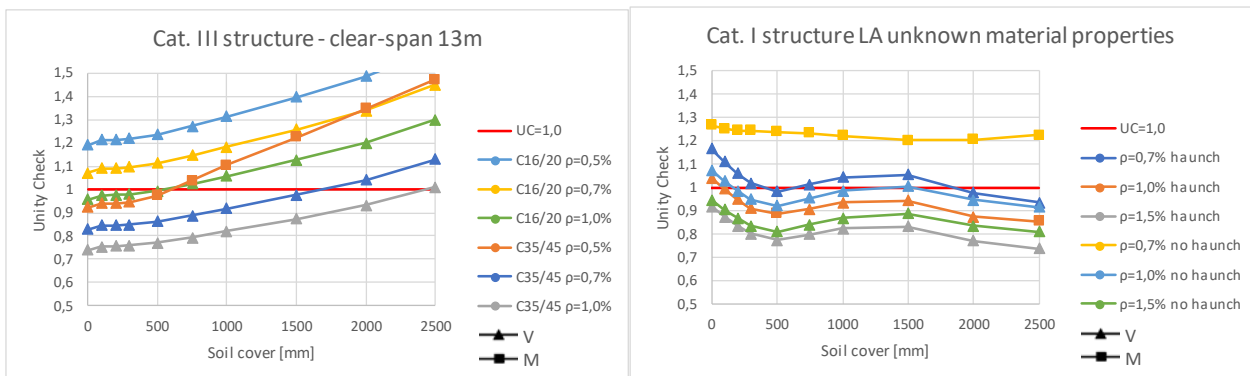
Figure 52 Influence of soil cover for RWS Cat. III structures with QR40 / FeB400 reinforcement (left) and Cat. I structures of Local Authorities with unknown material properties resulting in the use of C16/20 concrete and QR22 reinforcement for GBV 1962.

The three different structure categories show a different effect on an increase of the soil cover. For structures with a limited span, such as those of Category I, an additional effect occurs resulting in a different course of the graph. Initially, the UC decreases because more load distribution for TS occurs with a soil cover up to 500mm, but due to the limited span, a limit for the effective width b_w is quickly reached, so that the shear force due to TS does not decrease and the UC increases again as a result of additional dead load from the increased thickness of the soil layer on top of the deck. Ultimately, the UC decreases again because the distribution of TS through the soil reaches a point that part of the load no longer ends up on the considered deck, resulting in the undulating course of the graphs for category I structures. In theory with even greater coverage, the UC will increase again due to the high ground pressure. For the calculated variations of Category I structures from Figure 51, load combination according to 6.10b is governing, even with large soil cover. For underpasses and culverts with an average clear-span, Category II with 7m, an increase in soil coverage initially, up to approximately 750mm, will generally cause a drop in UC due to distribution of TS after which the UC will increase due to the dead load of the soil layer on top of the deck. However, the effect of load distribution of TS on the UC is smaller than with the Category I construction because the negative effect of the added deadload is relatively larger due to the increased span length. With large soil cover, both bending and shear force can be governing, which strongly depends on the concrete strength class. For the calculated variations of Category II structures from Figure 51, load combination according to 6.10b is

decisive. From previous calculations it appears that for such a construction 6.10a becomes governing from approximately 3,5m soil cover, where the applied assessment level also has a small influence due to the difference in the ratio of the load factors for deadload and traffic load. With large spans, such as Category III structures with a clear-span of 13m, the beneficial effect of load distribution of TS is smaller than the negative effect of the increased deadload with an increase of the soil cover, so that the UC does not decrease when the thickness of the soil cover is increased. For these structures with relatively large spans and the use of relative high steel grades, like QR40 or FeB400, shear force is mainly governing, bending can be governing for high concrete strength classes with a low reinforcement ratio. The relatively large span also ensures that load combination 6.10a with a smaller soil cover already becomes governing over 6.10b, namely from approximately 2,5m. Based on the found soil cover on structures in the data analysis from paragraph 2.4, load combination according to 6.10b will therefore be governing over 6.10a for most underpasses and culverts.

It is also investigated what the sensitivity of soil cover is on the UC of typical municipal structures, namely bicycle tunnels with a relatively small span with often an unknown concrete strength class and steel grade. The data analysis shows that it mainly occurs with small spans that no haunch is applied, therefore the influence on the UC for this type of construction is briefly investigated. Because shear force is often governing for these short spans, the lower steel grade to be used has no effect on the UC if shear force remains governing, which in most situations is the case with the same reinforcement ratio. With a relatively low reinforcement ratio for QR22, it can be seen that bending becomes decisive if no haunch is present, the moment capacity at the face of the supportive wall is significantly smaller due to a smaller internal lever arm in the absence of a haunch, resulting in the sum of the capacity of the sagging and hogging moment becomes smaller and redistribution cannot offer a way out. When no haunch is present, which is as long as thick with the same thickness as the deck so that the thickness in the section at the face of the wall is twice as large as at the end of the haunch and shear force remains governing, then the increase in the UC for the examined structures is only 5%. The limited increase of the UC for shear force is because the shear force due to TS is decisive, which in most cases is the same for the section at the face of the wall and the section at the end of the haunch because the control section is placed $2d$ out of the face of the wall, see paragraph 3.4.

Again, as in paragraph 4.3, it is clearly visible that the lower concrete strength class C16/20 ensures that shear force becomes governing in most cases. It is also visible that in the case of a C16/20 approximately twice as much longitudinal reinforcement, in terms of ρ_l, must be present to achieve the same shear capacity as a C35/45, when using QR40 or FeB400 reinforcement steel.

4.4.2   Structures from data

During the research, there are 64 structures in the database. Not all underpasses and culverts in the dataset can be assessed based on the Analytical model, of 23% of the structures insufficient data is available to perform a verification calculation and 25% of the structures have an intersection angle less than 80gon, which is approximately 72°, for which a model with beam elements would give too large deviations in the calculated section forces and is therefore not suitable. Of the total of 64 underpasses and culverts, it is possible to assess 33 structures with the analytical model. provides an overview of the development of the number of structures assessed with the analytical model.

Table 16 Overview available structures for assessment with Analytical model

	Number of structures	Share
Total number of structures in dataset	64	100%
Insufficient information available	15	23%
Intersection angle < 80gon	16	25%
Calculable with analytical model*	33	52%

*Assuming fully anchored reinforcement, for 27 structures (82%) anchorage was checked of which 96% was fully anchored

Figure 53 provides an analysis of the UC of the calculated underpasses and culverts with the failure modes and the critical cross-sections, the distribution of the UCs is shown graphically in the accompanying graph.
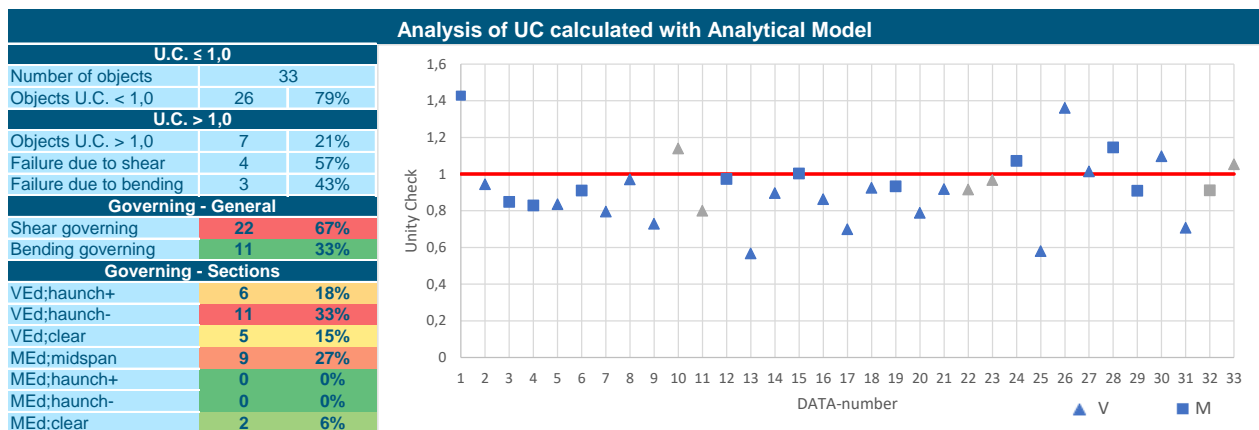
Figure 53 Analysis of UC for structures calculated with the Analytical model. Grey data points are structures for which the anchoring has been assumed as fully anchored.

Based on the calculations performed with the Analytical model, 79% of the calculated underpasses and culverts have a UC≤1,0, so a large part of the structures can be handled quickly and easily. Of the remaining 21%, which are disapproved based on the calculation with the analytical model, the distribution between bending moment and shear force as a determining mechanism is approximately equally divided with 43% and 57% respectively. On average, a fairly critical UC of 0,93 is found, but when only looking at the UC of the structures that are approved, the mean UC is 0,86. When a structure is disapproved it has on average an UC of 1,18, where some structures have just not been approved and other structures have a UC well above 1,0, as shown in Figure 53. Of the investigated culverts and underpasses with the analytical model, the mean UC where bending moment is decisive is 1,00, while for structures where shear force is governing it is slightly lower with an average UC of 0,89.

Figure 54 presents the number of structures in the database, for which a structural assessment with the analytical model is possible, compared to the number of structures with a UC > 1,0 per design code, where in addition a distinction is made between a UC > 1,0 due to bending moment and shear. The table shows that, just as in the data analysis from paragraph 2.4, the available data is concentrated in the period of the GBV 1962 design code, which can be logically explained by the wave of construction from that period as was shown in Figure 10 in combination with the end of the designed service life of structures from that period, as a result of which assessments are performed and research into the shear force problems was conducted by RWS.
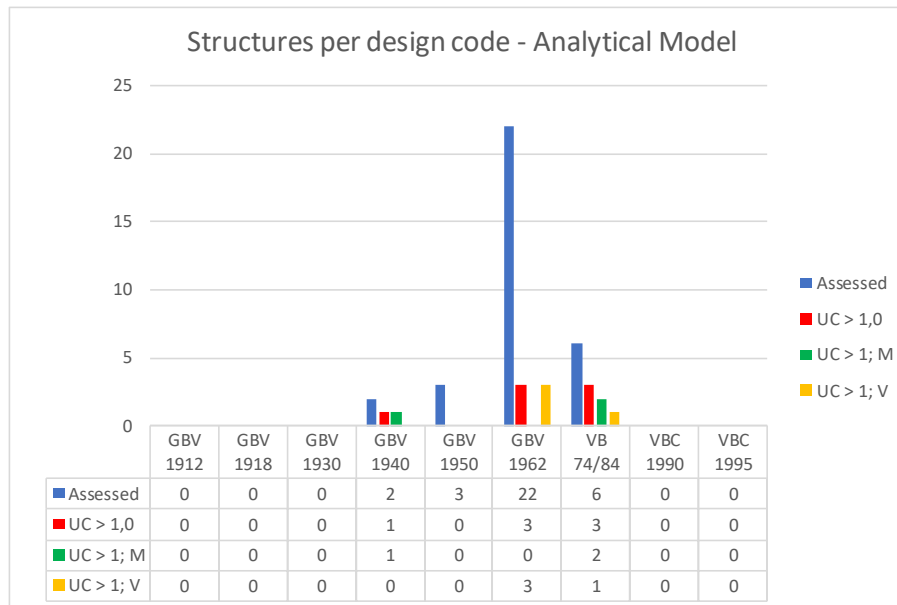
Figure 54 *Number of structures from database assessed with the analytical model per design code, showing the distribution of UC > 1,0 with associated failure mechanism*

The results from Figure 54 show that structures from the period before and after the GBV 1962 mainly are disapproved based on bending moment, structures from the GBV 1962 period are, in line with expectations as described in paragraph 2.3 based on the theory from the design codes, mainly disapproved on shear capacity. However, the number of structures with a calculated UC > 1,0 is relatively limited compared to the structures from VB 74/84, which are expected to be critical structures from the relevant period because they have already been assessed while it is expected that for a large part of the structures the designed service life had not yet been reached at the time these structures were assessed by RHDHV. However, the size of the dataset is so limited and the structures from the period of VB 74/84 only concern bicycle underpasses, that no general conclusion can be drawn about the entire set of approximately 12.500 underpasses and culverts in the Netherlands.

Comparing data results with available assessment reports

An old assessment report with the calculated UCs is available for several structures that have been assessed with the analytical model. The UCs from the available reports can be compared with the UCs obtained with the analytical model to further validate the analytical model and to investigate the distribution in the UCs from different reports of the same type of structures. A full report is available of 17 of the 33 structures calculated with the analytical model and the results are compared, shown in Table 17, and the distribution of the UCs is made visible in Figure 55.

Table 17 Comparison of assessment results from data reports and the analytical model

DATA reports			Analytical Model		
Number of objects	17		Objects compared	17	
Average UC	0,94		Average UC	0,98	
UC ≤ 1,0			UC ≤ 1,0		
Objects UC < 1,0	13	76%	Objects UC < 1,0	11	65%
Average UC < 1,0	0,88		Average UC < 1,0	0,86	
UC > 1,0			UC > 1,0		
Objects UC > 1,0	4	24%	Objects UC > 1,0	6	35%
Average UC > 1,0	1,13		Average UC > 1,0	1,20	
Failure due to shear	3	75%	Failure due to shear	4	67%
Failure due to bending	1	25%	Failure due to bending	2	33%
Governing - General			Governing - General		
Shear governing	10	59%	Shear governing	11	65%
Bending governing	7	41%	Bending governing	6	35%

The mean UC calculated with the analytical model is with a value of 0,98 slightly (4,3%) higher than the average UC of all structures considered where the mean UC is 0,93. The fact that the more critical objects are within this subset is also evident from the higher percentage of structures that are disapproved, the absolute number is only one lower while only half of the number of structures is within this subset for which reports are available. The ratio for governing mechanism between shear force and bending moment is however the same, where about two thirds shear force is governing. The mean calculated UC for shear force with a UC of 0,93 is higher than the UC of 0,88 from the reports, a difference of +5,7%. For the bending moment, however, a slightly lower UC is found on average, 0,83 compared to 0,87, which is a difference of -4,6%.
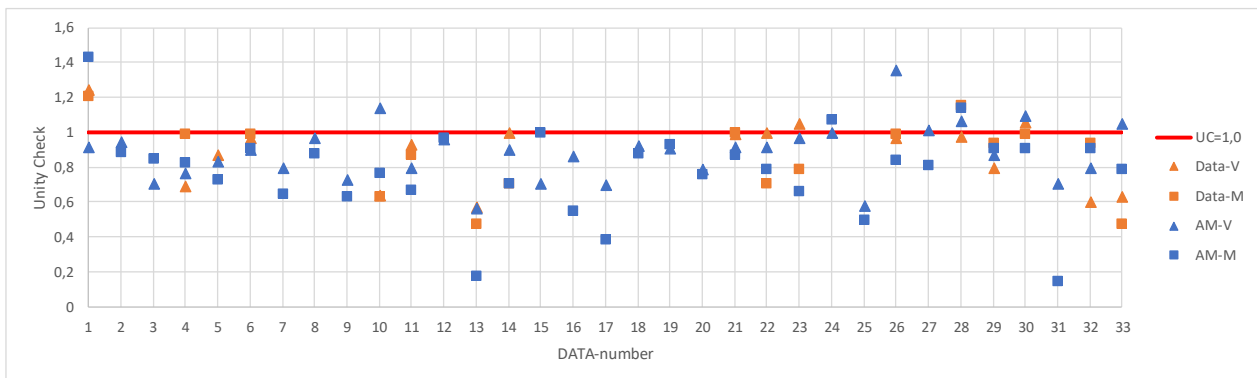
Figure 55 Unity Checks obtained from data reports compared with calculated Unity Checks from the Analytical model for both shear(V) and bending moment(M).

Based on Table 17 it appears that, on average, the results obtained with the analytical model hardly deviate from the results obtained and reported in the past. The average UC is slightly higher and more constructions are disapproved, which on the one hand is not desirable but on the other hand is more conservative and safer for a simple analytical model. In the reports of the performed assessments it appears that both 1D analytic beam models, 2D frame models with 1D member elements and 3D models with 2D plate elements have been made, where the 2D and 3D model are usually modelled in the FEM package SCIA Engineer. Looking at Figure 55, the differences per structure are visible and it appears that in some cases the calculated UCs are higher and in other cases lower again.

Data numbers 4, 6, 11 and 26 have a higher UC for bending moment in the reports than calculated with the analytical model, but it appears from the reports that these moments are not redistributed, which is allowed up to 20% because reinforcement with ductility class B has been applied, which means that these UCs can be lower, reducing the difference with the analytical model with regard to bending moment. Another reason why a higher UC is found in the reports is other significant load may be present which is not included in the

analytical model. This is the case for data number 11 for which a noise barrier, for which 35kN/m is used, has not been included in the calculation with the analytical model. Data number 23 is approved based on the analytical model but not according to the report from the data, a follow-up report from RHDHV, however, describes that the underpass will probably be approved with a good calculation and additional research. Remarkable is the very low UC for bending moment for the objects with numbers 13 and 31, but in those cases it concerns culverts with a small span of 1,4 and 1,5 meters both relatively heavily reinforced with Ø20-160. But it also happens the other way around, that a construction is disapproved based on the analytical model, but the report shows that an object is approved. A high UC for data number 1 for bending where QR22 is assumed because the steel grade is unknown. The remarkably high UC for bending suggests that a higher steel grade has been used, especially since in the past it was mostly designed based on bending. The remarkably high UC for shear force of data number 26 can be explained by the assumed C16/20 concrete because the concrete strength class is unknown from the design and the structure is the property of a province. In paragraph 4.3 it has been shown that this relatively low strength has a significant influence on the shear force capacity. In addition, a lower UC in the reports may be explained by the use of a more advanced model in a FEM package, typically a 3D model with 2D plate elements. Table 18 shows the distribution of the use of different model types in the available data.

Table 18 Distribution of different model types found in data reports

Model type	Objects	Share	$UC_{avg,reports}$	$UC_{avg,AM}$	Difference
1D analytical beam model	6	35%	0,95	0,93	-2%
2D FEM model, 1D beam elements	3	18%	0,87	0,98	+11%
3D FEM model, 2D plate elements	7	41%	0,97	0,94	-3%
3D FEM model, 3D solid elements	1	6%	1,25	1,43	+13%

No general trend has been found in terms of a higher or lower UC when applying a specific model type. Some reports are not comparable because additional load, such as a noise barrier, has been added, other load and safety factors have been used or in some cases there is strong doubt about the correctness of the modeling. However, in general it is expected that an analytical model or a framework model in FEM from the reports should yield the same or even slightly higher UCs and that with a model refinement to a plate model a reduction could be obtained by better modelling of load distribution.

4.5 Discussion

While performing the data analysis, as described in paragraph 2.4, it has been noticed that in some structures the top reinforcement just after the section at the end of the haunch is bent from the top to the bottom of the deck as bottom reinforcement. The change from top reinforcement to bottom reinforcement can ensure that the section at the end of the haunch is not decisive because in the section after bending the top reinforcement downwards there is significantly less top reinforcement present while it may still be possible that tension at the top of that cross-section occurs. However, the same data analysis also shows that the bending from top reinforcement to bottom reinforcement is only carried out in this way if very long haunches, with a length larger than approximately 1m, are used, so that the hogging moment in the section of the haunch is limited. Due to the occurrence of a limited hogging moment, or even a sagging moment, in the section just after the haunch it is not expected that bending of the top reinforcement to bottom reinforcement leads to problems.

Formula 6.2b for determining $V_{Rd,c,min}$ differs for RBK and EC, the difference in the constant factor in the v_{min}-formula has not yet been discussed. The difference in the constant factor in the formula for v_{min}, 0,83 for RBK and 0,77 for EC, can be traced to the assumption made for the internal lever arm z. RBK makes an estimate for z with $z = 0,95\ h$, while EC estimates this with $z = 0,90\ h$. This difference in internal lever arm leads to the difference in the constant factor in the formula for v_{min}, where a higher value leads to a higher calculated capacity. In paragraph 4.1.1, it is decided to apply the formulas from the EC with the addition of the plate factor k_p for this research. However, for slabs with reinforcement usually in the same layer and limited concrete coverage, the assumption of $z = 0,95\ h$ may not be too optimistic.

The angle of the compressive strut is assumed to be 45 degrees in accordance with current standards. Several conducted tests in (Muttoni, Rupf, & Ruiz, 2013) and (Olesen, Sozen, & Siess, 1965) show that this angle is more horizontal and tends more towards $\theta = 30°$, which would mean that the capacity is overestimated when using $\theta = 45°$. However, the tested beams and slabs nowadays always have stirrup reinforcement, which the RC slabs of the existing structures within the scope of this research do not have. The tests also made use of concentrated loads, while the loads on the deck mainly consist of distributed loads. In addition, tests have often been carried out on prestressed concrete, also in (Muttoni, Rupf, & Ruiz, 2013) and (Olesen, Sozen, & Siess, 1965), while prestressing also ensures a lesser angle. So, the question is whether the angle θ for RC slabs without shear reinforcement primarily loaded with distributed loads is 30 degrees.

Based on the models used, it would be expected that the results from the available reports of verification calculations with a 1D analytical beam model and a 2D FEM model with 1D beam elements would result in approximately the same UC as the analytical model described in chapter 3 and that a 3D FEM model, with 2D plate or 3D solid elements , results in a lower UC value. However, Table 18 from paragraph 4.4.2 shows this is not the case on average. What is particularly striking is that, on average, the calculated UC is 11% lower than the available calculations from reports with a 2D framework model, while the calculated UC is 3% lower than the UC from reports with a 3D FEM plate model. For comparison with a 2D framework model, only three calculation reports are available, of which two calculations, the correctness of which are doubted, come from one report set up by one engineer. The small average deviation found with the results of 3D FEM plate models is positive on the one hand because results from an advanced, more time-consuming 3D FEM model are achieved with an extensive but fast analytical model, on the other hand it raises questions about safety and reliability. First of all, one reason for the higher mean UC may be that in some cases additional load, such as a noise or wind screen, is accounted for in the model. In addition, one may wonder whether the 3D FEM plate models set up in the past are optimal or whether a minimal effort from the engineer for the modeling has been chosen because calculations have shown that the structure can already be approved.

In general, a fatigue check must also be carried out for existing concrete structures, but this check is not included within this research. The reason for choosing to disregard fatigue is that the preparation of a complete automated fatigue check is not within the time schedule of this research. The justification for this choice is threefold. First of all, according to NEN-EN 1992-2 art. 6.8.1 a fatigue check is generally not necessary for underground arch and frame structures with a minimum soil coverage of 1,00 m for road bridges. Secondly, with plain reinforcement, like QR24, the stresses are so low that fatigue will not be governing, which is to a limited extent also the case with the frequently used QR40 and FeB400 steel grades. It can also be stated that concrete pressure fatigue does not occur due to the increased concrete strength over time, certainly at C35/45.

For elements with a tapered height, such as the haunch in the deck, additional values are defined in the EC and EC 2020, shown in Figure 56, to account for the influence of inclined forces for the determination of the design shear force, replacing V_{Ed} by $V_{Ed} - V_{tcd} - V_{bcd}$.

a) internal forces at cross section   b) compression field, chord and prestressing forces
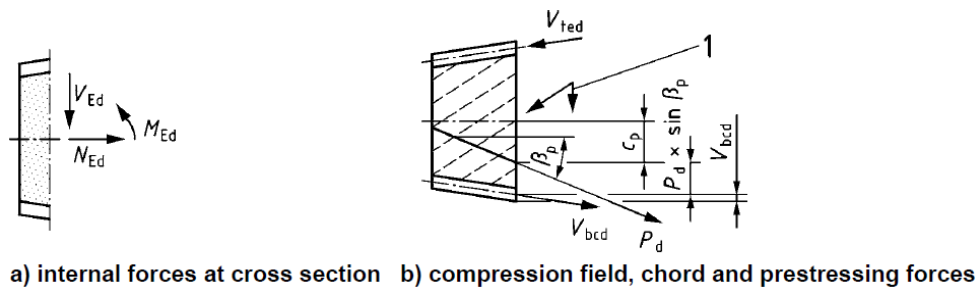
Figure 56 Shear components for members with inclined chords and/or prestressing (Source: Figure 8.4 EC 2020)

However, the favourable effect of V_{tcd} and V_{bcd} should, according to both EC and EC 2020, only be considered for members with shear reinforcement, which the concrete slabs in this research do not have. The favourable effect of a tapered height on the shear force as shown in Figure 56 is therefore not taken into account.

The shear capacity is increased by the arching effect, as demonstrated numerically in (Barten & 't Hart, 2018). By restraining the concrete slab by the walls and the surrounding ground, the slab is prevented from cracking, for cracks to occur in the slab the walls must deform but they are obstructed by the surrounding ground, a pressure arc is created in the slab through confinement whereby an increased shear capacity is achieved. This research does not take into account an increased shear capacity due to arching action, as the increased shear capacity must be demonstrated for which a non-linear FEA is required.

4.6   Conclusion

The relatively large difference in the calculated UCs and the governing mechanisms according to RBK and EC, presented in Table 13, is remarkable. It is expected that the shear capacity with formula 6.2b from RBK is overestimated, so that bending more often becomes governing, and that the EC underestimates the shear capacity for RC slabs, which is reflected in the high number of structures that would be disapproved based on the calculations performed. A confirmation is found in the draft versions of the new EC 2020 and NEN 8702 for the assessment of existing concrete structures. In the EC 2020 the yield stress f_{yk} is arithmetically released, so that a higher value of v_{min} is obtained for lower steel grades than FeB 500 and in NEN 8702 an increased shear force capacity with respect to EC is calculated by taking into account a plate effect but for both EC 2020 and NEN 8702 it applies that not both effects are applied at the same time. The remainder of this research is based on the current EC formula with the addition of the plate factor k_p, equivalent to the draft version of the NEN 8702.

If the angle $\theta = 45°$ for the concrete strut is maintained, it applies to 96% of the investigated structures that the reinforcement can be considered as fully anchored. Multiple tests, like shown in (Muttoni, Rupf, & Ruiz, 2013) and (Olesen, Sozen, & Siess, 1965), suggests that near supports a more conservative value of $\theta = 30°$ should be used. Maintaining $\theta = 30°$ resulted in an increased UC in more than 20% of the structures studied. A critical point that must be taken into account in the determination of the capacity is the bent reinforcement from the wall in the deck, this often does not extend far while there is significantly less reinforcement, resulting in a discontinuity, whereby the bent reinforcement must be partially anchored. Having to anchor main reinforcement at a location in the structure where potential shear cracks may occur can lead to dangerous situations. However, the tests were carried out with prestressed beams or slabs with stirrup reinforcement and concentrated loads, while the slabs in this study are not prestressed, have no stirrup reinforcement and are mainly loaded with distributed load, besides the current regulations do not say anything about an adjusted angle θ near supports, for which the standard $\theta = 45°$ has been maintained.

For structures managed by local authorities, such as provinces and municipalities, it often happens that the concrete strength class is unknown. The CUR 124 describes that research has found a large spread in concrete strength class of structures from local authorities, so that the relatively low EC concrete strength class C16/20 may be used if the concrete strength class is unknown. Because the distribution is so large, and a lower limit is maintained, there is a good chance that a significantly higher concrete strength will be found when testing concrete cylinders of an individual structure. The concrete strength class has a major influence on the shear force capacity, as it appears from calculations that for many structures the calculated normative UC dips just below the critical limit for the, based on the data analysis from paragraph 2.4, commonly used design concrete strength classes K300 and B30 in comparison with the C16/20 to be maintained. Research into the compressive strength of a specific structure owned by local authorities with an unknown concrete strength class offers serious possibilities if initial calculations show that the structure should be disapproved based on the calculated shear capacity. In contrast to RWS, in the CUR124 no distinction is made in the type of structure, perhaps the distribution in found concrete strengths becomes more limited when testing per structure type.

5

Load effect by Finite Element Method

This chapter examines the added value of a FEM model for the structural assessment of existing RC underpasses and culverts. First, the influence of additional effects that are not included in the analytical model is investigated based on FEM Model 1 - Framework. A further model refinement to FEM Model 2 - 3D space with 2D plate elements with enhanced load distribution is investigated and allows to analyse structures with intersection angle smaller than 80gon. The results of both FEM Model 1 and FEM model 2 are compared with the results of the analytical model.

5.1   FEM Model 1 – Framework

With a framework model in a finite element program, the influence of additional effects, which are not included in the analytical model, can be investigated relatively quickly and easily without having to build complex models. The effects of soil around the structure in the form of a modulus of subgrade reaction, a pile foundation, internal traffic, an increased stiffness and change of neutral line due to the presence of a haunch and loads from impact slabs are investigated. Note that model refinement from the analytical model to a framework model does not gain anything in terms of the occurring shear force. The influence of the additional effects is investigated based on a sensitivity analyses performed on three structures from the dataset for which bending moment is governing according to the analytical model and thus potentially benefiting from a model refinement where additional effects can be included. A total of five different model variants are made to investigate the influence of the model, the models are shown in Figure 57. Note that for each individual additional effect separate models have been made to isolate the considered effect, for which a total of 165 different models were made for this sensitivity analysis.
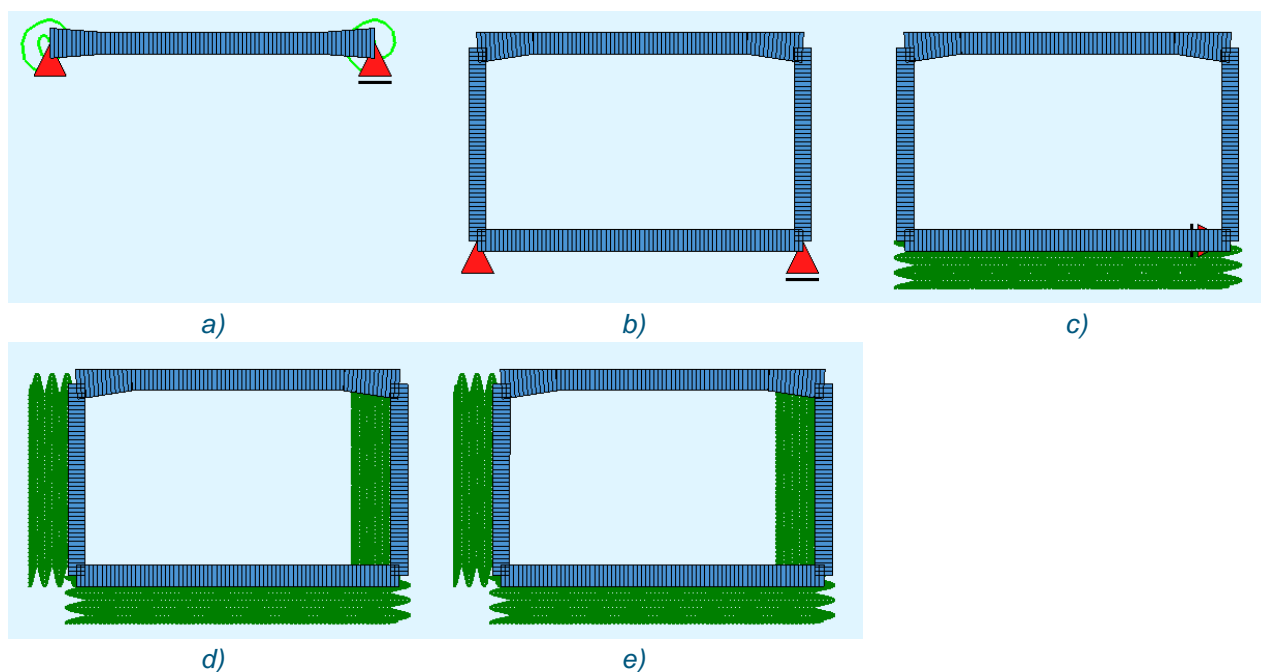
Figure 57 Model variants with 1D beam elements. a) 1D beam, b) 2D framework – fixed supports, c) 2D framework – bedding floor, d) 2D framework – bedding floor/wall ratio 1/1, e) 2D framework – bedding floor/wall ratio 2/1 (SOFiSTiK)

The 1D beam model acts as an additional verification of the analytical model in the ASA Tool. The 2D framework model with fixed supports is used to obtain the isolated effect of the floor slab, as the analytical model assumes complete clamping of the wall by the floor slab. The other variants provide insight into the difference in behaviour due to the soil around the structure. The variant where the stiffness of the soil, and thus the stiffness of the bedding, has a ratio between wall and floor of 1:2 is seen as the most realistic due to neutral soil pressure.

Modulus of subgrade reaction

The load-bearing capacity of the subgrade, consisting of the subsoil and the possible presence of a sand bed or foundation layer, is expressed in the modulus of subgrade reaction k. The modulus of subgrade reaction k is defined as the ratio between the pressure delivered by the subgrade and the settlement of an elastic plate, in this case the floor of an underpass or culvert, under a vertical load. In the model this means that a plate is linearly elastically supported with a spring stiffness equal to the modulus of subgrade reaction k. Determining the constant k is time-consuming and expensive because static plate load tests must be carried out on site, therefore such a soil mechanical investigation for the assessment of an existing structure is actually never done. Table 19 gives an indication of the modulus of subgrade reaction k for various types of subgrade, showing that there is a large spread in k, both between different subgrade types and within a type of subgrade.

Table 19 Global values of modulus of subgrade reaction k for various types of subgrades (source: (Vereniging Nederlandse Cementindustrie, 1993))

Subgrade	Modulus of subgrade reaction [MPa/m]
Well graded gravel and gravel/sand mix, hardly any fine material	80 – 130
Poor graded gravel, hardly any fine material	80 – 130
Gravel/sand/clay mixtures	50 – 130
Well graded sand and sand with gravel, hardly any fine material	50 – 100
Poor graded sand, hardly any fine material	40 – 100
Sand/clay mixtures	30 – 80
Very fine sand, sand with loam	30 – 50
Vast clay	10 – 30
Weak clay and peat	0 – 10

Based on Table 19, four values for k are taken for the sensitivity analysis, $k = 25 MPa$ representing a clay layer, $k = 50 MPa$ representing a layer with a mixture of sand and clay, $k = 75 MPa$ representing a layer of sand with gravel and a sound foundation layer with $k = 100 MPa$. The results of the sensitivity analysis on the modulus of subgrade reaction k are shown in Figure 58.

a)

b)

c)
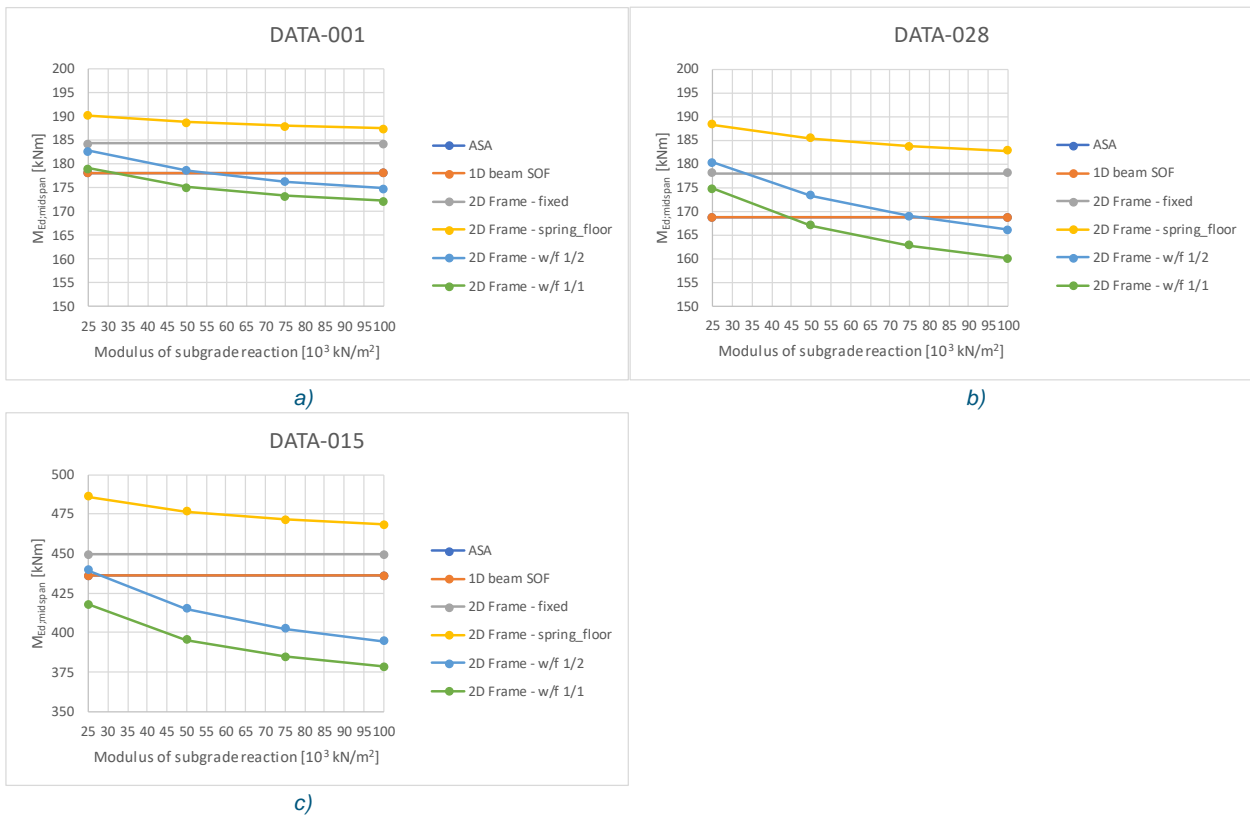
Figure 58 Influence of the modulus of subgrade reaction on the sagging bending moment in the span. The lines of the analytical model from ASA and the 1D beam from SOFiSTiK coincide.

Figure 58 shows based on an average 4% higher calculated sagging moment in the span for the framework with fixed supports that the clamping of the wall by the floor in the analytical model is assumed to be too stiff. When only calculating with a bedding under the floor, so with free walls, the moment shifts about 8% more to the span compared to the beam model. By adding an elastic horizontal support to the walls, the walls react stiffer to the vertical load on the deck and the moment shifts from the span to the support. The moment distribution of the framework with a ratio 1:2 between the k-values of the wall and the floor compared to the analytical model differs per structure, it cannot be said that a decrease in the sagging moment is always realized. For the most realistic k-values, however, based on the data from Figure 58, an equal value or a limited decrease of approximately 5% of the ratio between the sagging moment and the hogging moment will be expected. For structures with a large span or a large wall height, this error can be up to about 9%, but especially conservative because the moment in the span is smaller. A smaller sagging moment in the span is conservative because for structures where bending moment is governing, the moment in the span is in most cases, 82% based on Figure 53, critical.

Pile foundation

The data analysis in paragraph 2.4 shows that 14% of the structures investigated are founded on piles. The foundation piles are generally located under the walls because the top load is transferred down through the walls. The piles are usually made in pairs in opposite slanting positions to absorb horizontal forces. Because a detailed analysis of the foundation falls outside the scope of this study, the modeling is based on vertically oriented springs below the centreline of the walls where the spring stiffness is varied only to investigate the sensitivity of this parameter to the load effect. The results are comparable to the results of a shallow foundation with the modulus of subgrade reaction. For structures DATA-001 and DATA-028 the influence is very limited with less than 5%, for the structure DATA-015 the influence is more significant with a decrease of the sagging moment from 3% up to 10% compared to the analytical model. The graphs are similar to the

graphs in Figure 58, with the exception that no difference in moment distribution occurs between a 2D framework model with fixed supports and a 2D framework model where only the piles, independent of the stiffness, are modelled.

Internal traffic

In the data analysed, half of the structures concerned an intersection where mixed traffic passes through the underpass, approximately one third of the structures investigated concerns a bicycle underpass and in approximately one-sixth of the structures a culvert. A large part of the structures must therefore be calculated on internal traffic, especially since bicycle underpasses often also have to be calculated on a service vehicle. In addition to internal traffic, a hydrostatic load may also be present in the case of a culvert, but because culverts are generally smaller, the effect of internal hydrostatic load is expected to be smaller than that of internal traffic load based on LM1. If the effect of internal traffic is already negligible, it has no added value to investigate the effect of a hydrostatic load. The traffic load of LM1 has been investigated for two variants, one with minimal load distribution so that TS is regarded as separate loads and a variant where the UDL and TS from LM1 are distributed over a uniform load over the entire free space between the walls.

There is a clear difference in results between the 2D framework model with fixed supports or vertical springs, representing a pile foundation, with the addition of an elastic horizontal support of the walls, and the 2D framework models representing a shallow foundation. With a shallow foundation there is hardly any influence on the moment distribution as a result of internal traffic, both for a uniform load and a UDL with local loads of TS, with approximately 1% extra reduction in the sagging moment in the span compared to the 2D framework model with shallow foundation without internal traffic. The explanation for this is that an elastically supported plate with a uniform spring stiffness and a uniform load only undergoes a vertical displacement without bending, so that the moment distribution is not affected. In the case of a pile foundation, the influence is more significant because the reaction comes from the edge of the floor slab, while the internal traffic, whether concentrated or not, can be placed in the middle of the floor slab. For the structures studied, internal traffic with a foundation on piles results in a shift from the sagging moment to the hogging moment from 5% up to 14% compared to the 2D framework model without internal traffic.

Increased stiffness and change of neutral axis due to haunch

Due to the presence of a haunch, the thickness of the deck changes locally so that the stiffness is locally increased and the course of the neutral axis changes. Because the deck is part of a statically indeterminate system, a local change of the stiffness has an influence on the moment distribution, an increase of the stiffness near the support due to the extra height of the haunch causes a shift of the bending moment from the sagging moment in the span to the hogging moment above the supporting wall. A second effect of the presence of a haunch is that the neutral axis of the deck is not completely horizontal, the haunch creates a kink in the line, after which the axis continues under a slope up to the neutral axis of the wall. The oblique course of the neutral axis of the deck has an influence on the total moment that occurs, as this becomes smaller because part of the load is transferred via normal force.

The modeling of a gradient height of the deck results in a shift of the occurring moment with a large scatter from 5% to 23% in the structures studied. The influence of a locally increased stiffness due to the presence of the haunch depends on the geometric relationship between the deck and the haunch, but short spans with a thick haunch can have a significant influence on the moment distribution. The decrease of the total bending moment, the sum of the sagging moment and the hogging moment, due to a not completely horizontal course of the neutral axis of the deck also depends on the geometry. A reduction of the bending moment of 3% to 16%, resulting in a lower sagging moment from 4% to 11%, has been found for the structures studied. A combination of both effects results in a reduction of 11% to 18% of the sagging moment in the span compared to the 1D beam model. The effects of a locally increased stiffness and a change in the course of the neutral axis are correlated with each other, the sum of the isolated effects does not result in the result obtained with an analysis in which both effects are included. For the structure DATA-001 combining the two effects does not result in a larger shift of the moment, adding a gradient height results in a significant shift of 23% for this structure and the oblique neutral axis in a shift of 4% while the combination resulted in a shift of only 18%. Not in all cases combining a gradient neutral axis with and a gradient stiffness therefore results in a larger shift than either of the two individual effects.

Impact slab
Impact slabs are a transitional structure between the road in which an underpass or culvert is situated and the deck of the underpass or culvert. Because a structure generally has a proper foundation, it usually does not, or hardly, settle, unlike the main road. Any difference in settlement is, as it were, spread out over the length of the impact slab to ensure a good and safe transition. The weight of this slab and the soil resting on it is partly transferred near the top of the wall at a small distance from the centre line of the wall, this provides an extra moment. In order to investigate the influence of the impact slabs on the moment distribution, it is assumed that the self-weight of half the slab with the soil layer resting on it on the edge of the ridge on the wall is included in the modeling as a nodal load. The results obtained are compared with the moments of the same model without additional load from the impact slabs, showing that the extra moment as a result of a load by impact plates, with a maximum change found of less than 1%, has no significant influence on the moment distribution.

Conclusion FEM Model 1 - Framework
The advantage of a 2D FEM framework model consisting of 1D beam elements compared to the analytical 1D beam model is that additional effects influencing the moment distribution can be included in the model, which leads to a better approximation of the actual situation. Because the model still consists of a strip of 1m, no change in load distribution occurs, which is also calculated for the 2D framework model with Guyon-Massonnet to determine the occurring bending moment and the developed method, as described in 3.4, to determine the shear force. A framework model is therefore only interesting regarding the occurring bending moment compared to the analytical model. An overview of the mean influence of the additional effects on the moment distribution, defined as $M_{Ed,span}/M_{Ed,support}$, of the investigated structures is presented in Table 20.

Table 20 Overview of average influence of additional effects on the moment distribution based on studied structures.

Additional effect	Average influence on $M_{Ed,span}/M_{Ed,support}$
Modulus of subgrade reaction	-5%
Pile foundation relative to shallow foundation	-5%
Internal traffic load – shallow foundation	-1%
Internal traffic load – pile foundation	-8%
Modelling of the haunch	-15%[i]
Load from impact slabs	< -1%

[i] *partial reduction of total occurring bending moment.*

If the bending moment is governing based on a calculation with the analytical model, then the sagging moment in the span is in most cases, for 82% of the investigated structures, critical. Table 20 shows that the effects that are not included in the analytical model have a favourable effect, due to a shift from the sagging moment in the span to a hogging moment above the supportive wall, on the moment distribution. For a structure with a haunch which is disapproved based on the sagging moment in the span according to the analytical model there may still something to be achieved because the sagging moment is overestimated by about 15%. The estimated impact on a structure without haunch is limited with approximately 5%.

The results of the analytical model and thus the potential benefit are placed in perspective in Table 21.

Table 21 Results of structures from data calculated with the analytical model put into perspective

	Number of objects	Share
Total number of objects in dataset	64	100%
Structures with insufficient information	15	23%
Structures with intersection angle < 80$_{gon}$	16	25%
Calculated with analytical model	33	52%
Results analytical model	**Number of objects**	**Share**
UC ≤ 1,0	26	79%
UC > 1,0	7	21%
Bending	3	43%
Shear	4	57%

Since a model refinement to a 2D FEM framework is only beneficial for bending compared to the analytical model less than 5% of the total structures within the dataset has the potential to benefit from this model refinement. With a 3D FEM plate model these additional effects can also be included in the model and at the same time 25% more structures are assessable due to the possibility of modeling structures with an intersection angle smaller than 80gon. To this end, it is decided not to include the 2D FEM framework model in the ASA Tool, from the analytical model, if a structure is disapproved, it is immediately proceeded to a 3D FEM plate model. Due to significant influence on the total occurring bending moment and the distribution of it the additional effects of a elastically supported floor slab or a simplified pile foundation, the horizontal elastic support of the walls and the presence of a haunch are incorporated in the 3D FEM model with 2D plate elements.

5.2   FEM Model 2 – Plate model

The FEM Model 2 is a further model refinement to a model in a 3D space in which individual structural elements, such as the deck, the walls and the floor, are modelled with 2D plate elements to which a material with isotropic properties has been assigned. An example of such a 3D plate model is shown in Figure 59.
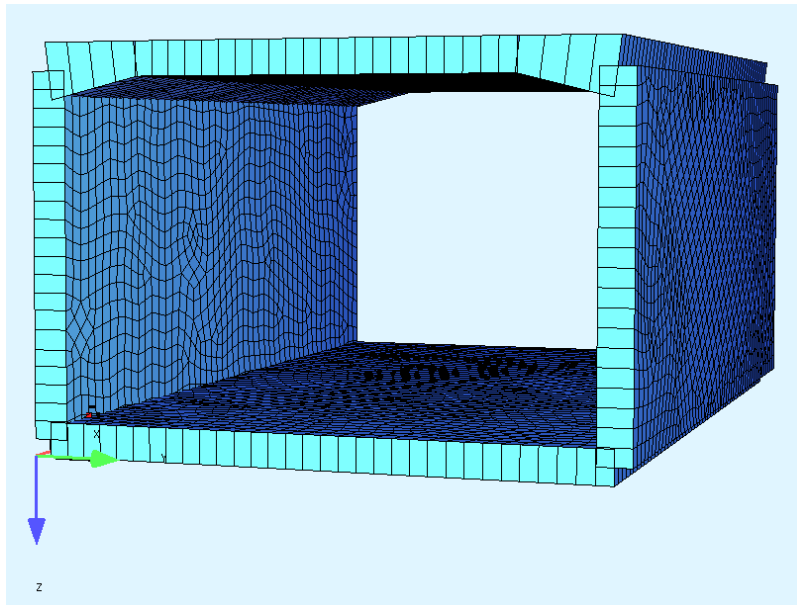
Figure 59 Example of an 3D FEM model build up with 2D plate elements (used Software: SOFiSTiK). Springs in global Z direction underneath the floor slab and springs in global X direction on the outer face of the walls are not shown.

The load effects calculated by the FEM model are compared with the cross-section capacity in the predetermined cross-sections at the location in the middle of the span, the end of the haunch and the face of the supportive wall. By using the predefined sections, the calculated cross-sectional capacity from the analytical model can be used.

According to RBK Table 3.1, a FEM model with plate elements is very suitable for modeling a box structure whose deck is seen as a slab. It is expected that a lower governing UC will be calculated by model refinement into a 3D plate model and taking into account a number of additional favourable effects. Structures with a critical UC based on the analytical model could be re-assessed with the FEM plate model, which may result in a lower governing UC, so that the structure is still approved. Within this research, the FEM plate model can also be used to validate the analytical model. In contrast to a model consisting of one or more beam elements, a model made up of plate elements offers the possibility to assess structures with an intersection angle smaller than 80gon, which increases the total set of structures to be assessed from the data analysis by approximately 25%.

In the 3D FEM plate model, the effects, shown in Table 22, are included in the modeling of the underpasses and culverts.

Table 22 Effects included in modelling 3D FEM plate model

Model	Loads
Increasing thickness and associated shifted neutral line due to the presence of a haunch	Self-weight of the concrete structure
Interaction with soil, vertical springs to represent bedding underneath the floor slab	Deadload in vertical direction by soil cover Deadload in horizontal direction by soil pressure
Interaction with soil, horizontal springs to represent the presence of soil on the outer face of the walls	Deadload in vertical direction by asphalt layer
	Traffic load – LM1 including a UDL and TS loads

Any traffic load in an underpass is not taken into account because the load does not always have to be present while it has a favourable effect on the moment distribution of the deck, in addition, paragraph 5.1 stated that the influence of internal traffic is very limited for most underpasses especially in case structures have a shallow foundation. The effect of any internal water table in a culvert is also neglected. The vertical component of load due to an internal water table has a positive effect and the horizontal component has a negative effect on the moment distribution of the deck. In general, the favourable vertical effect is larger than the negative horizontal effect due to the culvert's geometry, while the global effect of an internal water table is negligible and is therefore not included in the modeling. The load model for fatigue, and the corresponding check, is not included as discussed earlier in paragraph 4.5.

5.2.1 Script-based FEM analysis

In the classic way of using FEM software for the assessment of existing structures, an order comes in from a manager or contractor with the question whether an existing structure is still approved based on existing laws and regulations. Reasons for assessing an existing structure are described in paragraph 2.2.2. After analysing any available design drawings, design calculations and the original construction contract document an FEM model is drawn up, mostly graphically, by an engineer for the individual structure. The type of model, the development level of the modeling and the software used is a choice of the engineer, which refers to the first chapter where the "engineers' factor" was introduced. The classical approach involves a linear process which is prone to error and is time-consuming because for each structure to be assessed model considerations are repeatedly done and a new FEM model is drawn up.

Instead of a graphical construction of a FEM model, an input by scripting can be used, for this purpose the FEA Software from SOFiTiK is used. This software package offers the possibility to script the entire structure of the model, the analysis and the results to be displayed where the scripting takes place in a TEDDY file which is part of the software package. In the TEDDY script separate programs must be written for the tasks to be performed, an overview of the tasks to be performed with a description is given in Table 23.

Table 23 Overview and description of modules in the TEDDY script to perform a linear analysis with a 3D model with 2D elements

Module	PROG in SOFiSTiK	Description
Input parameters	template	Own template for storing the input parameters from the Excel database.
Running variables	template	Own template where variables are created which are used to generate the model and loads and determine the sections.
Materials and Cross-Sections	AQUA	Programme for the definition of materials with associated properties that will be used. No use has been made to define specific Cross sections.
Generate model	SOFIMSHC	Programme where the structural elements with its boundary conditions, support conditions and mesh are created based on the defined running variables.
Generate loads	SOFILOAD	Programme which defines the actions and load cases and generates the loads based on the running variables.
Linear analysis	ASE	Programme which executes the linear analysis for the given set of load cases.
Integrate forces over sections	SIR	Program where sections are created with a width of 4d which integrate the section forces so that afterwards an average over 4d, in accordance with RBK 6.2.1 (10), can be determined.
Superpositioning	MAXIMA	Part which finds the maximum and minimum section forces as a result of TS1 to TS3 and combines it into a new load case.
Combinations	MAXIMA	Programme which finds the maximum and minimum section forces as a result of the combined load cases.
Combinations for Mxy and redistribution	MAXIMA	Part which generates combinations to determine the corresponding torsional moments M_{xy} and moments in other sections for an occurring maximum or minimum.
Export results	RESULTS	Programme which exports selected results into an Excel file.

The advantage of a script-based FEM model is that in all programs self-defined variables can be used, so that a fully parametric FEM model can be set up. Having to start completely from scratch, the user can determine what will and will not be performed, so that no unnecessary calculations are performed, and the order of the tasks can be chosen so that in the right way combinations can be made with sections for which the forces are integrated so that an average over $4d$ can be calculated, something that is not going well with SCIA Engineer for example. These sections are automatically placed with an overlap of $2d$, shown in Figure 60. The sections at the edge have a width of $2d$ because of limited distribution at the edge of the slab. Figure 60 also shows the automatically generated TS loads which are moved step by step across the deck taking into account the intersection angle. Note that for the determination of the maximum occurring shear force the TSs are also placed out of line, while for bending moment it is assumed that the TSs are always in a line parallel to the supportive walls.

The background report of the 3D FEM plate model is given in Appendix D1.
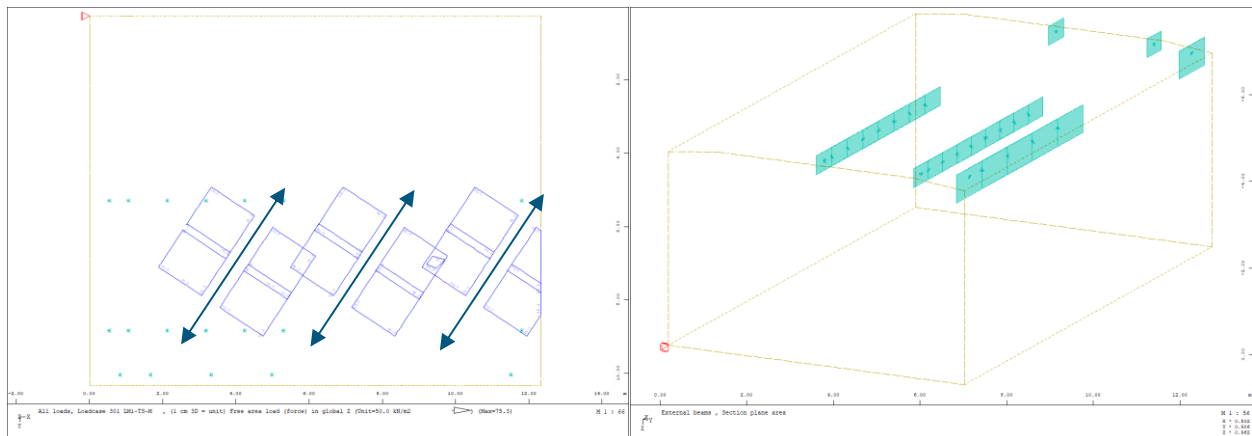
Figure 60 Example of TS loads in 3D FEM plate model, on the left an edge distance is given and on the right loads are cut-off because of a joint (no edge given) (left) and visualization of sections for integrating forces with standard width of $4d$ and overlap of $2d$, separate edge sections with a width of $2d$ (right).

5.2.2 Sensitivity of bedding stiffness reviewed

The sensitivity of the specified stiffnesses of the ground under the floor slab and next to the walls, expressed in spring stiffness k, is examined again to exclude that this input parameter can cause large differences in calculation results.

In the past, underpasses and culverts were almost always made on site, meaning that the ground was later backfilled. If clay or loam was present on the site it was not used as backfill, a better quality soil mix would then be used. Although the exact composition of the soil around an existing structure is often unknown, with a modulus of subgrade reaction of $k = 50\ MPa$ to $k = 100\ MPa$ it is considered that the spectrum of the soil around the structure is covered. This range is based on (Vereniging Nederlandse Cementindustrie, 1993) with which surrounding ground layers consisting of very fine sand or sand with loam to well graded gravel and gravel-sand mix with hardly any fine material are covered. In relation with horizontal stresses, a bedding with half the stiffness based on neutral soil pressure is used for the walls. As a starting point for the sensitivity analysis, a value of $k = 75\ MPa$ for the bedding of the floor and $k = 37,5\ MPa$ for the walls has been used.

Just as from the results of the analytical model from chapter 3 and the sensitivity analysis of the framework model from paragraph 5.1, the influence of the assumed stiffness of the surrounding soil on the occurring shear force appears to be very limited. When assigning a high stiffness of the surrounding soil, the occurring shear force for the assessed structures increases by a maximum of +0,6% in the controlled sections, when assuming a lower stiffness, the occurring shear force decreases by a maximum of -0,8%. The influence of the stiffness of the soil around the structure on the occurring shear force is therefore negligible.

Naturally, a higher assumed stiffness of the ground under and next to the structure leads to a shift from the sagging moment in the span to the hogging moment at the supportive walls and a lower assumed stiffness leads to a shift from the hogging moment to the sagging moment. With the found change from -2,8% to +3,8% of the bending moment in the span, it is unlikely that shifts in the moment distribution will occur larger than 5%, the effect on the moment distribution is therefore neglected and the values $k_{floor} = 75,0\ MPa$ and $k_{wall} = 0,5\ k_{floor}$ are taken as default values.

5.2.3 Comparison of 3D FEM plate model with Analytical model

The assessment of the existing underpasses and culverts from the database based on a calculation of the load effects with the 3D FEM plate model are compared with the assessment based on the analytical calculation model.

Bending

In the analytical model, the occurring moment is determined using the Guyon-Massonnet method, which approximates the load distribution of the UDL and TS load from LM1 so that an equivalent distributed load is obtained for application to a model consisting of a unit strip of 1m. In the case of a 3D FEM plate model, the distribution is calculated in the model itself. In line with expectations, the occurring moments calculated with the 3D FEM plate model are generally lower than the moments calculated with the analytical model. The calculated sagging moment at midspan, which in most cases is the decisive section for moment, is on average 20% lower with the 3D FEM plate model than the analytical model. An analysis of the results of the calculated structures from the database is presented in Table 24.

Table 24 Analysis of obtained bending moments (M) in which the ratio is defined as $M_{SOFiSTiK}/M_{Analytical}$. Q1 and Q3 represent the first quartile (25th percentile) and the third quartile (75th percentile), respectively.

	Ratio – MIN	Ratio – Q1	Ratio – AVG	Ratio – Q3	Ratio – MAX
$M_{Ed,span}$	0,57	0,76	0,82	0,87	1,08
$M_{Ed,hounch}^{-}$	0,32	0,55	0,69	0,82	1,19
$M_{Ed,hounch}^{+}$	0,00	0,00	0,22	0,25	1,00
$M_{Ed,face}$	0,19	0,69	0,76	0,88	1,02

Despite an average decrease of the occurring moments, it sometimes happens that the calculated occurring moment is higher with the 3D FEM plate model than the analytical model, an explanation can be given for why these are exceptions.

For the sagging moment in the span, denoted with $M_{Ed,span}$, a decrease in the occurring moment has been calculated for all structures with only one exception which is reflected in Table 24 as Ratio – Max with a value of 1,08. The specific case concerns a culvert with a limited distance in the clear of only 1,5m, the calculated moment of both the analytical model and the 3D FEM plate model is so small that a UC of 0,13 and 0,14 respectively is calculated making the error acceptable. The same culvert provides the remarkably low value of 0,19 for the minimum ratio found between the calculated hogging moments at the face of the supportive wall. With a calculated hogging moment far below the calculated capacity, this skewed ratio is also accepted because the absolute difference is small. Also, for the calculated hogging moments at the face of the supportive wall, it only happens once that a higher value is calculated with the 3D FEM plate model, which is reflected in Table 24 by the value 1,02 for Ratio – MAX. The ratios in the section at the end of the haunch are far apart. However, in several cases the ratios are far apart, but the actual differences are limited by small occurring bending moments. The results of the 3D FEM plate model show that the occurrence of a sagging moment in the section at the end of the haunch occurs significantly less often than the results of the analytical model suggest. Where the analytical model considers a sagging moment in the section at the end of the haunch possible for nineteen of the 26 structures with a haunch, the 3D FEM plate model only does so in five cases, which explains the skewed ratio for $M_{Ed,haunch}^{+}$ in Table 24 because $M_{Ed,haunch}^{+} = 0$ is used if no sagging moment can occur based on the calculation. The calculated positive moments in the section at the end of the haunch are usually so small that it does not cause any problems, however this means that the analytical model more often incorrectly checks a shear force under positive bending moment in the section at the end of the haunch while that has been found to potentially lead to problems.

Shear

For the determination of the occurring shear force in the analytical model, a beam model is used for evenly distributed loads and for the shear effect as a result of TS, the established method described in paragraph 3.4 based on method 7.3-7 from (CEB-fib, 2010) is used. In the 3D FEM plate model, the distribution in the plane of the concrete deck is modelled by the FEM model itself. In both cases the load is distributed vertically by the asphalt layer and by the presence of a possible soil layer to the top of the concrete deck. Contrary to expectations, the occurring shear forces calculated with the 3D FEM plate model are generally higher than the shear forces calculated with the analytical model. The calculated shear force in the section at the end of the haunch under a negative bending moment, which in most cases is governing, is on average 16% higher with the 3D FEM plate model than the analytical model.

One reason for the on average significantly higher calculated shear force with the 3D FEM plate model could be that a too large shear distribution in the plane of the concrete slab of TS was used in the method based on method 7.3-7 from (CEB-fib, 2010). To this end, the structures from the database were recalculated with an adjusted angle for the in-plane distribution of 30° and 60° to compare the results with the used value of 45°. The calculations show that when maintaining an angle of 30° for the distribution in the concrete slab for eight of the 23 structures with a haunch Case I, without overlap of wheel prints and effective width as described in paragraph 3.4, must be applied while in paragraph 3.4, based on a calculation and a general statement in (Lantsoght, 2012) where it was assumed that a situation like Case I does not occur, it was assumed that Case I practically does not occur. Case I has therefore not been elaborated in the module for determining the shear force effect as a result of TS, so that the results of these eight structures cannot be compared. For the other structures, an average increase of 7% of the calculated shear force in the section at the end of the haunch under a negative bending moment applies. An analysis of the results of the calculated structures from the database, excluding the eight non-computable structures, with an angle of 30° is presented in Table 25.

Table 25 Analysis of obtained shear forces (V) with the analytical model in which the ratio is defined as $V_{30°}/V_{45°}$ for the varying angle of in-plane distribution of shear force. Q1 and Q3 represent the first quartile (25th percentile) and the third quartile (75th percentile), respectively.

	Ratio – MIN	Ratio – Q1	Ratio – AVG	Ratio – Q3	Ratio – MAX
$V_{Ed,haunch^-}$	0,99	1,05	1,07	1,09	1,15
$V_{Ed,haunch^+}$	0,99	1,00	1,05	1,08	1,15
$V_{Ed,face}$	0,99	1,03	1,06	1,08	1,14

The calculations with an angle of 30° also yield values that are smaller than with an angle of 45°. The reasoning behind this is that by decreasing the horizontal distribution the shear force effect of TS1 is indeed increased, but that TS2 and TS3 must be placed further away from the control section in order to spread in the influence area of TS1, so that a lower total shear effect is calculated. For short spans, it can even result in TS2 and TS3 no longer having any influence at all on the considered strip of TS1. The increase in the calculated shear force by assuming an angle of 30° with respect to an in-plane distribution at an angle of 45° is on average, and even in the third quartile, lower than the increase with a 3D FEM plate model and in addition, an increase is not calculated for all structures studied, from which it is concluded that the angle of in-plane shear distribution of 45° is not the cause. When an angle of 60° is assumed, the calculated occurring shear force for all examined sections decreases by 0% to 15% with an average of 9% for all structures investigated from the database.

A further analysis of the results of the calculated shear forces for structures from the database is presented in Table 26.

Table 26 Analysis of obtained shear forces (V) in which the ratio is defined as $V_{SOFiSTiK}/V_{Analytical}$. Q1 and Q3 represent the first quartile (25th percentile) and the third quartile (75th percentile), respectively.

	Ratio – MIN	Ratio – Q1	Ratio – AVG	Ratio – Q3	Ratio – MAX
$V_{Ed,haunch^-}$	0,91	1,08	1,16	1,22	1,40
$V_{Ed,haunch^+}$	0,00	0,00	0,41	1,00	1,21
$V_{Ed,haunch^+}\,excl.\,0$	0,88	1,02	1,07	1,15	1,21
$V_{Ed,face}$	0,86	1,04	1,10	1,19	1,24

Table 26 shows that the difference in calculated shear force is larger than the difference obtained by adjusting the in-plane shear distribution angle from 45 to 30 degrees as shown in Table 25. Because no positive bending moment occurs more often in the section at the end of the haunch based on the 3D FEM plate model than in the analytical model, a ratio 0 is calculated for a significant number of structures, which is why the ratios excluding the zero values are considered separately. Because the method for determining the shear force as a result of TS can only calculate with whole TSs, it is possible that, based on geometry, the analytical model only takes one or two TSs into account where the 3D FEM plate model takes two or three TSs into account, which could explain a higher calculated shear force by the 3D FEM plate model. However, based on the geometry of the structures in the database this does not occur and if it occurs it will mainly occur that TS3 is not considered whose influence on the shear force in the considered strip in the analytical model is very limited, as in paragraph 3.4 is described and is confirmed by the results of the 3D FEM plate model. An explanation for the remarkably high maximum ratio for $V_{Ed,haunch^-}$ of 1,40 is that in the analytical model TS3 has just no influence on the shear force in the considered strip due to the limited bridge length, which makes the difference with the 3D FEM plate model even larger. An explanation based on geometry cannot be given because the structure in question does not have a deviating geometry from other structures in the database. For the few structures where a lower shear force is calculated with the 3D FEM plate model, it is not possible to give an unambiguous explanation based on geometric properties.

A further reasoning and discussion for the differences found between the calculated occurring shear force according to the analytical model and the 3D FEM plate model is described in paragraph 5.3 Discussion.

Skew intersections
In this research, skew intersections are understood to mean the skewed intersection between the overhead traffic and the underpass, where it is assumed that the slab of the underpass is perpendicular. Skewed slabs do occur, however, but have not been considered at this stage of the study.

According to RBK 6.2.1 (10) models with beam elements, such as a beam model or a 2D framework model, are only very good for structures with an intersection angle larger than 80gon, which is approximately 72°, where the shear force must still be determined manually. The database contains thirteen structures with an intersection angle less than 80gon of which enough data is available for a structural analysis. These skewed intersections were assessed with both the analytical model and the 3D FEM plate model in order to investigate the difference, the deviation.

In all examined sections for all studied structures with a skew intersection from the database, the occurring moment at midspan, which is usually the most critical section for bending, is on average overestimated by 34% with the analytical model. In an overview is given of the calculated ratios for the moment at midspan for structures with an intersection angle larger and smaller than 80gon.

Table 27 Analysis of obtained bending moments at midspan ($M_{Ed,span}$) in which the ratio is defined as $M_{SOFiSTiK}/M_{Analytical}$. Q1 and Q3 represent the first quartile (25th percentile) and the third quartile (75th percentile), respectively.

	Ratio – MIN	Ratio – Q1	Ratio – AVG	Ratio – Q3	Ratio – MAX
Angle > 80gon	0,57	0,73	0,80	0,87	1,07
Angle < 80gon	0,54	0,61	0,66	0,72	0,84

The calculated bending moments with the 3D FEM plate model are not only lower due to model refinement, the difference with the 3D FEM plate model is significantly smaller for structures with an intersection angle greater than 80gon compared to structures with an intersection angle smaller than 80gon. The 3D FEM plate model calculated for all investigated structures within this set no positive bending moment in the section at the end of the haunch, while the analytical model calculated this for all structures, except one. In a sense, this is not a bad thing because it is conservative, but it means that in some cases one must switch to the 3D FEM plate model since the bottom reinforcement in the section at the end of the haunch must then be checked, moreover the shear capacity with the lower reinforcement must then be checked which has proven to be critical in several cases. In terms of bending moment there is therefore a significant reserve in the analytical model, which means that it is very conservative for skew intersections at bending moment. If, despite a negative advice from the RBK, a structure with an intersection angle smaller than 80gon is nevertheless assessed with a model with bar elements and it is approved based on the calculation, one seems in any case on the safe side with regard to bending.

The calculated shear force in the section at the end of the haunch under a negative bending moment, which in most cases is governing, is, as shown in Table 28, on average 4% lower with the 3D FEM plate model than the analytical model. It is remarkable that the deviation found is so small, while in the module a straight crossing of 100gon is assumed to determine the shear force as a result of TS, which for most structures has the dominating share in the total occurring shear force.

	Ratio – MIN	Ratio – Q1	Ratio – AVG	Ratio – Q3	Ratio – MAX
$V_{Ed,haunch^-}$	0,89	0,90	0,96	0,97	1,11
$V_{Ed,face}$	0,73	0,85	0,93	0,97	1,28

Table 28 Analysis of obtained shear forces (V) in which the ratio is defined as $V_{SOFiSTiK}/V_{Analytical}$. Q1 and Q3 represent the first quartile (25th percentile) and the third quartile (75th percentile), respectively.

In Table 28 the values for a shear force under a positive bending moment have been omitted because with the 3D FEM plate model there is no positive bending moment calculated in the section at the end of the haunch for any of the investigated structures with an intersection angle less than 80gon. The minimum ratios are found for structures with a small intersection angle, as the intersection angle increases, the ratio also increases at which the maxima are found for a structure with the largest intersection angle of 78,7gon in the set under consideration.

5.2.4   Investigating calculated differences

In order to provide an explanation for the differences between the 3D FEM plate model and the analytical model found in paragraph 5.2.3, an intermediate model is used without additional effects compared to the analytical model, an overview of the assumptions is given in Table 29.

Table 29 Assumptions for the intermediate 3D FEM plate model

Assumptions – Intermediate 3D FEM plate model
Haunches are not modelled, meaning no inclined model line and no change in thickness of the slab.
Spring stiffness at the outer face of the walls neglected: $k_{wall} \approx 0$.
Spring underneath the floor is set practically to infinity to represent fully clamped walls: $k_{floor} \approx \infty$.
Intersection angle for loads fixed at 90° to match the analytical model.
Horizontal soil loads are neglected for the determination of the section forces.

To give a better impression of the comparison, the analytical model and the intermediate 3D FEM model are shown in Figure 61.
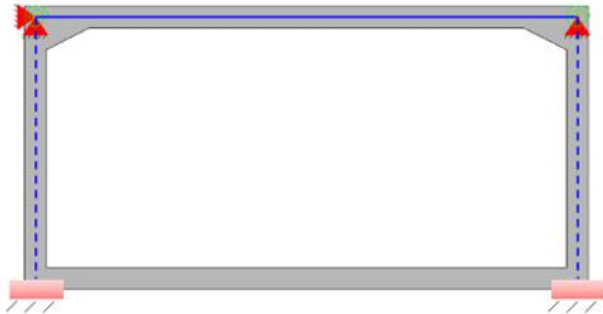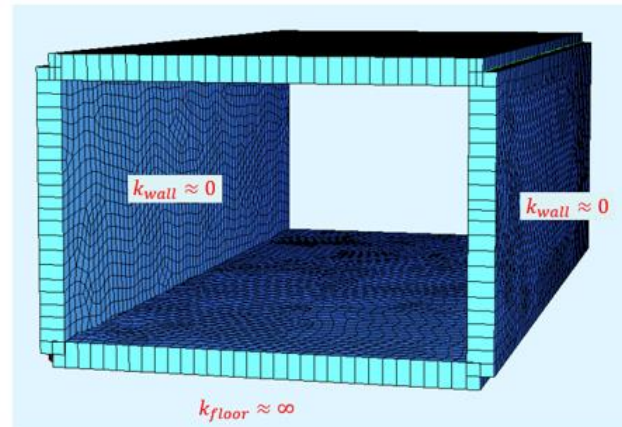
Figure 61 Graphical representation of Analytical model (left) and intermediate 3D FEM plate model (right). The rotational springs of the analytical model represent walls fully clamped by the floor, as assumed in chapter 3.

Comparison 1

First a comparison is made with the analytical model and the intermediate 3D FEM plate model without further adjustments to the determination of the load effect of the analytical model and the calculated capacity. In this comparison the calculated cross-sectional capacity as described in chapter 4 is used, both for the analytical model and the intermediate 3D FEM plate model. An overview of the obtained results is given in Table 30.

Table 30 Results of Comparison 1 of critical section forces of Analytical model and Intermediate 3D FEM plate model, in which the ratio is defined as $SOFiSTiK/Analytical$. Q1 and Q3 represent the first quartile (25th percentile) and the third quartile (75th percentile), respectively.

	Ratio – MIN	Ratio – Q1	Ratio – AVG	Ratio – Q3	Ratio – MAX
$M_{Ed,span}$	0,68	0,92	0,95	0,96	1,09
$V_{Ed,face}$	0,78	1,15	1,17	1,22	1,36

Table 30 shows that the calculated bending moment corresponds well with an average deviation of about 5%, the difference has been attributed to the effect of load distribution, which is slightly better in the 3D FEM plate model compared to the Guyon-Massonnet method in the analytical model. Table 30 also shows that the calculated shear force does not match, with an average deviation of +17%.

To narrow down the influence of the additional effects on the bending moment, separate models have been made to isolate the effect. An explanation for the differences in the calculated bending moment with the analytical model and a full 3D FEM model are provided in Table 31.

Table 31 Explanation for different calculated bending moments with 3D FEM plate models compared to the Analytical model.

Modelling aspect	$M_{Ed,3D\ FEM}/M_{Ed,Analytical}$ (%)
Full 3D FEM plate model	-18%
Horizontal soil loads	3%
Model refinement – Haunch and interaction with soil (springs)	10%
Intermediate 3D FEM plate model	-5%
Load distribution – Guyon-Massonnet method	5%

Comparison 2

For the second comparison, no vertical load distribution for the determination of the shear force due to TS of the analytical model is assumed and the calculated shear capacity of the 3D FEM plate model is adjusted to formulas in accordance with RBK, as shown Table 32, to bring the results of both models closer together.

Table 32 Additional assumptions for Comparison 2 between the analytical model and the intermediate 3D FEM plate model.

		Analytical model	Intermediate 3D FEM plate model
Load distribution		No vertical load distribution through asphalt and soil layer for the determination of the shear force of TS.[i]	Vertical load distribution through asphalt and soil layer to the top of the concrete deck for the determination of the shear force.
Shear capacity	6.2.a	$V_{Rd,c} = \left(0{,}12\ k_{cap}\ k\ (100\ \rho_l\ f_{ck})^{\frac{1}{3}} + k_1\ \sigma_{cp}\right) b_{wgem}\ d$	
	6.2.b	$V_{Rd,c} = \left(v_{min} + k_1\ \sigma_{cp}\right) b_w\ d$ $v_{min} = 0{,}035\ k_p^{\frac{3}{2}}\ k^{\frac{3}{2}}\ f_{ck}^{\frac{1}{2}}$	$V_{Rd,c} = \left(v_{min} + k_1\ \sigma_{cp}\right) b_w\ d$ $v_{min} = 0{,}83\ k_p^{\frac{3}{2}}\ k^{\frac{3}{2}}\ f_{ck}^{\frac{1}{2}}/f_{yk}^{\frac{1}{2}}$

i To avoid Case I from the method for determining V_{TS}, as in Table 10, vertical distribution through 5 cm of asphalt is maintained.

Due to the large calculated average difference of 17% for the shear force in Comparison 1, the question rises whether effects are not included twice with vertical load distribution through asphalt and soil, in-plane load distribution from the back of the load plane of TS as in method 7.3-7 (CEB-fib, 2010) and calculating with a plate factor k_p on the capacity side.

For the analytical model, the vertical load distribution through soil and asphalt is limited to only reach Case II, overlap of effective widths, to determine the occurring shear force as a result of TS with the method based on 7.3-7 from (CEB-fib, 2010). The reasoning for this assumption is that no soil or asphalt was present in the tests from (Muttoni, Rodrigues, & Burdet, 2006), so the vertical distribution through soil and asphalt has not been verified for this method to determine the shear force. In addition, the tests used slabs with a limited thickness to about 300 mm in combination with a load plate equal to the wheel print of TS, which is 400x400 mm, while the slabs of underpasses can reach larger thicknesses and load surfaces of TS many times larger than the wheel print due to vertical load distribution. It is expected that a certain scale effect will be present for the distribution, which is not present in the current method.

The vertical load distribution cannot be completely neglected. In paragraph 3.4 it is assumed, on the basis of (Lantsoght, 2012) and a simple calculation (Appendix B2), that in practice overlap of effective widths b_w always occurs due to the effective height d of the deck and the minimum asphalt thickness, for which it was decided not to elaborate this situation, Case I. However, if no vertical load distribution for the determination of the shear force due to TS through soil and asphalt is assumed, this situation would arise. In order to prevent an error, 5 cm of asphalt is therefore assumed so that, for the structures to be investigated, an overlap of effective widths b_w, Case II, is created.

The analytical model is not changed on the capacity side, 6.2.a – shear failure according to RBK, so with plate factor k_p, and 6.2.b – transition to flexure according to EC with addition of plate factor k_p, as described in chapter 4, are applied. For the 3D FEM model, the formulas from RBK are used for both formula 6.2.a and 6.2.b, so including the arithmetic release of the yield strength of the reinforcement f_{yk}. The background for this adaptation for the 3D FEM model is that low steel grades have more elongation before failure than the FeB500 steel grade used to determine the shear capacity formulas. Looking at the stress-strain curves, these steel grades have a longer horizontal branch and can therefore elongate relatively much and thus provide more redistribution. In the analytical model, this redistribution is incorporated in method 7.3-7 (CEB-fib, 2010) because it is calibrated for failure tests of concrete slabs (Muttoni, Rodrigues, & Burdet, 2006). The 3D FEM model is linearly elastic, which means that redistribution due to cracking at ULS is not included, in order to account for the effect of redistribution, it is processed on the capacity side for the linear elastic FEM model by arithmetically releasing the yield strength f_{yk} of the reinforcement.

The in-plane distribution of the TS load was further investigated by looking at the graphical representation of the calculated shear force as a result of TS in the quadrilateral elements from the 3D FEM plate model and comparing this with the calculated distribution width b_{eff} with corresponding shear force according to the method based on 7.3-7 from (CEB-fib, 2010). The assumed angle of 45° for in-plane load distribution to the control section in the method based on 7.3-7 from (CEB-fib, 2010) is acceptable based on graphical comparison with the 3D FEM plate models, with the exception for TSs placed close, $< 0,5m$, from the edge of the slab, for the graphical explanation see Appendix D2.

An overview of the obtained results for the comparison between the modified analytical model and the intermediate 3D FEM plate model with modified shear capacity is shown in Table 33.

Table 33 Results of Comparison 2 of critical section UCs of Analytical model and Intermediate 3D FEM plate model, in which the ratio is defined as $UC_{SOFiSTiK}/UC_{Analytical}$. Q1 and Q3 represent the first quartile (25th percentile) and the third quartile (75th percentile), respectively.

	Ratio – MIN	Ratio – Q1	Ratio – AVG	Ratio – Q3	Ratio – MAX
$M_{Ed,span}$	0,68	0,92	0,95	0,96	1,09
$V_{Ed,face}$	0,56	0,85	0,95	1,06	1,21

Table 33 shows that after the adjustments of the load distribution for the vertical distribution through soil and asphalt to determine the occurring shear force as a result of TS using the method based on 7.3-7 from (CEB-fib, 2010) and the shear capacity of the 3D FEM plate model, both for bending moment and for shear force an average 5% lower UC is calculated with the 3D FEM plate model. What can also be seen in Table 33 is that the analytical model fits very well with the 3D FEM plate model regarding bending moment, given the relatively small spread of result ratios, for shear force a larger spread is found with 50% of the data within a ratio of 0,85 to 1,06. For the investigated structures, the same shear capacity was calculated for the analytical model and the 3D FEM plate model in 45% of the cases, which means that for 45% of the investigated structures formula 6.2.a - shear failure is decisive and that for 55% of the investigated structures with the 3D FEM plate model formula 6.2.b – transition to flexure is decisive.

The calculated UC for shear force with the full 3D FEM plate model is on average 5% lower in the section at the end of the haunch, which is comparable with the intermediate model, and on average 12% lower in the section at the face of the wall, because a part of the shear force is transferred as normal force due to an inclined model line, both in favour of the full 3D FEM plate model.

Structures per design code

For the analysis of the UCs of the structures per design code, for the 3D FEM plate model, use was made of the shear capacity according to RBK formulas, as in Comparison 2 in this paragraph. Figure 61presents the number of structures in the database, for which a structural assessment is possible, compared to the number of structures with a UC > 1,0 per design code, where in addition a distinction is made between a UC > 1,0 due to bending moment and shear. In order to be able to compare the results with the results of the analytical model, shown in paragraph 4.4.2, the same structures are included in the overview, which means that structures with an intersection angle less than 80_{gon} are not included. The main explanation for the data concentration in the GBV 1962 is that there was a construction wave during that period in combination with the fact that many structures from that period have reached or are nearing the end of their designed service life, a more detailed explanation is given in chapter 2.

Structures per design code - 3D FEM plate model

	GBV 1912	GBV 1918	GBV 1930	GBV 1940	GBV 1950	GBV 1962	VB 74/84	VBC 1990	VBC 1995
Assessed	0	0	0	2	3	21	5	0	0
UC > 1,0	0	0	0	1	0	5	2	0	0
UC > 1;M	0	0	0	1	0	0	0	0	0
UC > 1;V	0	0	0	0	0	5	2	0	0

Structures per design code - 3D FEM plate model

	GBV 1912	GBV 1918	GBV 1930	GBV 1940	GBV 1950	GBV 1962	VB 74/84	VBC 1990	VBC 1995
Assessed	0	0	0	2	3	21	5	0	0
Bending	0	0	0	2	2	0	1	0	0
Shear	0	0	0	0	1	21	4	0	0

Figure 62 Number of structures from database assessed with the 3D FEM plate model per design code, showing the distribution of UC > 1,0 with associated failure mechanism (left) and the governing mechanism for all structures (right).

The expected pattern that bending moment for structures before and after the GBV 1962 is governing and for structures designed with the GBV 1962 shear is clearly the predominant failure mechanism, as was found with the analytical model in paragraph 4.4.2, is not found in the results of the assessment with the 3D FEM plate model shown in Figure 62. The 3D FEM model calculates on average 5% lower occurring shear forces than the analytical model, while using a higher shear capacity in the assessment for most structures due to a lower steel grade than FeB500. At the same time, however, the bending moment is estimated to be on average 18% lower based on the 3D FEM plate model. The result is that for structures with a $UC > 1,0$ shear is almost always, only one exception, governing. When not only looking at structures with a UC>1,0 but to which section forces are decisive, it can be seen that for structures before the GBV 1962 bending moment is decisive for most structures, for structures under the GBV 1962 shear force is always decisive for the investigated structures and that for the GBV 74/84 a mix of moment and shear force is found. Based on the 3D FEM plate model, the mean UC for shear with $UC_{avg,V} = 0,89$ is significantly higher than the mean $UC_{avg,M} = 0,65$ for bending moment.

5.2.5   Comparison with assessments from data

In this paragraph the results obtained with the 3D FEM plate model are compared with the calculated UCs for the sections forces, bending moment and shear, which are available from data reports of old assessments. In total, calculations of 17 structures are available for comparison, this is the same as for the comparison with the analytical model. The comparison of the results does not provide a full validation of the 3D FEM plate model, as different models have been used with a different elaboration level and additional loads such as a windshield may be applied, but it does indicate whether the calculated section forces are in the correct order of magnitude. What it also shows is the presence of the "engineers' factor" introduced in chapter 1.

Table 34 Comparison of assessment results from data reports and the 3D FEM plate model

DATA reports			3D FEM plate model		
Number of objects	17		Objects compared	17	
Average UC	0,94		Average UC	0,97	
UC ≤ 1,0			**UC ≤ 1,0**		
Objects UC < 1,0	13	76%	Objects UC < 1,0	11	65%
Average UC < 1,0	0,88		Average UC < 1,0	0,83	
UC > 1,0			**UC > 1,0**		
Objects UC > 1,0	4	24%	Objects UC > 1,0	6	35%
Average UC > 1,0	1,13		Average UC > 1,0	1,12	
Failure due to shear	3	75%	Failure due to shear	5	83%
Failure due to bending	1	25%	Failure due to bending	1	17%
Governing - General			**Governing - General**		
Shear governing	10	59%	Shear governing	13	76%
Bending governing	7	41%	Bending governing	4	24%

In general, the results of the 3D FEM plate model based on the mean UC from Table 34 seem to agree with the average results from the available reports. However, a further analysis shows that with the 3D FEM plate model more structures are disapproved with a UC just higher than 1,0, at the same time the mean UC of structures that do not comply is slightly lower, so this difference is not reflected in the mean UC. What is particularly striking is that in the reports approximately an equal ratio between bending moment and shear emerges as the decisive mechanism, while it follows from the 3D FEM plate model that shear force is decisive for most structures, an explanation for this is based on a deeper analysis.
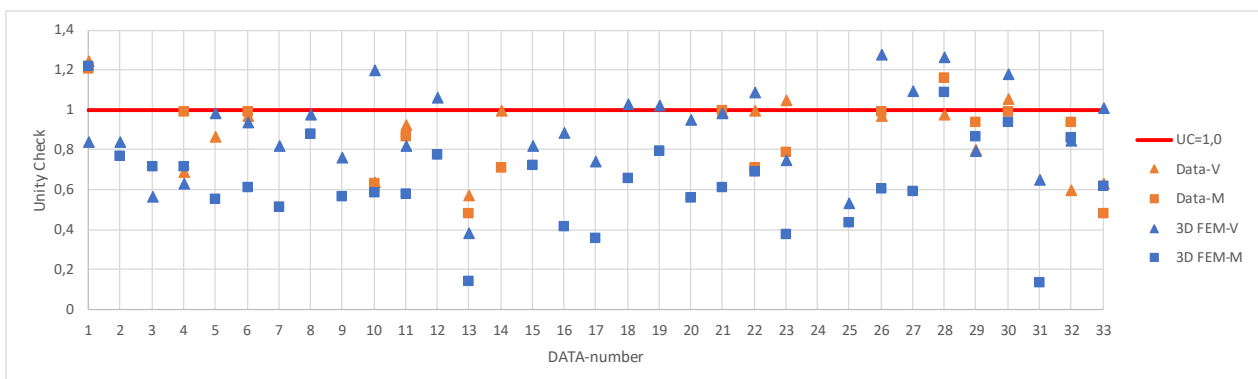
Figure 63 Unity Checks obtained from data reports compared with calculated Unity Checks from the 3D FEM plate model for both shear(V) and bending moment(M).

The available UCs from the reports are compared in Figure 63 with the calculated UCs from the 3D FEM plate model. The figure shows a remarkably low UC for DATA-013 and DATA-031, this concerns culverts with a distance in the clear of barely 1,5m in combination with a significant soil cover so that the occurring bending moment is minimal. For object number 13 an equivalent low UC for shear force is calculated in the available report. The high calculated UC for shear of DATA-026 can be explained using a C16/20 concrete

strength based on CUR 124 because the concrete strength class is unknown from the design, given the high UC, it is expected that a higher strength will be present. No clear explanation for the high UC for shear of DATA-028 can be given, it is expected to be a combination of a limited maintained concrete strength class B30 in combination with the absence of soil cover.

It is generally striking that in many cases no use has been made of the redistribution of bending moments in situations where it would lead to a lower normative UC. In addition, it is remarkable that relatively often engineers deviate from the RBK which states that the lowest concrete strength class from the design codes of the year of construction must be adhered to if the concrete quality is unknown, while often the engineer makes an estimate himself based on experience with equivalent structures for which a higher quality is maintained then the minimum of that time. At the same time, structures from local governments have been assessed in the past according to the regulation from the RBK that the lowest concrete strength class must be maintained if it is unknown, while since November 2019 the CUR 124 is available which allows to maintain C16/20, which results in most cases in an increase of the calculated capacity, especially the shear capacity.

5.3   Discussion

The sensitivity analysis of the impact slabs on the moment distribution did not look at the maximum bending moment in case no traffic load is present on the deck but only on the impact plate. However, this is not expected to be decisive, the own weight and the weight from soil and asphalt work against the effect of a TS above the baffle plates. Also, about half of the load from baffle plates is transferred to the substrate, it said at the end of the plate in a point or spread under the plate.

The analytical model incorrectly checks the shear capacity at the end of the haunch under a positive bending moment in a significant number of cases because it has calculated that a sagging moment can occur in the section in question, while the 3D FEM plate model shows that this is not the case. Since the analytical model is verified with a beam model in SOFiSTiK, this also applies to beam models. The moment distribution of the beam model has been compared with that of a framework model in SOFiSTiK, which shows that the difference is limited, so that it is also expected that the use of a 2D framework model will also result in incorrect checking of the shear capacity at the end of the haunch under a sagging moment for a significant number of structures. Which therefore gives another reason to switch directly to a 3D FEM plate model when a structure is disapproved based on the shear capacity in question with the analytical model. If the capacity at the end of the haunch is tested for a positive bending moment and is not disapproved, then there is of course no problem.

The calculated occurring shear force with the 3D FEM plate model appears in paragraph 5.2.3 to be on average 16% larger than the calculated shear force by the analytical model. In the analytical model, using the method according to 7.3-7 from (CEB-fib, 2010), one could distribute the TS load from the centre of the wheel print instead of the rear, although it is expected that this will not have sufficient effect to bridge the difference found in paragraph 5.2.3. The capacity is determined in the same way for the analytical model and the 3D FEM plate model, namely per considered section, and results for paragraph 5.2.3 also exactly in the same calculated capacity. A difference in calculated load effect with the same calculated capacity results in different UCs, which of course is not possible. Although both methods are an approximation of reality, the method based on (CEB-fib, 2010) is based on tests. In these tests from the research (Muttoni, Rodrigues, & Burdet, 2006) slabs were loaded until collapse followed, from the failure load it was calculated backwards how much effective plate width should be required to achieve the required calculated shear force capacity. In fact, the method from (CEB-fib, 2010) is a calibrated analytical approach to a non-linear problem. The 3D FEM plate model is made up of elements with isotropic properties and is only calculated linearly elastic. In the tests, after the first cracks have appeared, the internal forces are redistributed, resulting in the analytical model in a larger distribution and therefore a lower calculation value. This effect is not modelled by a linear elastic model, for which it can be discussed to assign a reduction factor, for example 1,1, over the calculated occurring shear force as a result of TS from the 3D FEM plate model. However, one may also wonder whether effects are double counted by first distributing vertically through soil and asphalt and then distributing the TS load horizontally from the rear of the load plane. In the tests performed described in (Muttoni, Rodrigues, & Burdet, 2006) for the preparation of the method 7.3-7 from (CEB-fib, 2010) there was no soil and asphalt on the slab, the slab had a limited thickness of about 300mm with a load plate about the same size as the thickness of the slab with dimensions 400x400mm equal to the wheel print of TS, while it is expected that a certain scale factor is present for large load planes and thicker slabs. In paragraph 5.2.4 it was shown that by limiting the vertical load distribution of TS for the method based on 7.3-7 from (CEB-fib, 2010) and using the full RBK formulas for the determination of the shear capacity, meaning the addition of f_{yk} in formula 6.2.b – transition to flexure, resulted in a limited deviation of an average of 5% for the calculated total occurring shear force. Another way is to look from the capacity side for the method based on 7.3-7 from (CEB-fib, 2010), it could be stated that when using this method for determining V_{TS}, the plate factor k_p or k_{cap} should not be applied because the method for determining V_{TS} is calibrated on tests that continued to the failure of RC slabs, which is a non-linear process. For most structures the calculated shear

capacity according to formula 6.2a from EC2 with the addition of k_{cap} is decisive, in case f_{yk} is not arithmetically released, in which the plate factor is processed by $k_{cap} = 1{,}20$, which is close to the mean deviation of 1,16 found. For structures for which formula 6.2.b is decisive, the plate factor k_p has an even larger influence with $k_p^{\frac{3}{2}} \approx 1{,}31$. For the structures investigated in paragraph 5.2.4, equivalent results are obtained with the analytical model and with the modified 3D FEM plate model. The investigated structures often have steel grade QR40 or FeB400, which means that the effect of the arithmetic release of f_{yk} is approximately 12% in case 6.2.b is decisive, which is for 55% of the investigated structures with the 3D FEM plate model the case. In case lower steel grades such as QR22 or QR24 are used, it may occur that a misalignment arises between the analytical model and the 3D FEM plate model, however, this was not always the case in the investigated structures with low stem grades.

5.4   **Conclusion**

Based on the sensitivity analysis from paragraph 5.1 it is concluded that for most cases a framework model, including additional effects that can be modelled, as intermediate variant for a 1D beam model and a 3D plate model does not offer significant added value, it is more effective to switch immediately from a beam model to a slab model if a structure is disapproved based on calculations with beam model, such as the analytical model in this research.

Setting up a FEM model based on a script has a steeper learning curve than drawing up a model graphically. The advantages of a script-based FEM analysis are that an engineer can determine for himself which tasks are performed and above all in which order these tasks are performed so that the desired results can be obtained, something that was often not possible in the past or that led to wrong results, for example when using sections with combined load cases in SCIA Engineer. In addition, it is easy to set up a parametric model from a script-based FEM analysis. The disadvantage of a script-based model, however, is that it is less robust, a small error in the script almost immediately results in an error, which means that the analysis is stopped. The step to a 3D FEM plate model turns out to be an added value for bending moment with a reduction of approximately 18% of the calculated bending moment compared to the analytical model. The analytical method based on 7.3-7 from (CEB-fib, 2010) for determining the shear force due to TS is calibrated on performed tests, which approximates a non-linear problem while the FEM model is a linear elastic approximation and thus results in higher calculated occurring shear forces, even with isotropic material properties. However, after adjustment of the vertical load distribution for the method based on 7.3-7 from (CEB-fib, 2010) and the shear capacity for the 3D FEM plate model to the RBK formulas, an average 5% lower UC for shear is calculated with the 3D FEM plate model than with the analytical model with the module based on method 7.3-7 from (CEB-fib, 2010). It can be concluded from this that vertical load distribution, as prescribed by the EC, works well for bending but less well for shear force, at least for the method according to 7.3-7 of (CEB-fib, 2010). A 3D FEM plate model can have an added value by reducing the calculated UC for shear, but the advantage will be small for most structures, since only an average UC reduction of 5% is found for the investigated underpasses and culverts.

6

Automated Structural Assessment Tool

This chapter describes the design of the ASA Tool and the choices that go with it. In addition, the value of the tool and the advantages of the new workflow associated with a script-based structural assessment compared to the traditional use of FEM software are discussed. Finally, a brief description is given of what the user can do if a structure is disapproved based on the ASA Tool.

6.1   Introduction

For a systematic approach to the structural assessment of existing concrete underpasses and culverts, it is important that the modeling to determine the load effect and the calculated capacity is automated. The automation takes place in the form of making the ASA Tool, where ASA stands for "Automated Structural Assessment" in the context of this research.

As expected at the start of this research and confirmed by the data analysis in chapter 2, the existing concrete underpasses and culverts in the Netherlands have been constructed with relatively simple cross-sections of which more than 80% have a box-shaped cross-section, which ensures that automation is feasible regarding the construction type. In the Preliminary study, outlined in chapter 2, an investigation was also carried out into the number of the structures within the scope of the research for which an estimate of the total was made. Due to the large number of existing underpasses and culverts in the Netherlands, an estimated total of approximately 12.500 of which 1.321 at RWS and over 11.000 at local authorities, in combination with the ageing of many of these structures, it also lends itself to the expected number of structures to be assessed to automate the structural assessment process. The advantage of an automated process and thus a systematic approach in which the same modelling is applied for all structures in a database is that mutual results can be compared and sensitivity analyses can be performed.

The ASA Tool includes the determination of the load effect on the basis of the Analytical model described in chapter 3 and the 3D FEM plate model described in chapter 5, for the determination of the capacity, the cross-section capacity is calculated for both modelling levels as described in chapter 4.

It should be noted that the tool was not set up last in the research process, the tool has been developed along the way. Because the tool has a modular structure, parts that were available earlier in the research are used to assess the structures from the database and to perform sensitivity analyses.

6.2   VBA versus Python

As described in (van der Aa & van den Bos, 2018), for the success of the automation of an entire workflow, it is important that programs can communicate with each other, for this it is important that a uniform language is used and that programs are mutually open so that they can exchange information and create or allow links. Various programs with different programming languages are available for automating processes by means of scripting, of which VBA, which stands for Visual Basic for Applications, and Python are two commonly used examples. VBA is an event-driven programming language developed by Microsoft intended to control and automate Microsoft Office applications. VBA is not a standalone program, it can only run in a host application of MS Office such as Excel. Although Microsoft stopped investing in VBA in 2008 and since then only came with updates for small changes, based on (TIOBE Index, 2020) it is still the 6th most popular programming language and it is a very easy language to learn. Python is a high-level open source programming language for general purposes which was first released in 1991 and as an open source

software it is still being developed by the Python Software Foundation. Python has grown in popularity over the years, where it now ranks second as the most popular programming language (TIOBE Index, 2020). The language is relatively easy to learn and with a vibrant community new features and libraries, pre-written code with a specific purpose, are in continuous development and because it is open source software they are widely available. Table 35 shows the main advantages and disadvantages for automating the structural assessment.

Table 35 Advantages (Pros) and disadvantages (Cons) of VBA and Python for automating the structural assessment

	Pros	Cons
VBA	a) Use of Excel's graphical in- and output; b) Low threshold for user due to the use of Excel; c) Easy to distribute.	d) Compared with Python less efficient with complex calculations and large datasets; e) Can only run script in logical order, meaning no multi-threading processing possible.
Python	f) Efficiency with complex calculations and large datasets; g) Multi-threading processing possible for running multiple of the same tasks at once (LOOP), which decreases the process time.	h) Requires installed software which most people are not familiar with (yet), creating a threshold; i) A graphical, user friendly, in and output must be completely built which is a lot of non-engineering work.

Calculating the 3D FEM plate model will take most of the time but is performed by SOFiSTiK, it does not matter for that part whether VBA or Python is used as the programming language for the ASA Tool. The calculations of the analytical model consist of Excel sheets which must be linked together, VBA is the native language for Excel and is best suited for this. It is expected that the computation time will remain limited within practical limits, so that the advantages of Python, which comes down to an expected shorter processing time, do not outweigh the disadvantages.

6.3   Design of the ASA Tool

A modular design has been chosen in which all separate modules can be considered as building blocks of the ASA Tool, a schematic flowchart of the tool with the so-called modules is shown in Figure 64. All modules are controlled using a VBA script and connected to each other to exchange data. In this way, the script forms the cement that makes a complete tool of all separate building blocks.

In the database the underpasses and culverts to be assessed are entered with data such as the general information, geometry, material properties, reinforcement layout and the thickness of the soil and asphalt layer. The database is supported by a materials module so that the correct material properties of material classes from old design codes are assigned. When all data has been entered, the calculation can be started.

The program first calculates all structures, apart from structures with an intersection angle less than 80gon, with the analytical model to avoid unnecessary start-up and closure of modules. The analytical model consists of a basic analytical model module which is supplemented by the modules Guyon-Massonet, for determining the equivalent traffic load from LM1, and the method based on 7.3-7 from (CEB-fib, 2010) for determining the shear force due to the TS. Optionally, it is possible to choose to use the calculated fictional stiffnesses E_f instead of the standard values for the E-moduli of the concrete parts, but this requires error-prone information regarding the reinforcement in the wall.

The capacity of the existing structure is calculated with the module the cross-sectional capacity which includes the sections in the middle of the span, at the end of the haunch and at the face of the supportive wall. The anchoring of the reinforcement is checked in a separate module anchorage, if it is calculated that the reinforcement is not fully anchored, the cross-sectional area of the reinforcement is reduced in proportion to anchoring. Since paragraph 4.2 shows that the reinforcement can be regarded as fully anchored for almost all investigated structures and because in practice it is often not possible to determine the available anchoring length properly, it is possible to assume the reinforcement as fully anchored. The calculated cross-sectional capacities of the existing structure are used for both the analytical model and the 3D FEM plate model.

As a second step, all structures may be calculated with the 3D FEM plate model. The basis for this process is the module Auto_SOFiSTiK in which the necessary input data is collected and an Excel variant of the Teddy script is created. A temporary Teddy script is generated with the help of a piece of code and is loaded into SOFiSTiK. In SOFiSTiK the entire analysis, as described in paragraph 5.2.1, is performed which exports the results to a separate temporary module called results. Once the results module is saved, identifiable as changed, the results are brought to the base file Auto_SOFiSTiK. This means that a single assessment with these separate modules can also be performed manually. The optimal redistribution of the occurring bending moments is performed in Auto_SOFiSTiK_redistribute. After exporting the results to the database, the following structure is automatically loaded into SOFiSTiK.
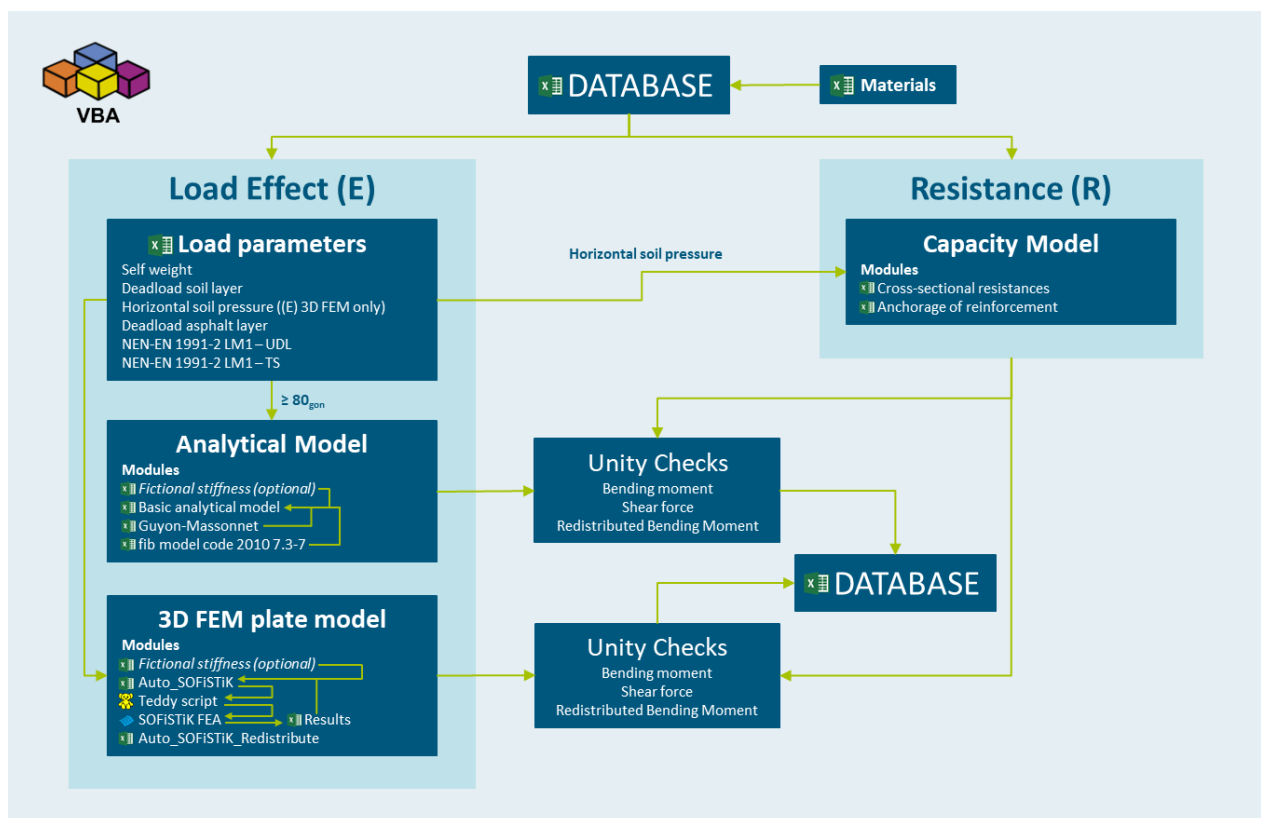
Figure 64 Schematic flowchart of the ASA Tool

In Appendix E1 an impression is given of the ASA Tool by showing the input sheet, the process indicator that becomes visible during the calculations and the table output.

6.3.1   Advantages of an ASA with script-based FEM analysis

An automated structural assessment with a script-based FEM analysis results in a completely new workflow compared to the traditional use of FEM software, which is accompanied by several interesting advantages for both research purposes and practical application.

A fully script-based structural analysis, which is set up completely parametrically, such as the ASA Tool in this research, offers the possibility to quickly and unambiguously perform structural assessments for batches of structures. With a standard mobile workstation, an enterprise level laptop, with a quad-core processor running at 2,70 GHz base speed, running the analytical model together with determining the capacity takes an average of 20 seconds per structure, which means that approximately 180 structures can be evaluated per hour. A more advanced analysis with the 3D FEM plate model takes about 5 minutes per structure. The structural assessment of an underpass or culvert thus takes approximately 5 minutes and 30 seconds, which means that approximately 11 structures can be assessed per hour. The analytical model is therefore significantly faster and certainly interesting for large batches.

An automated structural analysis which has been set up parametrically is ideal for performing sensitivity analyses within a research, through automation the process is consistent, and the results are obtained relatively easily and quickly. In addition, it offers a practical advantage because changes can be implemented quickly by simply adjusting the script and rerunning the structural assessment for a complete batch of structures. The introduction of the new EuroCode 2020, the release of NEN 8702 as a supplement to EC2 for existing concrete structures and changes within a project are some practical examples of this. Another practical advantage is that an optimal design can easily be sought within the set requirements of a project on the basis of an extensive structural calculation, while at the same time having the advantage that changes over the course of the project can be easily implemented and the associated consequences can be checked.

The advantage of a modular design is that the individual modules can also be used separately, for example the automated running of a 3D FEM plate model in SOFiSTiK without the analytical model and the calculated capacities, and these separate building blocks can be used again for other projects. This also applies to parts of the Teddy script for the FEM analysis, for example the part that determines all coordinates of the lanes and TSs of LM1 can easily be applied to an RC slab bridge since everything is defined with respect to a self-defined origin.

6.4   Disapproval by ASA Tool

When a structure based on the ASA Tool is disapproved, it does not immediately mean that structural safety is at risk. In case of disapproval by the ASA Tool, a single calculation can be performed, in this way the complete analytical model, the drawn up Teddy script and the used model of SOFiSTiK can be retained which can be reviewed and any adjustments, in the script, may be able to ensure that the structure is approved after all. If, after checking the input and the modeling, it appears that a structure is not approved based on the ASA Tool, there are still a number of options shown in Table 36 and Table 37. These options are divided into arithmetic options and intervening options. Arithmetic options are understood to mean the options without having to change anything to the structure and without changing anything for the user of the structure. Intervening options are the options where something must be done to the structure or where something changes for the user of the structure.

Table 36 Arithmetic options in case of disapproval by ASA Tool

Arithmetic		
Category	**Description**	**Expected impact on UC**
Additional effects	a) The default values used for the modulus of subgrade reaction k can be revised, this only changes the distribution of the bending moment; b) The loads from the dead load of internally present soil and asphalt layer can be added to the model.	a) The effect on the UC is limited, not meaningful if $UC > 1,1$; b) The influence is very limited, because the sensitivity analysis from paragraph 5.1 shows that the influence of internal traffic is already small, not meaningful if $UC > 1,1$;.
Load model	a) The decentralized load model from TNO, described in (Steenbergen, Allaix, la Gasse, & Vervuurt, 2018), is expected to be beneficial for both bending moment and shear. For the application of the decentralized load model, no vehicles for which an annual exemption is required (approx. 60t~100t) are allowed on the structure, as a result of which a form of load limitation is applied, because this is allowed when using LM1.	a) The effect is not investigated within this research but at least expected to be significant based on the limited span of underpasses and culverts, the reduction to 80% TS and findings in reports of old assessments in the data analysis.
Model refinement	a) With a non-linear FEA one could more accurately approximate the capacity of a structure in order to calculate a lower UC. However, good modeling requires a detailed reinforcement layout and material properties.	a) The effect is not investigated within this research
Assessment level	a) Adherence to a shorter residual service life and reference period, this results in lower partial safety factors for application to the load effects.	a) The influence on the UC will be very limited, so that this option is only useful if $UC < 1,1$. Deviation from the recommended 30 years to the minimum required 15 years results in a reduction of approximately 0,02.
Material testing	a) Determining the current concrete compressive strength, especially if it is unknown, can have a significant effect on the calculated shear capacity (Par. 4.2 & 4.3). b) If the steel grade is unknown and reinforcement with plain bars must be assumed, it makes primarily sense for bending moment but also for shear in case reinforcement cannot be assumed as fully anchored with plain bars to check, based on destructive testing, whether the reinforcement used is ribbed (par. 4.2 & 4.3). However, based on the data analysis from paragraph 2.4, it is not often the case that the reinforcement layout is known but the steel grade is unknown.	a) Very significant influence, up to drop of UC by 0,3 (Figure 45). b) Significant influence due to required anchorage length and allowable stress.

Table 37 Intervening options in case of disapproval by ASA Tool

Intervening		
Category	**Description**	**Expected impact on UC**
Soil cover	a) The calculations from paragraph 4.4.1 show that for structures with small to medium span and no or very limited soil cover which are disapproved based on shear, it is very effective to apply a small extra soil cover on top of the structure to achieve a lower UC (Figure 45, Figure 51 & Figure 52).	a) The effect depends on the current soil coverage in relation to the length of the span. Up to a 0,2 drop of the UC.
Load restriction	a) Imposing a load restriction by means of signage (NEN 8701). However, this is often not accepted for structures in the main road network of highways.	a) The significance of the effect on the UC depends on the share of traffic load in relation to the total load on the structure.
Upgrading	a) If load restrictions are undesirable and the adaptation of the soil cover is practically not possible or does not lead to the desired result and it is nevertheless desired to maintain the structure, it can be investigated whether the structure can be upgraded by means of auxiliary structures.	a) Depending on the situation.

6.5   Discussion

A comprehensive reliability analysis was placed outside the scope at the start of this research. At the same time, it is important that the ASA Tool has some form of validation for the results to be considered as valuable. The analytical model was pre-checked with hand calculations with Maple based on the ODEs, manually checked with 1D FEM beam models, compared with a 2D plate model in paragraph 3.4, additionally validated in the sensitivity analysis of paragraph 5.1 and validated based on reports from calculations performed by other engineers. The analytical model is therefore intensively checked. The 3D FEM plate model has been validated based on the analytical model and calculations from old reports from colleagues. It is therefore that the results of the structural assessment of the ASA Tool are acceptable. However, before the ASA Tool can be used in practice, an additional validation report must be drawn up in which the exceptions, limits and any bugs that have not yet been discovered are reported.

By using the ASA Tool, the engineers' factor is limited as much as possible, the source of error is limited to the input by the automated analysis. By means of conditional input, the engineers' factor is further limited, an example of this is the materials module and the restrictions or warnings on certain inputs. Further robustness of the ASA Tool could be achieved by upgrading the Graphical User Interface with further restrictions and warnings. These restrictions can be based on the data from the data analysis and give the user a warning in case the input is remarkable compared to the practical boundaries found in the data analysis.

7

Recommendations

This chapter provides recommendations for practice and future research. Recommendations for practice are specifically aimed at the use and deployment of the ASA Tool and an automated structural assessment with script-based FEM analysis in general. Recommendations for future research are given based on findings from this research.

7.1 Recommendations for practice

7.1.1 Recommendations based on results of the ASA Tool

In the structural assessment of existing RC underpasses and culverts, attention must be paid to checking the anchoring of rebars bent from the wall into the deck as top reinforcement. In several cases, this appears not to extend far beyond the face of the supportive wall or the end of the haunch, so that it cannot be considered as fully anchored when determining both the bending moment and shear capacity, certainly not in case the reinforcement must be anchored at a location where shear cracks occur.

Based on the data analysis described in paragraph 2.4, the concrete strength class is unknown in more than half of the structures studied, where structures of local authorities with an unknown concrete strength class are heavily over-represented. According to CUR 124, a concrete strength class equal to EC C16/20 may be used for these structures by local authorities, whereby it is stated that a relatively low strength had to be used because a large spread in the results was found in the investigation into the concrete compressive strength. Based on structures with a known design concrete strength class from the data analysis in combination with the large distribution in the tested concrete cores, it is expected that a higher current concrete strength can be determined. paragraph 4.3 showed that maintaining a higher concrete strength results in a significant increase in the shear capacity. It is therefore recommended to investigate the current strength of the concrete based on tests for structures of local authorities with an unknown concrete strength class where a $UC > 1,0$ is calculated for shear in a structural assessment. It should be noted that through ongoing hydration of the concrete, to a lesser extent, an increased capacity can also be determined in relation to the design concrete strength.

Despite the fact that 73% of the structures in the database are managed by RWS, based on the estimate of the total number of underpasses and culverts in the Netherlands from paragraph 2.2.1, it can be expected that there would be significantly more structures in the management of local authorities. Given the relatively large number of structures of local authorities with a UC > 1,0, whether or not due to the lack of data, and the limited spans of underpasses and culverts, a reduced UC can be obtained by using the decentralized load model of TNO (Steenbergen, Allaix, la Gasse, & Vervuurt, 2018) and is therefore recommended.

7.1.2 Future of Automated Structural Assessment of structures

An automated structural assessment is expected to play an important role mainly for the assessment of structures in the existing infrastructure. As chapter 2 shows, a large proportion of existing underpasses and culverts in the Netherlands is built in the 60s and 70s of the last century, this means that for many of these structures the end of their designed service life has been, or nearly is, reached for which many structural assessments have to be carried out in the near future. To achieve this a major efficiency boost is required compared to the current approach, as also described in (van der Ploeg, 2018). This applies not only to existing RC underpasses and culverts, but to the overall infrastructure, as has recently been shown for

bridges and quay walls in Amsterdam, where it has also been concluded that an efficiency improvement is necessary (NOS, 2020).

Everything is fixed in a certain sense for existing structures and is therefore ideal for automating the structural analysis. In principle, an automated workflow is feasible for structures, or sections of it, that can be reduced to a fixed number of orientation points with which all variations of parameters within the scope can be modelled. Whether it is also cost-efficient and can be of added value partly depends on the number of structures to be assessed. For standard types of bridges such as RC underpasses or culverts, as in this study, but also RC slab bridges or even a prestressed box bridges, an automated structural assessment is expected to be feasible and of added value. Combined with the developed tool in the research *"Reverse Engineering of existing reinforced concrete slab bridges"* (Harrewijn, 2019), an even more widely deployable automated tool can be created with which structures with unknown reinforcement layout can also be assessed.

In addition to the possibility of unambiguously and quickly carrying out a structural assessment for large batches of existing structures, the parametric design of the ASA Tool makes it possible to implement changes quickly and to provide insight into the consequences thereof on the existing infrastructure. In the event of a change in standards or regulations, such as the arrival of the new EuroCode, EC 2020, and the arrival of the NEN 8702 to supplement EC2 for existing concrete structures, a whole set of structures can then be reassessed relatively quickly by adjusting the ASA Tool just once.

It is expected that the role of an automated structural assessment including an automated FEM model in new construction will be more focused on optimizing the design within the specific requirements of the project, which also offers the advantage that changes to the design or to the requirements can be processed quickly and unambiguously by which insight into the consequences of design choices can be gained.

7.2   Recommendations for future research

Cracking behaviour near supports of RC slabs without transverse shear reinforcement
In many of the structures investigated, the reinforcement from the wall is bent over as top reinforcement in the deck due to the construction phasing, while the area of the continuous top reinforcement in the deck is often not even half of the bent reinforcement, resulting in a discontinuity, which means that a part of the force must be anchored in a zone with potential shear cracks. Research described in (Muttoni, Rupf, & Ruiz, 2013) and (Olesen, Sozen, & Siess, 1965), shows that shear cracks near supports run more horizontally at an angle of about 30°. In the current regulations nothing is said about an adjusted angle near supports and the standard angle for the diagonal strut of 45° may simply be used. Paragraph 4.2 showed that for 22% of the investigated structures the reinforcement can no longer be regarded as fully anchored when the angle is adjusted from 45° to 30°, resulting in a significant increase in the number of structures with a $UC > 1{,}0$. However, the tested beams and slabs nowadays always have stirrup reinforcement, which the RC slabs of the existing structures within the scope of this research do not have. The tests also made use of concentrated loads, while the loads on the deck mainly consist of distributed loads. So, further research should answer the question whether for the angle θ for RC slabs without shear reinforcement primarily loaded with distributed loads a 30° angle must be adhered to or that a 45° angle, as currently permitted by the codes, is safe to use at all times.

Shear distribution of TS load in RC slabs without transverse shear reinforcement
Further research into the load distribution of TS in RC slabs should clarify whether the observed factor, with an average of 1,16, between the calculated total shear force based on the linear elastic analysis of the 3D FEM model with 2D plate elements and the analytical model based on method 7.3-7 from (CEB-fib, 2010) is due to load distribution from TS loads, both in-plane in the concrete slab as vertical through soil and asphalt layers, or that an increased shear capacity may be assigned by limited redistribution in a linear elastic model.

In this study, the most conservative angle of 45° for the in-plane shear distribution prescribed in (CEB-fib, 2010) for a fully clamped slab was used. The sensitivity, described in paragraph 5.2.3, of a change from 45° to 30° or 60° was investigated resulting in a mean change of V_{TS} of 7% when changing from 45° to 30°. Further research into the developed method for determining the occurring shear force as a result of TS must determine which angle should be used for the in-plane shear distribution in relation to the degree of clamping of the deck by the walls in order to obtain a more accurate method, especially with applicable to structures with a larger span. At the same time, it should be investigated whether in-plane shear distribution from the rear of the load plane of the wheels is not too optimistic and should be distributed from the centre of the load plane. Paragraph 5.2.4 showed that with limited vertical load distribution of TS through soil and asphalt in the method based on 7.3-7 from (CEB-fib, 2010), together with an adjusted formula 6.2.b for shear to the RBK formula for the 3D FEM model, the UC for shear is more similar to the 3D FEM model. In paragraph 5.4 it was concluded that vertical load distribution at a certain angle, as prescribed by EC, gives good results for bending but not for shear, at least not for local loads in method 7.3-7 from (CEB-fib, 2010). Research into vertical load distribution for the determination of the occurring shear force of local loads must determine whether distribution at a fixed angle leads to the correct results. A validation of the method for determining V_{TS} must determine whether the method is suitable for use on other structures with RC slabs, such as application on an RC slab bridge.

Rules of thump for existing RC structures based on "big data"
Further research with automated structural analyses could generate enough data based on variations within the practical limits of underpasses and culverts in the Netherlands, so that, based on statistical models, under the term "big data", rules of thumb for the structural safety of existing RC underpasses and culverts can be set up. The moment an ASA Tool becomes available for other construction types, more structured knowledge of the existing infrastructure can be built on.

Predictive twins
In addition to a more efficient assessment method, through the use of automated structural assessment, a better distribution of the replacement task of existing structures in the Netherlands can be sought by being able to predict more precisely when a structure has really reached the end of its service life or having insight into which measures can still be taken to extend the service life, as reported by (Adriaanse, Borsboom, & Roef, 2020). Research must demonstrate the added value of the application of predictive twins in optimizing the replacement process of the existing infrastructure in the Netherlands.

8

Conclusion

A large part of the Dutch infrastructure, including underpasses and culverts, was built during a major construction wave in the 1960s and 1970s, with a designed service life of 50 to 80 years, many of these structures have reached the end of the designed service life or will soon reach them. It is practically impossible and financially unfeasible to replace all these constructions at once and for some of these structures it is also expected that the designed service life can be extended. In order to determine which structures are the most critical or whether a structure can still be approved based on current standards and guidelines many structural assessments must be carried out, even so much that there is a need for automation. The aim of this thesis is to achieve an automated structured consistent method for the structural assessment of existing reinforced concrete underpasses and culverts in the Netherlands with which unnecessary disapproval and unjustified approval can be avoided, a fast and cost-efficient structural analysis is delivered and objects where structural safety is at risk can be identified. To this end this research sought an answer to the question: *"How can the structural assessment of existing reinforced concrete underpasses be automated to provide a quick and cost-efficient generic method which prevents unnecessary disapproval and unjustified approval, which ultimately makes it possible to build structured knowledge of the existing underpasses?"*

The research started with a data analysis in which an estimate is made of the number of underpasses and culverts in the Netherlands and available data from RDHV of existing reinforced concrete underpasses and culverts in the Netherlands is gathered and examined. Based on exact numbers from RWS, there are an estimated 11.000 underpasses and culverts in the Netherlands, 1321 of which are structures in the management of RWS and the rest in the management of local authorities. Within the available data of 64 structures studied, 81% of the structures investigated has a box-shaped construction type, making it by far the most widely used construction type for underpasses and culverts in the Netherlands. The longitudinal reinforcement ratios for box-shaped structures are fairly spread apart with ρ_l from 0,35% to 1,00%. It is concluded that the "engineers' factor" was already present at the time, especially in periods of transition from old to new design codes with new calculation methods and materials. The available data is just like the structures concentrated in the period from the GBV 1962 to the VB74, regarding the development of the design code no clear connection with the new insight into shear capacity with the VB74 can be seen in the data. A high-quality steel, QR40 or FeB400, has been used for all structures from that period and there is no clear jump in the reinforcement ratio. Plain reinforcement steel, QR22 and QR24, is not common for underpasses and culverts which are designed in the period after the GBV 1950, since QR22 and QR24 have only be found in structures before the GBV 1962. The data does show that the reinforcement steel used makes a leap around the introduction of the GBV 1962 to the higher steel grade QR40, and later FeB400, while the development of the used concrete strength classes is lagging behind but is progressing gradually.

Research into the structural assessment started with drawing up an analytical model for determining the load effect, which was determined for structures from the database and a set of theoretical structures for the parameter studies. The theoretical structures are divided into three categories, CAT I representing culverts and bicycle underpasses with a relatively small span, CAT II representing small to medium sized mixed traffic underpasses with a medium size span and CAT III mixed traffic underpasses with a relatively large span. The limit values of the parameters are based on the data analysis. Most structures fall under CAT I and CAT II and have a limited soil coverage on which it can be concluded that the occurring section forces are dominated by the TS load from LM1. Only for structures from CAT III, with a large span, or

structures with a soil coverage from 1m applies that the occurring section force is determined for a maximum of 50% by the TS. This means that special attention must be paid to distribution of the TS load in order to minimize the load effect. In the analytical model a method is set up in this research as an extension of the method 7.3-7 from (CEB-fib, 2010) to determine the occurring shear force as a result of TS on the basis of the effective distribution width. A model refinement to a 3D FEM model with 2D plate elements results for the investigated structures compared to the analytical model in a significant decrease of the bending moment by an average of 18%, on which it is concluded that model refinement to a 3D FEM model with 2D plate elements is useful if a structure is disapproved based on bending moment. The difference in calculated bending moment between the analytical model and the 3D FEM plate model can be attributed for 10% to the model refinement by modeling the haunch and the interaction with the soil by springs, 3% is attributed to additional horizontal soil loads and 5% can be attributed to load distribution of the 3D FEM plate model compared to Guyon-Massonnet. For structures with a traffic intersection angle less than 80_{gon} ($\approx72°$), large deviations in the calculated bending moment with an average overestimation of 34% compared to the 3D FEM plate model are calculated by the analytical model and it is therefore concluded that for these structures the 3D FEM plate model thus also has added value. If, despite a negative advice from the RBK, a structure with an intersection angle smaller than 80_{gon} is nevertheless assessed with a model with bar elements and it is approved based on the calculation, one seems based on the results of the assessed structures in any case on the safe side with regard to bending.

For shear, a significantly higher occurring shear force is calculated with the 3D FEM plate model with an average of +16% compared with the analytical model. Method 7.3-7 from (CEB-fib, 2010) is based on failure tests of concrete slabs (Muttoni, Rodrigues, & Burdet, 2006) and is thus in fact a calibrated analytical method for a non-linear problem, the 3D FEM plate model is assumed to be isotropic, which results in the model for more distribution, but is still a linear approach to the problem. In the tests redistribution occurs through cracks, but not in a linear elastic FEM model. The research results show that a reduction of the in-plane shear distribution by a reduction of the distribution angle from 45° to 30°, which is less than the minimum recommended angle of 45° in (CEB-fib, 2010), has insufficient effect to explain the higher calculated shear force with the 3D FEM plate model. A comparison with a limited vertical load distribution for the method based on 7.3-7 from (CEB-fib, 2010), because in the tests described in (Muttoni, Rodrigues, & Burdet, 2006) no soil and asphalt was present either, and an adjustment of the calculated shear force capacity to the RBK formulas for the 3D FEM plate model, to account for the effect of a higher redistribution with low steel grades at the capacity side by arithmetically releasing the yield strength of the reinforcement f_{yk}, results in an average deviation of the UC for shear of -5% from the analytical model, whereby it can be concluded that vertical load distribution under a certain angle, as prescribed by EC, gives good results for bending but not for shear with method 7.3-7 from (CEB-fib, 2010). The model refinement of modelling the haunch provides an additional reduction of the calculated UC for shear by an average of 7% because of a change in stiffness due to the haunch and because a part of the shear force is transferred as normal force by an inclined model line. It has been concluded that a model refinement to a 3D FEM model with 2D plate elements may offer added value in terms of a lower UC compared to the method based on 7.3-7 from (CEB-fib, 2010), but the differences are limited with an average deviation of 5% found for the structures studied. In addition, when a structure is disapproved based on shear in the section at the end of the haunch under a sagging bending moment, the 3D FEM plate model does offer an added value with regard to shear because it has been found that the analytical model in a significant number of the examined cases incorrectly checks the shear capacity under a sagging bending moment at the section at the end of the haunch.

The influence of a haunch on both the calculated bending moment, due to stiffness differences, and shear force, because a part is transferred as normal force, is significant and the data analysis showed that most structures have a haunch, for which it is concluded that attention should be spent on the correct modeling of the haunch in the deck of an underpass or culvert. The sensitivity analysis showed that the modulus of subgrade reaction, the stiffness of the bedding, only influences the moment distribution but is limited with a maximum deviation of 3,8% found to which the stiffness of the soil around the structure is standardized.

The load bearing capacity of existing RC underpasses and culverts is determined for both the analytical model and the 3D FEM plate model based on the critical cross-sections of the deck at the face of the wall, at the end of the haunch and at midspan. Arithmetic research into the calculated cross-sectional shear capacity for existing structures has shown that formula 6.2b from RBK for determining the lower limit of the shear capacity probably overestimates the capacity. Formula 6.2.b, which should be the transition to flexure failure, is often governing for the structures studied over 6.2.a, which actually describes shear failure, while shear is governing over bending moment. Based on a further analysis it has been concluded that the arithmetic release of the yield strength of the reinforcement f_{yk} must be removed from the equation because it causes an overestimation of the capacity in case of steel grades lower than FeB 500. Based on the same arithmetic research, it is also concluded that the application of the plate factor k_p in both formula 6.2a and 6.2b to determine the shear force capacity is justified. Additional research with 3D FEM plate models compared to the analytical model has shown that for a linear elastic FEM model the arithmetic release of f_{yk} in formula 6.2.b leads to more comparable UCs for shear, which concludes that for linear elastic 3D FEM plate models the shear capacity formulas according to RBK can be used.

In many of the structures investigated, the reinforcement from the wall is bent over as top reinforcement in the deck due to the construction phasing, in several cases this reinforcement appears not to extend far beyond the face of the supportive wall or the end of the haunch. This results in a typical problem because the area of the continuous top reinforcement in the deck is often not even half of the bent reinforcement, resulting in a discontinuity, which means that a large part of the force must be anchored in a zone with potential shear cracks. The conclusion is that in many of these cases it cannot be considered as fully anchored resulting in both a decreased bending moment and shear capacity. Structures owned by local authorities with unknown concrete strength class, which means that a EC C16/20 concrete class may be maintained in accordance with CUR 124, are in many cases disapproved based on shear capacity, while calculations have shown that the same structures are approved with a higher concrete strength class. The CUR 124 describes that a large distribution in the results of the tested concrete cores was found, so that the relatively low C16/20 had to be maintained. It is therefore concluded that it can be expected that performing tests to determine the current concrete compressive strength is an effective way to make a structure with an unknown design concrete strength approved after all.

For a quick assessment of a large batch of structures, it is concluded that the analytical model with the Guyon-Massonnet method to determine the maximum occurring bending moment, taking into account the load distribution of LM1 and the method set up in this research as an extension of the method 7.3-7 from (CEB-fib, 2010) to determine the occurring shear force as a result of TS on the basis of the effective spreading width should be used first. The model refinement to the 3D FEM plate model does generally result in a 5% reduction of the UC for shear, but for bending it does have a more significant added value in terms of a reduction of the UC due to a decrease in the bending moment of approximately 18%. For structures with an intersection angle less than 80_{gon} it is concluded that the 3D FEM plate model should be used directly. For structures prior to the GBV 1962 bending is usually the governing failure mechanism, for structures from the GBV 1962 era shear force is clearly the governing failure mechanism and after the GBV 1962 shear force is still the determining factor for many underpasses, but bending is also more often seen as governing failure mechanism. This research has shown that an Automated Structural Assessment in which an analytical model is combined with a script-based FEM analysis leads to an ASA Tool of added value on the classic approach of assessing existing concrete underpasses and culverts by significantly improving efficiency and therefore to realize a cost-efficient method.

9
Bibliography

Abolmaali, A., & Garg, A. (2008). *Shear Behavior and Mode of Failure for ASTM C1433 Precast Box Culverts.* Journal of Bridge Engineering ASCE.

Abolmaali, A., & Garg, A. K. (2008). *Effect of Wheel Live Load on Shear Behavior of Precast Reinforced Concrete Box Culverts.* Journal of Bridge Engineering ASCE.

Adriaanse, P., Borsboom, W., & Roef, R. (2020, November 24). *Naar netwerken van Predictive Twins van de gebouwde omgeving.* Delft: De Nederlandse organisatie voor Toegepast-Natuurwetenschappelijk Onderzoek (TNO).

Barten, P., & 't Hart, M. (2018). Shear Capacity - Crossing Borders. In D. Hordijk, & M. Lukovic, *High Tech Concrete: Where Technology and Engineering Meet* (pp. 701-709). Springer International Publishing.

Blaauwendraad, J. (2010). *Plates and FEM.* Springer Science + Business Media B.V.

Bleijenberg, i., Maljars, P., Polder, P., Steenbergen, P., & Vervuurt, D. (2017, March 22). *De staat van onze bruggen*. Retrieved from https://tno.nl: https://www.tno.nl/nl/tno-insights/artikelen/de-staat-van-onze-bruggen/

Braam, R., & Lagendijk, P. (2010). *Constructieleer Gewapend Beton (CB2).* de Vrije Uitgevers.

Burns, J. C. (2006). *Experimental investigation of shear capacity of precast reinforced concrete box culverts.* The University of Texas at Arlington.

CEB-fib. (2010). *Model Code 2010.* Lausanna: the International Federation for Structural Concrete.

Cementindustrie, V. N. (1993). *Handleiding Betonwegen.* 's-Hertogenbosch.

Coleman, D. M., Harrison, J. A., & Woodson, S. C. (1990). *Evaluation Procedure for Reinforced Concrete Box Culverts under Airfield Pavements.* Mississippi: US Army Corps of Engineers.

CROW-CUR. (2019). *Aanbeveling 124:2019 Constructieve veiligheid bestaande bruggen en viaducten van decentrale overheden.* Ede: CROW.

Cullington, D. W., Daly, A. F., & Hill, M. E. (1996). *Assessment of Reinforced Concrete Bridges: Collapse Tests on Thurloxton Underpass.* London: E & FN Spon.

Ezi, E., Onuamah, P., Ugwuanyi, D., & Agbo, I. (2018, August). Advances in the Analysis of Simply Supported Concrete Bridge Deck. *Glabal Scientific Journal*, pp. 352-367.

Gantvoort, i. (1964, August). Betonstaal, overzicht van maten en eigenschappen. *Cement*, pp. 638-647.

Garg, A. K., & Abolmaali, A. (2009). *Finite-Element Modeling and Analysis of Reinforced Concrete Box Culverts.* Journal of Bridge Engineering ASCE.

Garg, A. K., Abolmaali, A., & Fernandez, R. (2007). *Experimental Investigation of Shear Capacity of Precast Reinforced Concrete Box Culverts.* Journal of Bridge Engineering ASCE.

Gijsbers, J. (2012, augustus). 100 jaar betonvoorschriften. *Cement online*, pp. 68-77.

Gijsbers, J., Dieteren, G., & van der Veen, C. (2012, april). Beoordelingskader bestaande constructies. *CEMENT Online*, pp. 18-25.

Harrewijn, T. (2019). *Reverse Engineering of existing reinforced concrete slab bridges.* Delft: Delft University of Technology.

Lantsoght, d. (2012). *Achtergrondrapport bij spreadsheet voor toetsing aan rand.* Delft: Delft Univeristy of Technology.

Latour, i. (1958, October). Tussentijdse wijziging van de G.B.V. 1950. *Cement*, p. 862.

Mulder, R. (2015). *Onderzoek gemeentelijke bruggen.* Zoetermeer: Bouwend Nederland.

Muttoni, A., Rupf, M., & Ruiz, M. F. (2013, June 15). Post-tensioned girders with low amounts of shear reinforcement: Shear strength and influence of flanges. *Engineering Structures*, pp. 357-371.

Muttoni, P., Rodrigues, V., & Burdet, D. (2006). *Large Scale Tests on Bridge Slabs Cantilevers Subjected to Traffic Loads.* Lausanne, Switzerland: Structural Concrete Laboratory, Ecole Polytechnique Fédérale de Lausanne.

NEN. (2011). *NEN 8700 Beoordeling van de constructieve veiligheid van een bestaand bouwwerk bij verbouw en afkeuren - Grondslagen.* Delft: NEN.

NEN. (2011). *NEN 8701 Beoordeling van de constructieve veiligheid van een bestaand bouwwerk bij verbouwen en afkeuren - Belastingen.* Delft: NEN.

NEN. (2015). *NEN-EN 1991-2+C1:2015.* Delft: NEN.

NEN. (2016). *NEN-EN 1992-2:2016.* Delft: NEN.

NEN. (2016). *NEN-EN 1992-2:2016 National Annex.* Delft: NEN.

NEN. (2018). *NEN 8702 [ONTWERP] Beoordeling van de constructieve veiligheid van een bestaand bouwwerk bij verbouw en afkeur - Betonconstructies.* Delft: NEN.

NEN. (2019). *NEN-EN 1991-1-1+C1+C11:2019 National Annex.* Delft: NEN.

NEN. (2019). *NEN-EN 1990+A1+A1/C2:2019.* Delft: NEN.

NEN. (2019). *NEN-EN 1990+A1+A1/C2:2019 National Annex.* Delft: NEN.

NEN. (2019). *NEN-EN 1991-1-1+C1+C11:2019.* Delft: NEN.

NEN. (2019). *NEN-EN 1991-2+C1:2015 National Annex.* Delft: NEN.

NOS. (2020, July 6). *Deel Amsterdamse bruggen en kades staat op instorten.* Retrieved from NOS.nl: https://nos.nl/artikel/2339738-deel-amsterdamse-bruggen-en-kades-staat-op-instorten.html

Olesen, S., Sozen, M. A., & Siess, C. P. (1965). *Investigation of prestressed reinforced concrete for highway bridges, part IV: strength in shear of beams with web reinforcement.* Illinois: University of Illinois College of Engineering.

Rijkswaterstaat. (2007). *Inventarisatie Kunstwerken.* Rijkswaterstaat Bouwdienst.

Rijkswaterstaat. (2008). *Eindrapportage beoordeling kunstwerken.* Rijkswaterstaat Bouwdienst.

Rijkswaterstaat. (2013). *Richtlijnen Beoordeling Kunstwerken v1.1.* Utrecht: RWS GPO.

Rijkswaterstaat. (2017). *Richtlijnen Ontwerp Kunstwerken v1.4.* Utrecht: RWS GPO.

Rijkswaterstaat. (2020, March 11). *Bouwwerken en monumenten van Rijkswaterstaat.* Retrieved from https://www.rijkswaterstaat.nl: https://www.rijkswaterstaat.nl/wegen/wegbeheer/aanleg-wegen/zorg-voor-cultuurhistorie-en-archeologie/bouwwerken-en-monumenten.aspx

Rijkswaterstaat. (2020, March 11). *DISK Webviewer app.* Retrieved from https://maps.rijkswaterstaat.nl: https://maps.rijkswaterstaat.nl/geoweb55/index.html?viewer=DISK.Webviewer_app

Steenbergen, R., Allaix, D., la Gasse, L., & Vervuurt, A. (2018). *Verkeersbelastingmodel voor wegverkeersbruggen in het onderliggend wegennet zonder jaarontheffingen, Technical report.* Delft: De Nederlandse Organisatie voor toegepast-natuurwetenschappelijk onderzoek (TNO).

TIOBE Index. (2020, November 30). Retrieved from TIOBE: https://www.tiobe.com/tiobe-index/

Uysal, H. (2017). *Numerieke en Experimentele Bepaling van het Draagvermogen van een Bestaande Prefab Duiker uit 1971.* Dordrecht: TU Delft, Arcadis.

van der Aa, P., & van den Bos, A. (2018, June). Parametrisch ontwerpen in DIANA. *Cement*, pp. 42-46.

van der Ploeg, C. (2018). De keuze voor parametrisch ontwerpen. *Cement Online*.

Vereniging Nederlandse Cementindustrie, (. (1993). *Handleiding Betonwegen.* 's-Hertogenbosch.

Vergoossen, i. (2008, July). Het afschuifdraagvermogen met dwarskrachtwapening. *Cement*, pp. 80-83.

Vergoossen, i. (2008, April). Het afschuifdraagvermogen volgens Nederlandse ontwerpnormen. *Cement*, pp. 83-87.

Vergoossen, i. (2008, May). Het afschuifdraagvermogen volgens Nederlandse ontwerpnormen (2). *Cement*, pp. 93-95.

Vergoossen, R. (2019). Bestaande bruggen algemeen (presentation).

Yang, Y. (2020). *CIE5127 Concrete Bridges - 6. Guyon Massonnet.* Retrieved from brightspace.tudelft.nl: not publicly available

A

Appendix – Chapter 2: Preliminary Study

A1   Summary of used Literature

Evaluation procedure for reinforced concrete box culverts under airfield pavements

The research in this report was conducted for the US Army Corps of Engineers from January 1983 to March 1990 by David M. Coleman, James A. Harrison and Stanley C. Woodson. For many airfields assessments are performed on regular basis to check whether the pavement meets the required structural capacity for traffic loads of today and the anticipated loads of the future. Their research was focused on the development of a standard procedure for determining the structural capacity of reinforced concrete box-shaped culverts in airfield pavements under aircraft loads. Just like in this research they wanted a method to be able to rapidly evaluate the structural capacity of a box-shaped structure. Their strategy was to look for methods already available and further develop that for evaluating culverts under aircraft loads. That is a completely different strategy than the strategy envisaged in this study. They came up with two alternatives. The first method called CANDE-1980 was a finite element analysis which, as they described: "Provides powerful modeling capabilities, and good level of detail when used properly". Nevertheless, this alternative was not chosen because it was too complicated and too asked too much computing power at the time. CORTCUL was chosen, a program that uses design rules from standard ACI-318 dating from 1963, where ACI stands for American Concrete Institute. This was a simple, straightforward and user-friendly method which did not require much computational power.

However, once a method was chosen, a study was conducted into the sensitivity of different parameters. A sensitivity analysis is also one of the research steps in this study.

They concluded that:
- The evaluation of box-shaped culverts is relatively insensitive to variations in the lateral earth pressure coefficient (k);
- The internal water level has a negative effect on the bending moment, especially in the midspan of the walls and deck. By an increase of the live load the effect of the internal water level on the culvert decreases, under aircraft load this effect drops below 10%. So, the influence of the internal water level is small compared to the influence of the much larger live load, therefore it is stated that the box-shaped construction is relatively insensitive to variations in the internal water level. It is advised that the internal water level is accounted for in the analysis if the culvert carries water most of the time.

They have also studied the variation of load factors for cases that the loads are well defined, in which case lower load factors could be used. But no specific, new, conclusions have been reached.

The conclusions of their study can be included in this study but will nevertheless have to be tested again. The main goal and background of their research is partly the same, but the strategy for finding the right model is different and the final product is outdated.

Assessment of reinforced concrete bridges: Collapse tests on Thurloxton underpass

Just like in the Netherlands many bridges in the UK have been found to have insufficient shear capacity. In 1996 as part of a research project an in-situ collapse test was carried out on a strip of a reinforced concrete underpass called Thurloxton underpass. The structure was 10m wide and had a effective span of 4,37m. The top slab was 300mm thick and had main reinforcement in the bottom face of 25mm diameter at 115mm centres. A cross-section of the Thurloxton underpass is shown in Figure 65.
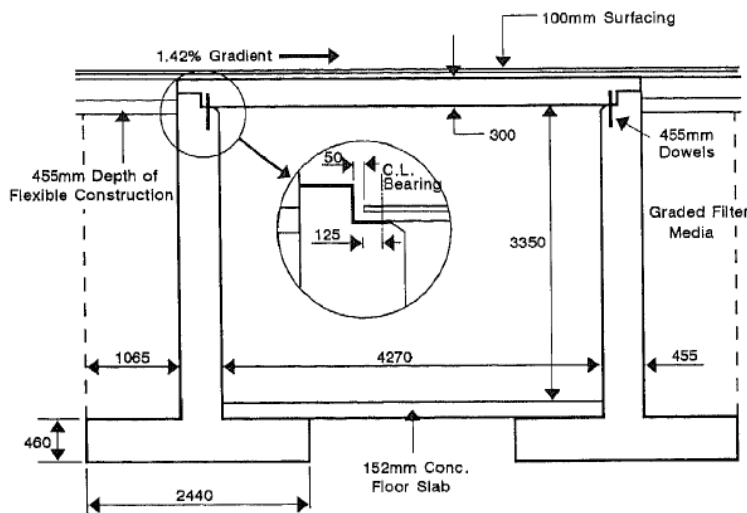
Figure 65 Cross-section of Thurloxton underpass

The anchorage length of the tensile reinforcement in the deck has a very large influence on the capacity of the structure. In the case of the Thurloxton underpass, the capacity changed from 3 tons for no anchoring, neglecting the steel, theoretically resulting in shear failure to 40 tons for fully anchored steel resulting in flexural failure. Another option is, a middle way, partial anchorage in which the steel surface is reduced by the ratio between the available anchorage and the required anchorage. For the Thurloxton underpass this partial anchorage theory led to a capacity of 17 tonnes. Which is therefore worthwhile in case the requirements regarding full anchoring are not met.

The strip tested on site had a shear span of 3,9d which resulted in a ductile flexural failure. The bending moment was approximately 30% greater than the calculated capacity, the associated shear force was 7% greater than calculated assuming fully anchored steel without any signs of shear cracking. The two tests conducted in the laboratory with a shorter shear span of d and 2d both ended in shear failure but at loads significantly larger than obtained by calculations assuming the steel to be fully anchored. They have observed evidence of shear enhancement despite the short anchorage at shear spans of d and 2d. The shear capacity where the load is placed within a distance 2d from the support seemed to be significantly higher. In NEN 1992-1-1 it is stated that loads within a distance 2d from the support, may be reduced for the calculation of the shear capacity. But this is only valid under the condition that the longitudinal reinforcement is fully anchored at the support, while the tests seem to suggest otherwise.

Shear Behaviour and Capacity of Precast Reinforced Concrete Box Culverts

In the period from 2007 to 2009 Anil K. Garg and Ali Abolmaali published multiple articles in the American journal of bridge engineering from ASCE about the research they have conducted on precast reinforced concrete culverts. With their research they tried to gain insight into the shear behaviour and capacity of precast reinforced concrete box culverts designed according to the American standard ASTM C1433.

The first article that appeared (Garg, Abolmaali, & Fernandez, Experimental Investigation of Shear Capacity of Precast Reinforced Concrete Box Culverts, 2007) reported on the experimental research into the shear capacity of concrete box culverts with a span of 1.2 meters. The results of six full-scale 2,4 m span box culverts were published in (Abolmaali & Garg, Effect of Wheel Live Load on Shear Behavior of Precast Reinforced Concrete Box Culverts, 2008), in this article they mentioned that other articles about the 0,91, 3,66 and 7,32 m spans culverts will be published but these articles were not found. Later that year results of the study that evaluates the shear behaviour and mode of failure were published in (Abolmaali & Garg, 2008). In (Garg & Abolmaali, Finite-Element Modeling and Analysis of Reinforced Concrete Box Culverts, 2009) they present the study of finite-element modeling and analysis of reinforced concrete box culverts. A comprehensive overview of the experiment design and results of the 1,22 m span culverts can be found in (Burns, 2006).

Tested culverts

Since their focus was on prefabricated concrete box culverts the span and internal height combinations came in a standard range, limited by the shipping weights and sizes. In total they have tested 24 cases with various spans, the internal height was kept constant at 1,22 m. Spans of 0,91, 1,22, 2,44 and 3,66 m were tested as stated in (Abolmaali & Garg, 2008), probably no tests were eventually performed on a culvert with a span of 7.32 m. Depending on the span the thickness of the top slab, bottom slab and walls varied. The culverts are reinforced with smooth welded wire reinforcement mesh as per ASTM standard A185 (2001). A typical cross-section and a detail of the reinforcement at the haunch of the tested precast reinforced concrete box culverts is shown in Figure 66.
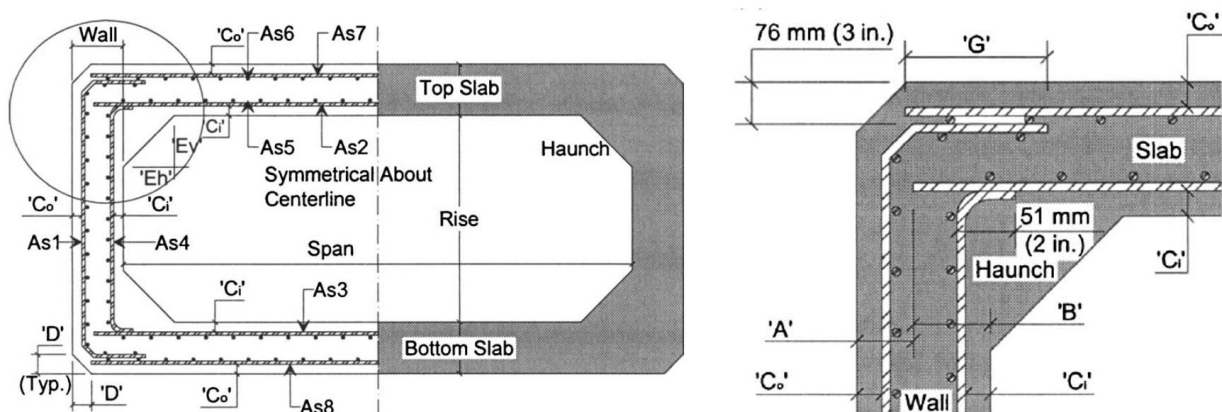
Figure 66 Typical cross-section of box culvert (left) and detail of reinforcement at haunch (right)

Each culvert was subjected to an incrementally increasing load through a steel plate which represented the wheel of the truckload HS20 as stated in AASHTO 2005. The load was applied at three different locations on the top slab to capture the location at which the maximum shear force is induced. They have tested at 127, 1675 and 292 mm from the tip of the haunch. The test set-up is shown in Figure 67.

The soil layer on top of the culvert has been neglected because the most critical situation for the top slab was considered, if the soil layer were to be taken along there would be more load in total on the top slab,

but the concentrated wheel load is spread, which significantly reduces its effect. The soil on the sides of the culvert has also be neglected as it decreases the effect of the wheel load on the top slab, even though the influence turned out to be relatively small, this was checked separately.
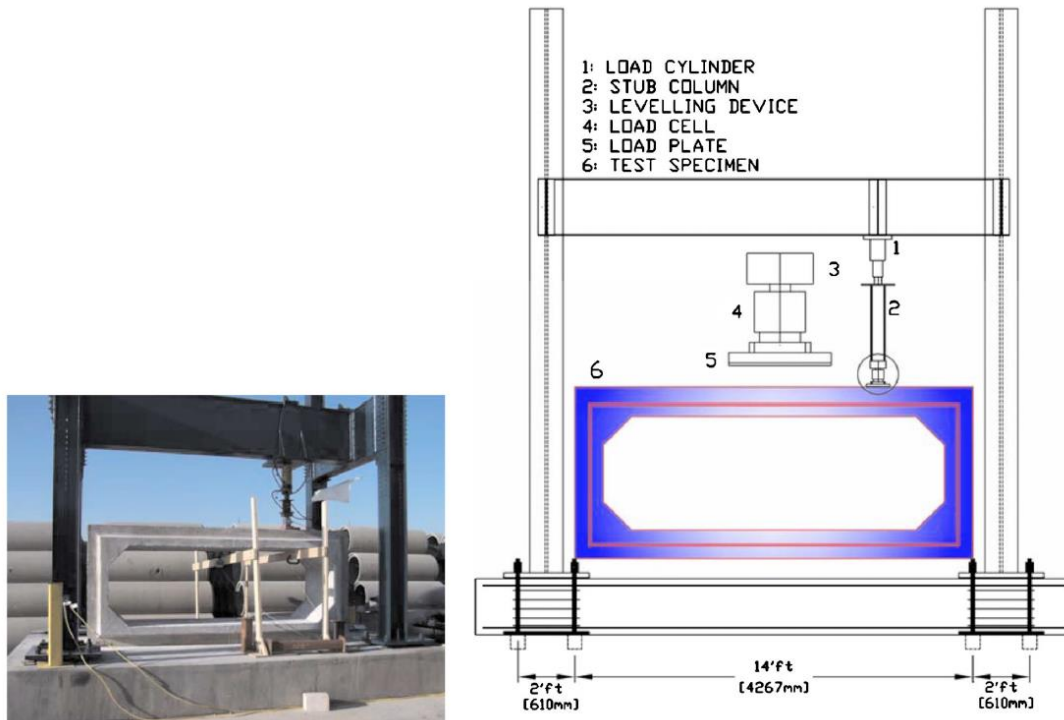
Figure 67 Typical test set-up (left) and schematization with instrumentation (right)

Test results

The tested culverts with a span of 1,22 m all behaved in a similar way with initial flexural cracks forming at the top of the bottom slab and the bottom of the top slab followed by failure cracks as a combination of bond and shear cracks. The failure load for the 1,22 m specimen ranged from 578 kN to 712 kN. It must be noted that all the test specimens failed at loads 1,5 to 2 times above the strength limit state for live load used in design per AASHTO (2005).

Six 2,4 m span box culverts were tested to failure which showed that initially flexural cracks governed the behaviour even at loading somewhat above the design load but in the end a combination of flexure, shear and bond slippage was the cause of the failure for all the tested culverts. But shear cracks did not arise until after almost twice the design load was applied. The failure load for the 2,44 m specimens ranged from 391 kN to 543 kN, which is an average decrease of 28% compared to the results from the 1,22 m span culverts.

The critical location for the wheel load for shear failure has been investigated, this turned out to be at a distance d from the tip of the haunch, where d is the effective height of the bottom reinforcement at midspan in the top slab.

Modelling

To simulate the experimental results a NLFEA with a 3D model of the concrete box specimen was made. Both material and geometrical non-linearities were accounted for. The culvert was modelled in 3D by shell and solid elements, the reinforcement was modelled using rebar, embedded, elements placed on the surface elements and the interface between the bottom of the bottom slab and the reaction floor was modelled by using a nonlinear node to surface contact analysis. Based on the meshes in Figure 68, obtained

from (Garg & Abolmaali, Finite-Element Modeling and Analysis of Reinforced Concrete Box Culverts, 2009), quadrilateral elements have been used, the number of elements in the coarsest and finest models were 1.055 and 16.166 respectively. The material properties used in the model are known and can be found in (Garg & Abolmaali, Finite-Element Modeling and Analysis of Reinforced Concrete Box Culverts, 2009). It was chosen to model discrete cracking of concrete using the smeared cracking model. Disadvantage of that is that the results are mesh dependent and can result in non-convergence for a unique result. The load was incrementally applied using the Newton-Raphson method to determine the iterative increment of the displacement vector. If no convergence was found, they reduced the increment.
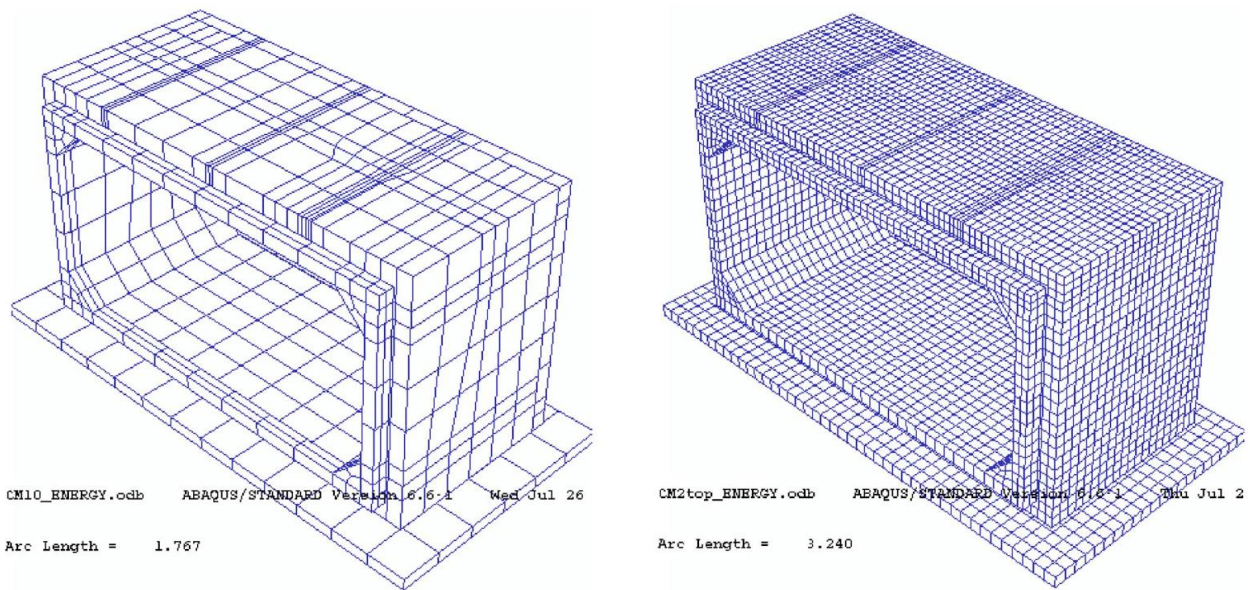
Figure 68 FEA Model with coarsest mesh with 1.055 elements (left) and finest mesh with 16.166 elements (right)

A close correlation was found between the FEM model, comprised of brick and shell elements, and the experimental results for the crack initiation and propagation. The order, with associated load, of cracking development is quite consistent with the results of the experiments. The load-deflection plot and the experimental results are shown together in Figure 69, which also shows that the FEM model and the experimental results are close to each other.
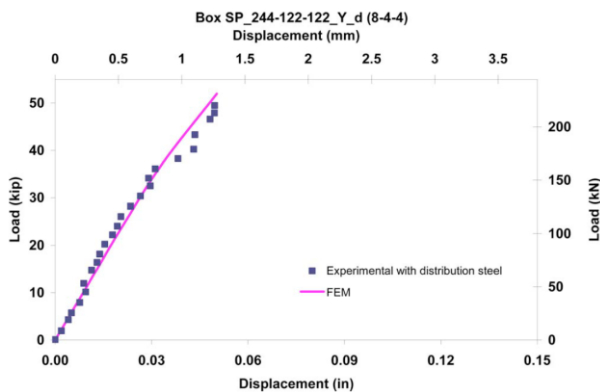
Figure 69 Load-deflection relation for FEM and experimental results

Conclusion

The results of the tested culverts with a span of 1,22 m show a cause of failure by a combination of bond and shear, while the culverts with a span of 2.4 m, in addition to bond and shear failure, also have flexure in the combination of failure mechanism. Based on these test data, shear is decisive for a relatively small span and that an increase in the span in combination with a higher slenderness will cause bending to occur in the failure mechanisms. Although the data of the larger spans is not known, it is to be expected that bending will become governing for larger spans.

A comparison between the results from the FEM model and the experiments shows that it is possible to get very close to the actual failure behaviour of a reinforced concrete culvert with a model. The only caveats are that much information about material properties must be known and that an NLFEA takes a relatively long time and can end in non-convergence.

The model, or models, of this research can be validated by the test results from Abolmaali and Garg. By giving the tool the input that most closely corresponds to the test situation, it is possible to determine to what extent the model corresponds to reality. However, the interaction between the structure and the surrounding ground cannot be checked with this validation.

"Numerieke en Experimentele Bepaling van het Draagvermogen van een Bestaande Prefab Duiker uit 1971"

The thesis title translates to *Numeric and experimental determination of the load bearing capacity of an existing prefab culvert from 1971*.

The province of Zuid-Holland has developed a uniform model for the assessment of the structural safety of existing prefabricated reinforced concrete culverts. The model developed by the province is based on a simply supported beam with rotational springs at the supports representing the deck of the culvert. All calculations and checks are performed within an EXCEL-sheet.

The research conducted by Uysal focusses on the ultimate load bearing capacity of a precast reinforced concrete culvert called "Schaapswegduiker", which was built in 1971. For that structure the method of the province is compared with two other models, one linear elastic analysis with a framework and one non-linear analysis with 2D elements in a 2D space.

Tested culvert

The tested culvert called "Schaapswegduiker" is situated in the area access road N498 and consists of precast concrete elements with a length of 1 m which are coupled together using post-tensioning. It is built in 1971, based on that year it would be assumed that it was designed according to the GBV 1962. However, experiments showed that the reinforcement was of the higher quality FeB 500, which later appeared in the VB 74. It is more common that structures from the period just before the publication of the VB 74 already have reinforcement, which is described in this standard because the design values were already known in practice before the standard was officially published. Both the span, from wall to wall, and internal height of the structure are 2,50 m. The culvert has a foundation on grade and on top of the structure a layer of soil, rubble and asphalt are present. A typical cross-section of the culvert is shown in Figure 70.
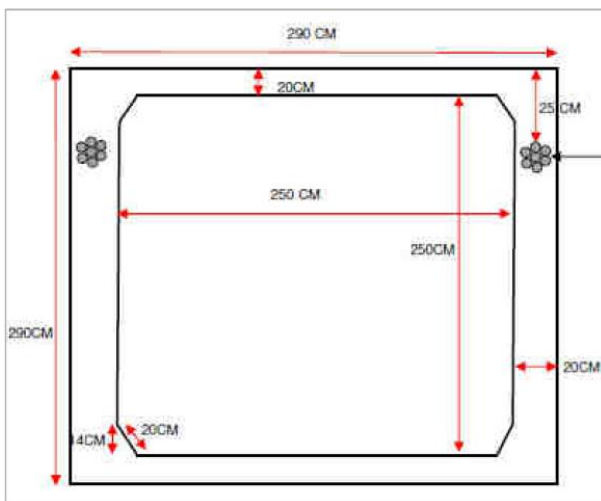
Figure 70 Typical cross-section of the culvert Schaapswegduiker

Used models

His report describes three different models, a simple and an advanced model that he has set up himself and the uniform model of the province which must be validated. All variants of models use EC, NEN8700 series and RBK.

The first model, *"Eigen gangbare berekening"* which translates to own common calculation, is a 2D framework model built in Technosoft Raamwerken. The beam elements represent one meter of the culvert

length which is exactly one precast element. He made two different frames, one with only four beams and one where the haunch was accounted for. The first mentioned variant will give a normative sagging moment at midspan, the second model will provide the normative hogging moment at the supportive wall. Uysal has also noted that the model that accounts for the haunch overestimates the hogging moment. The first model is shown in Figure 71. The following loads are included in this model: self-weight, vertical and horizontal ground and water loads, weight of asphalt and LM1 or LM2. The UDL and Tandem of LM1 have been distributed and translated to a representative uniform load in kN/m.
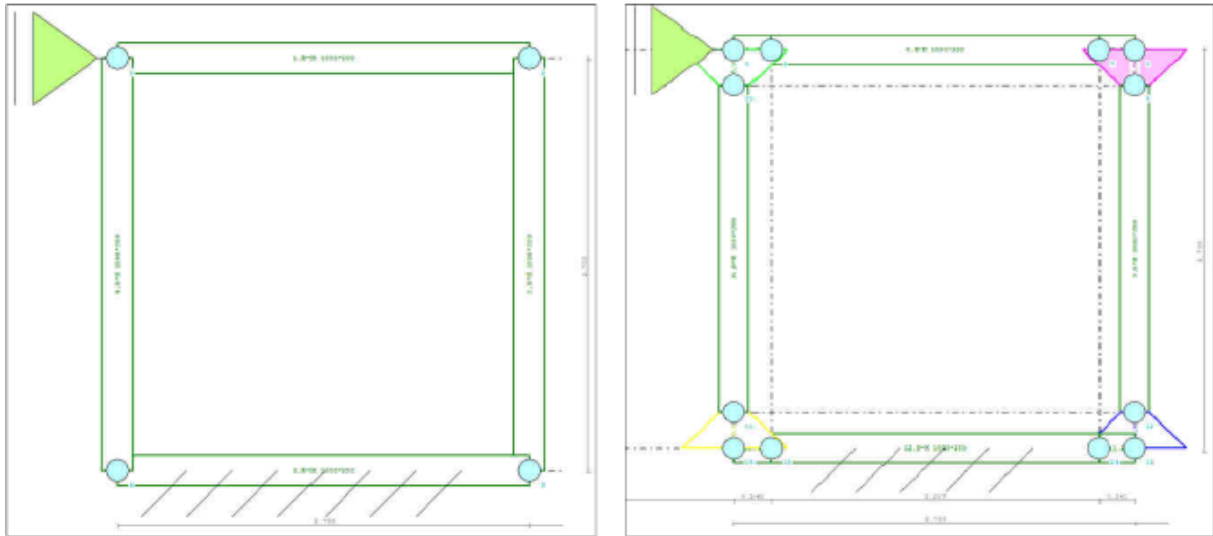
Figure 71 Model 1 common calculation

The uniform model of the province, in the report called as *"Uniform model, gangbare berekening PZH"*, is a simply supported beam with rotational springs at the end which represent the connection of the deck with the walls as presented in Figure 72. The province estimates that the deck of culverts is almost completely clamped by its walls, resulting in $\frac{1}{20} \cdot q \cdot L^2$ for sagging moment and $\frac{3}{40} \cdot q \cdot L^2$ for the hogging moment which together is $\frac{1}{8} \cdot q \cdot L^2$ again. It is expected that the deck will behave less like a clamped beam, which means that the sagging moment at midspan is assumed to be too small and the hogging moment at the supports are overestimated. Note that this has no influence on the shear force distribution. The loads are basically the same as mentioned for model 1, with the exception that the soil and water loads on the walls are not accounted for.
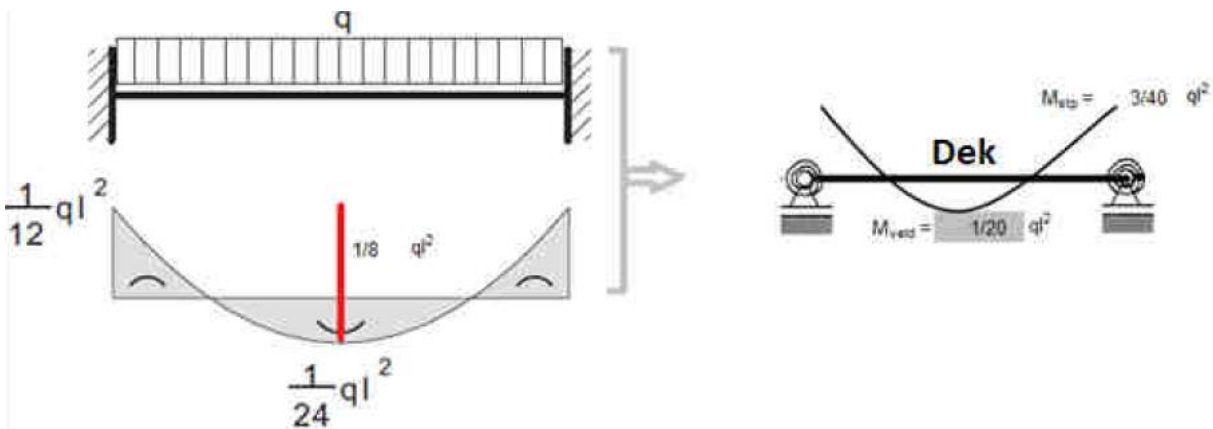
Figure 72 Model 2 drawn up by the province, to be validated

Finally, an advanced 2D NLFEA model is made in DIANA FEA. This model acts as a predictor model for the experiment to be performed and can be calibrated afterwards. His goal was to determine the failure load, check the crack patterns and failure mechanism and obtain a force-displacement graph. The model consists of 2D plane stress elements for the concrete, beam elements with a bond-slip interface for the reinforcement and the support blocks are modelled as 2D line interface elements. For the concrete a total strain-based crack model is used, for the reinforcement a Von Mises plasticity model is used and for the support linear material properties are used. The model is shown in Figure 73. The load is applied as a line force which should represent a single wheel load, but load distribution is not taken into account for the span direction since a width of 400 mm is applied. He applied the load at three different positions which would result in the greatest chance of flexure failure, shear failure and failure due to a combination of flexure and shear.
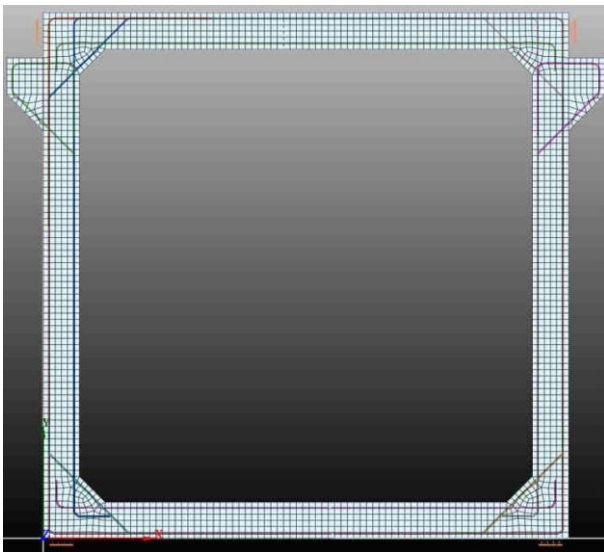
Figure 73 Model 3 NLFEA DIANA

Test set-up
The test specimen, a precast concrete culvert element, is placed in a steel frame consisting of standard HEA profiles. The load is applied using a jack and introduced through a HEA profile with a 400 mm plate welded to it. The test set-up is shown in Figure 74 and Figure 74.
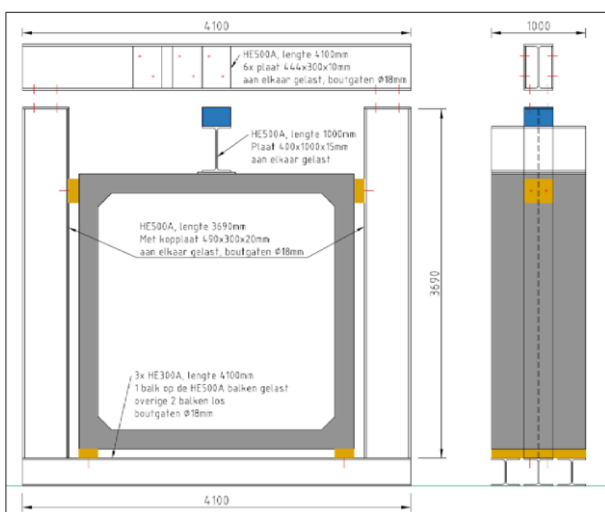
Figure 74 Schematic test set-up
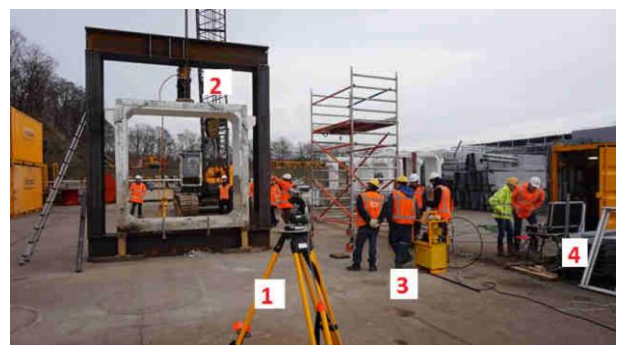
Figure 75 Photograph actual test set-up

Results

The results of the first model show that LM1 is governing over LM2, both for bending moment and shear. In the combination with LM1 the culvert has insufficient bending moment capacity at midspan and insufficient shear capacity at the supportive wall of which the first mentioned is slightly governing. The construction in question complies with LM2 for which bending moment resistance is slightly governing again. The results of the first simple model show that in his case material research makes only a very small positive contribution to the normative unity check, which is improved from 1.14 to 1.08 for the sagging moment at midspan. The unity check for shear in the deck near the walls improves from 1.09 to 1.02. In the specific case of Uysal, material research for the input of a framework model therefore does not yield significant gains in terms of capacity. It is assumed that the reinforcement layout is known in both situations.

For the uniform model of the province only a combination with LM1 has been checked. According to this model the structure does not fail on shear and satisfies both for sagging and hogging bending moments. But it must be noted that the sagging bending moment will be substantially larger than the estimated $\frac{1}{20} \cdot q \cdot L^2$. For the model of the province the material research seems to have a significant added value in terms of a lower unity check, since it dropped from 1,24 to 0,89 for shear. Which means that according to this model the test object will not be rejected with the values from the material study. Not much can be said about the influence of the material study on model 2, because in the calculation with material study not only the resistance has been adjusted due to better known material properties, but also other loads have been used. This means that the influence of the material study cannot be isolated. But the most important thing is that you would expect that simplified calculations would be on the safe side, resulting in higher unity checks, which is not the case for this model since it results in lower unity checks and that is strange and seems dangerous.

Based on the prediction model, it was expected that all three test situations would fail on shear. The model intended for bending was expected to fail on punching shear, which is also a form of shear. The models intended for flexure failure, shear failure and failure due to a combination of flexure and shear were expected to have a failure load of 325 kN, 550 kN and 318 kN respectively. The situation resulting in the maximum bending moment in the deck resulted in shear failure of the deck at an average load of 554 kN. The crack propagates from the edge of the loading plate under an angle of approximately 45 degrees through the deck. The case which was intended to fail on shear in the deck actually failed on shear in the wall. The failure load was significantly higher than the prediction model would suggest, namely 1205 kN. The deck itself does not seem to tend to fail on shear but on flexure based on the cracks. The test situation intended for a combined failure on bending and shear in the deck has failed to shear in the wall at a load of 589 kN. The results from the experiment differ from the expected failure loads from the prediction model, the actual failure loads are approximately a factor of 1,8 higher. The main reasons for this deviation are probably the assumed characteristic value for the tensile strength of the concrete instead of the tested value and afterwards it turned out that there was more reinforcement in the concrete elements than expected. Uysal calibrated his model by changing these two parameters and the bond-slip factors. Ultimately, his calibrated DIANA model concluded that the culvert was constructively safe under the combined loads including LM1, the governing unity check was 0,53 at shear in the wall.

Conclusion

Uysal's research was focused on the ultimate load bearing capacity of the "Schaapswegduiker". So, within his research the focus was entirely on one single structure, with a given geometry and material properties. Therefore, further analysis of the involved parameters gives a more realistic view of the sensitivity and importance of each parameter. Based on his model, it appears, as expected, that for higher values of the bed constant a higher failure load is found. Uysal decide to not make a 3D model since the structure was build up with small precast elements with a limited length. Furthermore, he expected that a more advanced model would not give much better results, it would take much longer to run and would be more difficult to

model. However, he did not investigate that but only assumed it. In the Netherlands and in this research, however, we see many structures that were built in-situ, which probably benefits from a larger 3D model because of load distribution. The tests show that the deck is not always governing, it is to be expected that it occurs more often that the walls are governing for failure of the cross section of the underpass when the concentrated load is on the deck near the wall. In this case, an advanced analysis of the construction in the form of an NLFEA makes a positive contribution to the calculated failure load by a factor of 1,9 compared to the less refined LE framework model, so in that sense it offers perspective for this research. At the same time, Uysal reports that the reinforcement configuration appears to have a major impact on the failure load, which means that much of the construction data must be known for reliable analysis.

The methodology he recommends provides one stage with a calculation using the design values and the uniform model. After that, immediately a material research has to be conducted, without first a model refinement. The question of this study is whether it is not possible to get more out of the structure by modelling before all kinds of studies have to be carried out.

The model, or models, of this research can be validated by the model and test results from (Uysal, 2017). By giving the tool the input that most closely corresponds to the test situation conducted in Uysal's research, it is possible to determine to what extent the model corresponds to reality.

A2 Overview of materials with material properties including previous design codes

Concrete strength classes

Project	Materials	-	0
Omschrijving	Validatieberekening		
Status	SO		
Versie	0		
Opgezet door	D.Jilissen	Datum	2-12-2020
Gecontroleerd	V.Achternaam	Datum	dd-mm-yyyy

Royal HaskoningDHV — *Enhancing Society Together*

Eurocode conversiewaarden conform RBK v1.1. Tabel 2.2. Betoneigenschappen berekend volgens NEN-EN 1992-1-1 Tabel 3.1.

BETON

Betonkwaliteit	Eurocode conversie	f_{ck}	f_{cm}	f_{cd}	f_{ctm}	$f_{ctk,0,05}$	f_{ctd}
				N/mm^2			
RWS b.j. vóór 1976	C35/45	35	43	23,33	3,21	2,2	1,50
Onbekend - GBV 1930	C16/20	16	24	10,7	1,90	1,3	0,89
Onbekend - GBV 1940	C16/20	16	24	10,7	1,90	1,3	0,89
Onbekend - GBV 1950	C16/20	16	24	10,7	1,90	1,3	0,89
Onbekend - GBV 1962	C16/20	16	24	10,7	1,90	1,3	0,89
Onbekend - VB 74 + VB 74/84	C16/20	16	24	10,7	1,90	1,3	0,89
Onbekend - VBC	C16/20	16	24	10,7	1,90	1,3	0,89
Onbekend - EC	C16/20	16	24	10,7	1,90	1,3	0,89
GBV 1930 Beton	C8/10	8	16	5,33	1,20	0,8	0,56
GBV 1940 K 150	C8/10	8	16	5,33	1,20	0,8	0,56
GBV 1940 K 200	C11/14	11	19	7,33	1,48	1,0	0,69
GBV 1940 K 250	C14/18	13,5	21,5	9,00	1,70	1,2	0,79
GBV 1950 K 150	C8/10	8	16	5,33	1,20	0,8	0,56
GBV 1950 K 200	C11/14	11	19	7,33	1,48	1,0	0,69
GBV 1950 K 250	C14/18	13,5	21,5	9,00	1,70	1,2	0,79
GBV 1962 K 160	C9/11	9	17	6,00	1,30	0,9	0,61
GBV 1962 K 225	C13/16	13	21	8,67	1,66	1,2	0,77
GBV 1962 K 300	C19/24	19	27	12,67	2,14	1,5	1,00
GBV 1962 K 400	C28/35	28	36	18,67	2,77	1,9	1,29
GBV 1962 K 450	C32/41	32	40	21,33	3,02	2,1	1,41
RVB 1962 + 1667 K 500	C33/42	33	41	22,00	3,09	2,2	1,44
RVB 1962 + 1667 K 600	C40/50	40	48	26,67	3,51	2,5	1,64
VB 74 + VB 74/84 B 12,5	C10/13	10	18	6,67	1,39	1,0	0,65
VB 74 + VB 74/84 B 17,5	C14/18	14	22	9,33	1,74	1,2	0,81
VB 74 + VB 74/84 B 22,5	C18/23	18	26	12,00	2,06	1,4	0,96
VB 74 + VB 74/84 B 30	C25/30	25	33	16,67	2,56	1,8	1,20
VB 74 + VB 74/84 B 37,5	C30/37	30	38	20,00	2,90	2,0	1,35
VB 74 + VB 74/84 B 45	C35/45	35	43	23,33	3,21	2,2	1,50
VB 74 + VB 74/84 B 52,5	C47,5/58	47,5	55,5	31,67	3,93	2,8	1,84
VB 74 + VB 74/84 B 60	C50/60	50	58	33,33	4,07	2,9	1,90
VBC B15	C12/15	12	20	8,00	1,57	1,1	0,73
VBC B25	C20/25	20	28	13,33	2,21	1,5	1,03
VBC B35	C28/35	28	36	18,67	2,77	1,9	1,29
VBC B45	C35/45	35	43	23,33	3,21	2,2	1,50
VBC B55	C45/55	45	53	30,00	3,80	2,7	1,77
VBC B65	C53/65	53	61	35,33	4,16	2,9	1,94
EC C12/15	C12/15	12	20	8,0	1,57	1,1	0,73
EC C16/20	C16/20	16	24	10,7	1,90	1,3	0,89
EC C20/25	C20/25	20	28	13,3	2,21	1,5	1,03
EC C25/30	C25/30	25	33	16,7	2,56	1,8	1,20
EC C30/37	C30/37	30	38	20,0	2,90	2,0	1,35
EC C35/45	C35/45	35	43	23,3	3,21	2,2	1,50
EC C40/50	C40/50	40	48	26,7	3,51	2,5	1,64
EC C45/55	C45/55	45	53	30,0	3,80	2,7	1,77
EC C50/60	C50/60	50	58	33,3	4,07	2,9	1,90
EC C55/67	C55/67	55	63	36,7	4,21	3,0	1,97
EC C60/75	C60/75	60	68	40,0	4,35	3,0	2,03
EC C70/85	C70/85	70	78	46,7	4,61	3,2	2,15
EC C80/95	C80/95	80	88	53,3	4,84	3,4	2,26
EC C90/105	C90/105	90	98	60,0	5,04	3,5	2,35
Uit proeven k_t=0,85	C34/41	34	42	22,7	3,15	2,2	1,47

Reinforcement steel grades

Project	Materials	-	0		
Omschrijving	Validatieberekening				
Status	SO				
Versie	0				
Opgezet door	D.Jilissen			Datum	2-12-2020
Gecontroleerd	V.Achternaam			Datum	dd-mm-yyyy

Eurocode conversie waarden conform NEN 8702 2018 Tabel 2. In tegenstelling tot RBK v1.1 wordt een materiaal factor 1,15 gebruikt voor alle staalkwaliteiten.

WAPENINGSSTAAL

Staal kwaliteit	f_{yk} N/mm^2	f_{yd} N/mm^2	Ductiliteits-klasse	Staal profiel
Onbekend - GBV 1930	220	191	B	Glad
Onbekend - GBV 1940	220	191	B	Glad
Onbekend - GBV 1950	220	191	B	Glad
Onbekend - GBV 1962	220	191	B	Glad
Onbekend - VB 74 + VB 74/84	220	191	B	Geribd
Onbekend - VBC	220	191	B	Geribd
GBV 1930 1. B	220	191	B	Glad
GBV 1940 HK	-	191	B	Glad
GBV 1940 St.37	220	191	B	Glad
GBV 1940 L. St. 52	340-360	296-313	B	Glad
GBV 1940 Speciaal staal sv 36	360	313	B	Glad
GBV 1940 Speciaal staal sv 48	480	417	B	Glad
GBV 1950 QR22	220	191	B	Glad
GBV 1950 QR24	240	209	B	Glad
GBV 1950 QR30	300	261	B	Geribd
GBV 1950 QR36	360	313	B	Geribd
GBV 1950 QR42	420	365	B	Geribd
GBV 1950 QRn36	360	313	A	Geribd
GBV 1950 QRn42	420	365	A	Geribd
GBV 1950 QRn48	480	417	A	Geribd
GBV 1950 QRn54	540	470	A	Geribd
GBV 1962 QR22	220	191	B	Glad
GBV 1962 QR24	240	209	B	Glad
GBV 1962 QR32	320	278	B	Geribd
GBV 1962 QR40	400	348	B	Geribd
GBV 1962 QR48	480	417	B	Geribd
GBV 1962 QRn32	320	278	A	Geribd
GBV 1962 QRn40	400	348	A	Geribd
GBV 1962 QRn48	480	417	A	Geribd
VB 74 + VB 74/84 FeB 220 HW	220	191	B	Geribd
VB 74 + VB 74/84 FeB 400 HW, HWL	400	348	B	Geribd
VB 74 + VB 74/84 FeB 500 HW	500	435	B	Geribd
VB 74 + VB 74/84 FeB 400 HK	400	348	B	Geribd
VB 74 + VB 74/84 FeB 500 HK	500	435	B	Geribd
VB 74 + VB 74/84 FeB 500 HKN, HWN	500	435	A	Geribd
VBC FeB 220 HWL	220	191	B	Geribd
VBC FeB 400 HWL, HK	400	348	B	Geribd
VBC FeB 500 HWL, HK	500	435	B	Geribd
VBC FeB 500 HKN	500	435	A	Geribd
Uit proeven	220	191	B	Geribd

A3   Data analysis

Introduction

General introduction
In this data analysis information about underpasses in the Netherlands is gathered which will be used for further structural research. General information about the underpass, the geometry of the structure and information about the materials were searched for. To substantiate the relevance of this research, an attempt was made to estimate the number of structures in the Netherlands within the predetermined scope. This scope is limited to underpasses with a construction type box, portal or a concrete deck on sheet piles as presented in 1.4.

The purpose
It is of importance to have an understanding about what kind of construction types are present in the Netherlands and how old these structures are. In addition, it is important to know how many there are and between what the underpass facilitates an intersection. Based on the information found an equivalent structure, based on average geometrical data, can be used to draw up the first-generation model.

Another reason for this analysis is to investigate if typical changes in the underpass constructions can be found in relation with different codes used for their design. One typical change in codes is that with the advent of the VB 74 the capacity of concrete with regard to shear force changed, which may result in changes in the structures as well.

Furthermore, the scope can be further substantiated and, if necessary, adjusted or reduced based on the data obtained. The scope at this stage of the research determines which typical construction types of underpasses are worth to be automated based on occurrence.

Ultimately, the data gathered can give founded arguments to use certain default input values and limitations for the automated calculation later on. In case some data of an existing structure is unknown, a default value will be used so the calculation can still be performed.

Starting points

Predefined scope
For this analysis, only existing underpasses with a concrete main loadbearing structure of the type box, portal or concrete plate on sheet piles were searched. It concerns both underpasses in the main road network, owned by Rijkswaterstaat, and underpasses that are not part of the main road network which are owned by local authorities.

The predefined scope for this data analysis is described in more detail in paragraph 1.4.

Available data
Rijkswaterstaat has basic information about its structures publicly available on the DISK GeoWeb website. The number of underpasses and culverts, in the main road network, per foundation year can be obtained from this database.

The data concerning the underpasses itself comes from structural assessments of existing underpasses already carried out by RoyalHaskoningDHV itself as well as some other parties and is available on the online database of RoyalHaskoningDHV. Unfortunately, most projects are not tagged based on construction type, they are given a project number, which makes it hard to find the structures within the scope. Therefore, the number of different objects strongly depends on the experience of employees.

Evaluation used data

Investigated structures
The available documents of a total of 63 structures were examined. Documents include DISK reports, reports of structural assessments, calculations, shape drawings and reinforcement drawings.

Procedure stocktaking
To make an inventory of the required data, the available drawings were first examined. If the drawings present do not provide sufficient usable data, any available calculations will be inspected. In addition, data from inspection reports have been examined, but these mainly contain brief information regarding the geometry of the structure and the layout of the reinforcement.

Sequence in case of conflicting information:
1. Shape drawings
2. Reinforcement drawings
3. Calculations
4. DISK report
5. Inspection reports

The reason why DISK and inspection reports which contain actual measured dimensions are at the bottom of the list is because these measurements can contain errors and may include defects to a structure. Therefore, they do not give a good value for the dimensions keeping in mind that these objects represent a much larger group of objects in the same category.

The underpasses and culverts are further categorized by the road or waterway they are in or cross, as shown in Table 38.

Situated in	Crossing
Highway	Highway (ramp/exit)
	B-road
	Byroad
	Cycling path
	Waterway
Area access road	Byroad
	Cycling path
	Waterway
byroad	Cycling path
	Waterway

Table 38 Overview of crossing categories.

Highways are the national roads which are indicated in the Netherlands with the letter A and have a flow function. Area access roads are regional roads which in the Netherlands are indicated with the letter N an also have a flow function, but at a regional level. Byroads are local roads and do not have a special letter designation in the Netherlands, these roads have an exchange function.

Information about a construction is considered complete provided that at least the following data is known:
- General data (name, year, crossing, in, etcetera)
- Geometry (dimensions structure)
- Applied concrete
- Applied reinforcement, including reinforcement ratio

- Presence of shear reinforcement
- Presence of prestressing

Availability of data

The number of objects included in the database is limited, 63 different structures are investigated and added. Most of the data for these objects was available.

- Of the structures in the "Byroad-box" category, about 14% of the structures have no or insufficient data;
- Of the structures in the "Cycling path-Box" category, about 20% of the structures have no or insufficient data;
- Of the structures in the "Culvert-Box" category, about 25% of the structures have no or insufficient data;
- Of the structures in the "Byroad-Portal" category, about 29% of the structures have no or insufficient data;
- On average about 19% of the structures have no or insufficient data.

Usability of data

The starting point is that all available information from RoyalHaskoningDHV's online database is used, including drawings, calculations and reports. If the data is incomplete or missing, the object is nevertheless added, either with an "unknown" entry for the unknown parameters.

It has been found that the material properties of concrete and steel usually can be obtained from the shape and reinforcement drawings, if they are available and readable.

Predefined input and limitations

To prevent data entry errors, much of the input parameters must be chosen from predefined options or is restricted to certain input limits. The predefined input for material properties is based on prescriptions given in the RBK. The concrete and reinforcement classes are based on table 2.2 and 2.6 of RBK respectively, which can be found in Appendix A2. For the geometry some practical limits are set, as an example no negative values for dimensions are allowed.

The concrete underpasses which are included in the dataset are designed according to loads specified in the VOSB, of which several editions were published in 1933, 1938 and 1963. Most constructions that have been examined fall into the Class 60 category from VOSB 1963, other found categories are Class 45 from VOSB 1963 and Class A from VOSB 1938. The total distribution of the cases examined is shown in Figure 76.
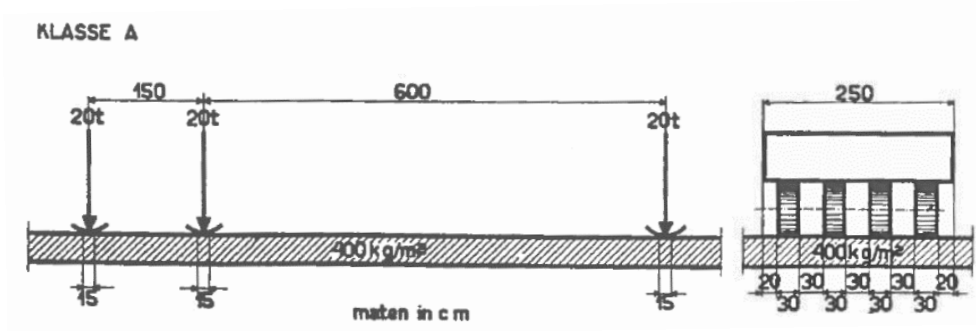
Class A VOSB 1938
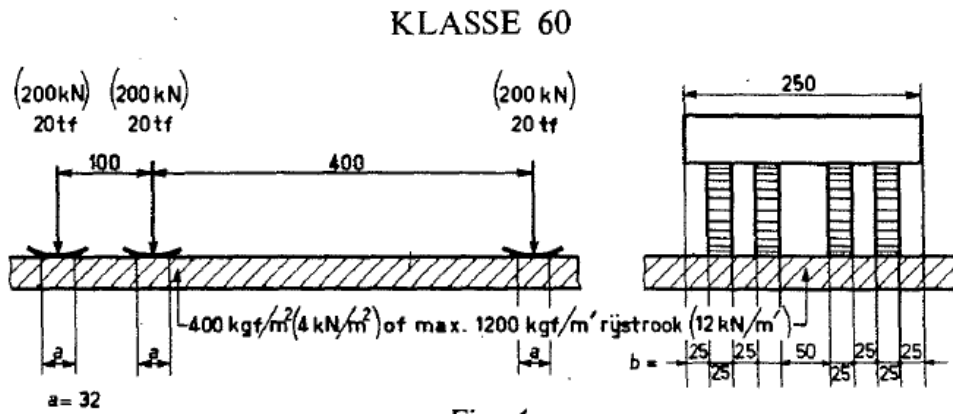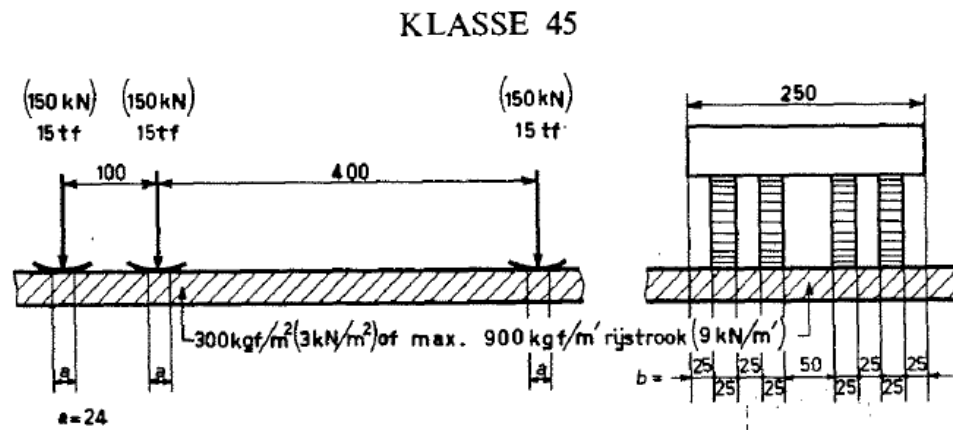
Figure 76 Class 60 and Class 45 VOSB 1963

Model types

For the verification calculation of, primarily, box-shaped structures models with the following element types have been found within available reports:

- 1D beam elements
- 2D shell elements
- 3D solid elements

According to RBK 1.1 Table 3.1 all these types of models are able to capture the structural behaviour in a very good way.
According to (Rijkswaterstaat, 2013) the substructure only needs to be included in case there is a direct cause to do so.

Analytical model or 1D beam elements

The use of 1D beam elements is the most easiest way to model the underpass, by means of analytical equations or a simple beam modeling, the critical cross-section of each construction element is checked, whereby it is assessed per failure mechanism whether the occurring section force can be withstand by the cross-section. In the past, when no powerful computer analysis were available, specific beam models which include load distribution in transverse direction of plates were developed based on the method of Guyon-Massonnet. Such method will be suitable to quickly gain insight in the structural behaviour and in some cases the model will be accurate enough for the assessment. Since the underpasses in the scope of this research only have one cell, the shear force is equally distributed over the two walls. Since the deck will be modelled with beam elements, RBK Table 3.1 states that the intersection angle must be larger than 80^{gon} = 72° so that the span can be assumed perpendicular. The cross-sectional resistance can be calculated by a hand, by means of a verified Excel sheet, or with Dbet. According to RBK it is allowed, in case no reinforcement with ductility class A is used, to redistribute bending moments up to 20% from sagging to hogging moment or the other way around. The horizontal loads on the walls results in compressive forces in the deck structure, which works favourably and is therefore neglected in the first instance. If the construction does not prove to be satisfactory, this favourable effect can still be included.

One method to model these underpasses is to just model the deck as a beam on two supports and account for the walls by means of rotational springs at the ends of the beam, the mechanical system is shown in Figure 77.

Figure 77 Mechanical system

The stiffness of the rotational springs at the end of the beam can easily be calculated by hand with the traditional "forget-me-nots" as shown in Figure 78.

$$k_r = M/\varphi = \frac{4 \cdot EI}{L}$$
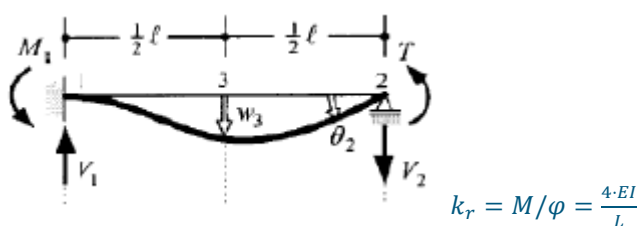
Figure 78 "forget-me-not" for clamped beam with supported end

The calculations regarding cross-sectional forces will be performed in the FEA software ALP2000 which can be checked by hand calculations. The advantage of using ALP2000 software is that the old materials are available in the software. Simple checks can be performed since the results of the model of the deck structure must be between that of a simply supported beam and a two-sided clamped beam. It is possible to model prestressed beams including prestressing losses. For the distribution of traffic load the method of Guyon-Massonnet is embedded in the software.

A second method to model underpasses is to create a 2D framework model with 1D beam elements having a unity width of one meter. The elements and nodes coincidence with the centre line of the cross section and the connections between the deck, walls and floor will be fixed. A foundation on grade will be modelled using a subgrade reaction modulus, an underpass with pile foundation will be modelled with springs representing the piles. An example of the mechanical system of a box-shaped underpass founded on grade is shown in Figure 79.
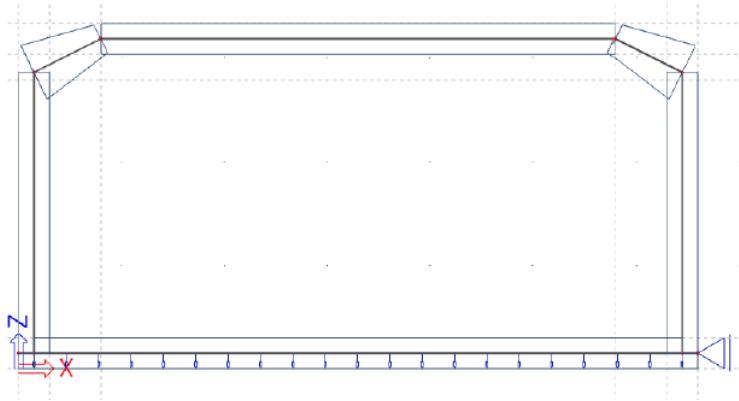
Figure 79 Example of mechanical system of framework with 1D beam elements, foundation on grade

2D plate elements

To achieve a more realistic approximation of the load transfer in both longitudinal and transverse direction, a model with plate elements can be used as an alternative to the beam model. As with a beam model, the results of a model with plate elements include section forces that can be compared with the calculated resistance of the corresponding cross-section. If much more reinforcement is present in the span direction compared to the transverse direction, the plate does not behave like an isotropic plate but will behave more like an orthotropic plate. A plate with orthotropic properties can be used. In this case a different stiffness for longitudinal and transverse direction is accounted for which is a better representation of the real structural behaviour in case longitudinal and transverse reinforcements are not quite the same. In case the transverse reinforcement is calculated to be insufficient ($M_{uy} < M_{dy}$), using different stiffnesses in longitudinal and transverse direction result in a decrease in bending moment in transverse direction and an increase in bending moment in longitudinal direction.

In case plate elements are used to model the underpass structure, elements of Mindlin-Reissner type must be used according to the RBK. Furthermore, mesh refinement must be performed on the free edges over a width equal to the plate thickness using element size of half the plate thickness.

The first and most simple way to use 2D elements for modelling the underpass would be if one slice, of one meter, of the cross section is modelled using a 2D element. The next step in complexity would be to make a model using 2D elements in a 3D model space.

3D solid elements

In the available data one report was found in which a model with 3D solid elements in a non-linear FEA were used. 3D solid elements are used for structures where the geometry has a significant influence on the

force distribution and a more precise analysis is required. However, section forces are used to check the cross-sections and the stresses over the relevant cross-section must be integrated. However, this is a method with relatively little experience and where the translation into section forces requires specific attention. This places specific demands on both the experience of the engineer and the validation of the model and the results. In addition, calculating 3D volume models is an intensive exercise that requires the necessary computational capacity.

Refinements

Refinements can be applied within the calculation model to come closer to reality. Several refinements are commonly used:
- Assume the stiffness of cracked concrete in longitudinal and transverse direction
- Set Poisson's ratio equal to zero (0), assuming cracked concrete, according to NEN-EN 1992-1-1 art. 3.1.3 (4). In this way the calculated bending moments in transverse direction become smaller.
- Account for the spring stiffness of the supports. In case the underpass is founded on grade the support is modelled as bedding, with a bedding constant. In case of a pile foundation the piles can be modelled as springs, instead of fixed supports. Since foundation piles are placed almost directly under the wall, it is expected that the influence will not be significant. Further refinement can be achieved by taking into account the deformation of the supports, for rubber supports 1 mm and rigid steel supports 0,1 mm may be assumed. The latter effect will be placed outside the scope of this research and will not be accounted for.
- In case requirements are not met locally near supports, the actual size and number of the supports can be accounted for to reduce stress concentrations in de model.
- Reduce bending moment peak values by using distributed loads instead of concentrated loads.
- Redistribution of bending moments between support and span by using both moment capacities. Redistribution is allowed up to 20%.

Damage

There are cases that underpasses have structural damage that cannot be ignored for the structural assessment. In case of crack formation, in longitudinal or transverse direction, the stiffness in the direction perpendicular to the crack must be reduced based on the actual crack width. This results in an orthotropic behaviour in that specific part of the structure. The shear modulus G is still depending on $E_{uncracked}$, if the crack width is limited to $0,3\ mm$.

Prestressed plate

In case prestressing is applied, the plate can be modelled using orthotropy. In longitudinal direction the concrete is uncracked, due to prestressing, and in transverse direction the concrete is assumed to be cracked. This results in a stiffness ratio of approximately 2:1.

Non-Linearity

Physically non-linear

The refinements earlier mentioned are mainly focussed on changes of the model assuming a linear elastic material behaviour. A linear elastic analysis results in a conservative load distribution because materials do not behave with a linear relation between stresses and strains. Taking these physical non-linear effects into account leads to more realistic and less conservative results. Since the deck structure of a typical underpass is statically undetermined, redistribution of forces is possible between span and support and therefore a non-linear analysis may be beneficial.

Geometrically non-linear

When geometric non-linearity is considered, second order effects due to eccentricities are considered in the analysis as well. If the deformation is large, the equilibrium equations must be written with respect to the

deformed structural geometry. This is the case with buckling of a slender column or the deformation of a cable but seems not be important for the typical constructions for the underpasses.

B

Appendix – Chapter 3: Load effect with analytical model

B1 Standards, guidelines and regulations

Assessment of a civil structure must be executed conform *Bouwbesluit 2012*, which refers to the Eurocode, NEN8700 and NEN8701. The Eurocode provides principles for the structural design, the load models and rules regarding the calculation of concrete structures. The NEN8700 is designated in *Bouwbesluit 2012* to be used with existing structures calculated with NEN6702, part of *Bouwbesluit 2003*, and older. For structures designed with Eurocode which have reached the age of 15 years NEN8700 also applies. The NEN8701 is an elaboration of the guidelines from NEN8700 which refers to the loads on the structure. This code is based on the Eurocode NEN-EN 1991 and must be read in conjunction with it. Loads may be reduced in relation with the remaining service life in case it is less than the design service life. These reductions are discussed later in this Appendix. On top of that RBK and CUR124 are used, which supply additional guidelines and requirements for the assessment of existing civil structures owned by *Rijkswaterstaat* and local authorities respectively.

In case of contradictions, the following pick order is guiding:
1. Demands from the contract with the owner
2. RBK and CUR124 provisions
3. NEN8700 and NEN8701 (and NEN 8702)
4. ROK provisions
5. Guidelines from *Rijkswaterstaat*
6. Eurocode with National Annex, other NEN-codes, CUR-recommendations and CROW-documents.

For the assessment of existing structures applies that during the residual service life it should be safe and usable. The structural safety is determined by ultimate limit state (ULS) verifications. The NEN8700 does not state any requirements regarding serviceability limit state (SLS) that are legally obligated. This means that the assessment does not have to meet the design requirements for usability and durability from the material-related standards. Table 39 lists the standards, guidelines and regulations that apply within the verification.

Document	Title	Organization
NEN-EN 1990+A1+A1/C2:2019 incl. NB:2019	Eurocode: Basis of structural design	NEN
NEN-EN 1991-1-1+C1+C11:2019 incl. NB:2019	Actions on structures – Part 1-1: General actions – Densities, self- weight,imposed loads for buildings	NEN
NEN-EN 1991-2+C1:2015 incl. NB:2019	Actions on structures - Part 2: Traffic loads on bridges including National Annex	NEN
NEN-EN 1992-2 incl. NB:2016	Design of concrete structures - Concrete bridges - Design and detailing rules	NEN
NEN 8700:2011 NEN 8700:2011/ A1:2018 Ontw.	Assessment of existing structures in case of reconstruction and disapproval - Basic Rules	NEN
NEN 8701:2011 NEN 8701:2011/ A1:2018 Ontw.	Assessment of existing structures in case of reconstruction and disapproval - Actions	NEN
NEN 8702:2018 Draft	Assessment of existing structures in case of reconstruction and disapproval – Concrete structures	NEN
RBK v1.1	Richtlijnen Beoordeling Kunstwerken	RWS
ROK v1.4	Richtlijnen Ontwerp Kunstwerken	RWS
CROW-CUR 124:2019	Constructieve veiligheid bestaande bruggen en viaducten van decentrale overheden	CROW

Table 39 Standards, guidelines and regulations that apply within the verification

Classification of the structure

Structures are classified based on consequence class, assessment level, reference period and remaining service life. For the assessment of existing structures is, as mentioned before, RBK governing.

Consequence Class

Constructions are classified in a consequence class (CC) looking at the consequences in loss of life and economic damage from collapse or malfunction of the construction. Table 40 can be drawn up based on the Eurocode with the Dutch national annex, this table also applies to assessments of existing structures.

Consequence Class	Definition of consequence classes NEN-EN 1990:2019 NB Table NB.23 – B1	Examples of applications NEN-EN 1990:2019 NB Table NB.24 – B1
CC3	**Major** consequences in terms of loss of life, or **very large** economic, social or environmental consequences	Bridges in and over main roads, main waterways and national railways. This concerns bridges: • in and over the main infrastructure or on main waterways with intensive (sea) shipping or • where the collapse has disruptive consequences for the society;
CC2	**Mediocre** consequences with regard to loss of life, or **significant** economic, social or environmental impacts	Bridges not classified in CC1 or CC3
CC1b	**Minor** impacts on loss of life and **minor** or **negligible** economic, social or environmental impacts	Bridges for which the entire design life applies: • the bridge is not in an economically important route, • the number of trucks is less than 2.000 per lane per year, and • there is a limited risk of major social or personal injury. Bridges in country roads, residential areas, etc.
CC1a	**Virtually excluded** loss of life and very small or **negligible** economic, social or environmental impact	

Table 40 Overview of consequence classes

For structures owned by local authorities the CUR124 may be used, which refers to NEN8700 which again refers to NEN-EN 1990 which means Table 40 can be used. But since RWS only owns structures in or over main roads, main waterways or over national railways all their existing structures must be assessed according to CC3, RBK therefore gives only the option of CC3.

Classification of an existing structure into a consequence class has a direct effect on the load factor which must be applied (Appendix B2).

Assessment levels

Together NEN8700 and RBK have four assessment levels, these are in order of decreasing reliability index β:

- **New construction**   for design of new structures (level conform Eurocode 0);
- **Reconstruction**   for assessment of the parts of a structure to be reconstructed;
- **Usage**   for assessment of a structure, or parts of it, that is in use but will not be renovated;
- **Disapproval**   To determine whether the statutory minimum level of structural safety is reached.

The assessment level of a new construction is only meant for new constructions and for the complete renovation of constructions, therefore it is too conservative and not applicable for the assessment of an existing structure with no or minor changes.

The reconstruction level is for partially renewing, changing or enlarging of a construction and has a lower reliability index which manifests itself in lower partial safety factors. It must be noted that renovation must involve a physical change of the construction. The renovation level therefore does not include a change of load without this being accompanied by a structural change on the construction. A change in load may be a reason to conduct an assessment for which, from a public law point of view, the rejection level must be met.

Rijkswaterstaat introduced the usage level of assessment to fill the gap between reconstruction and disapproval level, where a reliability factor is used higher than that of disapproval level but lower than that of reconstruction. This usage level is the lower limit that is used for the structural safety of the structures of RWS. This assessment level may only be applied to existing (parts of) structures that are not being reconstructed. Please note that this assessment level only applies to structures of *Rijkswaterstaat* and are therefore only classified in CC3.

The level of disapproval is the bare minimum and is meant to determine whether a structure is safe or not, if this level is not met, measures are required immediately, which translates to within a year, to ensure structural safety. It must be clear that this is not the desired level of safety if an assessment is conducted, since a construction preferably should last much longer.

Remaining service life

The remaining service life is the assumed period during which an existing or renovated construction, or part of it, can be used for the intended purpose. This means that within this period the minimum level of structural safety must always be met.

The NEN8700 states that for existing structures a remaining service life of 15 years should be the absolute minimum, but that in many cases it will be better to keep a remaining service life of 30 years. This has been interpreted as an advice to maintain a 30-year remaining service life. In case of assessment level renovation, the remaining service life must not end before the end of the original design life of the other structural parts.

Structures owned by RWS should have, based on RBK, a remaining service life of 30 years, but a project-specific longer remaining service life can be agreed.

Reference period

Load models in the Eurocode, for new construction, are based on a trend and a reference year 2060. A construction can have a residual life, as a result of which the reference year 2060 is not reached. The reference period is the period in which the construction is still used before 2060. A reference period ending before the year 2060 results in a reduction of the variable loads. Therefore, the reference period does not have to be equal to the remaining service life.

According to NEN8700 Table B.2 the minimum reference period for all consequence classes is 15 years, with the exception for CC1a at rejection level which has a minimum reference period of 1 year.

RWS demands in RBK a longer reference period for its structures with a reference period of 30 years for assessment levels use and renovation, where a project-specific longer reference period can be agreed.

It should be noted that a reference period of 15 years must be used for the rejection level, instead of its remaining service life of just 1 year.

B2   Background of the Analytical Model

Introduction

This Appendix describes the background of the Analytical Model. The underpasses box-shaped structure is modelled as a simply supported beam, which represent the deck, with rotational springs which represent the walls. Vertical loads that are included in this model are self-weight, dead load and traffic loads.

The goal of this model is to be able to quickly assess whether a structure fails or not, and if it does due to what. Furthermore, this model will be used to verify further detailed analysis of structures with FEA models, resulting in the end in the first-generation model. Besides, some parts of this model will be used later together with the FEA model as well.

First an overview is given of the used standards, guidelines and regulations, thereafter this report is divided into chapters according to the tabs in the calculation sheet:

- Model
- Loads
- GEO
- MEd
- VEd
- Resistance
- Check
- Restrictions

Model

For the modelling of the superstructure of concrete bridges, a distinction is made between the types of plates, beams, boxes and tubes. Underpasses and culverts are box structures, while its deck can be seen as a plate. Due to the geometry, the dimensions of subparts and the fact that the walls are horizontally elastically supported by soil it is that in general the deck of the underpass box-shaped structure is the most critical part. Therefore, only the deck is modelled for this calculation by hand. The model consists of a simply supported beam which represents a strip of the deck of one meter. The connection with the walls is accounted for by adding rotational springs at the supports, which stiffness depends on the stiffness of the walls. The basic model is shown in Figure 22, in which k_r is the rotational stiffness at the supports, EI is the bending stiffness and L the model length of the beam.

Figure 80 Basic model of calculation by hand

Depending on the rotational stiffness of the springs, this basic model can be considered as a simply supported beam with two hinges or clamped with both sides. Since the deck structure is primarily loaded by uniformly distributed load, the occurring bending moments will be approximately within the limits shown in Table 41. The rotational stiffness K_r will be somewhere between zero and infinity.

Rotational stiffness K_r [kN/m]	Sagging moment	Hogging moment
$K_r = 0$	$\frac{1}{8} \cdot q \cdot L^2$	0
$K_r = \infty$	$\frac{1}{24} \cdot q \cdot L^2$	$\frac{1}{12} \cdot q \cdot L^2$
$0 < K_r < \infty$	$\frac{1}{24} \cdot q \cdot L^2 < M_{sagging} < \frac{1}{8} \cdot q \cdot L^2$	$0 < M_{hogging} < \frac{1}{12} \cdot q \cdot L^2$

Table 41 Approximated limits of bending moment for basic model of calculation by hand

Geometry
The span of the model consists of the measure in the clear plus two times half the wall thickness. The cross-section of the model beam is limited to a massive rectangular cross-section, i.e. without any holes, with the same concrete quality meaning prefab girders with an infill deck are out of the scope. The slab has a width of one meter and the height of the deck at midspan, any haunches present, which increase the deck thickness near the supports, are neglected for the beam stiffness. However, haunches have been taken into account in the determination of cross-sectional resistances (Appendix C1), therefore the length and height of the haunch is required. Although the model only represents a one-meter strip, the width of the deck from joint to joint is required for the determination of load distribution.

Although the model is focussed on the deck, information of the walls is needed to determine the rotational stiffness at the connection between the deck and the wall.

Bending stiffness
Since the cross-section of the model beam is limited to a massive rectangular shape, the bending stiffness can be determined quite easily. The value of the E-modulus of the deck can be defined as user input, based on concrete class, or can be determined as fictional stiffness E_f based on NEN-EN 1992-1-1 NB Table NB-1. The moment of inertia I is be determined with: $I_{deck} = \frac{1}{12} \cdot b_{model} \cdot h_{deck}^3$. The bending stiffness of the deck is then defined as $EI_{deck} = E_{deck} \cdot I_{deck}$. The reinforcement, with a much higher stiffness, is neglected in the determination of the bending stiffness unless the module of fictional stiffness E_f is used.

Rotational springs
The stiffness of the rotational springs at the end of the beam can easily be calculated by hand with the traditional "forget-me-not" with one end clamped, representing the connection with the floor, and the other end hinged, representing the connection with the deck with the external moment, as shown in Figure 81. Formula B.1 gives the rotational stiffness.
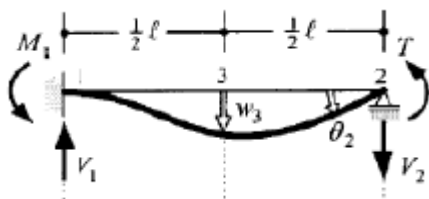
Figure 81 "Forget-me-not" clamped-hinged beam

$$k_r = M/\varphi = \frac{4 \cdot EI}{L} \tag{B.1}$$

Where,

EI is the bending stiffness of the wall, of which E may be user defined input or determined based on the fictional stiffness E_f based on NEN-EN 1992-1-1 NB Table NB-1 and I is defined as $I_{wall} = \frac{1}{12} \cdot b_{model} \cdot h^3_{wall}$.

L is model height of the wall, defined as the sum of half the deck height plus the internal height of the box plus half the thickness of the floor slab. $\left(L = \frac{1}{2} \cdot h_{deck} + h_{internal} + \frac{1}{2} \cdot h_{floor} \right)$

The reinforcement, with a much higher stiffness, is neglected in the determination of the rotational stiffness of the springs unless the module of fictional stiffness E_f is used.

Fictional Stiffness E_f

Since it is expected that the wall of the box construction will have a higher stiffness due to the presence of a normal force from top load, the fictitious stiffness E_f, from NEN-EN 1992-1-1 NB Table NB-1, can be used to determine the stiffnesses of the deck and the wall.

Research, described in paragraph 3.3 of the main report, shows that in principle a stiffness ratio of 1:1 between the walls and the deck can be assumed, which means that an equal E-modulus is used for both elements.

Based on the structures studied within the research, it is stated that the sagging moment in the span is usually governing of the mechanism bending moment. If a structure is disapproved based on bending moment and additional data regarding the reinforcement in the walls is present, the module *Fictional stiffness E_f* can still be used to determine E_f.

It should be noted that by changing the stiffness ratio, using the method for *Fictional stiffness E_f*, the total occurring moment is not decreased, the occurring moment is merely shifted.

Background of E_f

The fictitious E-modulus E_f is based on the slope of the M-N-κ diagram between the origin and the point $M = 0,8 \, M_{Rd}$, which means that a load of 80% of failure load is assumed, $M_{Ed} = 0,8 \, M_{Rd}$, with occurring normal force N_{Ed}. A so-called E-heavy cross-section, with reinforcement, and the bi-linear stress (σ) - strain (ε) diagram is assumed. At $0,8 \, M_{Rd}$ the reinforcement is still in the linear elastic branch, while the concrete compression zone is usually no longer. If the load is substantially lower or higher, the calculated stiffness E_f is therefore not correct. Calculations for the structures in the dataset however show that the load does not deviate substantially from 80% failure load with an average UC of $UC_{avg} = 0,85$. The bending stiffness EI of the deck and the wall is determined by the moment of inertia I of the E-heavy cross-section. The construction height h, the amount of reinforcement ρ in the deck and the wall and the occurring moment M_{Ed} and normal force N_{Ed} are the influencing parameters. When the section forces are so low that the concrete is uncracked, the bending stiffness is $E_c I_c + E_s I_s$. The moment cracking occurs, the bending stiffness EI decreases. In the fictional modulus of elasticity it is assumed that the moment of inertia I is constant, $\frac{1}{12} \, b \, h^3$ for rectangular cross-sections, which means that the E_f changes to realize the decrease in bending stiffness EI for cracked cross-sections.

Fictional stiffness module input

Compared to the standard analytical model, addition of the fictional stiffness module requires additional input with regard to the reinforcement. To determine the stiffness of the deck, in addition to the tensile reinforcement, the compression reinforcement is now also required, which means that the additional data

required are the compression reinforcement in the deck and the tension and compression reinforcement in the wall. Use of Table 42 is recommended for the determination of the available reinforcement.

Element	Reinforcement
Deck	Bottom and top reinforcement from the section at midspan.
Wall	Reinforcement from both the compressive and tension zone from the section halfway of the height of the wall.

Table 42 Recommended sections for determination of A_s for use of E_f module

The normal force in the deck, due to the horizontal ground pressure, is calculated in the GEO part. The normal force in the wall is equated to the shear force in the section at the face of the wall, it is assumed that the shear force in the deck completely passes into the normal force in the wall.

For the concrete strength class and the steel grade all materials from previous design codes as shown in Appendix A2 can be used. For concrete strength classes which are not listed in Table NEN-EN 1992-1-1 NB-1 Fictitious elastic modulus E_f is interpolated linearly. This is allowed since all values in tables of the Eurocode can be based on linear interpolation.

Fictional stiffness module output
Stiffnesses are determined according to NEN-EN 1992-1-1. NB Table NB-1 - Fictional modulus of elasticity E_f with starting point bending and normal force, symmetrically reinforced rectangular cross-section.

The module checks the utilization degree of normal force α_n of the element under consideration and determines whether the stiffness must be determined according to $\alpha_n \leq 0,45$ or $0,45 < \alpha_n \leq 0,9$. The utilization ratio is defined as:

$$\alpha_n = N_{Ed}/N_{Rd} \tag{B.2}$$
with,
$$N_{Rd} = Ac\, f_{cd} + (A_{st} + A_{sc})\, f_{yd} \tag{B.3}$$
In which
A_{st} is the cross-sectional area of the reinforcement in tension;
A_{sc} is the cross-sectional area of the reinforcement in compression.

For most structures the formula according to $\alpha_n < 0,45$ will be used.
The following applies to the reinforcement ratio within the fictional stiffness module: $\rho = (A_{st} + A_{sc})/A_c$.
The output of the module is the stiffness ratio expressed in $E_{f,wall}/E_{f,deck}$.

NEN-EN 1992-1-1 Dutch National Annex Table NB.1

	E_f MPa	
Sterkte-klasse	**Buiging en normaalkracht, symmetrisch gewapende rechthoekige doorsnede**	
	$\alpha_n \leq 0{,}45$	$0{,}45 < \alpha_n \leq 0{,}9$
C12/15	$[1{,}30 + 410\rho + (\ 9{,}0 - 130\rho)\alpha n\ ]10^3 \geq 2900$	$(\ 6{,}8 + 517\rho)(1 - 0{,}5\alpha n)10^3$
C16/20	$[1{,}45 + 415\rho + (11{,}5 - 145\rho)\alpha n\ ]10^3 \geq 3250$	$(\ 8{,}5 + 514\rho)(1 - 0{,}5\alpha n)10^3$
C20/25	$[1{,}60 + 420\rho + (14{,}0 - 160\rho)\alpha n\ ]10^3 \geq 3600$	$(10{,}0 + 510\rho)(1 - 0{,}5\alpha n)10^3$
C25/30	$[1{,}75 + 425\rho + (16{,}5 - 175\rho)\alpha n\ ]10^3 \geq 3950$	$(11{,}7 + 506\rho)(1 - 0{,}5\alpha n)10^3$
C30/37	$[1{,}96 + 432\rho + (20{,}0 - 196\rho)\alpha n\ ]10^3 \geq 4450$	$(14{,}0 + 501\rho)(1 - 0{,}5\alpha n)10^3$
C35/45	$[2{,}20 + 440\rho + (24{,}0 - 220\rho)\alpha n\ ]10^3 \geq 5000$	$(16{,}7 + 495\rho)(1 - 0{,}5\alpha n)10^3$
C40/50	$[2{,}35 + 445\rho + (26{,}5 - 235\rho)\alpha n\ ]10^3 \geq 5350$	$(18{,}3 + 491\rho)(1 - 0{,}5\alpha n)10^3$
C45/55	$[2{,}50 + 450\rho + (29{,}0 - 250\rho)\alpha n\ ]10^3 \geq 5700$	$(20{,}0 + 487\rho)(1 - 0{,}5\alpha n)10^3$
C50/60	$[2{,}65 + 455\rho + (31{,}5 - 265\rho)\alpha n\ ]10^3 \geq 6050$	$(21{,}6 + 484\rho)(1 - 0{,}5\alpha n)10^3$
C55/67	$[2{,}86 + 462\rho + (34{,}6 - 258\rho)\alpha n\ ]10^3 \geq 6400$	$(23{,}8 + 480\rho)(1 - 0{,}5\alpha n)10^3$
C60/75	$[3{,}10 + 470\rho + (37{,}0 - 170\rho)\alpha n\ ]10^3 \geq 6400$	$(25{,}5 + 480\rho)(1 - 0{,}5\alpha n)10^3$
C70/85	$[3{,}10 + 470\rho + (41{,}5 - 170\rho)\alpha n\ ]10^3 \geq 6400$	$(28{,}1 + 480\rho)(1 - 0{,}5\alpha n)10^3$
C80/95	$[3{,}10 + 470\rho + (46{,}5 - 170\rho)\alpha n\ ]10^3 \geq 6400$	$(31{,}1 + 480\rho)(1 - 0{,}5\alpha n)10^3$
C90/105	$[3{,}10 + 470\rho + (51{,}0 - 170\rho)\alpha n\ ]10^3 \geq 6400$	$(33{,}7 + 480\rho)(1 - 0{,}5\alpha n)10^3$
	waarin: $\rho = (A_{st} + A_{sc})/A_c \quad \alpha_n = N_{Ed}/(f_{cd} A_c + (A_{st} + A_{sc}) f_{yd})$ A_{st} is de oppervlakte van de wapening aan de meest getrokken zijde A_{sc} is de oppervlakte van de wapening aan de meest gedrukte zijde	

Basic model design

A simply supported beam model can be described with the Euler-Bernoulli beam theory. This theory only includes bending of the beam, no shear deformation, but since the deck of underpasses is relatively slender the error will be negligible. The classical displacement method is used to find the ODEs for the basic load cases, the model of this method is shown in Figure 23.
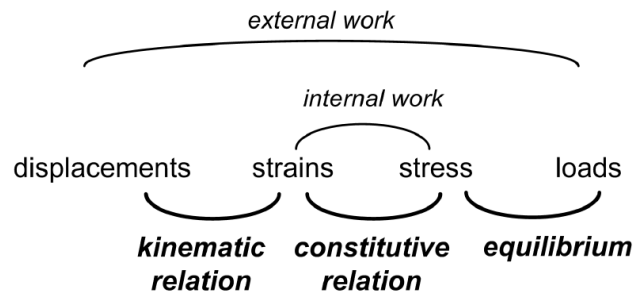
Figure 82 Classical displacement method

In order to find the ODEs first, the kinematic relations are formulated from which the constitutive relations are drawn up and finally the equilibrium conditions are formulated. These relations and conditions result in the ODEs.

It is generally known that for the Euler-Bernoulli theory the following applies:

- Kinematic relation: $\varphi = -\frac{dw}{dx}; \kappa = \frac{d\varphi}{dx};$ (B.4)
- Constitutive relation: $M = EI \cdot \kappa;$ (B.5)
- Equilibrium: $\frac{dV}{dx} = -q; \frac{dM}{dx} = V;$ (B.6)
- ODE: $EI \cdot \left(\frac{d^4w}{dx^4}\right) = q$ (B.7)

The general solution to this single ODE is:

$$w = \frac{q \cdot x^4}{24 \cdot EI} + \frac{C1 \cdot x^3}{6} + \frac{C2 \cdot x^2}{2} + C3 \cdot x + C4$$ (B.8)

The integration constants, in this single ODE case four, can be found by formulating an equivalent amount of boundary conditions as the number of integration constants. If loads are applied at only a single location two ODEs are necessary, in case of a uniformly distributed load over a part of the beam three ODEs are needed. Between two ODEs matching conditions need to be formulated to find the extra integration constants. Each fourth order ODE results in four extra integration constants, unknowns, meaning four matching conditions, equations, are needed in order to be able to solve the problem. Boundary and matching conditions are equations which say something about the displacement, rotation, moment or shear force at a certain point.

To speed up the process, MAPLE software is used for the mathematical calculations to determine all solutions. The advantage of approaching the problem with ODEs is that equations are obtained with which the moment and the shear force can be calculated for each cross-section.

Limitations of the basic analytical model

Modelling the deck of the underpass by a strip of one-meter width as beam gives good results for the bending moment, but according to RBK the shear force should be determined by hand. This mainly applies to local load effects and their distribution over the deck slab to the edge supports.

Although it is better for traffic safety and constructional simplicity to cross an underpass at an angle of 100^{gon} (90 degrees) with its overlying path, it often happens that the angle of intersection is considerably less than 100^{gon}. Since loads are placed on a beam model as a 100^{gon} intersection, the moment distribution is no longer correct when the angle of intersection becomes significantly smaller, because the stiffness of the concrete deck depends on the direction. The angle of intersection found in the preliminary study is in almost 75% of the investigated cases within the range from 80^{gon} to 100^{gon}, which is according to RBK a requirement if a construction is modelled with beam elements to obtain bending moment s whose error is negligible.

Loads

The loads acting on the structure are divided into permanent loads and variable loads. In principle the permanent loads, like self-weight, the weight of soil and asphalt, are always present. Variable loads, primarily traffic loads, are not always present but must naturally be represented.

In this model only vertical loads are considered. The horizontal forces have been disregarded except for the horizontal ground tension which introduces a normal force on the deck. Horizontal loads, like breaking forces, are relevant for the walls but are not modelled in this calculation by hand, this will be done in the FEA models.

Permanent loads

In principle, permanent loads are always present on the construction, however during the (remaining) service life of the construction these loads can change as a result of renovations or alterations. In this model self-weight, and the weight of soil and asphalt are considered.

Self-weight

For the calculation of the self-weight of the deck, the specific weight of concrete is considered in the model, which is standard 25 kN/m^3, but can be adjusted as required. This weight of the reinforcement steel is included in the weight of concrete. For the model it is assumed that the self-weight of the deck is a uniformly distributed load that engages in the neutral line. For the determination of the uniform load the average height of the deck is considered, which is the height of the deck at midspan, meaning the haunches are ignored. The uniform load for self-weight is formulated as:

$$q_{EG} = \rho_{concrete} \cdot b_{model} \cdot h_{deck;midspan} \qquad [kN/m] \tag{B.9}$$

Soil loads

In most cases a layer of soil is present between the asphalt and the top of the concrete deck, the weight of this soil layer is accounted for. For the model it is assumed that the weight of the soil layer is uniformly distributed and engages at the top of the concrete deck. The specific weight of the soil layer depends on the type of soil, but since in most cases a layer of sand is applied the standard value is 17,5 kN/m^3. For the determination of the uniform load the average height of the soil layer is considered. The uniform load for the weight of soil is formulated as:

$$q_{soil} = \rho_{soil} \cdot b_{model} \cdot h_{soil} \qquad [kN/m] \tag{B.10}$$

Asphalt load

Regardless of the type of asphalt, a specific weight of 23 kN/m^3 is used as standard, but a user can change this value. Based on an average thickness of the asphalt layer a uniform load due to the weight of asphalt is determined. According to ROK, the asphalt layer on the structure must be at least 120 mm. For the model it is assumed that the weight of the asphalt layer is uniformly distributed and engages at the top of the concrete deck. The uniform load for the weight of asphalt is formulated as:

$$q_{asphalt} = \rho_{asphalt} \cdot b_{model} \cdot h_{asphalt} \qquad [kN/m] \qquad \text{(B.11)}$$

Other loads
Other loads such as the tiling of a footpath, railings on the bridge or loads from noise barriers are not included in this model.

Variable loads
For the variable load the traffic load conform NEN-EN 1991-2, including Dutch national annex, load model 1 (LM1) is considered. A lane layout must be made before LM1 can be used.

Lane layout
The lane layout is determined in accordance with NEN-EN 1991-2 Table 4.1, which is shown below.

Width of the roadway w	Number of theoretical lanes	Width of a theoretical lane w_l	Width of the remaining area
$w < 5,4\ m$	$n_1 = 1$	$3\ m$	$w - 3\ m$
$5,4\ m \leq w < 6\ m$	$n_1 = 2$	$\frac{w}{2}\ m$	0
$w \geq 6\ m$	$n_1 = Int\left(\frac{w}{3}\right)$	$3\ m$	$w - 3 \cdot n_1$

Table 43 Number and width of the theoretical lanes (Table 4.1 of NEN-EN 1991-2)

For sake of simplicity the width of the roadway w is calculated as the width of the deck structure minus the two edge distances. The number of lanes, width of the theoretical lanes and width of the remaining area are determined in accordance with Table 43.

The lanes are positioned in such a way that the most unfavourable effect, both for bending and shear, for the bridge deck is created, which is the case when lane 1 is placed as much as possible on the edge of the deck and lanes 2 and 3 directly adjacent.

If the roadway on top of an underpass deck is physically separated into two parts by the presence of a central reservation the width of the deck must be changed accordingly, resulting into two sets of theoretical lane layouts. The disadvantage of this model is that the load is not distributed from one side of the middle reservation to the other, because the model has been reduced to only half of the structure.

Load Model 1
Load model 1, conform NEN-EN 1991-2 paragraph 4.3.2, consists of concentrated and uniformly distributed loads, which covers most of the effects of freight and passenger car traffic. This model is used for bending and shear assessments.

The concentrated loads of LM1 are double axle loads, hereafter called tandem system (TS), where the load per axle is given by:

$$\alpha_Q \cdot Q_k \qquad \text{where } \alpha_Q \text{ is a correction factor} \qquad \text{(B.12)}$$

The centre to centre distance of the axels in driving direction is 1,2 m, the centre to centre width of the TS is 2,0 m. The load of one axle is evenly distributed over two wheels which each have a length and width of 0,4 m. The tandem systems are all placed centrically in the corresponding lane.

The uniformly distributed load, called UDL, has a load per square meter of theoretical lane:

$$\alpha_q \cdot q_k \qquad \text{where } \alpha_q \text{ is a correction factor} \qquad \text{(B.13)}$$

The evenly distributed loads should only be applied to the unfavourable parts of the area of influence, which is the entire deck in this model.

The characteristic values of TS and UDL per lane are presented in Table 44, the application of LM1 is shown in Figure 83.

Position	Tandem system TS Axle load Q_{ik} [kN]	Uniformly distributed load UDL q_{ik} or q_{rk} [kN/m^2]
Lane number 1	300	9
Lane number 2	200	2,5
Lane number 3	100	2,5
Other lanes	0	2,5
Remaining area (q_{rk})	0	2,5

Table 44 Load model 1: Characteristic values (Table 4.2 of NEN-EN 1991-2)
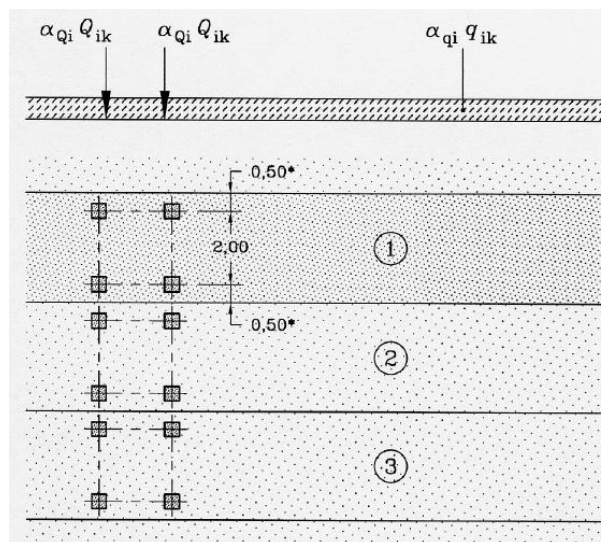
Figure 83 Application of LM1 (Figure 4.2a of NEN-EN 1991-2)

LM1 is applies at every theoretical lane and on the remaining areas.

If it can be shown that the number of heavy trucks in the lane for heavy traffic N_{obs} is less than 2.000.000, the load of LM1 will be reduced. The correction factors α_{Q1} and α_{q1} apply to all lanes. The correction factors α_{Q1}, α_{q1} and α_{qr} are determined based on the number of heavy trucks in the lane for heavy traffic N_{obs} and the length of the model L_{span}, Table 45 shows an overview of predefined values for which intermediate values are linearly interpolated. For lengths smaller than 20 meters the value belonging to 20 meters is taken.

Aantal vrachtwagens per jaar per rijstrook voor zwaar verkeer N_{obs} [a]	α_{Q1} en α_{q1}				α_{qr}
	Lengte van de overspanning of invloedslengte (L)				
	20 m	50 m	100 m	$\geq$ 200 m	
$\geq$ 2 000 000	1,0	1,0	1,0	1,0	
200 000	0,97	0,97	0,95	0,95	0,90
20 000	0,95	0,94	0,89	0,88	0,80
2 000	0,91	0,91	0,82	0,81	0,70
200	0,88	0,87	0,75	0,74	0,60
[a] Tussengelegen waarden mogen worden geïnterpoleerd.					

Table 45 Correction factors from Table NB.1 NEN-EN 1991-2 NB

In case of a roadway with three or more theoretical lanes and $N_{obs} \geq$ 2.000.000 per year, like most highways, applies $\alpha_{q1} = 1,15$ and for $i > 1$ applies $\alpha_{qi} = 1,40$.

Load combinations and load factors
Load combinations
In the assessment, only the ULS has been considered with the fundamental load combinations 6.10a and 6.10b from NEN-EN 1990.

$$6.10a: \sum_{j\geq1} \gamma_{G;j} \cdot G_{k;j} + \gamma_{Q;1} \cdot \psi_{0;1} \cdot Q_{k;1} + \sum_{i>1} \gamma_{Q;i} \cdot \psi_{0;1} \cdot Q_{k;i} \tag{B.14}$$

Since only one variable load, LM1, is present in this model, formula (B.14) can be reduced to:

$$6.10a: \sum_{j\geq1} \gamma_{G;j} \cdot G_{k;j} + \gamma_{Q;1} \cdot \psi_{0;1} \cdot Q_{k;1} \tag{B.15}$$

$$6.10b: \sum_{j\geq1} \xi \cdot \gamma_{G;j} \cdot G_{k;j} + \gamma_{Q;1} \cdot Q_{k;1} + \sum_{i>1} \gamma_{Q;i} \cdot \psi_{0;1} \cdot Q_{k;i} \tag{B.16}$$

Since only one variable load, LM1, is present in this model, formula (B.16) can be reduced to:

$$6.10b: \sum_{j\geq1} \xi \cdot \gamma_{G;j} \cdot G_{k;j} + \gamma_{Q;1} \cdot Q_{k;1} \tag{B.17}$$

The least favourable of the two formulas 6.10a and 6.10b is used.

6.10a applies an instantaneous factor $\psi_{0;1} = 0,8$ on traffic loads and the reduction factor for unfavourable permanent loads G in 6.10b is $\xi = 0,89$, according to the Dutch national annex.

Therefore, in most cases 6.10b will be decisive due to the relatively large share of traffic load. Only in case a large soil cover is present on the underpass will 6.10a become normative due to the increased share of permanent load.

Load factors

The load factors depend on the applied assessment level and the assigned consequence class. The applicable load factors are shown in Table 46, these factors do not include any correction factors.

Assessment level	Consequence Class	Permanent $6.10a$ $(\gamma_{G;j} \cdot G_{k;j})$	Permanent $6.10b$ $(\xi \cdot \gamma_{G;j} \cdot G_{k;j})$	Permanent favourable	Traffic $\gamma_{Q;1}$
New construction	CC1	1,20	1,10	0,90	1,20
	CC2	1,30	1,20	0,90	1,35
	CC3	1,40	1,25	0,90	1,50
Reconstruction	CC1	1,10	1,10	0,90	1,10
	CC2	1,25	1,10	0,90	1,20
	CC3	1,30	1,15	0,90	1,30
Usage	CC3	1,25	1,15	0,90	1,25
Disapproval	CC1	1,00	1,00	0,90	1,00
	CC2	1,10	1,10	0,90	1,10
	CC3	1,25	1,10	0,90	1,25

Table 46 Load factors applicable in the calculation

Correction factor for shorter reference period

According to NEN 8701 section 5.1.2, for the vertical loads by road traffic, including LM1, ψ-factors may be applied in accordance with Table 47 if the reference period is less than 100 years. The ψ-factor depends on the reference period and the length of the span, for which the model length is used, and intermediate values are interpolated linearly.

Referentieperiode	Ψ-factor [a]			
	Lengte van de overspanning of invloedslengte *L*			
	20 m	50 m	100 m	≥ 200 m
100 jaar	1,00	1,00	1,00	1,00
50 jaar	0,99	0,99	0,99	0,99
30 jaar	0,99	0,99	0,98	0,97
15 jaar	0,98	0,98	0.96	0,96
1 jaar	0,95 [b]	0,94 [b]	0,89	0,88
1 maand	0,91 [b]	0,91 [b]	0,81	0,81

Table 47 ψ-factor for shorter reference period (Table 1 of NEN 8701)

In case the length of the span is smaller than 20 meters, the value for 20 meters is taken.

Correction factor reduced trend

In accordance with NEN 8701 section 5.1.3 a trend reduction over the period from 2010 to 2060 is applied to the load size of LM1, which depends on the current year and the influence length, in this case the model

length. The table to determine the reduction factor α_{trend} is presented in Table 48, intermediate values are linearly interpolated.

Invloedslengte L [m]	Reductiefactor α_{trend} [a]					
	2010	2020	2030	2040	2050	2060
0	1,00	1,00	1,00	1,00	1,00	1,00
20	0,89	0,91	0,93	0,96	0,98	1,00
50	0,82	0,86	0,89	0,93	0,96	1,00
75	0,78	0,83	0,87	0,91	0,96	1,00
100	0,76	0,81	0,85	0,90	0,95	1,00
150	0,75	0,80	0,85	0,90	0,95	1,00
≥ 200	0,75	0,80	0,85	0,90	0,95	1,00

Table 48 Reduction factor α_{trend} (Table 2 of NEN 8701)

GEO – soil stresses

The GEO part is included to determine the load in plane of the underpass deck due to horizontal soil stresses and later this data is used for the horizontal loads on the 3D FEM plate model. The in-plane load increases the shear capacity of the deck and is therefore determined. The horizontal ground pressure is derived from the vertical ground stresses.

User input
Reference system
All layers are linked to a reference system based on the level of the top of the deck of the underpass. Based on this level and the layer thickness all other top and bottom levels of layers and the bottom of the structure are determined.

The level of the top of the deck of the underpass was chosen because it is often known, in $m\,NAP$, from drawing and has not changed over time.

Groundwater table
The groundwater table influences both vertical and horizontal soil stresses. In most soils the vertical stresses increase because pores fill with water increasing the specific weight. Because water stress is the same in all directions, a saturated soil increases the horizontal soil stresses.

In case a structure is completely dry, the groundwater level must be placed under the structure.

Top load
If an additional top load is present, it can be entered in kN/m^2 so that it is included in the calculation of vertical and horizontal ground stresses. As standard this value is set equal to zero, since it is most unfavourable to have traffic load on the deck and no traffic on the soils before and after underpass.

Soil layers
The user can choose to enter 0, 1, 2 or 3 layers of soil on top of the structure. The user is responsible for entering the soil type with the associated properties for each individual layer. It is strongly recommended and the standard value, based on NEN-EN 1991-2, to apply a coefficient of internal friction of 30° for all soil types.

Recommended values for various soil types:

Soil type	Specific weight dry $\gamma_{G;dry}$ $[kN/m^3]$	Specific weight saturated $\gamma_{G;sat}$ $[kN/m^3]$	Coefficient of internal friction φ_G [°]
Sand	17,5	17,5	30
Clay	16	20	30

Table 49 Recommended values for various soil types

Structure
The information about the structure is obtained from the geometry part, except for information about the ground next to the construction, which must be entered by the user himself. For the soil next to the structure, the same applies as the soil layers on top of the structure, see the relevant paragraph.

Vertical soil stresses
The vertical soil stress is determined by the top load plus the weight of asphalt and soil:

$$\sigma_v = P_{top} + \rho_{asphalt} \cdot h_{asphalt} + \sum_{i \geq 1}(\rho_{soil;i} \cdot h_{soil;i})$$ (B.18)

Where,
i is the number of layers soil in the total reference system from ground level to the bottom of the structure.

The value of $\rho_{soil;i}$ depends on whether the soil is dry or wet, in case the groundwater table is situated in a soil layer, the layer is split in two separate layers, one dry and one wet.

Above the groundwater table the groundwater stress σ_w is naturally zero, thereafter it increases with 10 kPa every meter of depth into the ground independently of soil type.

The effective vertical soil stress σ_v' is determined as the vertical soil stress minus the water stress:

$$\sigma_v' = \sigma_v - \sigma_w$$ (B.19)

Horizontal soil stresses
The horizontal ground stress σ_h is made up of effective horizontal soil stress σ_h' plus the water pressure σ_w.

$$\sigma_h = \sigma_h' + \sigma_w$$ (B.20)

The effective horizontal soil stress σ_h' depends on whether the soil is active K_a, passive K_p or neutral K_0 and its coefficient of internal friction $\varphi_{G;i}$. The underpass wall is believed to be stiff enough so that no significant displacement of soil occurs, so that the soil is considered neutral K_0. The formula for the determination of K_0 is:

$$K_0 = 1 - \sin(\varphi_{G;i})$$ (B.21)

Most soil types have an internal friction coefficient of about 30 degrees $\varphi_G \approx 30°$ resulting in a K_0 of 0,5. With K_0 known the effective horizontal soil stress σ_h' can be calculated with:

$$\sigma_h' = K_0 \cdot \sigma_v'$$ (B.22)

Normal force on deck structure

From the horizontal soil stress σ_h the normal force acting in plane on the deck of the underpass can be determined. An example situation is schematically visualized in Figure 84.
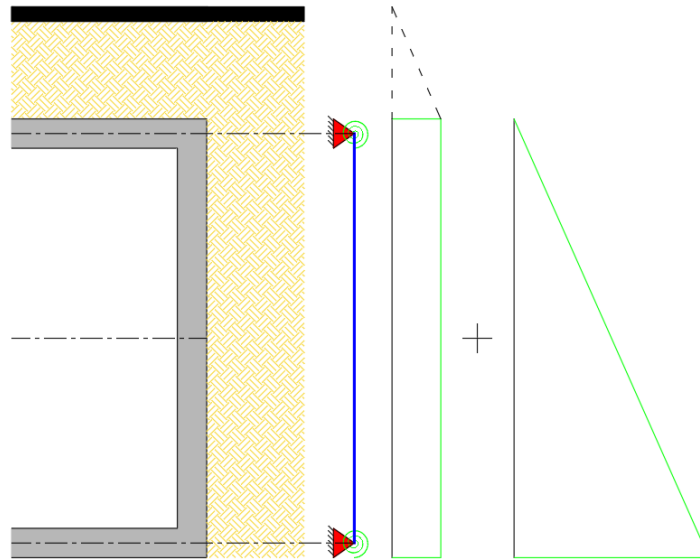
Figure 84 Schematization horizontal soil load on the structure

As a result of the ground above the deck level of the construction, or any top load, a constant horizontal pressure is created against the wall, the ground next to the structure creates a horizontal ground pressure rising from zero.

To determine the reaction force in the deck, the wall is modelled as a simply supported beam. The rotational stiffness at the supports, due to its connections with the deck and the floor slab, is ignored since it has no influence on the shear force distribution if the stiffness is comparable.

To solve this problem completely parametrically, including the possible presence of groundwater, the classic displacement method and solving of the ODEs were used. For the classic displacement method, reference is made to Bending Moment – MEd of this Appendix. In order to capture the presence of groundwater two ODEs are drawn up. The reaction force in the deck is found by asking for the shear force at the top support. Calculations by hand have been made to verify the script. The script is presented in Figure 85.

Simply supported Euler-Bernoulli beam - GEO

```
> restart :
```

Define loads

```
> q1 := q_boven + q_droog·(x) :
> q2 := q_boven + q_droog·(x_WL − x_BK) + q_nat·(x − x_WL) :
```

ODE, BC&MC,Solver

```
> ODE1 := EI·diff (w1(x), x$4) = q1 :
> ODE2 := EI· diff (w2(x), x$4) = q2 :
> sol := dsolve({ODE1, ODE2}, {w1, w2}) : assign(sol) :
> w1 := w1(x) : w2 := w2(x) :
> phi1 := −diff (w1, x) : Kappa1 := diff (phi1, x) : M1 := EI·Kappa1 : V1 := diff (M1, x) :
> phi2 := −diff (w2, x) : Kappa2 := diff (phi2, x) : M2 := EI·Kappa2 : V2 := diff (M2, x) :
> x := x_BK : eq1 := w1 = 0 : eq2 := M1 = 0 :
> x := x_WL : eq3 := w1 = w2 : eq4 := phi1 = phi2 : eq5 := M1 = M2 : eq6 := V1 = V2 :
> x := x_OK : eq7 := w2 = 0 : eq8 := M2 = 0 :
> sol := solve({eq1, eq2, eq3, eq4, eq5, eq6, eq7, eq8}, {_C1, _C2, _C3, _C4, _C5, _C6, _C7,
    _C8}) : assign(sol);
> x := 'x':
```

Convert reference system m NAP to x-coordinates

```
> x_BK := BK − BK :
> x_WL := abs(BK − WL) :
> x_OK := abs(BK − OK) :
```

Set x to top level of structure:
```
> x := x_BK:
```

Ask for V(x=0);
```
> V1
```

$$-\frac{1}{6\,|BK - OK|}\left(-3\,q\_droog\,|BK - OK|^2\,|BK - WL| + 3\,q\_droog\,|BK - OK|\,|BK - WL|^2 \right.$$
$$- q\_droog\,|BK - WL|^3 - q\_nat\,|BK - OK|^3 + 3\,q\_nat\,|BK - OK|^2\,|BK - WL|$$
$$\left. - 3\,q\_nat\,|BK - OK|\,|BK - WL|^2 + q\_nat\,|BK - WL|^3 - 3\,q\_boven\,|BK - OK|^2\right)$$

(1)

Figure 85 MAPLE script for the determination of normal force in the deck due to horizontal soil loads

The formula for $V1$ in Figure 85 is converted to Excel which links the parameters to the corresponding cells, the result is the normal force in plane on the deck in kN per linear meter.

Limitations

Although the calculation method allows, the model has chosen not to apply more than three layers of soil on top of the construction. This was chosen because of complexity, and in practice it is rare that there are more than three different layers of soil on top of the construction. The same story holds for the maximum layers of soil next to the structure, which is limited to just one layer.

It is possible that due to a closed clay layer the water pressure at the bottom of this clay layer is higher than its depth location suggests, this increased groundwater pressure cannot be included in the model.

Bending moment – MEd

The underpass is modelled as a simply supported beam, representing the deck, with rotational springs at the supports, representing the walls, with a model width of one meter.

For the load distribution of LM 1 the method of Guyon-Massonnet is used, this method translates the UDL and TS to two uniform loads which can be applied on the beam model together with the uniform loads of self-weight and the weight of the soil and asphalt layer.

The classical displacement method is used to determine the ODEs which give formulas for the occurring moments. General information about this method in this model is later described in this Appendix. This method was chosen because the occurring moment must be determined at various sections in the beam, and this method gives a generic formula for the occurring moment.

Load distribution of Load Model 1 with Guyon-Massonnet

The method of Guyon-Massonnet is used for the load distribution of load model 1. This was chosen because it is generally known that load distribution of LM1 at a distribution angle, for concrete 45 degrees, results in too conservative values.

Background

The background information of the method of Guyon-Massonnet is based on (Ezi, Onuamah, Ugwuanyi, & Agbo, 2018) and (Yang, 2020).

In the Guyon-Massonnet method a 4th order differential equation (B.23) describes the orthotropic slab behaviour with as input the geometry, elastic modulus of the concrete, flexural stiffness θ (B.30) and torsional stiffness α (B.26) of the slab. The method assumes that the slab is deformed as a half-sine wave.

$$\rho_{xx} \frac{\partial^4 w}{\partial x^4} + 2H \frac{\partial^4 w}{\partial x^2 \partial y^2} + \rho_{yy} \frac{\partial^4 w}{\partial y^4} = \rho(x,y) \tag{B.23}$$

Where,

$$2H = 2\alpha \sqrt{\rho_{xx}\rho_{yy}} \tag{B.24}$$

In which ρ is the flexural rigidity per unit width of the plate.

In formula (B.23) $\rho_{xx} \frac{\partial^4 w}{\partial x^4}$ and $\rho_{yy} \frac{\partial^4 w}{\partial y^4}$ represent ideal beam strip action, the term $2H \frac{\partial^4 w}{\partial x^2 \partial y^2}$ includes twisting. Since the cross-section of the deck is a rigid rectangular plate the flexural rigidity per unit width can be easily determined:

$$\rho_{xx} = \rho_{yy} = EI = E \cdot \left(\frac{1}{12} \cdot b_{model} \cdot h_{deck}^3 \right) \tag{B.25}$$

The centre-to-centre distance of both main- and transverse beams have been replaced in formula (B.25) by the model width b_{model}, which is $1\ m$, since the deck is a massive plate and the model has a unit width.

The torsional stiffness α is given by:

$$\alpha = \frac{\gamma_{xy} + \gamma_{yx} + \nu\rho_{xx} + \nu\rho_{yy}}{2\sqrt{\rho_{xx}\rho_{yy}}} \tag{B.26}$$

In which γ is the torsional rigidity per unit width.

Since the cross-section of the deck is a rigid rectangular plate the torsional rigidity per unit width can be easily determined:

$$\gamma_{xx} = \gamma_{yy} = GI_t = G \cdot \left(\frac{1}{6} \cdot b_{model} \cdot h_{deck}^3 \right) \tag{B.27}$$

Where,

$$G = \frac{E}{2 \cdot (1+v)} \tag{B.28}$$

And again the centre-to-centre distance of both main- and transverse beams have been replaced in formula (B.27) by the model width b_{model}, which is 1 m, since the deck is a massive plate and the model has a unit width.

From formulas (B.27) and (B.28) it appears that Poisson ratio v influences the torsional rigidity γ and therefore the torsional stiffness α. In this model setting the Poisson ratio equal to zero $v = 0$ results in $\alpha = 1$, by increasing the Poisson effect the torsional stiffness becomes smaller resulting in less load distribution.

Increasing the torsional stiffness α results in larger load distribution.

In 1946 Guyon started with a torsionless deck. By setting the torsional stiffness equal to zero $\alpha = 0$ and assuming a displacement field equal to $p(x, y) = p_m \cdot \sin\left(\frac{m \cdot \pi \cdot x}{L}\right)$, formula (B.23) becomes:

$$\left(\frac{\theta L}{b}\right)^4 \frac{\partial^4 w}{\partial x^4} + \frac{\partial^4 w}{\partial y^4} = \frac{\rho_m}{\rho_{yy}} \cdot \sin\left(\frac{m \cdot \pi \cdot x}{L}\right) \tag{B.29}$$

With the flexural stiffness θ given by:

$$\theta = \frac{b}{l} \sqrt[4]{\rho_{xx}/\rho_{yy}} \tag{B.30}$$

The solution of equation (B.29) is of the form:

$$w_m = Y_m \cdot \sin\left(\frac{m \cdot \pi \cdot x}{L}\right) \tag{B.31}$$

Where Y_m is the amplitude, the maximum deflection, and given by:

$$Y_m = \frac{L^4 \cdot p_m}{m^4 \cdot \pi^4 \cdot \rho_{xx}} \tag{B.32}$$

If we take this theory to a simple bridge type, as shown in Figure 86, and load it with a line-load:

$$p(x) = P_1 \cdot \sin\left(\frac{\pi \cdot x}{L}\right) \tag{B.33}$$

The slab deflects in both x- and y-direction according to:

$$w(x, y) = W(y) \cdot \sin\left(\frac{\pi \cdot x}{L}\right) \tag{B.34}$$

In which, $W(y)$ is a function of y determining the maximum deflection, amplitude, over the y-coordinate.

In the x-direction, the plate deforms according to a half sine.
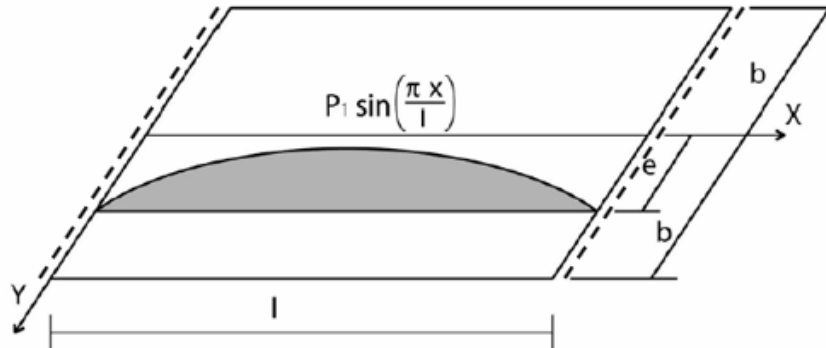
Figure 86 The system of a simple bridge type (edited from: (Yang, 2020))

If the load from equation (B.33) is smeared out over the whole width $2b$ of the slab this equation turns into:

$$p_0(x) = \frac{P_1}{2b} \cdot \sin\left(\frac{\pi \cdot x}{L}\right)$$
(B.35)

Because the load is distributed evenly over the width of the slab, it does not bend in y-direction anymore. Due to the load defined by (B.35) the slab deforms as a cylindrical surface:

$$w_0(x) = W_0 \cdot \sin\left(\frac{\pi \cdot x}{L}\right)$$
(B.36)

In which, W_0 determines the maximum deflection, amplitude, over the width of the slab, but does not depend on y-coordinate.

The ratio between the deflections (B.34) and (B.36), caused by the line load (B.33) and the distributed load (B.35) respectively, is called "the principal coefficient of lateral distribution" and is denoted with K.

$$K(\alpha)_v = \frac{w(x,y)}{w_0(x)} = \frac{W(y)}{W_0}$$
(B.37)

The coefficient K is influenced by:

- The flexural stiffness θ;
- The torsional stiffness α;
- The relative eccentricity of the line-load e/b;
- The relative coordinate of the considered point y/b.

In 1950 Massonnet, unlike Guyon, also considered torsion, based on many numerical investigations Massonnet deduced the interpolation formula:

$$K_\alpha = K_0 + (K_1 - K_0)\sqrt{\alpha}$$
(B.38)

Where,

K_0 is $K(\alpha)_v$ with $\alpha = 0$

K_1 is $K(\alpha)_v$ with $\alpha = 1$

In this way $K(\alpha)_v$ does not have to be recalculated in its entirety every time when changing the torsional stiffness α.

Module: Guyon-Massonnet

The Guyon-Massonnet module, *"Guyon-Massonnet plaat Eurocode.xlsm",* is a modified version of an Excel sheet from RHDHV. Permission to use this sheet has been granted by R.P.H. Vergoossen, employee and thesis supervisor of RHDHV.

Sections 1 and 2 of this spreadsheet concern the geometry of the bridge deck and the load from LM1. The input regarding the geometry of the bridge deck and the loads are loaded automatically via a script. As standard the Poisson ratio is fixed at $v = 0.20$, because lowering the Poisson ratio leads to more load spreading. Since it is assumed that the tandem system is placed centrally in the lanes, the eccentricity of TS is fixed at zero. Adjustment to the sheet was made by not setting the values of α_{q1} and α_{Q1} to 1,0 but importing them from the calculation sheet, which in some cases has a positive effect in the form of a reduction on the applicable loads from LM1.

In section 3 constants depending on the geometry of the deck, which are needed for further calculations, are calculated.

The K_0-factors and K_1-factors are calculated in section 4 and 5 respectively.

In section 6 the K_α-factor is calculated with formula (B.38). The representative loads for the UDL and TS at a certain y-location are calculated by summing up all the TS loads and all the UDL loads, multiply them by the corresponding K_α-factor and spread the load across the width of the deck. In formula:

$$q_{UDL;y} = \frac{K_{\alpha;q} \cdot q_{tot}}{2b} \tag{B.39}$$

$$q_{TS;single\;;y} = \frac{K_{\alpha;Q} \cdot Q_{tot}}{2b} \qquad \text{(single axle)} \tag{B.40}$$

Then the script continues and the bridge deck is divided into 100 pieces across the width, resulting in 100 y-locations. The corresponding q_{UDL} and $q_{TS;single}$ are then calculated per location and exported to the calculation sheet under "Uitvoer Guyon-Massonnet". The calculation sheet then determines the maximum load with corresponding location. In case the decisive location is $y < d$, where d is estimated with $d \approx 0,9 \cdot h$, then $y = d$ is entered in the module and the values for q_{UDL} and $q_{TS;single}$ are extra exported to the calculation sheet and used. This is because the normative value at $y = 0$ would be too conservative and there should be a relation with the thickness of the deck, so in that case the value at $y = d$ of the strip is used.

The characteristic value for the whole TS is calculated with:

$$Q_{TS;k} = \frac{2 \cdot q_{TS;single;y}}{L_{wheelprint}} \tag{B.41}$$

Projection of TS on the concrete deck

According to NEN-EN 1991-2 section 4.3.6 local loads, like TS from LM1, may be distributed to the neutral line of the concrete deck as shown in Figure 87.
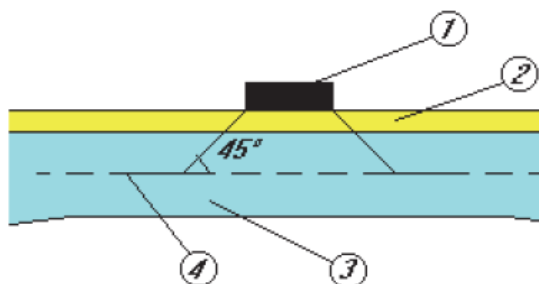
Figure 87 Load distribution of local loads (Figure 4.4 of NEN-EN 1991-2)

According to art. (2) of this section the angle for load distribution of concrete and asphalt must be equal to 45°. As standard, it is recommended to maintain a spread angle of 30° for soil.

The spreading width from the edge of the wheel is denoted as s, shown in Figure 88, and is calculated as:

$$s = h_{asphalt} \cdot \sin(\varphi_{asphalt}) + h_{soil} \cdot \sin(\varphi_{soil}) + \frac{1}{2} \cdot h_{deck} \cdot \sin(\varphi_{concrete}) \qquad \text{(B.42)}$$

Where,

$$\varphi_{asphalt} = \varphi_{concrete} = 45° \qquad \text{(NEN-EN 1991-2 art. 4.3.6 (2))}$$

φ_{soil} is the spread angle for soil, standard set to $\varphi_{soil} = 30°$
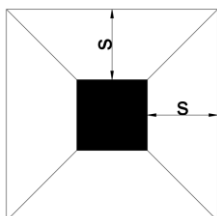
Figure 88 Display of distance s

Because the axles are only 1,2 meters center to center in the direction of travel, the wheel prints can overlap. This is checked by calculating the space between the two wheel prints, in case a negative value is calculated the prints overlap each other. This can be checked with:

$$L_{Ts} - L_{wheel} - 2 \cdot s < 0 \qquad \text{(B.43)}$$

Where,

$$L_{TS} = 1,2 \ m; \quad L_{wheel} = 0,4 \ m$$

If formula (B.43) is true situation as shown in Figure 89 (B) applies, otherwise situation (A) applies.
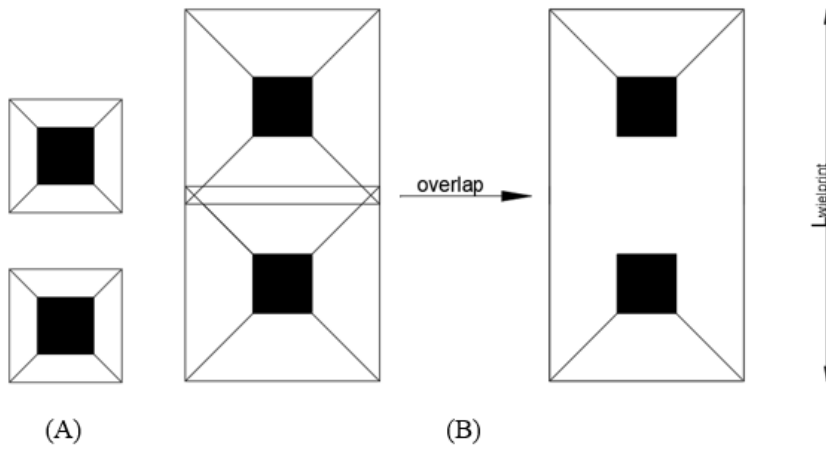
Figure 89 (A) no overlap, (B) with overlap

Based on the available data and the minimum asphalt thickness according to ROK of 120 mm, situation (B) almost always occurs. In case situation (A) occurs, the gap is so small that situation (B) is still assumed accepting a negligible error. The length of the combined wheel print $L_{wheel\ print}$ is determined by:

$$L_{wheelprint} = L_{TS} + L_{wheel} + 2 \cdot s \qquad \text{(B.44)}$$

Since the load of the Guyon-Massonnet module only contains one TS axle, the load of the two axles must be combined:

$$q_{TS} = 2 \cdot q_{TS;single}/L_{wheelprint} \qquad \text{(B.45)}$$

Determination of bending moment based on ODE
The sheet allows the user to select which loads must be applied in the model, if a checkbox is marked the load is naturally applied. An overview of all the loads is given with the corresponding load factor obtained from the tab loads. The loads due to self-weight, soil, asphalt and UDL act on the whole length of the deck and are summed up as one load denoted as q_q. The load of the TS is kept isolated since it does not act over the full beam length. A schematic overview of the model is shown in Figure 90.
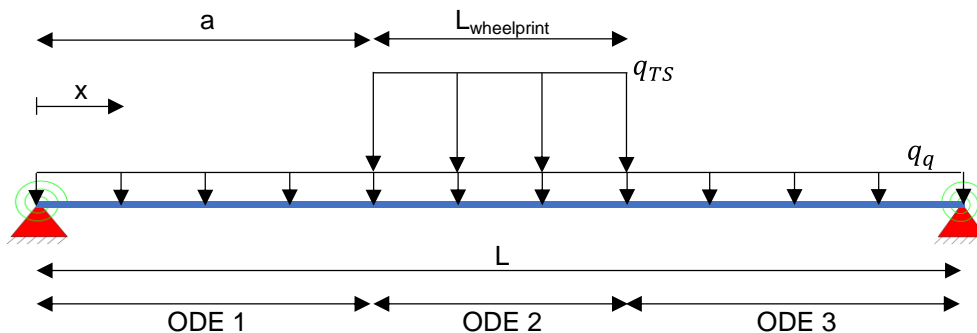
Figure 90 schematization of the model

To capture the behaviour of this model correctly, three ODEs must be drawn up. Although the location of the TS differs for maximum sagging moment, maximum hogging moment at the haunch and maximum hogging moment in the clear, the ODEs, kinematic and constitutive relations, equilibrium conditions, matching and boundary conditions and the general solution to the ODEs are in all situations the same. The ODEs are:

$$ODE_1 = EI \cdot \frac{\partial^4 w_1(x)}{\partial x^4} = q_q \tag{B.46}$$

$$ODE_2 = EI \cdot \frac{\partial^4 w_2(x)}{\partial x^4} = q_q + q_{TS} \tag{B.47}$$

$$ODE_3 = EI \cdot \frac{\partial^4 w_3(x)}{\partial x^4} = q_q \tag{B.48}$$

The general solution to this set of ODEs is:

$$w_1(x) = \frac{qx^4}{24EI} + \frac{C1x^3}{6} + \frac{C2x^2}{2} + C3x + C4 \tag{B.49}$$

$$w_2(x) = \frac{qx^4}{24EI} + \frac{C5x^3}{6} + \frac{C6x^2}{2} + C7x + C8 \tag{B.50}$$

$$w_3(x) = \frac{qx^4}{24EI} + \frac{C9x^3}{6} + \frac{C10x^2}{2} + C11x + C12 \tag{B.51}$$

The kinematic relations are:

$$\varphi_1 = -\frac{\partial w_1}{\partial x}; \quad \kappa_1 = \frac{\partial \varphi_1}{\partial x}; \quad \varphi_2 = -\frac{\partial w_2}{\partial x}; \quad \kappa_2 = \frac{\partial \varphi_2}{\partial x}; \quad \varphi_3 = -\frac{\partial w_3}{\partial x}; \quad \kappa_3 = \frac{\partial \varphi_3}{\partial x}; \tag{B.52}$$

The constitutive relations are:

$$M_1 = \kappa_1 \cdot EI; \quad M_2 = \kappa_2 \cdot EI; \quad M_3 = \kappa_3 \cdot EI; \tag{B.53}$$

The equilibrium equations are:

$$V_1 = \frac{\partial M_1}{\partial x}; \quad V_2 = \frac{\partial M_2}{\partial x}; \quad V_3 = \frac{\partial M_3}{\partial x}; \tag{B.54}$$

The boundary conditions at the left support, $x = 0$, are:

$$eq_1: w_1 = 0; \quad eq_2: M_1 = K_r \cdot \varphi_1; \tag{B.55}$$

In which K_r is the rotational stiffness.

The matching conditions between ODE_1 and ODE_2 at $x = a$ are:

$$eq_3: w_1 = w_2; \quad eq_4: \varphi_1 = \varphi_2; \quad eq_5: M_1 = M_2; \quad eq_6; V_1 = V_2 \tag{B.56}$$

The matching conditions between ODE_2 and ODE_3 at $x = a + L_{wheelprint}$ are:

$$eq_7: w_2 = w_3; \quad eq_8: \varphi_2 = \varphi_3; \quad eq_9: M_2 = M_3; \quad eq_{10}; V_2 = V_3 \tag{B.57}$$

The boundary conditions at the right support, $x = L$, are:

$$eq_{11}: w_3 = 0; \quad eq_{12}: M_3 = -K_r \cdot \varphi_3; \tag{B.58}$$
In which K_r is the rotational stiffness.

The solution for the integration constants $C1$ to $C12$ can be found with the equations for the boundary and matching conditions eq_1 to eq_{12}.

Since everything is scripted in MAPLE, the bending moment and shear force at a certain value of x can simply be asked for. Which section force, like $M_1, M_2 \ or \ M_3$, to be requested depends on which ODE the section is located. The formulas obtained with MAPLE for the section forces are rather long but completely parametric. These formulas are exported to Excel and linked to the correct cells. The resulting section forces are checked for a simple situation by a calculation by hand and for the more complex situation verified with SOFiSTiK FEA software.

The parametric solution for the bending moment of ODE_1 denoted with $M_1(x)$ is defined as: (B.59)

$$EI\left(-\frac{qq\,x^2}{2\,EI}+\frac{1}{2\,L^2\,EI\,(Kr\,L+6\,EI)}\left(\left(Kr\,L^4\,qq+2\,Kr\,L^3\,qTS\,Lwheelprint-6\,Kr\,L\,a^2\,qTS\,Lwheelprint-6\,Kr\,L\,a\,qTS\,Lwheelprint^2-2\,Kr\,L\,qTS\,Lwheelprint^3+4\,Kr\,a^3\,qTS\,Lwheelprint+6\,Kr\,a^2\,qTS\,Lwheelprint^2\right.\right.\right.$$

$$+4\,Kr\,a\,qTS\,Lwheelprint^3+Kr\,qTS\,Lwheelprint^4+6\,EI\,L^3\,qq+12\,EI\,L^2\,qTS\,Lwheelprint-12\,EI\,a\,qTS\,Lwheelprint\,L-6\,EI\,qTS\,Lwheelprint^2\,L)\,x)-\frac{1}{12\,EI\,L\,(Kr^2\,L^2+8\,EI\,Kr\,L+12\,EI^2)}(Kr\,(Kr\,L^5\,qq$$

$$+12\,Kr\,L^3\,a\,qTS\,Lwheelprint+6\,Kr\,L^3\,qTS\,Lwheelprint^2-24\,Kr\,L^2\,a^2\,qTS\,Lwheelprint-24\,Kr\,L^2\,a\,qTS\,Lwheelprint^2-8\,Kr\,L^2\,qTS\,Lwheelprint^3+12\,Kr\,L\,a^3\,qTS\,Lwheelprint+18\,Kr\,L\,a^2\,qTS\,Lwheelprint^2$$

$$+12\,Kr\,L\,a\,qTS\,Lwheelprint^3+3\,Kr\,L\,qTS\,Lwheelprint^4+6\,EI\,L^4\,qq+48\,EI\,L^2\,a\,qTS\,Lwheelprint+24\,EI\,L^2\,qTS\,Lwheelprint^2-72\,EI\,L\,a^2\,qTS\,Lwheelprint-72\,EI\,L\,a\,qTS\,Lwheelprint^2-24\,EI\,L\,qTS\,Lwheelprint^3$$

$$\left.\left.\left.+24\,EI\,a^3\,qTS\,Lwheelprint+36\,EI\,a^2\,qTS\,Lwheelprint^2+24\,EI\,a\,qTS\,Lwheelprint^3+6\,EI\,qTS\,Lwheelprint^4)\right)\right)\right)$$

The parametric solution for the shear force of ODE_1 denoted with $V_1(x)$ is defined as: (B.60)

$$EI\left(-\frac{qq\,x}{EI}+\frac{1}{2\,L^2\,EI\,(Kr\,L+6\,EI)}(Kr\,L^4\,qq+2\,Kr\,L^3\,qTS\,Lwheelprint-6\,Kr\,L\,a^2\,qTS\,Lwheelprint-6\,Kr\,L\,a\,qTS\,Lwheelprint^2-2\,Kr\,L\,qTS\,Lwheelprint^3+4\,Kr\,a^3\,qTS\,Lwheelprint+6\,Kr\,a^2\,qTS\,Lwheelprint^2+4\,Kr\,a\,qTS\,Lwheelprint^3\right.$$

$$\left.+Kr\,qTS\,Lwheelprint^4+6\,EI\,L^3\,qq+12\,EI\,L^2\,qTS\,Lwheelprint-12\,EI\,a\,qTS\,Lwheelprint\,L-6\,EI\,qTS\,Lwheelprint^2\,L)\right)$$

The parametric solution for the bending moment of ODE_2 denoted with $M_2(x)$ is defined as: (B.61)

$$\frac{1}{2\,L^2\,(Kr\,L+6\,EI)}\left(\left(Kr\,L^4\,qq+2\,Kr\,L^3\,a\,qTS+2\,Kr\,L^3\,qTS\,Lwheelprint-6\,Kr\,L\,a^2\,qTS\,Lwheelprint-6\,Kr\,L\,a\,qTS\,Lwheelprint^2-2\,Kr\,L\,qTS\,Lwheelprint^3+4\,Kr\,a^3\,qTS\,Lwheelprint+6\,Kr\,a^2\,qTS\,Lwheelprint^2+4\,Kr\,a\,qTS\,Lwheelprint^3\right.\right.$$

$$+Kr\,qTS\,Lwheelprint^4+6\,EI\,L^3\,qq+12\,EI\,L^2\,a\,qTS+12\,EI\,L^2\,qTS\,Lwheelprint-12\,EI\,a\,qTS\,Lwheelprint\,L-6\,EI\,qTS\,Lwheelprint^2\,L)\,x)-\frac{qTS\,x^2}{2}-\frac{qq\,x^2}{2}-\frac{1}{12\,L\,(Kr^2\,L^2+8\,EI\,Kr\,L+12\,EI^2)}(Kr^2\,L^5\,qq+6\,Kr^2\,L^3\,a^2\,qTS$$

$$+12\,Kr^2\,L^3\,a\,qTS\,Lwheelprint+6\,Kr^2\,L^3\,qTS\,Lwheelprint^2-24\,Kr^2\,L^2\,a^2\,qTS\,Lwheelprint-24\,Kr^2\,L^2\,a\,qTS\,Lwheelprint^2-8\,Kr^2\,L^2\,qTS\,Lwheelprint^3+12\,Kr^2\,L\,a^3\,qTS\,Lwheelprint+18\,Kr^2\,L\,a^2\,qTS\,Lwheelprint^2$$

$$+12\,Kr^2\,L\,a\,qTS\,Lwheelprint^3+3\,Kr^2\,L\,qTS\,Lwheelprint^4+6\,EI\,Kr\,L^4\,qq+48\,EI\,Kr\,L^2\,a^2\,qTS+48\,EI\,Kr\,L^2\,a\,qTS\,Lwheelprint+24\,EI\,Kr\,L^2\,qTS\,Lwheelprint^2-72\,EI\,Kr\,L\,a^2\,qTS\,Lwheelprint-72\,EI\,Kr\,L\,a\,qTS\,Lwheelprint^2$$

$$\left.-24\,EI\,Kr\,L\,qTS\,Lwheelprint^3+24\,EI\,Kr\,a^3\,qTS\,Lwheelprint+36\,EI\,Kr\,a^2\,qTS\,Lwheelprint^2+24\,EI\,Kr\,a\,qTS\,Lwheelprint^3+6\,EI\,Kr\,qTS\,Lwheelprint^4+72\,EI^2\,L\,a^2\,qTS)\right)$$

The parametric solution for the shear force of ODE_2 denoted with $V_2(x)$ is defined as: (B.62)

$$\frac{1}{2\,L^2\,(Kr\,L+6\,EI)}(Kr\,L^4\,qq+2\,Kr\,L^3\,a\,qTS+2\,Kr\,L^3\,qTS\,Lwheelprint-6\,Kr\,L\,a^2\,qTS\,Lwheelprint-6\,Kr\,L\,a\,qTS\,Lwheelprint^2-2\,Kr\,L\,qTS\,Lwheelprint^3+4\,Kr\,a^3\,qTS\,Lwheelprint+6\,Kr\,a^2\,qTS\,Lwheelprint^2+4\,Kr\,a\,qTS\,Lwheelprint^3$$

$$+Kr\,qTS\,Lwheelprint^4+6\,EI\,L^3\,qq+12\,EI\,L^2\,a\,qTS+12\,EI\,L^2\,qTS\,Lwheelprint-12\,EI\,a\,qTS\,Lwheelprint\,L-6\,EI\,qTS\,Lwheelprint^2\,L)-qTS\,x-qq\,x$$

The solutions for ODE_3 are not shown since no cross-sections are taken in that part of the structure. All bending moments are calculated for both 6.10a and 6.10b, naturally the maximum value is used. Solutions for ODE_3 are used within the analytical model to create a Moment-line.

Sagging moment
The maximum sagging bending moment naturally occurs in the cross-section in the middle of the span if the TS is situated in the middle of the span as well. The distance a is in this situation defined as:

$$a = \frac{L-L_{wheelprint}}{2} \tag{B.63}$$

The sagging bending moment at the centre of the span denoted as $M_{Ed;span}$ and defined as $M_2\left(x = \frac{L}{2}\right)$.

For the situation of the maximum sagging moment, the shear force and bending moment in the clear are also determined for verification.

The distance from the support to the face of the wall x_{clear} is defined as:

$$x_{clear} = \frac{h_{wall}}{2} \tag{B.64}$$

The hogging bending moment at the section in the clear denoted as $M_{Ed;clear}$ is defined as $M_1(x = x_{clear})$. The shear force occurring at the section in the clear denoted as $V_{Ed;clear}$ is defined as $V_1(x = x_{clear})$.

Hogging moment at end of haunch
The section with the connection of the haunch is illustrated in Figure 91. The location of the TS for the maximum hogging moment in the section with the connection of the haunch is determined by solving the ODE and analytically maximizing the moment in the relevant section minus a distance d. The moment M_{Ed} is read at a distance d from the section, in accordance with NEN-EN 1992-1-1 section 9.2.1.3, which states that the moment line must be shifted over a distance $a_l = d$ in the negative direction.

Figure 91 Illustration of section at haunch with hogging moment

The distance a is determined by differentiating M_1, formula (B.59), with respect to a and solving the found equation equal to zero. The equation for the slope of the moment line is defined as $\frac{\partial M_1}{\partial a}$: (B.65)

$$M1\_helling := EI\left(\frac{(-12\,KrL\,aqTSLwheelprint - 6\,KrL\,qTSLwheelprint^2 + 12\,Kr\,d^2\,qTSLwheelprint + 12\,Kr\,aqTSLwheelprint^2 + 4\,Kr\,qTSLwheelprint^3 - 12\,EILqTSLwheelprint)\,x}{2\,L^2\,EI\,(KrL + 6\,EI)}\right.$$
$$-\frac{1}{12\,EIL\,(Kr^2L^2 + 8\,EI\,KrL + 12\,EI^2)}\left(Kr\left(12\,KrL^3\,qTSLwheelprint - 48\,KrL^2\,aqTSLwheelprint - 24\,KrL^2\,qTSLwheelprint^2 + 36\,KrL\,d^2\,qTSLwheelprint + 36\,KrL\,aqTSLwheelprint^2\right.\right.$$
$$+ 12\,KrL\,qTSLwheelprint^3 + 48\,EIL^2\,qTSLwheelprint - 144\,EI\,aqTSLwheelprintL - 72\,EI\,qTSLwheelprint^2\,L + 72\,EI\,d^2\,qTSLwheelprint + 72\,EI\,aqTSLwheelprint^2$$
$$\left.\left.\left.+ 24\,EI\,qTSLwheelprint^3\right)\right)\right)$$

The critical distance a for the hogging bending moment at the haunch is found by solving $\frac{\partial M_1}{\partial a} = 0$: (B.66)

$$\frac{1}{6\,Kr\,(KrL^2 - 2\,KrLx + 2\,EIL - 4\,EIx)}\left(4\,L^3\,Kr^2 - 6\,Kr^2\,L^2x - 3\,Kr^2\,L^2\,Lwheelprint + 6\,Kr^2\,Lx\,Lwheelprint + 12\,L^2\,Kr\,EI - 12\,EI\,Kr\,Lx - 6\,EI\,Kr\,L\,Lwheelprint + 12\,EI\,Kr\,x\,Lwheelprint\right.$$
$$+ \sqrt{4\,Kr^4\,L^6 - 24\,Kr^4\,L^5x + 36\,Kr^4\,L^4x^2 - 3\,Kr^4\,L^4\,Lwheelprint^2 + 12\,Kr^4\,L^3\,x\,Lwheelprint^2 - 12\,Kr^4\,L^2\,x^2\,Lwheelprint^2 + 24\,EI\,Kr^3\,L^4 - 168\,EI\,Kr^3\,L^3\,x + 288\,EI\,Kr^3\,L^2\,x^2 - 12\,EI\,Kr^3\,L^2\,Lwheelprint^2 + 48\,EI\,Kr^3\,L^2\,x\,Lwheelprint^2 - 48\,EI\,Kr^3\,Lx^2\,Lwheelprint^2 + 48\,EI^2\,Kr^2\,L^4 - 384\,EI^2\,Kr^2\,L^3\,x + 720\,EI^2\,Kr^2\,L^2\,x^2 - 12\,EI^2\,Kr^2\,L^2\,Lwheelprint^2 + 48\,EI^2\,Kr^2\,Lx\,Lwheelprint^2 - 48\,EI^2\,Kr^2\,x^2\,Lwheelprint^2 - 288\,EI^3\,Kr\,L^2x + 576\,EI^3\,Kr\,Lx^2}\right)$$
$$\frac{1}{6\,Kr\,(KrL^2 - 2\,KrLx + 2\,EIL - 4\,EIx)}\left(4\,L^3\,Kr^2 - 6\,Kr^2\,L^2x - 3\,Kr^2\,L^2\,Lwheelprint + 6\,Kr^2\,Lx\,Lwheelprint + 12\,L^2\,Kr\,EI - 12\,EI\,Kr\,Lx - 6\,EI\,Kr\,L\,Lwheelprint + 12\,EI\,Kr\,x\,Lwheelprint\right.$$
$$- \sqrt{4\,Kr^4\,L^6 - 24\,Kr^4\,L^5x + 36\,Kr^4\,L^4x^2 - 3\,Kr^4\,L^4\,Lwheelprint^2 + 12\,Kr^4\,L^3\,x\,Lwheelprint^2 - 12\,Kr^4\,L^2\,x^2\,Lwheelprint^2 + 24\,EI\,Kr^3\,L^4 - 168\,EI\,Kr^3\,L^3\,x + 288\,EI\,Kr^3\,L^2\,x^2 - 12\,EI\,Kr^3\,L^2\,Lwheelprint^2 + 48\,EI\,Kr^3\,L^2\,x\,Lwheelprint^2 - 48\,EI\,Kr^3\,Lx^2\,Lwheelprint^2 + 48\,EI^2\,Kr^2\,L^4 - 384\,EI^2\,Kr^2\,L^3\,x + 720\,EI^2\,Kr^2\,L^2\,x^2 - 12\,EI^2\,Kr^2\,L^2\,Lwheelprint^2 + 48\,EI^2\,Kr^2\,Lx\,Lwheelprint^2 - 48\,EI^2\,Kr^2\,x^2\,Lwheelprint^2 - 288\,EI^3\,Kr\,L^2x + 576\,EI^3\,Kr\,Lx^2}\right)$$

In which x is defined as the distance from the support to the section with the haunch x_{haunch}:

$$x_{haunch} = \frac{h_{wall}}{2} + L_{haunch} - d \tag{B.67}$$

In which L_{haunch} is the length of the haunch.

With the critical location of the TS known the maximum hogging moment at the section at the haunch denoted as $M_{Ed;haunch^-}$ is defined as $M_1(x = x_{haunch})$.

For the situation of the maximum hogging moment at the section at the connection with the haunch, the shear force in the clear and bending moment at midspan are also determined for verification. The distance from the support to the face of the wall x_{clear} is defined as formula (B.64).

The corresponding maximum sagging moment in the span is determined for the location of TS for the maximum hogging moment in the section at the end of the haunch $M_{Ed,haunch^-}$ and the shear force at the

section in the clear $V_{Ed;clear}$ is defined as $V_1(x = x_{clear})$. Note that this will not result in the same values as determined for other sections, since the location of the TS has been changed.

Sagging moment at end of haunch
The section with the connection of the haunch is illustrated in Figure 92. The location of the TS for the maximum sagging moment in the section with the connection of the haunch is determined by solving the ODE and analytically maximizing the moment in the relevant section plus a distance d. The moment M_{Ed} is read at a distance d from the section, in accordance with NEN-EN 1992-1-1 section 9.2.1.3, which states that the moment line must be shifted over a distance $a_l = d$ in the negative direction.
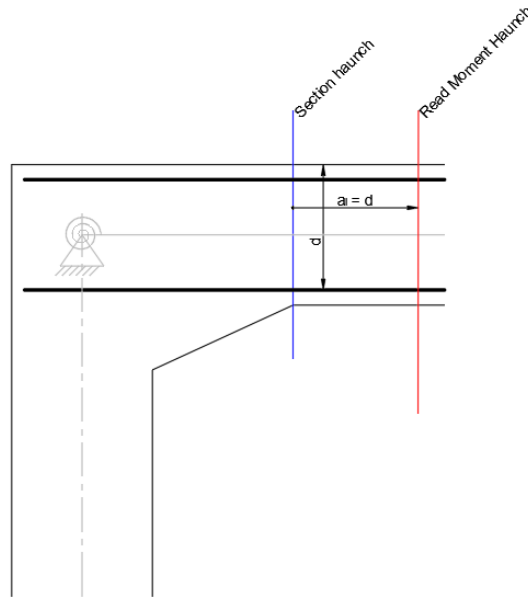
Figure 92 Illustration of section at haunch with sagging moment

Because it is not clear in advance which position is decisive both M_1 and M_2 are differentiated, to determine the distance a at which TS is located from the support shown in formulas (B.68) and (B.69) respectively, with respect to a and solving the found equation equal to zero. The equation for the slope of the moment line is defined as $\frac{\partial M_1}{\partial a}$ and $\frac{\partial M_2}{\partial a}$ respectively:

(B.68)

$$M1\_helling := EI\left(\frac{\left(-12\,Kr\,L\,a\,qTS\,Lwheelprint - 6\,Kr\,L\,qTS\,Lwheelprint^2 + 12\,Kr\,a^2\,qTS\,Lwheelprint + 12\,Kr\,a\,qTS\,Lwheelprint^2 + 4\,Kr\,qTS\,Lwheelprint^3 - 12\,EI\,L\,qTS\,Lwheelprint\right)x}{2\,L^2\,EI\,(Kr\,L + 6\,EI)}\right.$$
$$-\frac{1}{12\,EI\,L\left(Kr^2\,L^2 + 8\,EI\,Kr\,L + 12\,EI^2\right)}\left(Kr\left(12\,Kr\,L^3\,qTS\,Lwheelprint - 48\,Kr\,L^2\,a\,qTS\,Lwheelprint - 24\,Kr\,L^2\,qTS\,Lwheelprint^2 + 36\,Kr\,L\,a^2\,qTS\,Lwheelprint + 36\,Kr\,L\,a\,qTS\,Lwheelprint^2\right.\right.$$
$$\left.\left.\left. + 12\,Kr\,L\,qTS\,Lwheelprint^3 + 48\,EI\,L^2\,qTS\,Lwheelprint - 144\,EI\,L\,a\,qTS\,Lwheelprint - 72\,EI\,L\,qTS\,Lwheelprint^2 + 72\,EI\,a^2\,qTS\,Lwheelprint + 72\,EI\,a\,qTS\,Lwheelprint^2 + 24\,EI\,qTS\,Lwheelprint^3\right)\right)\right)$$

(B.69)

$$\frac{\left(2\,Kr\,L^3\,qTS - 12\,Kr\,L\,a\,qTS\,Lwheelprint - 6\,Kr\,L\,qTS\,Lwheelprint^2 + 12\,Kr\,a^2\,qTS\,Lwheelprint + 12\,Kr\,a\,qTS\,Lwheelprint^2 + 4\,Kr\,qTS\,Lwheelprint^3 + 12\,EI\,L^2\,qTS - 12\,EI\,L\,qTS\,Lwheelprint\right)x}{2\,L^2\,(Kr\,L + 6\,EI)}$$
$$-\frac{1}{12\,L\left(Kr^2\,L^2 + 8\,EI\,Kr\,L + 12\,EI^2\right)}\left(12\,Kr^2\,L^3\,a\,qTS + 12\,Kr^2\,L^3\,qTS\,Lwheelprint - 48\,Kr^2\,L^2\,a\,qTS\,Lwheelprint - 24\,Kr^2\,L^2\,qTS\,Lwheelprint^2 + 36\,Kr^2\,L\,a^2\,qTS\,Lwheelprint\right.$$
$$+ 36\,Kr^2\,L\,a\,qTS\,Lwheelprint^2 + 12\,Kr^2\,L\,qTS\,Lwheelprint^3 + 96\,EI\,Kr\,L^2\,a\,qTS + 48\,EI\,Kr\,L^2\,qTS\,Lwheelprint - 144\,EI\,Kr\,L\,a\,qTS\,Lwheelprint - 72\,EI\,Kr\,L\,qTS\,Lwheelprint^2$$
$$\left. + 72\,EI\,Kr\,a^2\,qTS\,Lwheelprint + 72\,EI\,Kr\,a\,qTS\,Lwheelprint^2 + 24\,EI\,Kr\,qTS\,Lwheelprint^3 + 144\,EI^2\,L\,a\,qTS\right)$$

The critical distance a for the sagging bending moment at the haunch is found by solving $\frac{\partial M_1}{\partial a} = 0$ and $\frac{\partial M_2}{\partial a} = 0$: $\hspace{2cm}$ (B.70)

$$\text{[complex equation — illegible at given resolution]}$$

(B.71)

$$\text{[complex equation — illegible at given resolution]}$$

In which x is defined as the distance from the support to the section with the haunch x_{haunch}:

$$x_{haunch} = \frac{h_{wall}}{2} + L_{haunch} - d$$ $\hspace{2cm}$ (B.72)

In which L_{haunch} is the length of the haunch.

The critical value between $M_1(x_{haunch})$ and $M_2(x_{haunch})$ is automatically taken into account denoted as $M_{Ed;haunch^+}$.

For the situation of the maximum hogging moment at the section at the connection with the haunch, the shear force in the clear and bending moment at midspan are also determined for verification. The distance from the support to the face of the wall x_{clear} is defined as formula (B.64).

The corresponding maximum sagging moment in the span is determined for the location of TS for the maximum sagging moment in the section at the end of the haunch $M_{Ed,haunch^+}$ and the shear force at the section in the clear $V_{Ed;clear}$ is defined as $V_1(x = x_{clear})$. Note that this will not result in the same values as determined for other sections, since the location of the TS has been changed.

Hogging moment at the face of the support (clear)
The location of the section in the clear is visualized by Figure 93. The location of the TS for the maximum moment at the section in the clear is determined by solving the ODE and analytically maximizing the moment at the location of the support. The moment M_{Ed} is read at the support because NEN-EN 1992-1-1 section 9.2.1.3 states that the moment line must be shifted over a distance $a_l = d$ in the negative direction, but this location would be out of model for most cases. Based on the available data, the probability that d_{deck} is less than half the wall thickness is so small that this assumption is accepted. Note that the extra thickness due to the haunch is only ignored for determining the section forces, for determination of the sectional resistance, described in Appendix C1, the increased effective height is taken into account.

Figure 93 Illustration of section in the clear

The distance a is determined by formula (B.65) from the previous paragraph. The difference is the x-location which is in this case defined as the location of the support:

$$x_{clear} = 0 \qquad (B.73)$$

With the critical location of the TS known the maximum hogging moment at the section at the haunch denoted as $M_{Ed;clear}$ is defined as $M_1(x = 0)$.

For the situation of the maximum hogging moment at the section in the clear, the shear force in the clear and bending moment at midspan are also determined for verification. The distance from the support to the face of the wall x_{clear} is defined as formula (B.64).

The corresponding maximum sagging moment in the span is determined for the location of TS for the maximum hogging moment in the section at the face of the supportive wall $M_{Ed,clear}$ and the shear force at the section in the clear $V_{Ed;clear}$ is defined as $V_1(x = x_{clear})$. Note that this will not result in the same values as determined for other sections, since the location of the TS has been changed.

Check of maximum shear force and reaction forces with Guyon-Massonnet load
The Guyon-Massonnet method is limited to the transverse load distribution of bending moment, making this method not applicable for the TS. Although the critical shear force is determined according to the method 7.3-7 from (CEB-fib, 2010) the shear force is still calculated according to Guyon-Massonnet for verification.

The maximum value of V_{Ed} is obtained when the TS is located as close as possible to the support, however, due to direct load transfer of local loads to the supports V_{Ed} may be reduced for loads placed close to the supports. According to NEN-EN 1992-1-1 section 6.2.2 art. (6) V_{Ed} may be reduced with a factor $\beta = a_v/2d$ for loads placed within a distance $2d$ of the support with a minimum of $\beta = 0{,}25$ for $a_v \leq 0{,}5d$.

For a simply supported beam with a span L loaded with a concentrated load F, as shown in Figure 94, the shear force at the left side of F is defined as:

$$V_{Ed} = F \cdot \frac{L - a_v}{L} \qquad (B.74)$$
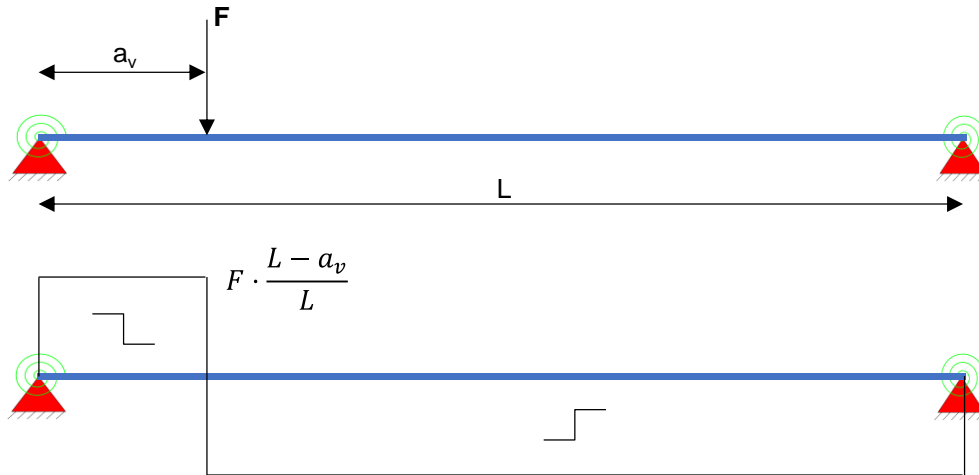
Figure 94 Example of simply supported beam loaded with concentrated load

In case the load is placed at a distance $2d$, or further, from the support, no reduction β is applicable. The shear force when the load is placed at a distance $2d$ is:

$$V_{Ed;2d} = F \cdot \frac{L-2d}{L} \tag{B.75}$$

For loads with placed within $2d$ of the support the shear force to be charged is defined as:

$$V_{Ed;\beta} = F \cdot \frac{L-a_v}{L} \cdot \beta \tag{B.76}$$

Where,

$$\beta = \frac{a_v}{2d} \qquad \text{and } 0,25 \leq \beta \leq 1 \tag{B.77}$$

The cases when locating the load within $2d$ from the support is governing is when:

$$F \cdot \frac{L-2d}{L} < F \cdot \frac{L-a_v}{L} \cdot \beta \quad \rightarrow \quad L - 2d \leq (L - a_v) \cdot \frac{a_v}{2d} \tag{B.78}$$

The inequality described in (B.78) is only valid if:

$$a_v \leq 0,5d: \quad L < 2,5d \tag{B.79}$$

$$0,5d < a_v < 2d: \quad L < a_v + 2d \tag{B.80}$$

The equations above prove that it is theoretically possible that the maximum shear force is not found when the load is paced at a distance $2d$ from the support, when the shear force is reduced by a factor β in case the load is placed within a distance $2d$ from the support. However, practically it is very unlikely that such a situation occurs due to the dimensions of the box-shaped structures. The first possible situation, described by (B.79), requires a slenderness $\frac{L}{d} < 2,5$ of the deck which is very unlikely based on the data analysis. The second situation (B.80) requires a relatively short span of $L < 2,5d$ to $L < 4d$, depending on the value of a_v. This also means that the slenderness should be smaller than 2,5 to 4, depending on the value of a_v. Even the largest span for which a load at a distance $2d$ from the support is not decisive, $L < 4d$, is very unlikely when looking at the available data. Therefore, it can be concluded that, based on NEN-EN 1992-1-1 section 6.2.2 art (6), the critical distance for the load for shear force is located at a distance $2d$ from the support.

Tests at Delft University of Technology, published in (Lantsoght, 2012), have even shown that concentrated loads can be counted with a $\beta = a_v/2{,}5d$ reduction, while distributed loads are still reduced with $\beta = a_v/2d$. Nevertheless, it was decided to place the load at a distance $2d$ in order to meet the requirements in the Eurocode.

The considered sections to check the shear force according to values calculated with load from Guyon-Massonnet method are shown in Figure 95. The shear force to be taken into account at the section in the clear is taken at a distance d from the clear of the wall, based on NEN-EN 1992-1-1 section 6.2.1 art. (8).
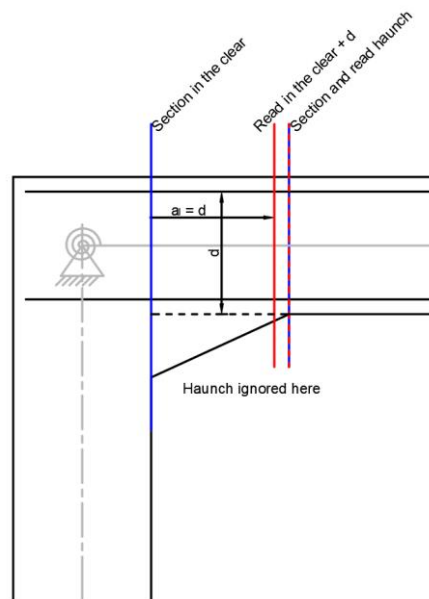
Figure 95 Illustration of sections for shear (Guyon-Massonnet)

In general, the shear force for the section at the connection with the haunch will be read from that section. In case the length of the haunch L_{haunch} is smaller than the effective height of the deck d, the shear force for the section at the haunch is read at the location for the section in the clear plus a distance d.

Because it is possible that the section to be read sometimes falls into ODE1 and the other time into ODE2, it is first checked into which ODE the section is situated.

For the section in the clear the shear force formula of ODE1 is applied if:

$$x_{clear} + d < a \tag{B.81}$$

In which,
x_{clear} is the distance from the model support to the clear of the wall;
d is the effective height of the deck, excluding the haunch;
a is the distance between the edge of q_{TS} and the model support.

If formula (B.81) is not satisfied ODE2 is applied. The shear force in the section in the clear is denoted as $V_{Ed;clear+d}$ and is defined as:

$$V_i(x = x_{clear} + d) \tag{B.82}$$

Where,

$i = 1 \; or \; 2$

For the section at the connection with the haunch the shear force formula of ODE1 is applied if:

$$x_{clear} + L_{haunch} < a \tag{B.83}$$

If formula (B.83) is not satisfied ODE2 is applied. The shear force in the section at the connection with the haunch is denoted as $V_{Ed;haunch}$ and is defined as:

$$V_i(x = x_{clear} + L_{haunch}) \tag{B.84}$$

Where,

$i = 1 \; or \; 2$

As an additional check, the moment at midspan and in the clear are determined. The bending moment at midspan is determined with $M_2\left(x = \frac{L}{2}\right)$ and the hogging moment in the clear is determined with $M_1(x = 0)$. An explanation for $x = 0$ is given earlier in this Appendix.

Verification based on support reactions
A small check of the model is performed by checking if the total load applied on the model corresponds with the sum of the reaction forces at the supports. The situation for maximum shear using the Guyon-Massonnet method is used for the check, this also gives the maximum reaction force on the supportive wall. The reaction force on the wall can be used to say something about the stiffness of the wall, the load from LM1 can be switched off.

The reaction forces in the wall under supports is determined with $V_1(x = 0)$ and $V_3(x = L)$ for the left and right support respectively. The sum of the reaction forces is denoted with $\sum R$, the sum of the applied load is denoted with $\sum E$. Naturally the difference between the applied load and the reaction forces should be zero.

Shear force – VEd

The shear force due to the distributed loads, self-weight, the weight of soil and asphalt and the UDL from LM1, is determined with the ODEs based on the Euler-Bernoulli beam theory. The Guyon-Massonnet method, used for the load distribution of LM1 for the determination of M_{Ed}, is limited to the transverse load distribution of bending moment, making this method not applicable for the TS of LM1. The shear force due to TS is determined by an additional module using the "French Method". This module is a calculation by hand and is in line with Table 3.1 from RBK, which states that the shear force must be determined manually in a model with beam elements. All the shear forces are calculated using both combination 6.10a and 6.10b, the maximum value between the two is automatically taken.

Shear force due to distributed loads
The shear force due to the distributed loads is determined with the ODEs based on the classical Euler-Bernoulli beam theory. General information about this method in this model is described in Bending Moment – MEd. This method was chosen because the occurring shear force must be determined at various sections in the beam, and this method gives a generic formula for the occurring shear force.

Determination of shear force formulas based on ODE
The sheet allows the user to select which loads must be applied in the model, if a checkbox is marked the load is naturally applied. An overview of all the loads is given with the corresponding load factor obtained from the tab loads. The load due to self-weight acts on the whole length of the deck and is denoted with

q_{SW}. The load of the weight of the soil and asphalt layers and the UDL form LM1 are summed up and denoted with q_{SAU}, in which SAU stands for soil, asphalt and UDL. q_{SAU} is not placed over the full length of the model, the reason for this is that based on NEN-EN 1992-1-1 section 6.2.2 art. (6) the shear force may be reduced when it is situated within a distance $2d$ from the support. To capture the behaviour of this model correctly, three ODEs must be drawn up. A schematic overview of the model is shown in Figure 96.
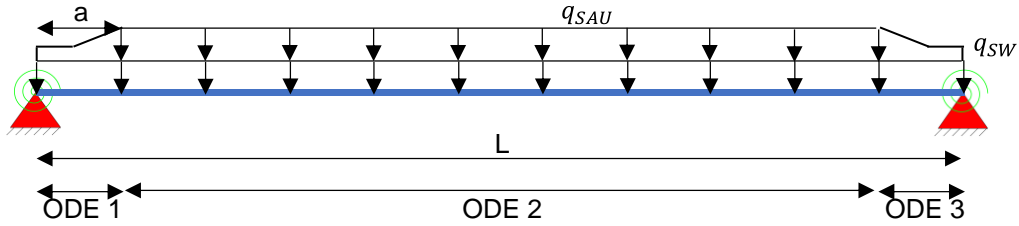
Figure 96 schematization of the model

The ODEs are:

$$ODE_1 = EI \cdot \frac{\partial^4 w_1(x)}{\partial x^4} = q_{SW} \tag{B.85}$$

$$ODE_2 = EI \cdot \frac{\partial^4 w_2(x)}{\partial x^4} = q_{SW} + q_{SAU} \tag{B.86}$$

$$ODE_3 = EI \cdot \frac{\partial^4 w_3(x)}{\partial x^4} = q_{SW} \tag{B.87}$$

The general solution to this set of ODEs is:

$$w_1(x) = \frac{qx^4}{24EI} + \frac{C1x^3}{6} + \frac{C2x^2}{2} + C3x + C4 \tag{B.88}$$

$$w_2(x) = \frac{qx^4}{24EI} + \frac{C5x^3}{6} + \frac{C6x^2}{2} + C7x + C8 \tag{B.89}$$

$$w_3(x) = \frac{qx^4}{24EI} + \frac{C9x^3}{6} + \frac{C10x^2}{2} + C11x + C12 \tag{B.90}$$

The kinematic relations are:

$$\varphi_1 = -\frac{\partial w_1}{\partial x}; \quad \kappa_1 = \frac{\partial \varphi_1}{\partial x}; \quad \varphi_2 = -\frac{\partial w_2}{\partial x}; \quad \kappa_2 = \frac{\partial \varphi_2}{\partial x}; \quad \varphi_3 = -\frac{\partial w_3}{\partial x}; \quad \kappa_3 = \frac{\partial \varphi_3}{\partial x}; \tag{B.91}$$

The constitutive relations are:

$$M_1 = \kappa_1 \cdot EI; \quad M_2 = \kappa_2 \cdot EI; \quad M_3 = \kappa_3 \cdot EI; \tag{B.92}$$

The equilibrium equations are:

$$V_1 = \frac{\partial M_1}{\partial x}; \quad V_2 = \frac{\partial M_2}{\partial x}; \quad V_3 = \frac{\partial M_3}{\partial x}; \tag{B.93}$$

The boundary conditions at the left support, $x = 0$, are:

$$eq_1: w_1 = 0; \quad eq_2: M_1 = K_r \cdot \varphi_1; \tag{B.94}$$
In which K_r is the rotational stiffness.

The matching conditions between ODE_1 and ODE_2 at $x = a$ are:

$$eq_3: w_1 = w_2; \quad eq_4: \varphi_1 = \varphi_2; \quad eq_5: M_1 = M_2; \quad eq_6; V_1 = V_2 \tag{B.95}$$

The matching conditions between ODE_2 and ODE_3 at $x = L - a$ are:

$$eq_7: w_2 = w_3; \quad eq_8: \varphi_2 = \varphi_3; \quad eq_9: M_2 = M_3; \quad eq_{10}; V_2 = V_3 \tag{B.96}$$

The boundary conditions at the right support, $x = L$, are:

$$eq_{11}: w_3 = 0; \quad eq_{12}: M_3 = -K_r \cdot \varphi_3; \tag{B.97}$$
In which K_r is the rotational stiffness.

The solution for the integration constants $C1$ to $C12$ can be found with the equations for the boundary and matching conditions eq_1 to eq_{12}.

Since everything is scripted in MAPLE, the shear force at a certain value of x can simply be asked for. Which section force, like V_1, V_2 or V_3, to be requested depends on which ODE the section is located. The formulas obtained with MAPLE for the section forces are rather long but completely parametric. These formulas are exported to Excel and linked to the correct cells. The resulting section forces are checked for a simple situation by a calculation by hand and for the more complex situation verified with SOFiSTiK FEA software.

Two sections have been chosen to check the shear capacity, the first section is in the clear of the wall. The second section is located in the connection of the haunch, which has a lower shear capacity than in the section in the clear of the wall. Because calculations are made with a so-called oblique section, the various load cases are read at other x-coordinates.

Shear crack angle
The angle of the shear force crack is determined according to NEN 8702 section 6.2, which states that for the determination of V_{Rd}, the angle (as defined in NEN-EN 1992-1-1) must be taken equal to the slope of the compressive strut, where:

- $\theta = 45°$ for elements with $\sigma_{cp} = 0\ MPa$;
- $\theta = 30°$ for elements with $\sigma_{cp} = 5\ MPa$;

In which,
σ_{cp} according to Appendix C1 formula C9.

Values of σ_{cp} between $0\ MPa$ and $5\ MPa$ are interpolated linearly to determine θ.

Section at the end of the haunch
overview of the section is shown in Figure 97.
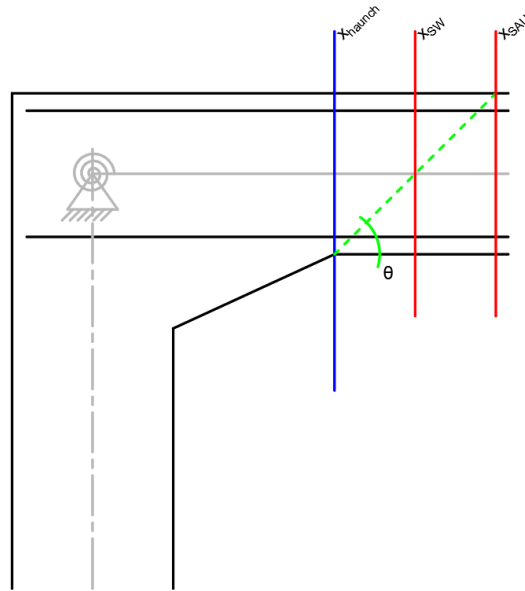
Figure 97 Overview section at the connection with the haunch

Since the uniform load due to self-weight, which engages in the neutral line of the deck, is constant over the full length of the model beam, the shear force formula is easy to determine and does not depend on which ODE the section is taken:

$$V_{Ed;SW} = q_{SW} \cdot \frac{L}{2} - x_{SW} \cdot q_{SW} \tag{B.98}$$

Where,

$$x_{SW} = x_{haunch} + 0.5h/\tan(\theta) \tag{B.99}$$

For the shear force due to soil, asphalt and UDL load which is denoted as $V_{Ed;SAU}$ and engages on top of the deck, the distance of the section x_{SAU} must be determined first in order to choose for the shear force equation of $ODE1$ or $ODE2$.

$$x_{SAU} = x_{haunch} + h/\tan(\theta) \tag{B.100}$$

The shear force equation of $ODE1$ is taken in case:

$$x_{SAU} \leq a \tag{B.101}$$

Where,

$$a = 2d + 0.5h_{wall} - 0.5h_{deck} \tag{B.102}$$

Otherwise the shear force equation of $ODE2$ is taken.
The shear force equation, due to soil, asphalt and UDL load, of $ODE1$ is denoted with $V_{SAU;1}(x)$ and is defined as:

$$\frac{\left(2\,Kr\,L^3 - 2\,Kr\,L\,LqGAV^2 - 6\,Kr\,L\,LqGAV\,a - 6\,Kr\,L\,a^2 + Kr\,LqGAV^3 + 4\,Kr\,LqGAV^2\,a + 6\,Kr\,LqGAV\,a^2 + 4\,Kr\,a^3 + 12\,EIL^2 - 6\,EIL\,LqGAV - 12\,EIL\,a\right)\,LqGAV\,qSAU}{2\,L^2\,(Kr\,L + 6\,EI)}$$

The shear force equation, due to soil, asphalt and UDL load, of $ODE2$ is denoted with $V_{SAU;2}(x)$ and is defined as:

$$EI\left(-\frac{qSAUx}{EI} + \frac{1}{2\,L^2\,(Kr\,L + 6\,EI)\,EI}\left(qSAU\left(2\,Kr\,L^3\,LqGAV + 2\,Kr\,L^3\,a - 2\,Kr\,L\,LqGAV^3 - 6\,Kr\,L\,LqGAV^2\,a - 6\,Kr\,L\,LqGAV\,a^2 + Kr\,LqGAV^4 + 4\,Kr\,LqGAV^3\,a + 6\,Kr\,LqGAV^2\,a^2\right.\right.\right.$$
$$\left.\left.\left. + 4\,Kr\,LqGAV\,a^3 + 12\,EIL^2\,LqGAV + 12\,EIL^2\,a - 6\,EILqGAV^2\,L - 12\,EILqGAV\,aL\right)\right)\right)$$

The total shear force due to distributed loads in the section with the connection with the haunch is denoted with $V_{Ed;haunch}$ and is defined as:

$$V_{Ed;haunch} = V_{Ed;SW} + V_{Ed;SAU} \tag{B.103}$$

Section at the face of the wall (clear)
An overview of the section is shown in Figure 98.
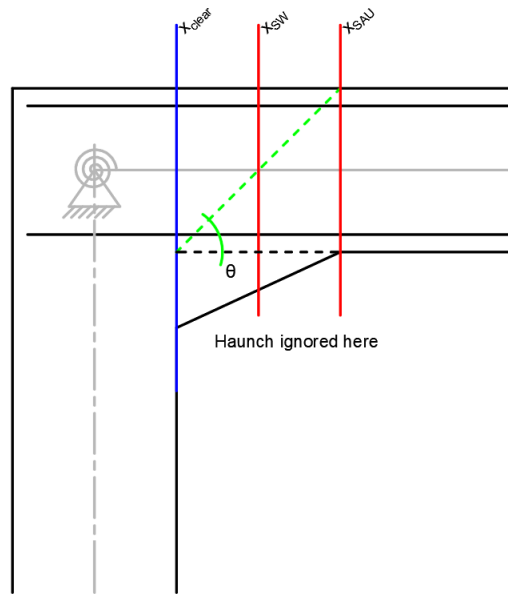
Figure 98 Overview section in the clear of the wall

Since the uniform load due to self-weight, which engages in the neutral line of the deck, is constant over the full length of the model beam, the shear force formula is easy to determine and does not depend on which ODE the section is taken:

$$V_{Ed;SW} = q_{SW} \cdot \frac{L}{2} - x_{SW} \cdot q_{SW} \tag{B.104}$$

Where,

$$x_{SW} = x_{clear} + 0{,}5h/\tan(\theta) \tag{B.105}$$

For the shear force due to soil, asphalt and UDL load which is denoted as $V_{Ed;SAU}$ and engages on top of the deck, the distance of the section x_{SAU} must be determined first in order to choose for the shear force equation of $ODE1$ or $ODE2$.

$$x_{SAU} = x_{clear} + h/\tan(\theta) \tag{B.106}$$

The shear force equation of $ODE1$ is taken in case:

$$x_{SAU} \leq a \tag{B.107}$$

Where,

$$a = 2d + 0{,}5h_{wall} - 0{,}5h_{deck} \tag{B.108}$$

Otherwise the shear force equation of $ODE2$ is taken.

The shear force equation, due to soil, asphalt and UDL load, of $ODE1$ is denoted with $V_{SAU;1}(x)$ and is defined as:

$$\frac{\left(2\,Kr\,L^3 - 2\,Kr\,L\,LqGAV^2 - 6\,Kr\,L\,LqGAV\,a - 6\,Kr\,L\,a^2 + Kr\,LqGAV^3 + 4\,Kr\,LqGAV^2\,a + 6\,Kr\,LqGAV\,a^2 + 4\,Kr\,a^3 + 12\,EI\,L^2 - 6\,EI\,L\,LqGAV - 12\,EI\,L\,a\right)LqGAV\,qSAU}{2\,L^2\,(Kr\,L + 6\,EI)}$$

The shear force equation, due to soil, asphalt and UDL load, of $ODE2$ is denoted with $V_{SAU;2}(x)$ and is defined as:

$$EI\left(-\frac{qSAU\,x}{EI} + \frac{1}{2\,L^2\,(Kr\,L + 6\,EI)\,EI}\left(qSAU\left(2\,Kr\,L^3\,LqGAV + 2\,Kr\,L^3\,a - 2\,Kr\,L\,LqGAV^3 - 6\,Kr\,L\,LqGAV^2\,a - 6\,Kr\,L\,LqGAV\,a^2 + Kr\,LqGAV^4 + 4\,Kr\,LqGAV^3\,a + 6\,Kr\,LqGAV^2\,a^2\right.\right.\right.$$
$$\left.\left.\left. + 4\,Kr\,LqGAV\,a^3 + 12\,EI\,L^2\,LqGAV + 12\,EI\,L^2\,a - 6\,EI\,LqGAV^2\,L - 12\,EI\,LqGAV\,a\,L\right)\right)\right)$$

The total shear force due to distributed loads in the section with the connection with the haunch is denoted with $V_{Ed;clear}$ and is defined as:

$$V_{Ed;clear} = V_{Ed;SW} + V_{Ed;SAU} \tag{B.109}$$

Shear force due to TS with method 7.3-7 from CEB-fib Model Code 2010

The shear force as a result of TS from LM1 is calculated based on the "French Method", whereby the distribution of the shear force per tandem system is worked out graphically. Different embodiments of this method can be found in different publications, among which the method is described in (Lantsoght, 2012) and (CEB-fib, 2010). In the first mentioned publication, the load is placed at a distance $2{,}5d$ from the support and spread to the heart of the support, while in the latter publication the load is placed at a distance $2d$, which matches with the reduction factor β up to $2d$, and the load is distributed to a control section some distance away from the support. Calculations, comparing the different calculated shear force values due to TS, have shown that the method described in (CEB-fib, 2010) results in somewhat more conservative values. To ensure that the calculation is not too optimistic, the method as in (CEB-fib, 2010) is used in the rest of this study. The method used is shown in Figure 31 a) and c).
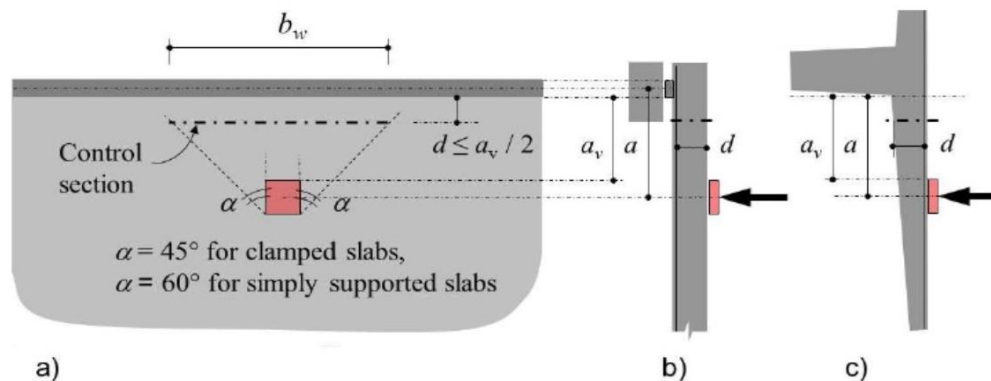
Figure 7.3-7: *Location and length of the control section, bw, for the determination of the shear resistance of slabs with point loads located near a support-line; (b) simple edge support; (c) clamped edge support*

Figure 99 Method used as "French Method" from CEB-fib Model Code 2010 Figure 7.3-7

Overlapping of the effective widths b_w of two wheel prints of a single axle is considered as in (CEB-fib, 2010), which describes that in case b_w of two wheel prints from a single axle overlap each other at the control section the load and effective width may be merged and distributed evenly over the combined b_w. This is further elaborated in the next section and graphically displayed in Figure 32.

The load distribution of TS according to the "French Method" is elaborated in a separate spreadsheet, '*Dwarskracht TS Franse Methode V0.xlsm*', and is called up via a script, filled in and exported to the calculation sheet. It has been decided to work this out in a separate module so that this method can also be used for other bridges with a concrete bridge deck. First, the background of this external module is described, then it is explained how the link was made.

Model info

For this calculation the geometry of the bridge deck, properties of the soil layer, properties of the asphalt layer, partial load factor for LM1, the edge distances at the left and right and the number of heavy trucks is required. An overview of the input parameters is given in Table 50.

Input parameter	Symbol	Explanation
Span length	L	The span length of the deck from support to support.
Deck width	b_{deck}	The width of the concrete deck structure. In case of a joint, the width of the element or section should be taken, because it is assumed that load spread does not continue through the joint.
Deck thickness	h_{deck}	The average thickness of the concrete deck.
Model width	b_{model}	The width of the modelled section, as standard this is 1,0 m.
Thickness soil layer	h_{soil}	The combined thickness of all soil layers above the concrete deck.

Spread angle	φ	The angle under which a load is transferred from the top of the layer to the bottom. In accordance with NEN-EN 1991-2 art. 4.3.6 (2) the spread angle for asphalt is 45°. For soil an angle of 30° is recommended and therefore set as standard.
Thickness asphalt layer	$h_{asphalt}$	The combined thickness of all asphalt layers on top of the concrete deck.
Angle of in-plane load distribution	α	The angle of load distribution in the horizontal plane of the concrete, as standard 45° in accordance with FIB model code 2010 fig. 7.3-7. By narrowing the angle, the effective width becomes smaller and thus the maximum shear force in the observed strip increases. In case the bridge deck is not monolithic connected to the walls, as is the case with a sheet pile, it is recommended to use $\alpha = 60°$.
Partial load factor	γ_Q	Safety factor for load of tandem system from load model 1 of NEN-EN 1991-2.
Edge distance left	$Edge_L$	The distance at the left side between the edge of the concrete bridge deck and the edge of a loaded lane or remaining area.
Edge distance right	$Edge_R$	The distance at the right side between the edge of the concrete bridge deck and the edge of a loaded lane or remaining area.
Number of heavy trucks	N_{obs}	The number of heavy trucks per year per lane. If unknown, 2.000.000 must be entered.

Table 50 Overview of input parameters of module "Method 7.3-7 CEB-fib model code 2010"

The lane layout and the load TS to be charged are determined as described in earlier in this Appendix.

Load distribution cases

In contrast to the bending moment, TS for shear is spread only to the top of the concrete deck. The spreading width from the edge of the wheel is denoted as s, shown in Figure 100, and is calculated as:

$$s = h_{asphalt} \cdot \sin(\varphi_{asphalt}) + h_{soil} \cdot \sin(\varphi_{soil}) \tag{B.110}$$

Where,

$$\varphi_{asphalt} = 45° \qquad \text{(NEN-EN 1991-2 art. 4.3.6 (2))}$$

φ_{soil} is the spread angle for soil, standard set to $\varphi_{soil} = 30°$
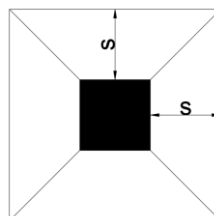
Figure 100 Display of distance s

With the distribution distance s increasing the wheel prints may overlap, in driving direction or in both directions. This is checked by calculating the space between the wheel prints, in case a negative value is calculated the prints overlap each other. This can be checked with:

$$L_{Ts} - L_{wheel} - 2 \cdot s < 0 \qquad\qquad\qquad\qquad (B.111)$$

Where,

$$L_{TS} = 1,2\ m; \quad L_{wheel} = 0,4\ m$$

And:

$$b_{TS} - b_{wheel} - 2 \cdot s < 0 \qquad\qquad\qquad\qquad (B.112)$$

Where,

$$b_{TS} = 2,0\ m; \quad b_{wheel} = 0,4\ m$$

Formula (B.111) checks for overlap in driving direction, formula (B.112) checks for overlap in the width of the TS. Because s spreads equally in both directions, only an overlap in width direction cannot occur because $b_{TS} - b_{wheel} = 1,6\ m$ and $L_{TS} - L_{wheel} = 0,8\ m$.

It is then necessary to check whether overlap of b_{eff} from wheels on one axle occurs, in the event that they overlap, the wheel prints and effective width are merged as shown in Figure 32.
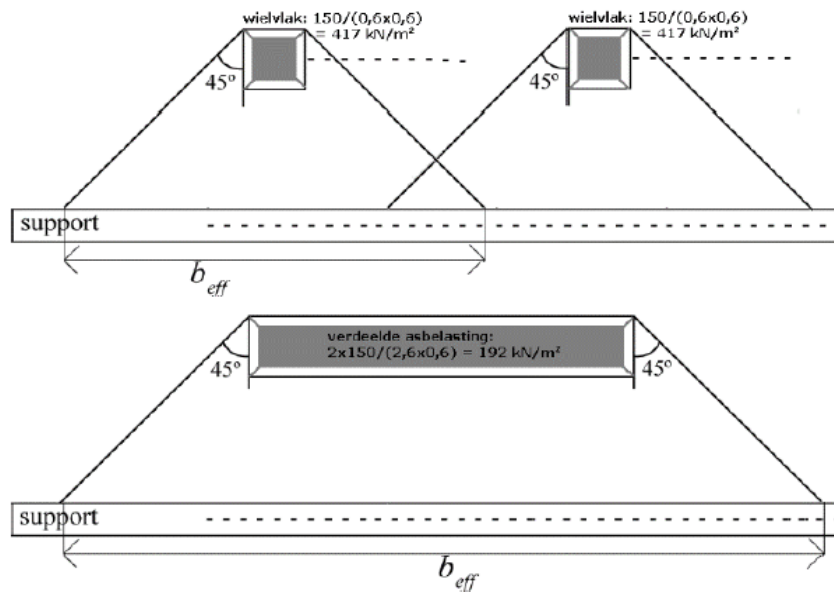
Figure 101 Overlap of beff from wheels on one axle

In the event that the distance between the wheel prints after spreading to the top of the concrete deck is less than the effective spreading width b_{eff} of one wheel load, the effective widths of the wheels of one axle overlap and both load and effective width may be joined as shown in Figure 32. In formula:

$$b_{TS} - b_{wheel} - 2 \cdot s < \left(\left(2d + L_{wheelprint}\right) \cdot \tan(\alpha) \right) \cdot 2 \qquad\qquad (B.113)$$

Where,

d is estimated with $d = 0,9 \cdot h$;

$2d$ is the distance within which no load will be placed, because within a distance $2d$ from the support the load may be reduced by a factor β;

$L_{wheelprint}$ is the length, driving direction, of the wheel print depending on whether there is overlap between the first and second axle or not;

α is the assumed angle of the load distribution in the horizontal plane.

In total, four situations are conceivable based on formulas (B.111), (B.112) and (B.113) for overlap of wheel print in length, overlap of wheel print in width and overlap of effective width respectively:

Case	Overlap $L_{wheelprint}$ (x.xx)	Overlap $b_{wheelprint}$ (x.xx)	Overlap of effective width (x.xx)
Case I	✖	✖	✖
Case II	✖	✖	✔
Case III	✔	✖	✔
Case IV	✔	✔	✔

Table 51 Overview of different load distribution cases

In addition to Cases I to IV based on vertical load distribution, a further distinction is made between two load cases, namely load case "middle" and load case "edge". In load case middle, the TSs are placed in such a way that a maximum is created between lane 1 and lane 2, in "the middle" of the plate. In load case edge, the TSs are placed in such a way that a maximum is created at the edge.

Case I
Not overlapping b_{eff} of wheel prints of one axle is rare and is therefore not (yet) elaborated. A worked-out example to support this:

$$h_{deck;min} = 300\ mm \rightarrow d = 270\ mm$$

$$h_{soil} = 0\ mm; \quad h_{asphalt} = 120\ mm \qquad \text{(Minimum according to ROK)}$$

$$\theta = 30°$$

In the data analysis, Appendix A3, a minimum deck thickness of $300\ mm$ is found and therefore it is unlikely that much thinner decks occur. According to ROK the minimum asphalt thickness on a bridge deck should be $120\ mm$. The small angle of the assumed load distribution in horizontal plane $\theta = 30°$ results in less load distribution. But for this theoretical lower bound there is still an overlap of b_{eff} of the two wheels from one axle.

It can be questioned whether there is as much as $120\ mm$ asphalt on structures of local authorities. For a deck thickness of $300\ mm$, the minimum asphalt thickness for which overlap still takes place is $85\ mm$. Since the occurrence of a structure with a thinner deck or even less asphalt is small, this situation is not addressed at this stage of the investigation.

The outcome of this calculation, which concludes that Case I hardly occurs in practice, is confirmed by the same statement in (Lantsoght, 2012).

Case II – Middle
In load distribution Case II-Middle:

- Load spread from asphalt to top of concrete deck in width direction **does not** overlap;
- Load spread from asphalt to top of concrete deck in length direction **does not** overlap;
- Spread of wheel prints to support of one axle **do** overlap;
- Width of the overlap strip is $4d$.

Load distribution takes place from the back of the wheel prints since this situation corresponds to the situation as described in both (Lantsoght, 2012) and (CEB-fib, 2010). An example situation of Case II-Middle is presented in Figure 102.

	Tandemstel 1		Tandemstel 2		Tandemstel 3	
Effectieve breedte 1^e as	**4.71**	m	**5.42**	m	**8.37**	m
Effectieve breedte 2^e as	**5.91**	m	**7.82**	m	**8.37**	m
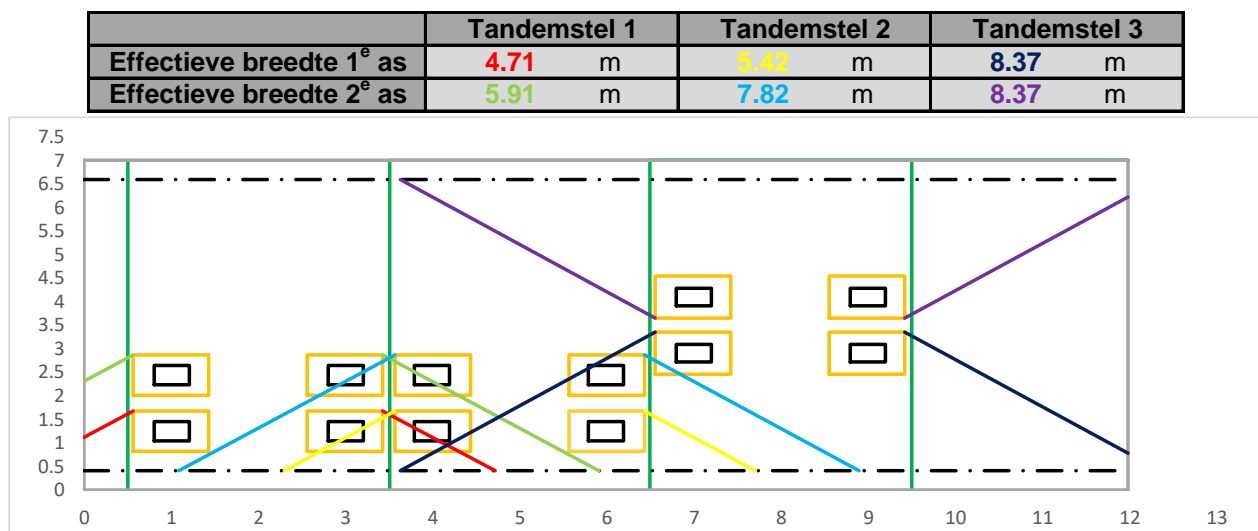
Figure 102 Example situation of Case II-Middle (overlap TS3 1,08m < 1,62m (4d) in relation with short span)

Case III – Middle
In load distribution Case III-Middle:

- Load spread from asphalt to top of concrete deck in width direction **does not** overlap;
- Load spread from asphalt to top of concrete deck in length direction **does** overlap;
- Spread of wheel prints to support of one axle **do** overlap;
- Width of the overlap strip is $4d$.

Load distribution takes place from the back of the wheel prints, where the print of the first axle ends in the middle of the two axles. An example situation of Case III-Middle is presented in Figure 103.

	Tandemstel 1		Tandemstel 2		Tandemstel 3	
Effectieve breedte 1^e as	5.22	m	6.44	m	8.40	m
Effectieve breedte 2^e as	6.43	m	8.86	m	9.01	m
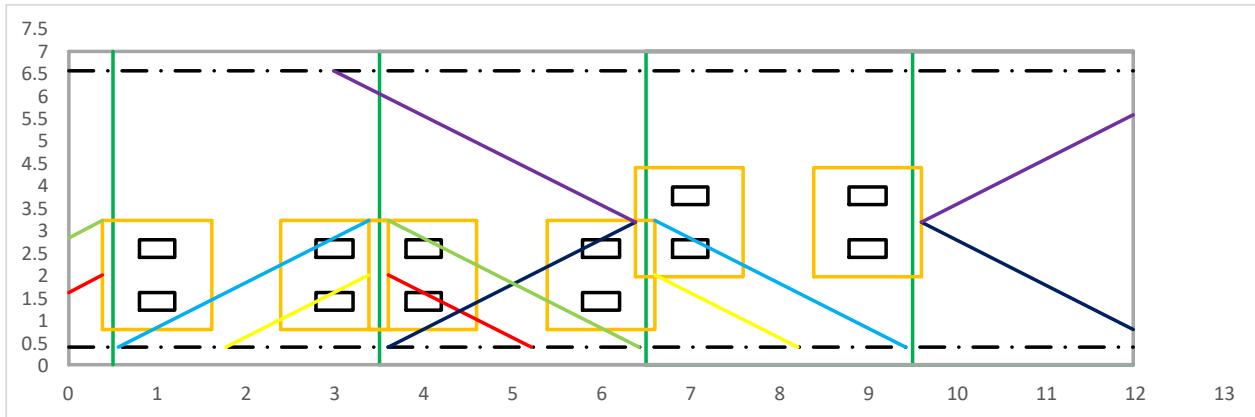
Figure 103 Example situation of Case III-Middle (overlap strip width of 4d)

Case IV – Middle

In load distribution Case IV-Middle:

- Load spread from asphalt to top of concrete deck in width direction **does** overlap;
- Load spread from asphalt to top of concrete deck in length direction **does** overlap;
- Spread of wheel prints to support of one axle **do** overlap;
- Width of the overlap strip is $4d$.

Load distribution takes place from the back of the wheel prints, where the print of the first axle ends in the middle of the two axles. An example situation of Case IV-Middle is presented in Figure 104.

	Tandemstel 1		Tandemstel 2		Tandemstel 3	
Effectieve breedte 1^e as	6.03	m	8.06	m	8.03	m
Effectieve breedte 2^e as	7.64	m	10.64	m	9.64	m
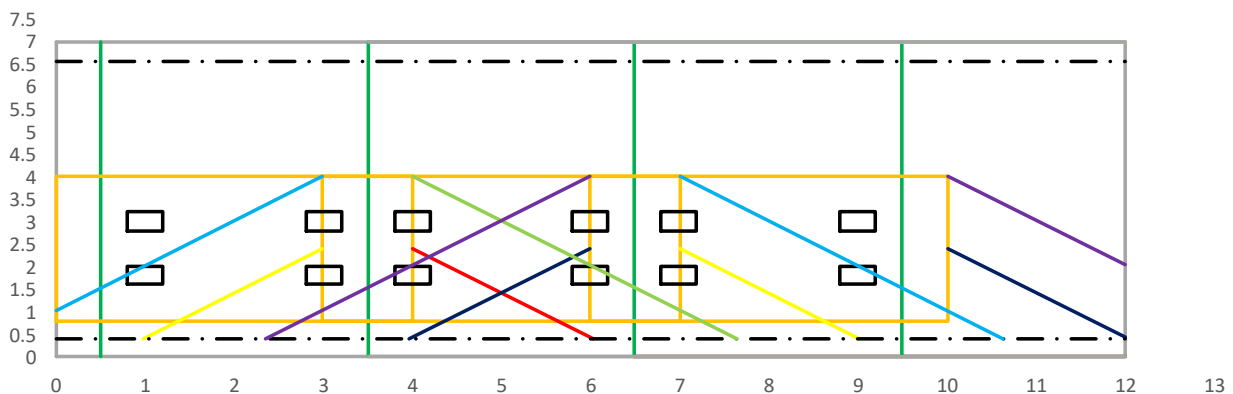
Figure 104 Example situation of Case IV-Middle (TS3 placed at 2d from face of support)

Determination of V_{TS} for load case Middle

In Figure 102 to Figure 104 the dash-dot-dash line represents the control section and is situated at a distance d from the clear of the wall. The tandem system(s) are placed from the left to the right, depending on the number of theoretical lanes n_l one, two or three TS are placed. The edges of the lanes are represented by the green lines, where lane 1 is at the far left and counting continues to the right. TS1 is placed on the edge

to ensure minimal load distribution for this heaviest TS, since the load of a TS is distributed evenly over b_w. The tandem systems are automatically placed in such a way that an overlap with a minimum of $4d$ is created between all the effective widths, resulting in the maximum load averaged over $4d$. But note that the load is not placed within $2d$ from the face of the wall since loads may be reduced with a factor β when they do. As standard the width of the overlapping strip, represented in figures by the distance between the red and dark blue line in lane 2, is $b_{overlap} = 4d$. The width of $4d$ of the overlap strip corresponds to RBK requirement 6.2.1 (10) that the calculation value of the shear force V_{Ed} must be determined by averaging over a width of $4d$ when calculating slabs using 2D slab modeling. An increase in the vertical load distribution or placing TS1 further from the control section by an increase in the effective height d of the deck provides a larger effective width b_w of TS1. As a result, TS2 and TS3 may need to be moved further away from the control section to create an overlap of $4d$. However, this shift of TS stops when the centre of TS is halfway through the span because then the maximum distribution of that TS has been reached, recognizable by the "envelope" that arises as shown by TS3 in the figures above. The load distribution in plane of the slab takes place by bending, if TS were to be placed further it would be closer to the other support point, resulting in a smaller effective width b_w. This means that the overlap strip can be smaller than $4d$ due to a limited span length. This is typical for culverts and underpasses, but for normal bridges with relatively larger spans this does not occur.

The edge distances left $Edge_L$ and right $Edge_R$ can be entered separately, the minimum distance is used to place TS1. The other edge distance is important if it is not possible to drive near the edge of the deck, but load distribution does take place. The edge distance on the left determines the distance lane 1 from the edge is placed. The edge distance on the right determines whether lane 2 or lane 3 still fits or what width of lane 1 should be taken.

In the case of a large soil cover, it may happen that the TS load is distributed so much vertically that part of the load does not end up on the bridge deck, in that case only the part of the load that ends up on the deck is included.

With the tandem systems in place the shear force in the critical strip for load case Middle is calculated. Each TS has two effective widths, denoted with $b_{eff;ij}$ where i stands for the number of TS and j stands for the axle number. The shear force due to one single axle is calculated according to:

$$V_{Ek;TSi;j} = \frac{Q_{k;i} \cdot \alpha_{Q1}}{b_{eff;ij}} \cdot \frac{b_{overlap}}{b_w} \cdot \left(\frac{L_{span} - L_{ij}}{L_{span}}\right) \tag{B.114}$$

In which,
$\frac{b_{overlap}}{b_w}$ is the proportion of the overlap with regard to the effective width ($b_w = 4d$);
L_{ij} is the distance from the support to the back of axle j of TS i.
The shear force due to TSi is described as:

$$V_{Ek;TSi} = V_{Ek;TSi;1} + V_{Ek;TSi;2} \tag{B.115}$$

The characteristic value of shear force in the critical strip with width b_w is denoted with $V_{Ek;TS}$ and defined as:

$$V_{Ek;TS} = \sum_i V_{Ek;TSi} \tag{B.116}$$

The shear force to be taken into account based on an averaged value over a width of $b_w = 4d$ is:

$$V_{Ed;TS} = \gamma_Q \cdot V_{Ek;TS} \tag{B.117}$$

In which,

γ_Q is the partial load factor for traffic of LM1 including correction factors.

Case II – Edge

In load distribution Case II-Edge:

- Load spread from asphalt to top of concrete deck in width direction **does not** overlap;
- Load spread from asphalt to top of concrete deck in length direction **does not** overlap;
- Spread of wheel prints to support of one axle **do** overlap;
- Width of the overlap strip is $2d$.

Load distribution takes place from the back of the wheel prints since this situation corresponds to the situation as described in both (Lantsoght, 2012) and (CEB-fib, 2010). An example situation of Case II-Edge is presented in Figure 105.

	Tandemstel 1		Tandemstel 2		Tandemstel 3	
Effectieve breedte 1^e as	4.71	m	10.00	m	12.00	m
Effectieve breedte 2^e as	5.91	m	11.20	m	12.00	m
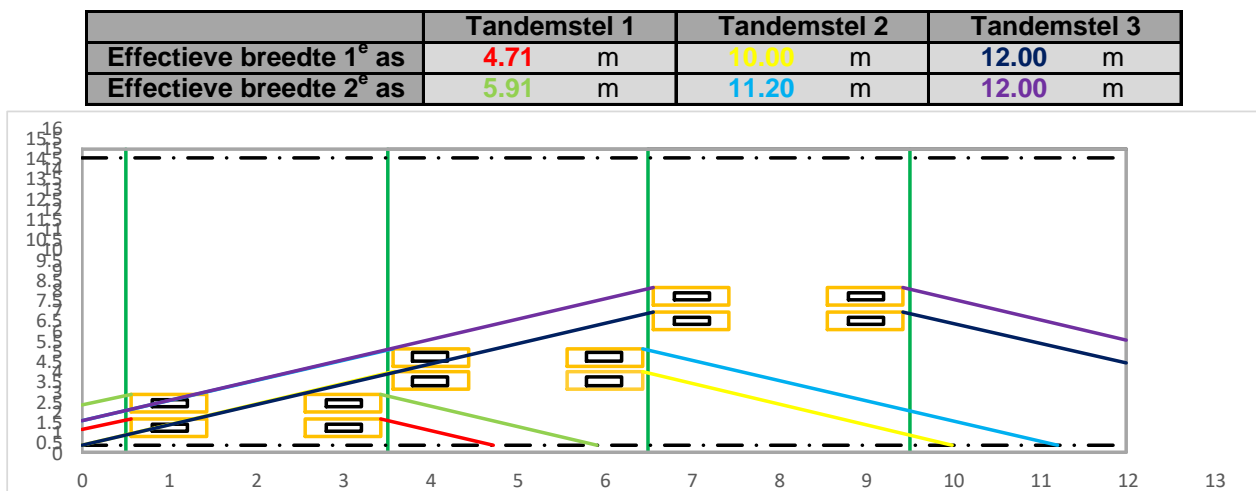
Figure 105 Example situation of Case II-Edge (with of overlap strip 2d taken from edge x=0)

Case III – Edge

In load distribution Case III-Middle:

- Load spread from asphalt to top of concrete deck in width direction **does not** overlap;
- Load spread from asphalt to top of concrete deck in length direction **does** overlap;
- Spread of wheel prints to support of one axle **do** overlap;
- Width of the overlap strip is $2d$.

Load distribution takes place from the back of the wheel prints, where the print of the first axle ends in the middle of the two axles. An example situation of Case III-Edge is presented in Figure 106.

	Tandemstel 1		Tandemstel 2		Tandemstel 3	
Effectieve breedte 1^e as	5.22	m	10.00	m	10.20	m
Effectieve breedte 2^e as	6.43	m	11.21	m	10.20	m
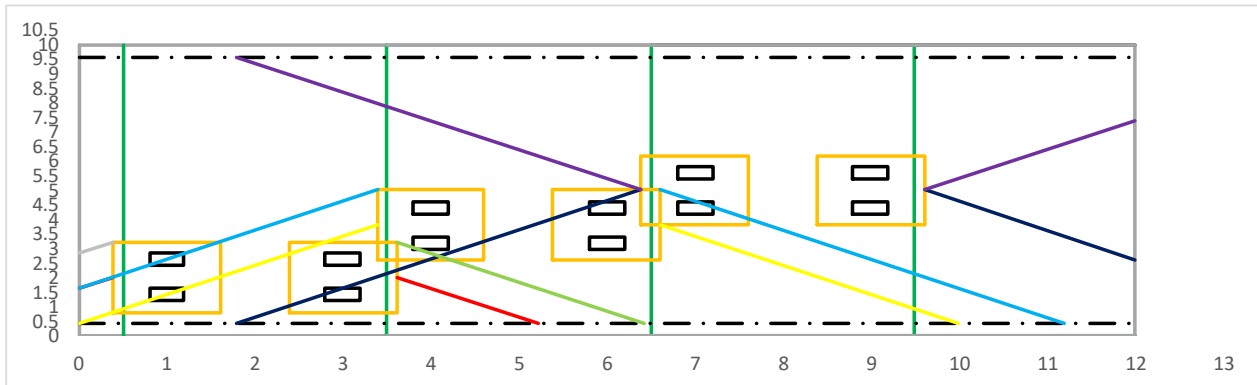
Figure 106 Example situation of Case III-Edge (No overlap with TS3 due to short span)

Case IV – Edge

In load distribution Case IV-Edge:

- Load spread from asphalt to top of concrete deck in width direction **does** overlap;
- Load spread from asphalt to top of concrete deck in length direction **does** overlap;
- Spread of wheel prints to support of one axle **do** overlap;
- Width of the overlap strip is $2d$.

Load distribution takes place from the back of the wheel prints, where the print of the first axle ends in the middle of the two axles. An example situation of Case IV-Middle is presented in Figure 107.

	Tandemstel 1		Tandemstel 2		Tandemstel 3	
Effectieve breedte 1^e as	**6.03**	m	**10.00**	m	**9.11**	m
Effectieve breedte 2^e as	**7.64**	m	**10.22**	m	**9.11**	m
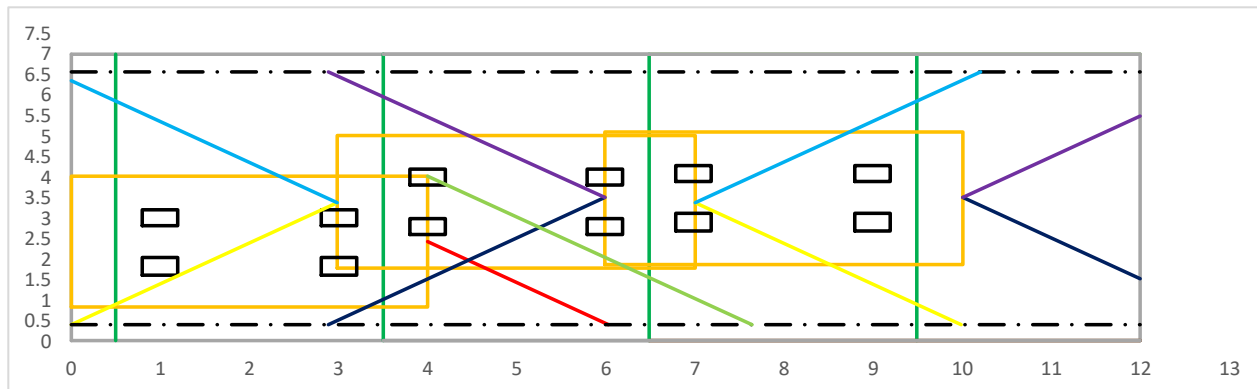
Figure 107 Example situation of Case IV-Edge (No overlap with TS3 due to short span)

Determination of V_{TS} for load cases Edge

The determination of the shear force as a result of TS for the load case where the TSs are placed in such a way that a maximum is created at the edge of the plate, named load case Edge, is largely in accordance with the determination of V_{TS} for load case Middle. The changes are:

- TSs are placed so that distribution to $x = 0$ (left lower corner in the figures) takes place, unless this is impossible due to limited bridge length.
- Width of the overlap strip reduced to $2d$, placed from the edge of the slab ($x = 0$) inwards;

Note that for underpasses and culverts with a relatively short span load case Edge does not result in the governing load case because TS3, and in some cases also TS2, cannot contribute to the shear force in the considered strip due to limited span.

For the determination of V_{TS} for load case Edge, reference is made to the determination of V_{TS} for load case Middle.

Export data to analytical model module
The steps involved within the script to export the data to the calculation sheet are:

- Clear the current data in the calculation sheet;
- Open the module *'Dwarskracht TS Franse Methode V0.3.xlsm'*;
  - As long as the main calculation sheet and the sub modules in the map *'Modules'* are saved at the same location and their names are unchanged, the user is allowed to choose a location on their computer or server to store these files.
- The input cells from the module "French Method" are linked with the corresponding data from the main calculation file;
- Based on the load distribution case the tandem systems are placed and the shear forces calculated;
- The output data will be exported from the external module to the main calculation sheet;
- The layout of the main calculation sheet is adjusted to the data obtained from the external module;
- The external module will be saved and closed;

In Figure 108 and Figure 109 an example of the output is shown.

Project	XX9999	-	Duiker Molentocht		
Omschrijving	Validatieberekening				
Status	SO				
Versie	0.2				
Opgezet door	D.Jilissen			Datum	7-12-2020
Gecontroleerd	V.Achternaam			Datum	dd-mm-yyyy

Royal HaskoningDHV
Enhancing Society Together

DWARSKRACHT T.G.V. TANDEMSTEL
Gebaseerd op fib model code 2010 7.3-7

MODEL INFO

Dagmaat brugdek	L	7 m
Breedte dek	b_{dek}	12 m
Dekdikte	h_{dek}	0.45 m
Model breedte	b_{model}	1.0 m
Dikte grondlaag	h_{grond}	0.2 m
Spreidingshoek grond		30 °
Dikte asfasltlaag	h_{asfalt}	0.120 m
Spreidingshoek asfalt		45 °
Hoek spreiding in het vlak	45 ° → tan(45)	1.00 -
Partiële belasting factor	$\gamma_{Q;6.10a}$ 0.947 $\gamma_{Q;6.10b}$	1.18 -

Rijstrook indeling   -   Werkelijk

Randafstand links	$Rand_L$	0.50 m
Randafstand rechts	$Rand_R$	0.50 m
Breedte rijweg	w	11 m
Aantal theoretische rijstroken	n_l	3 rijstroken
Breedte van een theoretische rijstrook	w_l	3 m
Breedte van het resterende oppervlak		2 m
Aantal vrachtwagens per jaar per rijstrook	N_{obs}	125000 stuks

LM1 - Tandemstel
Plaatsing tandemstel centrisch in rijstroken

Breedte TS	b_{TS}	2 m
Lengte TS	L_{TS}	1.2 m
Wielprent breedte	b_{wiel}	0.4 m
Wielprent lengte	L_{wiel}	0.4 m

	Aslast Q_k [kN]	Correctiefactor α_{Q1}	$Q_k * \alpha_{Q1}$ [kN]
Rijstrook 1	300	0.962	289
Rijstrook 2	200	0.962	192
Rijstrook 3	100	0.962	96
Overige stroken	0	0.962	0

	asfalt + grond		
Asfalt naar bovenkant betondek	s = 0.120 + 0.115	s	0.235 m

Overlapping breedte richting: 1.129 > 0 dus geen overlap van assen in breedte richting
Overlapping lengte richting: 0.329 > 0 dus geen overlap van assen in lengte richting

Wielprint breedte op bovenkant betondek	$b_{wielprint}$	0.871 m
Wielprint lengte op bovenkant betondek	$L_{wielprint}$	0.871 m
Aantal overlappende wielen per prent		1 stuks
Oppervlakte per wielprent		0.76 m²

Controle op overlap van b_{eff} van wielen van één as

Afstand tussen wielen na spreiding tot bovenkant betondek	1.13 m
Spreiding vanaf achterkant wiellast (binnen 2d geen belasting)	2.55 m

Omdat 1.13 < 2.55 overlappen de wielen van een as elkaar.

Belasting: Geval II

Figure 108 Example output of module 7.3-7 CEB-fib model code 2010 – Part I

PLAATSEN TANDEMSTELSELS - GEVAL II - MIDDEN

Lastspreiding van asfalt naar bovenkant betondek breedte overlapt niet
Lastspreiding van asfalt naar bovenkant betondek lengte overlapt niet
Spreiding wielprinten naar support van een as overlappen wel

Spreiding vanaf achterkant wielprint per as

	Tandemstel 1		Tandemstel 2		Tandemstel 3	
Effectieve breedte 1^e as	4.71	m	5.42	m	8.37	m
Effectieve breedte 2^e as	5.91	m	7.82	m	8.37	m

Visualisatie effectieve breedtes per as per tandemstel

DWARSKRACHT IN ZWAARST BELASTE STROOK

De zwaarst belaste strook heeft een breedte van 1.62 meter. (4d)

Karakteristieke waarde dwarskracht (bw = 1,0 m)		$V_{Ek;TS}$	124.3 kN/m
Partiële belasting factor	$\gamma_{Q;6.10a}$ 0.95 -	$\gamma_{Q;6.10b}$	1.18 -
In rekening te brengen dwarskracht (bw = 1,0 m)	$V_{Ed;TS;6.10a}$ 117.7 kN/m	$V_{Ed;TS;6.10b}$	147.1 kN/m

Tandemstel 1

Belasting per as		$Q_k * \alpha_{Q1}$	289 kN
Effectieve breedte TS1 as 1		$b_{eff;11}$	4.71 m
Dwarskracht t.g.v. TS1 as 1	$((Q_k * \alpha_{Q1}) / b_{eff;11}) * ((L_{span} - L_{11;achter})/L_{span})$	$V_{Ek;TS1;1}$	46.5 kN/m
Effectieve breedte TS1 as 2		$b_{eff;12}$	5.91 m
Dwarskracht t.g.v. TS1 as 2	$((Q_k * \alpha_{Q1}) / b_{eff;12}) * ((L_{span} - L_{12;achter})/L_{span})$	$V_{Ek;TS1;2}$	28.7 kN/m
Dwarskracht t.g.v. TS1		$V_{Ek;TS1}$	75.2 kN/m

Tandemstel 2

Belasting per as		$Q_k * \alpha_{Q1}$	192 kN
Effectieve breedte TS2 as 1		$b_{eff;21}$	5.42 m
Overlappingspercentage TS2 as 1		$\%_{lap;21}$	100%
Dwarskracht t.g.v. TS2 as 1	$((Q_k * \alpha_{Q1}) / b_{eff;21}) * ((L_{span} - L_{21;achter})/L_{span})$	$V_{Ek;TS2;1}$	27.0 kN/m
Effectieve breedte TS2 as 2		$b_{eff;22}$	7.82 m
Overlappingspercentage TS2 as 2		$\%_{lap;22}$	100%
Dwarskracht t.g.v. TS2 as 2	$((Q_k * \alpha_{Q1}) / b_{eff;22}) * ((L_{span} - L_{22;achter})/L_{span})$	$V_{Ek;TS2;2}$	14.5 kN/m
Dwarskracht t.g.v. TS2		$V_{Ek;TS2}$	41.4 kN/m

Tandemstel 3   Overlap TS3 1.08 m < 1.62 m (4d) i.v.m. bruglengte

Belasting per as		$Q_k * \alpha_{Q1}$	96 kN
Effectieve breedte TS3 as 1		$b_{eff;31}$	8.37 m
Overlappingspercentage TS3 as 1		$\%_{lap;31}$	67%
Dwarskracht t.g.v. TS3 as 1	$((Q_k * \alpha_{Q1}) / b_{eff;31}) * ((L_{span} - L_{31;achter})/L_{span})$	$V_{Ek;TS3;1}$	4.0 kN/m
Effectieve breedte TS3 as 2		$b_{eff;32}$	8.37 m
Overlappingspercentage TS3 as 2		$\%_{lap;32}$	67%
Dwarskracht t.g.v. TS3 as 2	$((Q_k * \alpha_{Q1}) / b_{eff;32}) * ((L_{span} - L_{32;achter})/L_{span})$	$V_{Ek;TS3;2}$	3.6 kN/m
Dwarskracht t.g.v. TS3		$V_{Ek;TS3}$	7.6 kN/m

Figure 109 Example output of module 7.3-7 CEB-fib model code 2010 – Part II

C

Appendix – Chapter 4: Load bearing capacity of existing structures

C1   Background of the Capacity model

The bending moment and shear force capacity in the selected sections are determined based on data and formulas from RBK and EC.

Materials

The RBK, and to a lesser extent the CUR recommendation 124, supplements the materials from the EC for old standards. In these additions, the design values for existing structures without material research are given in terms according to the EC.

Concrete

The cube compressive strength of the concrete can be determined based on the design value. RBK gives the values from Table 52 for concrete from the old standards, this is a supplement to NEN-EN 1992-1-1 table 3.1.

Standard	Quality	f_{ck} N/mm^2	Standard	Quality	f_{ck} N/mm^2
GBV 1930		8		B 12,5	10
GBV 1940	K 150	8		B 17,5	14
	K 200	11		B 22,5	18
	K 250	13,5		B 30	25
GBV 1950	K 150	8	VB 74 + VB 74/84	B 37,5	30
	K 200	11		B 45	35
	K 250	13,5		B 52,5	47,5
GBV 1962	K 160	9		B60	50
	K 225	13		B15	12
	K 300	19	VBC	B25	20
	K 400	28		B35	28

	K 450	32		B45	35
RVB 1962 + 1967	K 500	33		B55	45
	K 600	40		B65	53

Table 52 Material properties of old standards for EC based checks (Acquired from RBK v1.1 Tabel 2.2)

If from the available data it cannot be determined according to which concrete quality a construction has been designed, the lowest cube compressive strength following the original design standard must be used. There are two exceptions to this.

In the event that a construction is managed by RWS or it can be demonstrated that the construction has been owned by RWS and a building inspection has taken place, based on RBK v1.1 art. 3.1.2 (10) for structures founded before 1976 a concrete strength class C35/45 may be used. The condition for this is that the construction must not show any visible phenomena, there must be no direct reason to doubt the condition of the concrete construction and the construction must be made of normal concrete. By phenomena is understood excessive deflections or subsidence, cracks, loose stones, rust or efflorescence. For structures in the management of local authorities, if no data concerning the concrete quality is known, a C16/20 concrete quality can be assumed in accordance with CUR recommendation 124 paragraph 6.2. The prerequisite for this is that there is no damage to the concrete construction. The CUR recommendation 124 says nothing about a foundation year other than that due to the large spread of data, no reliable material strength can be determined and therefore comes to the relatively low strength.

It sometimes happens that the concrete strength class is determined from material research. One reason for this is that shear strength of older structures often depends to a large extent on the quality of the concrete because no specific shear reinforcement is present. Because values obtained from a material research often deviate from the standard values, the user is given the option of entering the characteristic and design value of a certain strength class in the "Restrictions" tab. It must be noted that in cases that not the design value is used a k_t factor of $0{,}85$ has to be used, resulting in lower f_{cd} and f_{ctd} by the same factor of $0{,}85$.

Reinforcement steel
In most cases no material research will be performed, the material properties are determined based on design values. The characteristic and design values for reinforcement steel to be used for structures of RWS and local authorities are the same since the CUR recommendation 124 refers to the values in the RBK. The RBK provides an overview of old rebar types for application with NEN-EN 1992-1-1.

Without investigation of the reinforcement steel, the material strength as used in the design should be used for the calculation. Table 53 shows the characteristic and design values of the yield strength and the ductility class for the old steel types known from the old concrete standards.

Old standard		NEN-EN 1992-1-1		
	Reinforcement steel	$f_{yk}\ [N/mm^2]$	$f_{yd}\ [N/mm^2]$	Ductility class
GBV 1930	1. B	220	191	B
	HK	-	191	B
GBV 1940	St. 37	220	191	B
	L. St. 52	340-360	296	B

	Speciaal staal s_v 36	360	313	B
	Speciaal staal s_v 48	480	417	B
GBV 1950	QR22	220	191	B
	QR24	240	209	B
	QR30	300	261	B
	QR36	360	313	B
	QR42	420	365	B
	QRn36	360	313	A
	QRn42	420	365	A
	QRn48	480	417	A
	QRn54	540	470	A
GBV 1962	QR22	220	191	B
	QR24	240	209	B
	QR32	320	278	B
	QR40	400	348	B
	QR48	480	417	B
	QRn32	320	278	A
	QRn40	400	348	A
	QRn48	480	417	A
VB 74 + VB 74/84	FeB 220HW	220	191	B
	FeB 400 HW, HWL	400	348	B
	FeB 500 HW	500	435	B
	FeB 400 HK	400	348	B
	FeB 500 HK	500	435	B
	FeB 500 HKN, HWN	500	435	A
VBC	FeB 220 HWL	220	191	B
	FeB 400 HWL, HK	400	348	B
	FeB 500 HWL, HK	500	435	B
	FeB 500 HKN	500	435	A

Table 53 Overview of properties from reinforcement of old standards for use of NEN-EN 1992-1-1 (Acquired from RBK v1.1 tabel 2.6)

In RBK, a higher material factor is used for some types of reinforcement than the usual $\gamma_s = 1,15$. The new NEN 8702, released for comment, states that a material factor of $\gamma_s = 1,15$ can be used for all reinforcement. This recommendation has been adopted for the design values of the reinforcement.

If the steel reinforcement cannot be determined from the available data or even the year of construction is unknown, RBK and CUR 124 give the same advice. If it is not possible to determine which reinforcement steel type has been used in the construction from the available data, the lowest reinforcement steel type following the original design standard must be used. In case it is not clear which design standard has been used, a minimum strength can be used based on the year of construction. For constructions built before 1964 it is never necessary to use a value lower than $f_{yd} = 191\ N/mm^2$, constructions built later than 1964 no value lower than $f_{yd} = 209\ N/mm^2$ should be used.

Sections

Cross-sectional resistances of the deck structure are determined in the sections called:
- Midspan;
- Connection with haunch;
- In the clear.

The location of the sections is visualized in Figure 110.
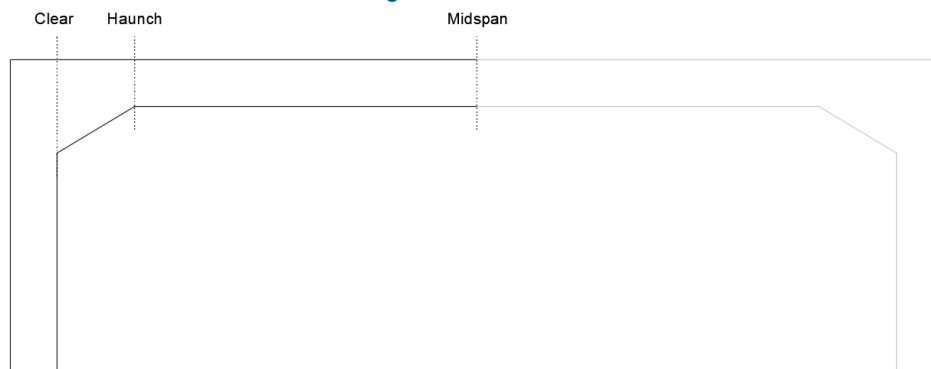
Figure 110 Overview of location sections

Bending moment capacity

The bending moment capacity is determined for sections:

- Midspan, as positive bending moment;
- Connection with haunch, both positive and negative bending moment;
- In the clear, as negative bending moment.

As defined in Figure 110.

Method
The moment capacity of a cross-section is calculated by making a moment equilibrium assuming that the reinforcement yields before the concrete fails. The basic principle is shown in Figure 111.
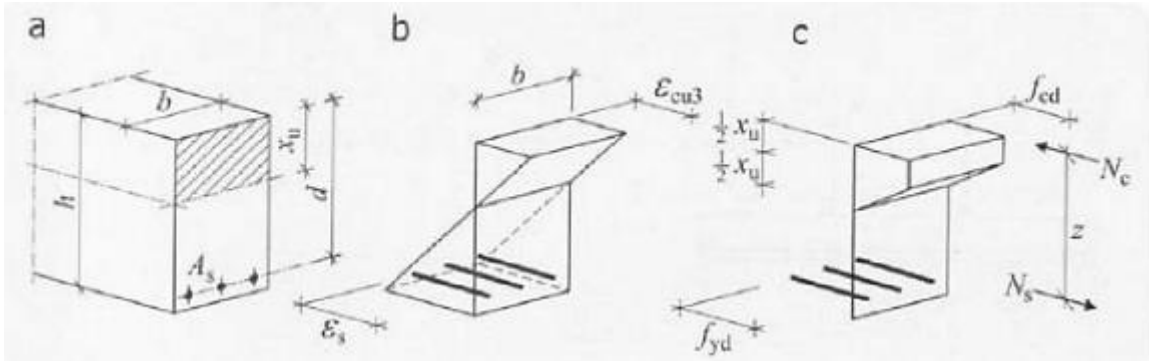
Figure 111 Concrete cross-section with deformation and stress diagram (Source: (Braam & Lagendijk, 2010))

The horizontal load on the walls due to the surrounding ground results in a normal force in the deck. This normal force has a positive effect on the moment resistance of the section and is therefore taken into account for determining the moment capacity of the section.

There must be a balance in horizontal forces and internal moment:

$$\sum H = 0 \quad \xrightarrow{yields} \quad N_c + N_{soil} = N_s \tag{C.1}$$

$$\sum M = 0 \quad \xrightarrow{yields} \quad M_{Rd} = (N_c + N_{soil}) \cdot z = N_s \cdot z = A_s \cdot f_{yd} \cdot z \tag{C.2}$$

Where,

z is the internal lever am and determined with: $z = d - \beta \cdot x_u$ (C.3)

$$N_c + N_{soil} = N_s \quad \xrightarrow{yields} \quad \alpha \cdot b \cdot x_u \cdot f_{cd} = A_s \cdot f_{yd} - N_{soil}$$

d is the effective height and determined with: $d = h_w - c - \frac{\emptyset}{2}$ (C.4)

In case the reinforcement in span direction is not in the outer layer, the diameter of the first layer can be given at the top of the *Resistance* tab, the reinforcement diameter in the first layer will then be subtracted from d.

x_u is the height of the compressive zone and determined with: $x_u = \frac{A_s \cdot f_{yd} - N_{soil}}{\alpha \cdot b \cdot f_{cd}}$ (C.5)

By including the normal force N_{soil} as a result of the ground load in the calculation, the height of the compressive zone x_u becomes smaller. As a result of a smaller compressive zone x_u, the internal lever arm z and thus the moment capacity M_{Rd} increases. The determination of N_{soil} is described in Appendix B2.

NEN-EN 1992-1-1 section 3.1.7 gives the engineer two options for stress-strain relationships for calculating cross sections, the parabola-rectangle and the bi-linear diagram for concrete. For a concrete strength class $\leq C50/60$ the values for α and β are constant:

- Parabola-rectangle diagram: $\alpha = \frac{17}{21} \approx 0{,}81, \beta = \frac{99}{238} \approx 0{,}42;$
- Bi-linear diagram: $\alpha = 0{,}75, \beta = 0{,}39.$

In this calculation the values for α and β according to the parabola-rectangle diagram are used since they result in a slightly favourable resistance. The reason behind is that the change in α and β result in a lower x_u and thus a larger internal arm z thus a larger moment capacity M_{Rd}.

The cross-sectional area of the reinforcement A_s, in case fully anchored, is calculated from the given input, which is limited to two layers of reinforcement. The input is defined as bar diameter $\emptyset$ every certain distance. For a single layer A_s is calculated with:

$$A_{s;i;section} = \frac{1}{4} \cdot \pi \cdot \emptyset^2 \cdot \frac{1000}{s} \tag{C.6}$$

Where,

s is the centre-to-centre distance of the reinforcement in mm.

The cross-sectional area of the reinforcement in a cross-section is defined as:

$$A_{s;section} = A_{s;1;section} + A_{s;2;section} \tag{C.7}$$

When two layers are present in one section to take up the bending moment, the layer with the biggest bar diameter should be layer 1 since the effective height of the deck d is defined based on the diameter $\emptyset$ of layer 1. In case only one layer is present to take up the bending moment, layer 2 should be set to zero by setting the diameter to 0. When more than one layer of reinforcement is present, it is assumed that both are of the same steel grade. Since it is very unlikely that within a structure, let alone within a part of it, different steel grades have been used for the reinforcement.

The concrete cover c can be defined for every single cross-section, c is user defined input. In case the concrete cover is unknown, $c = 40\ mm$ may be used. This value refers to the upper limit from the data analysis for the concrete cover. The reason for choosing the upper limit is that greater coverage results in a smaller internal lever arm and therefore a lower bending moment and shear force capacity.

Shear capacity

The determination of the shear capacity of existing concrete structures has received special attention in this research and is described in detail in paragraph 4.1.1 of the main report. Only the formulas studied are elaborated in this appendix.

Eurocode
The shear capacity for elements that do not require calculated shear reinforcement is described in NEN-EN 1992-1-1 section 6.2.2 art. (1) and formulated as:

$$V_{Rd;c} = \left(C_{Rd;c} \cdot k \cdot (100 \cdot \rho_l \cdot f_{ck})^{\frac{1}{3}} + k_1 \cdot \sigma_{cp} \right) \cdot b_w \cdot d \qquad (6.2.a) \tag{C.8}$$

With a minimum of:

$$V_{Rd;c;min} = \left(v_{min} + k_1 \cdot \sigma_{cp} \right) \cdot b_w \cdot d \qquad (6.2.b) \tag{C.9}$$

In which,

$$C_{Rd;c} = \frac{0,18}{\gamma_c} = \frac{0,18}{1,5} = 0,12; \qquad \text{(NEN-EN 1992-1-1 NB 6.2.2 (1))}$$

$$k = 1 + \sqrt{\frac{200}{d}} \leq 2,0 \quad with\ d\ in\ mm;$$

ρ_l is the longitudinal reinforcement ratio defined as: $\rho_l = \frac{A_{sl}}{b_w \cdot d} \leq 0,02$. In case the reinforcement is not fully anchored, $A_{s;red}$ as in (C.24) is taken;

A_{sl} is the area of the tensile reinforcement, which extends $\geq (l_{bd} + d)$ beyond the considered cross-section. (see Figure 26). Which in the case of a box-shaped section means that the reinforcement must be bent. In case the reinforcement is not fully anchored, $A_{s;red}$ as in (C.24) is taken;

f_{ck} is the characteristic cylinder compressive strength in MPa;

k_1 equals 0,15 taken in accordance with NEN-EN 1992-1-1 NB 6.2.2 (1)

σ_{cp} $\frac{N_{Ed}}{A_c} < 0,2 \cdot f_{cd}\ in\ MPa$;

N_{Ed} is the normal force in the cross-section due to horizontal soil load. Since the bending moment and shear effect of the soil load is governing over the effect of normal force due to the same soil load a load factor for unfavourable is used despite the normal force has a positive effect;

A_c is the cross-sectional area of the concrete in mm^2;

b_w is the smallest width of the cross-section in the area under tension in mm, for a section with a width of 1 meter $b_w = 1000\ mm$. Note that the assumption is made that the slab is massive, i.e. without holes, with the same concrete quality meaning no prefab girders with an infill deck;

d is the effective height of the cross-section. For the three sections it is defined as:

$$d_{midspan} = h_{midspan} - c_{midspan} - \frac{\emptyset_{midspan}}{2};$$

$$d_{haunch^+} = h_{haunch} - c_{haunch} - \frac{\emptyset_{haunch^+}}{2};$$

In which,

     d_{haunch^+} is the effective height of the deck at the section haunch with a sagging bending moment;

     $\emptyset_{haunch^+}$ is the bar diameter of the reinforcement under tension at section haunch with a sagging bending moment;

$$d_{haunch^-} = h_{haunch} - c_{haunch} - \frac{\emptyset_{haunch^-}}{2};$$

In which,

     d_{haunch^-} is the effective height of the deck at the section haunch with a hogging bending moment;

$\emptyset_{haunch-}$ is the bar diameter of the reinforcement under tension at section haunch with a hogging bending moment;

$$d_{clear} = h_{clear} - c_{clear} - \frac{\emptyset_{clear}}{2}.$$

In the EC, NEN-EN 1992-1-1 NB 6.2.2 (1), is stated that:

$$v_{min} = 0{,}035 \cdot k^{\frac{3}{2}} \cdot f_{ck}^{\frac{1}{2}} \tag{C.10}$$

The design value for the shear force capacity of a certain cross-section according to EC is defined as:

$$V_{Rd;c;section} = \max\left(V_{Rd;c;min}; V_{Rd;c}\right) \tag{C.11}$$

RBK

In RBK, the formulas (6.2.a) and (6.2.b) of NEN-EN 1992-1-1 section 6.2.2 for the calculation of the shear capacity without shear reinforcement have been replaced by:

$$V_{Rd;c} = \left(0{,}12 \cdot k_{cap} \cdot k \cdot (100 \cdot \rho_l \cdot f_{ck})^{\frac{1}{3}} + 0{,}15 \cdot \sigma_{cp}\right) \cdot b_{wgem} \cdot d \qquad (6.2.a) \tag{C.12}$$

$$V_{Rd;c} = \left(v_{min} + 0{,}15 \cdot \sigma_{cp}\right) \cdot b_{wgem} \cdot d \qquad (6.2.b) \tag{C.13}$$

In which,

$k, \rho_l, f_{ck}, \sigma_{cp}, b_{wgem}$ and d are the same as for EC and specified in Eurocode;

$k_{cap} = 1{,}2$ RBK states that $k_{cap} = 1{,}2$ if the deck is considered to be a solid reinforced plate.

For non-prestressed solid reinforced plates, v_{min} may be determined by the formula:

$$v_{min} = 0{,}83 \cdot k_p^{\frac{3}{2}} \cdot k^{\frac{3}{2}} \cdot f_{ck}^{\frac{1}{2}}/f_{yk}^{\frac{1}{2}} \tag{C.14}$$

Where,

k_p is the plate factor and is defined by RBK as: $k_p = k_{cap} = 1{,}2$.

The design value for the shear force capacity of a certain cross-section according to RBK is defined as:

$$V_{Rd;c;section} = \max\left(V_{Rd;c;min}; V_{Rd;c}\right) \tag{C.15}$$

RBK v_{min-k_p}

This is a studied variant based on RBK without the plate factor k_p, the formulas 6.2a and 6.2b are then formulated as:

$$V_{Rd;c} = \left(0{,}12 \cdot k_{cap} \cdot k \cdot (100 \cdot \rho_l \cdot f_{ck})^{\frac{1}{3}} + 0{,}15 \cdot \sigma_{cp}\right) \cdot b_{wgem} \cdot d \qquad (6.2.a) \tag{C.16}$$

$$V_{Rd;c} = \left(v_{min} + 0{,}15 \cdot \sigma_{cp}\right) \cdot b_{wgem} \cdot d \qquad (6.2.b) \tag{C.17}$$

In which,

$k, \rho_l, f_{ck}, \sigma_{cp}, b_{wgem}$ and d are the same as for EC and specified in Eurocode;

$k_{cap} = 1,2$ RBK states that $k_{cap} = 1,2$ if the deck is considered to be a solid reinforced plate.

For non-prestressed solid reinforced plates, v_{min} may be determined by the formula:

$$v_{min} = 0,83 \cdot k^{\frac{3}{2}} \cdot f_{ck}^{\frac{1}{2}} / f_{yk}^{\frac{1}{2}} \tag{C.18}$$

The design value for the shear force capacity of a certain cross-section according to RBK is defined as:

$$V_{Rd;c;section} = \max\left(V_{Rd;c;min}; V_{Rd;c}\right) \tag{C.19}$$

EC v_{min+k_p}

This is a studied variant which is a combination of RBK and EC formulas. Formula 6.2a is the same as within RBK, including plate factor k_p. For formula 6.2b the constant factor in the v_{min}-formula from EC, based on the assumption $z = 0,9\, h$, is used with the addition of the plate factor k_p from RBK. Formulas 6.2a and 6.2b are then formulated as:

$$V_{Rd;c} = \left(0,12 \cdot k_{cap} \cdot k \cdot (100 \cdot \rho_l \cdot f_{ck})^{\frac{1}{3}} + 0,15 \cdot \sigma_{cp}\right) \cdot b_{wgem} \cdot d \qquad (6.2.a) \tag{C.20}$$

$$V_{Rd;c} = \left(v_{min} + 0,15 \cdot \sigma_{cp}\right) \cdot b_{wgem} \cdot d \qquad (6.2.b) \tag{C.21}$$

In which,

$k, \rho_l, f_{ck}, \sigma_{cp}, b_{wgem}$ and d are the same as for EC and specified in Eurocode;

$k_{cap} = 1,2$ RBK states that $k_{cap} = 1,2$ if the deck is considered to be a solid reinforced plate.

For non-prestressed solid reinforced plates, v_{min} may be determined by the formula:

$$v_{min} = 0,035 \cdot k_p^{\frac{3}{2}} \cdot k^{\frac{3}{2}} \cdot f_{ck}^{\frac{1}{2}} \tag{C.22}$$

The design value for the shear force capacity of a certain cross-section according to RBK is defined as:

$$V_{Rd;c;section} = \max\left(V_{Rd;c;min}; V_{Rd;c}\right) \tag{C.23}$$

Anchorage

Reinforcing bars must be anchored so that the bonding forces can be safely transferred to the concrete so that longitudinal cracks and spalling are avoided. This has been less taken into account in the past, which means that the reinforcement cross-section may need to be theoretically reduced to prevent cracking and spalling of the concrete or slipping of the reinforcement bar.

The user has the option to choose whether the reinforcement is assumed to be fully anchored or that the anchorage will be checked based on a provided length in relation with a certain point in the structure and the calculated required anchorage length. The check for anchorage length takes place in a separate module called *"Verankeringslengte V0.xlsx"*. In case the reinforcement is not fully anchored the reduced cross-sectional area is defined as:

$$A_{s;red} = \min \left(\frac{l_{bd;prov;start}}{l_{bd}} ; \frac{l_{bd;prov;end}}{l_{bd}} \right) \cdot A_s \qquad (C.24)$$

The anchorage length of a bar to be considered fully anchored is calculated on the basis of NEN-EN 1992-1-1 section 8.4 with additions from RBK. For the verification calculation of existing underpasses, a distinction is made between the anchoring method with a straight and a bent bar as shown in Figure 112.
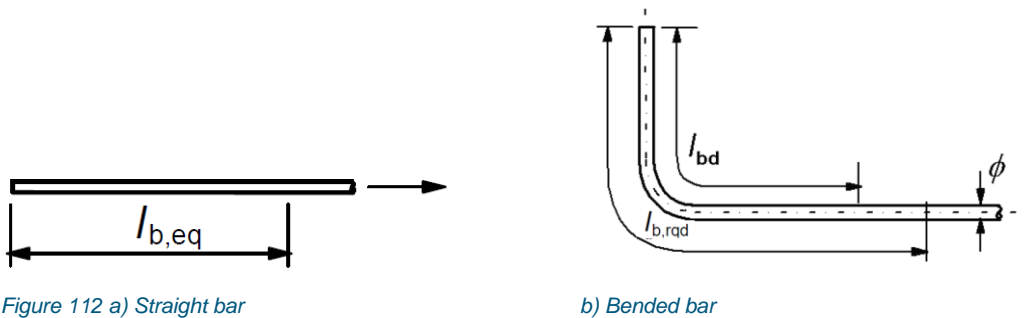
Figure 112 a) Straight bar   *b) Bended bar*

Required anchorage length

Ultimate bond stress
Before the basic anchorage length can be calculated, the ultimate bond stress f_{bd} must be determined. The ultimate bond capacity must be sufficient to prevent anchor failure. The design value of the ultimate bond stress f_{bd} is taken as follows:

$$f_{bd} = 2{,}25 \, \eta_1 \, \eta_2 \, \eta_3 \, f_{ctd} \qquad (C.25)$$

Where,

η_1 is the coefficient on the quality of bonding conditions, for which it is assumed that reinforcement bars at the bottom always have good bonding conditions with $\eta_1 = 1{,}0$ and reinforcement bars at the top have poor bonding conditions meaning $\eta_1 = 0{,}7$ unless the concrete element is less then $250 \, mm$ thick. The explanation for top and bottom reinforcement relates to the direction of pouring.

η_2 is the coefficient on the bar diameter. For which holds that $\eta_2 = 1{,}0$ for $\emptyset \leq 32 \, mm$ and $\eta_2 = (132 - \emptyset)/100$ for $\emptyset > 32 \, mm$.

η_3 is the coefficient on bar profiling, for which applies that for ribbed reinforcement steel $\eta_3 = 1{,}0$ and smooth reinforcement steel $\eta_3 = 0{,}5$.

f_{ctd} is the design value of the tensile strength of concrete.

Basic anchorage length

When calculating the required anchorage length for full anchorage, the type of steel and the bonding properties of the respective bar are taken into account. The required basic anchoring length $l_{b;rqd}$ for anchoring the force $A_s \cdot \sigma_{sd}$ in a straight bar assuming a constant bonding stress equal to f_{bd} follows from:

$$l_{b;rqd} = (\emptyset/4)\,(\sigma_{sd}/f_{bd}) \tag{C.26}$$

In which,

σ_{sd} is the design value of the stress in the bar at the point from which the anchoring was measured. For a reinforcement bar to be fully anchored $\sigma_{sd} = f_{yd}$ applies.

Design value of anchorage length

The design value of the anchorage length l_{bd} is:

$$l_{bd} = \alpha_1\,\alpha_2\,\alpha_3\,\alpha_4\,\alpha_5\,l_{b;rqd} \geq l_{b;min} \tag{C.27}$$

Where,

α_1 is the coefficient for the effect of the shape of the reinforcement bar, where it is assumed that there is sufficient concrete coverage. The value of α_1 depends on the type of anchorage and the profiling of the reinforcement bar;

α_2 is the coefficient for the minimum concrete cover c_d and depends on whether the bar is anchored as a straight or bended bar. It is assumed that $c_1 = c$, resulting in $c_d = \min\left(\frac{s}{2}; c\right)$.

α_3 is the coefficient for the effect of confinement by transverse reinforcement. But since it is assumed that there is no transverse (shear) reinforcement present in the structures to be investigated $\alpha_3 = 1,0$.

α_4 is the coefficient for the effect of confinement by welded transverse reinforcement. Although no (welded) transverse reinforcement is present, the value of α_4 is fixed by EC to $\alpha_4 = 0,7$.

α_5 is the coefficient for the effect of confinement by transverse pressure p in the ULS along l_{bd}. Transverse pressure has a positive effect on the anchorage of the reinforcement and is therefore conservatively maintained as $p = 0$ by default.

An overview for determining the individual α-coefficients is shown in Table 54, for which holds that the product of $(\alpha_2\,\alpha_3\,\alpha_5) \geq 0,7$.

The minimum anchorage length $l_{b;min}$ for tension anchors is:

$$l_{b;min} \geq \max\{0,3\,l_{b;rqd};\,10\emptyset;\,100\ mm\} \tag{C.28}$$

Influence factor	Type of anchorage	Steel profiling	Coefficient α
Shape of the reinforcement bar α_1	Straight	Ribbed / Smooth	$\alpha_1 = 1,0$
	Bended	Ribbed	$\alpha_1 = 1,0$ if $c_d \leq 3\,\emptyset$ $\alpha_1 = 0,7$ if $c_d > 3\,\emptyset$
		Smooth	$\alpha_1 = 1,0$ if $c_d \leq \emptyset$ $\alpha_1 = 0,7$ if $c_d > \emptyset$
Minimum concrete cover α_2	Straight	Ribbed / Smooth	$\alpha_2 = 1 - 0,15\,(c_d - \emptyset)/\emptyset$ But $0,7 \leq \alpha_2 \leq 1,0$
	Bended	Ribbed / Smooth	$\alpha_2 = 1 - 0,15\,(c_d - 3\,\emptyset)/\emptyset$ But $0,7 \leq \alpha_2 \leq 1,0$
Effect of confinement by transverse reinforcement (not welded to main reinforcement) α_3	Straight / Bended	Ribbed / Smooth	$\alpha_3 = 1,0$ Assumed: no transverse (shear) reinforcement present
Effect of confinement by welded transverse reinforcement α_4	Straight / Bended	Ribbed / Smooth	$\alpha_4 = 0,7$
Effect of confinement by transverse pressure p	Straight / Bended	Ribbed / Smooth	$\alpha_5 = 1 - 0,04\,p$ But $0,7 \leq \alpha_5 \leq 1,0$

Table 54 Overview for determining the α-coefficients (Adapted from NEN-EN 1992-1-1+C2 Table 8.2)

Provided anchorage length

For the determination of the provided anchorage length, please refer to section 4.2.2 of the main report.

Checks

Unity Checks

The unity check (UC) is defined as the effect (E) divided by the resistance (R). An overview of the checks performed is shown in Table 55.

Section	Corresponding moment	Corresponding reinforcement	M_{Ed}/M_{Rd}	V_{Ed}/V_{Rd}
Midspan	Sagging (+)	Bottom	✔	✘
Haunch	Sagging (+)	Bottom	✔	✔
	Hogging (-)	Top	✔	✔
Clear	Hogging (-)	Top	✔	✔

Table 55 Overview of performed checks

An overview of the checks with corresponding cross-section is presented in Figure 113.
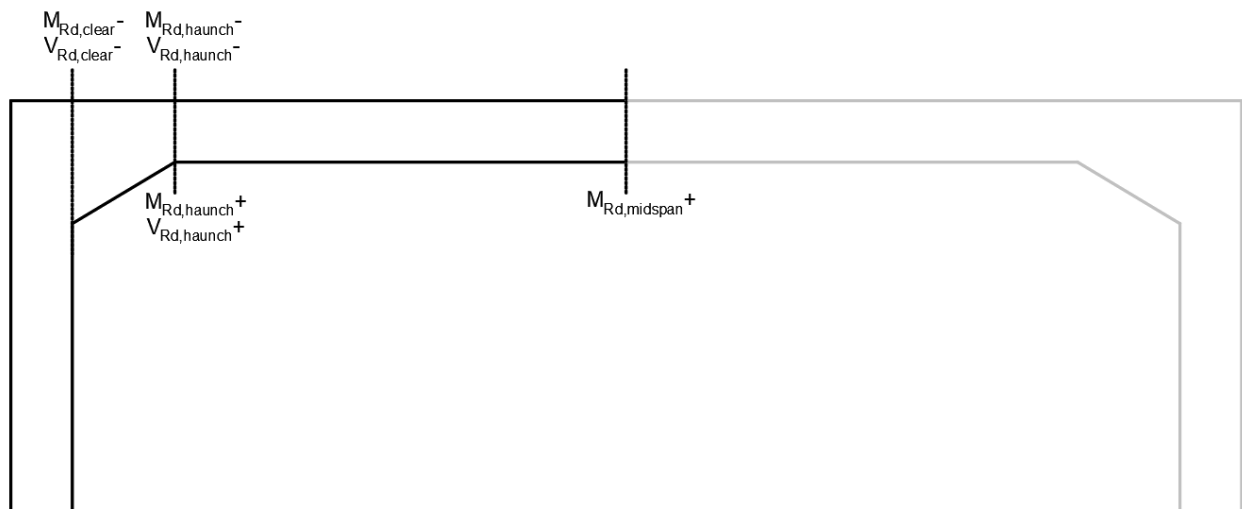
Figure 113 Overview of checks with corresponding section

For the bending moment and the shear force, it is determined per load situation whether the combination according to 6.10a or 6.10b is decisive, this is also shown for each situation and in the overview.
The bending moment checks that are performed are defined as:

$$\frac{M_{Ed;midspan}}{M_{Rd;midspan}} \leq 1,0 \quad \xrightarrow{yields} \quad okay \tag{C.29}$$

$$\frac{M_{Ed;haunch^-}}{M_{Rd;haunch^-}} \leq 1,0 \quad \xrightarrow{yields} \quad okay \tag{C.30}$$

$$\frac{M_{Ed;haunch^+}}{M_{Rd;haunch^+}} \leq 1,0 \quad \xrightarrow{yields} \quad okay \tag{C.31}$$

$$\frac{M_{Ed;clear}}{M_{Rd;clear}} \leq 1,0 \quad \xrightarrow{yields} \quad okay \tag{C.32}$$

The shear resistance checks that are performed are defined as:

$$\frac{V_{Ed;haunch^-}}{V_{Rd;haunch;EC^-}} \leq 1,0 \quad \xrightarrow{yields} \quad okay \qquad \text{(EC)} \tag{C.33}$$

$$\frac{V_{Ed;haunch^-}}{V_{Rd;haunch;RBK^-}} \leq 1,0 \quad \xrightarrow{yields} \quad okay \qquad \text{(RBK)} \tag{C.34}$$

$$\frac{V_{Ed;haunch^+}}{V_{Rd;haunch;EC^+}} \leq 1,0 \quad \xrightarrow{yields} \quad okay \qquad \text{(EC)} \tag{C.35}$$

$$\frac{V_{Ed;haunch^+}}{V_{Rd;haunch;RBK^+}} \leq 1,0 \quad \xrightarrow{yields} \quad okay \qquad \text{(RBK)} \tag{C.36}$$

$$\frac{V_{Ed;clear}}{V_{Rd;clear;EC}} \leq 1,0 \quad \xrightarrow{yields} \quad okay \qquad \text{(EC)} \tag{C.37}$$

$$\frac{V_{Ed;clear}}{V_{Rd;clear;RBK}} \leq 1,0 \quad \xrightarrow{yields} \quad okay \qquad \text{(RBK)} \tag{C.38}$$

Redistribution of bending moment

In case the moment capacity of the deck is not sufficient with the fully elastic calculated moment distribution, may according to RBK section 5.5 art. (105) a maximum of 20% of the moment be redistributed. Under the condition that reinforcement with a ductility class B has been applied. Moment redistribution is only applied between the bending moment at midspan and in the clear.

In the event that the midspan moment does not suffice, the midspan moment, up to a maximum of 20%, is redistributed to the moment in the clear of the same load case.

In the event that the moment in the clear does not suffice, the moment in the clear, up to a maximum of 20%, is redistributed to the midspan moment of the same load case.

In case a positive bending moment in the section at the end of the haunch is governing, the moment is up to a maximum of 20% redistributed to the corresponding negative moment in the section at the face of the wall from the same load case.

In case a negative bending moment in the section at the end of the haunch is governing, the moment is up to a maximum of 20% redistributed to the corresponding sagging moment in the span from the same load case.

When the sum of the occurring midspan moment and moment in the clear is greater than the sum of the moment capacity in these sections, the tool gives a warning because it is unlikely that the structure can still meet the requirements even with redistribution.

D
Appendix – Chapter 5: Load effect by Finite Element Method

D1   Background of the 3D FEM plate model

Introduction

This Appendix is the background report of the script-based FEM analysis. Within the study, the module for automatically running the FEM software is called Auto_SOFiSTiK, named after the FEM software SOFiSTiK which is used for the analysis. The script is set up in a TEDDY file, which is part of SOFiSTiK, and has its own programming language.

The TEDDY script is divided into a few self-defined templates and several dedicated programs from SOFiSTiK. The script is divided into:

- Template: Input parameters;
- Template: Running variables;
- AQUA: Materials and Cross-Sections;
- SOFIMSHC: Generate model;
- SOFILOAD: Generate loads;
- ASE: Linear Analysis;
- SIR: Integrate forces over sections;
- MAXIMA: Superpositioning;
- MAXIMA: Combinations;
- MAXIMA: Combinations for redistribution;
- RESULTS: Excel output.

This chapter is organized according to the programs in the script with the addition of the Auto_SOFiSTiK sub tool.

Template: Input parameters

In the program "Template: Input parameters" the input parameters are defined which are linked to the input file of Auto_SOFiSTiK which can be updated per structure from the Excel database for assessing a set of structures. The user of Auto_SOFiSTiK, or as part of the ASA Tool, therefore does not have to do anything in the TEDDY script file. The program "Template" is no official program from SOFiSTiK but one is able to use the general functions of TEDDY like STO to store a parameter for use in other programmes.

In case the user wants to adjust a specific setting, it is best to try the change in the TEDDY script first, with the assistance of the SOFiSTiK help file under F1 key, and then adjust the change in Auto_SOFiSTiK on the sheet *"Int_Sofistik"*. In the TEDDY script, green text, starting with a $, is supporting text for the explanation of variables and equations.

Template: Running variables

In the program "Template: Running variables" parameters which are used later for generating the model, generating the loads and the determination of the sections are stored. This program is not part of the standard SOFiSTiK programs, but variables can be stored using the TEDDY command STO for storing a variable in the SOFiSTiK database which can be recalled in other programs. Note that the command LET is only valid for the current program, in this case Template: Running variables.

Global coordinates for structural points

A joint-to-joint segment of an underpass or culvert can be reduced to 12 points with which the model can be generated, and the parameters considered can be changed. An overview of the assigned numbers of the global structural points, orientation points, is shown in Figure 114.
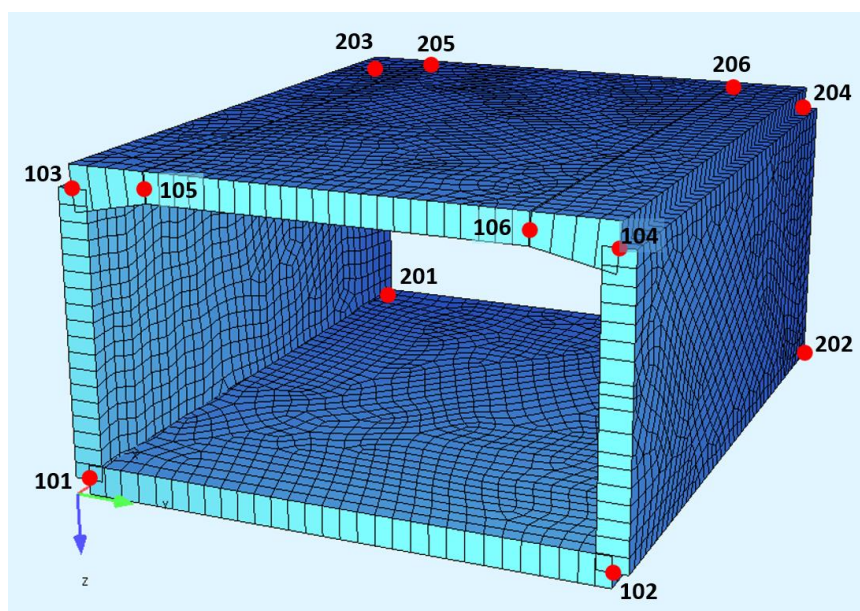
Figure 114 Overview of global coordinates of 3D FEM plate model

Every node showed in Figure 114 is defined as:

```
STO#Node_x(101)
STO#Node_y(101)
STO#Node_z(101)
```

Using parentheses () ensures that all global coordinates are stored by TEDDY in some sort of list and can be called up later.

Load distribution

Due to the presence of an asphalt layer and soil cover, the traffic loads are distributed vertically. For the calculation of the occurring bending moment loads are distributed up to the centre line of the deck of the structure, for the calculation of the shear force is distributed to the top of the deck of the structure.

Coordinates – LM1 UDL & TS

For the application of LM1, consisting of the UDL and TS loads, all coordinates for the load planes are stored as variables. The principle is shown graphically in Figure 115, after which it is explained textually.
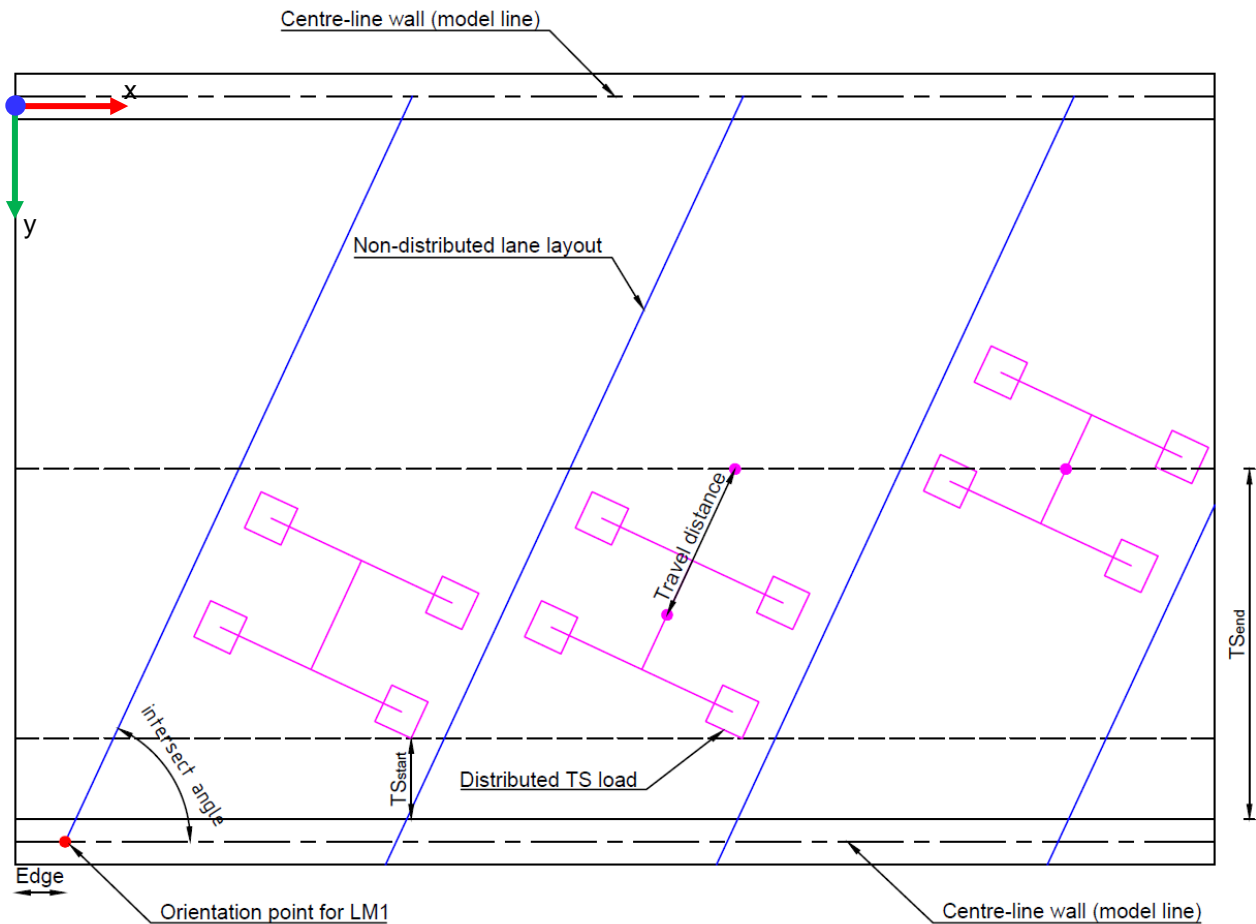
Figure 115 Principle for placing LM1 loads in 3D FEM plate model.

The positioning of the loads from LM1, including the UDL and TS loads, is based on the orientation point indicated by the red dot in Figure 115. By changing the $Edge$ distance the user can shift the placement of lanes across the width of the deck. The coordinates of the lanes, and remaining area, in Figure 115 are based on non-distributed loads, vertical load distribution is processed in a later step for a load case for bending moment and a load case for shear. The distributed TS loads are used to determine the locations of the TSs because the placement depends on the edge of the load plane in relation to the face of the supportive wall, called TS_{start}. The last position of TS is the location for maximum bending moment in the span and is by default in the middle of the span, the distance from the face of the supportive wall to the centre of gravity of TS is called TS_{end}. The default for TS_{start} is $2d_{span}$ and for TS_{end} $L_{clear}/2$, but the user can adjust these values if desired. Together TS_{start} and TS_{end} define the travel distance. Given the limited spans of underpasses and culverts, the number of steps is 10 by default, the user can increase this number in multiples of 10. However, it should be borne in mind that increasing the number of steps results in a significant increase in processing time of SOFiSTiK. The entire set of loads is automatically rotated based on the intersection angle as indicated in Figure 115.

Aqua: Materials and Cross-Sections

Aqua is the first program from SOFiSTiK, in this program the materials and cross-sections are defined. In this case only a material for concrete is defined, so no cross-sections are defined. A material can be created by using MATE. For concrete the E-modulus is standard 10.000 for all elements, in case use is made of the fictional stiffness E_f separate values can be given. A Poisson ratio of $v = 0{,}20$ and a G-modulus of $G = E/(1 + v)$ are used.

Sofimshc: Generate Model

SOFiMSHC is the programme for creating and processing geometric models and finite element structures. The very first thing SOFiSTiK needs to know is that a 3D system with gravity in the positive z-direction will be used.

Structural points (SPT) must be created to later create the 2D elements, the structural points correspond to the previously defined global coordinates. An extra structural point is created which is fixed in global x-direction, this must prevent translations in the x-direction (length of the underpass or culvert).

The elements of the structure are created by use of the function SAR, which stands for structural area. In order to create a structural area (SAR), four boundaries must be given, so-called SARB. These boundaries are linked to the global coordinates.

The mesh generation is started by the CTRL function, a mesh with quadrilateral elements only has been chosen since 3-noded elements are more prone to shear locking.

Sofiload: Generate Loads

Loads are generated in the SOFILOAD program.

Control Warnings
Before loads can be generated, several warnings are suppressed.

CTRL WARN 909 $No warning for loads activated with less than 100 percent (partially of the structure)
CTRL WARN 185 $No warning for loads activated with less than 100 percent (partially of the structure)

Part of the UDL and TS loads can turn off the deck, SOFiSTiK solves this itself by cutting the evenly load on the edge of the deck. A check of the sum of the vertical forces has been performed and this appears to be correct.

Actions

Before loads can be defined, the load groups must first be created, for this in SOFiSTiK use the function ACT (Definition of an Action). In the actions, too partial safety factors and way of superposition are processed. An overview of the actions is given in Table 56.

ACT – Definition of an Action	Description	Superposition
G	Permanent loads: self-weight and dead load	PERM
QUDM	LM1 – UDL distributed for determination of bending moment	EXCL
QUDV	LM1 – UDL distributed for determination of shear force	EXCL
QTSM	LM1 – TS distributed for determination of bending moment (incl. up to 3 TS)	EXCL
QV1	LM1 – TS1 distributed for determination of shear force	EXCL
QV2	LM1 – TS2 distributed for determination of shear force	EXCL
QV3	LM1 – TS3 distributed for determination of shear force	EXCL
QTSV	Consists of the MAXIMA from QV1, QV2 and QV3	EXCL

Table 56 Overview of defined actions (ACT) in SOFiSTiK 3D FEM plate model

Action "G" with superposition PERM is naturally always present, meaning loads defined in action group "G" will always be added to a combination. All the other action groups are given the superposition property EXCL, which means that loads within the action are never combined but they will be combined with other loads in case they are added to the combination.

Overview of Load Cases

Before loads can be created, the load class must first be created in which the loads fall. A load case is created in SOFiSTiK by the LC function. Table 57 shows an overview of the Load Cases for the applied loads. The number of Load Cases for LM1-TS load cases depends on the number of steps defined, as standard the number of steps is 10. Note that the number of steps may only be defined in multiple of 10.

Load Case number	Type	Title
100	G	Self-weight
110	G	Deadload of Soil-Vertical
111	G	Deadload of Soil-Horizontal
120	G	Deadload of Asphalt
220	Q	LM1 – UDL – M (vertical distribution to centre-line of concrete deck)
230	Q	LM1 – UDL – V (vertical distribution to top of concrete deck)
301	Q	LM1 – TS – M (vertical distribution to centre-line of concrete deck) – Step 1
⋮	Q	LM1 – TS – M (vertical distribution to centre-line of concrete deck) – Step i
300+#steps	Q	LM1 – TS – M (vertical distribution to centre-line of concrete deck) – Step #steps
401	Q	LM1 – TS1 – V (vertical distribution to top of concrete deck) – Step 1
⋮	Q	LM1 – TS1 – V (vertical distribution to top of concrete deck) – Step i
400+#steps	Q	LM1 – TS1 – V (vertical distribution to top of concrete deck) – Step #steps
501	Q	LM1 – TS2 – V (vertical distribution to top of concrete deck) – Step 1

⋮	Q	LM1 – TS2 – V (vertical distribution to top of concrete deck) – Step i
500+#steps	Q	LM1 – TS2 – V (vertical distribution to top of concrete deck) – Step #steps
601	Q	LM1 – TS3 – V (vertical distribution to top of concrete deck) – Step 1
⋮	Q	LM1 – TS3 – V (vertical distribution to top of concrete deck) – Step i
600+#steps	Q	LM1 – TS3 – V (vertical distribution to top of concrete deck) – Step #steps

Table 57 Overview of defined Load Cases for applied loads

The self-weight is stored in a separate load case and activated by adding FACD 1.0, the other loads are created with AREA loads.

Permanent Loads
Self-weight
The self-weight is stopped in load case 100, falls under TYPE "G" and is triggered as self-weight load case by FACD 1.0.

Soil loads
The vertical soil loads are classified in load case 110 and fall under action group "G". The load is generated by the AREA function, the size of the load comes from Auto_SOFiSTiK or the Excel database, the load is of course in the global z-direction and is created based on the defined global coordinates. It is assumed that a uniform load applies across the entire deck.

The horizontal soil loads are classified in load case 111 and fall under action group "G". The load is generated by the AREA function, the size of the load comes from Auto_SOFiSTiK or the Excel database, the load is in the global y-direction and is created based on the defined global coordinates. The WIDE function is used to allow the horizontal load to also engage the oblique centre line of the haunches. The WIDE function indicates how far in a certain direction an element may be searched to execute the created load. In this case, the x-coordinates of the wall can be used and WIDE searches an extra distance with the length of the haunch plus half a wall thickness for applying the horizontal soil loads.

Asphalt
The asphalt load is classified in load case 120 and falls under action group "G". The load is generated by the AREA function, the size of the load comes from Auto_SOFiSTiK or the Excel database, the load is of course in the global z-direction and is created based on the defined global coordinates. It is assumed that a uniform load applies across the entire deck.

Live Loads
The Live Loads consists of loads from Load Model 1, conform NEN-EN 1991-2 paragraph 4.3.2, which includes concentrated and uniformly distributed loads, which covers most of the effects of traffic load.

LM1 – UDL
Two load cases have been created for the UDL, load case 220 with vertical load distribution to the centre of the deck to determine the bending moment and load case 230 with vertical distribution to the top of the deck to determine the shear force that occurs.

The loads are generated by the AREA function and projected in the global z-direction, because the neutral line at the haunches varies in the vertical plane, a WIDE function is added with the size of the deck thickness at the face of the supportive wall. The size of the load is determined based on the non-distributed UDL load from Auto_SOFiSTiK input or the database and is distributed separately for LC 220 and LC 230.

<u>LM1 – TS – M</u>

It is assumed that the maximum bending moment occurs when TSs are placed in one line with the same y-coordinate, which results in that the number of Load Cases of TS for bending moment is limited to the number of steps. Depending on the number of lanes, 3, 2 or 1 TS are placed, this process is repeated with the number of steps, standard 10, whereby the travel distance from TS_{start} to TS_{end} is covered. Depending on the number of steps, default 10, the load cases for LM1-TS-M are created from 301 to 300 plus the number of steps. Standard 301 to 310.

<u>LM1 – TS – V</u>

The mutual locations of the TSs for the maximum occurring shear force are unknown, this means that in addition to the number of steps, it must also be possible to vary the locations of individual TSs. The number of Load Cases for TS to determine shear force is therefore divided per step per lane. LC 400 series is for TS1, LC 500 series is for TS2 and LC 600 series is for TS3, increasing numbers within these load cases are the steps bridging the travel distance from TS_{start} to TS_{end}. The load cases from the 400, 500 and 600 series LM1-TS-V are later combined to find the maximums and minimums for shear.

Ase: Linear Analysis

The linear analysis is carried out by the ASE program, which calculates the forces and moment. The analysis is performed for all defined load cases.

As was previously the case with the loads, several warnings are suppressed:

CTRL WARN 185 $No warning for loads activated with less than 100 percent (partially of the structure)
CTRL WARN 398 $No warning for no loads in certain LC (soil cover for example)

Sir: Integrate forces over sections

In the cross-section of the underpass or culvert, three main cuts are made, at the face of the wall, at the end of the haunch and at midspan, as was showed in Figure 25. With the 3D FEM plate model, a third dimension is added and must be averaged over a distance of $4d$.

Sections are created by function SIR, an overview of the section series is given in Table 58.

Section Series	Description	Section Height
100	Sections in the deck at the face of the supportive wall	$h_{deck,face}$
200	Sections in the deck at the end of the haunch	$h_{deck,haunch}$
300	Sections in the deck at midspan	$h_{deck,midspan}$

Table 58 Overview of SIR sections series for 3D FEM plate model.

All load cases are used, are relevant, for the integration of forces by SIR. Sections with a width of $4d$ and an overlap of $2d$, sketched in Figure 116, are created for each section series. If a structure has a deck width that can accommodate more than two lanes, only cuts up to half the width of the deck are created to save computation time. This does not affect the maxima because TS1 is always placed from one side, meaning that the other half of the deck is less loaded. In addition, two sections, per section series, with a width of $2d$ are always placed at the edge of the deck.
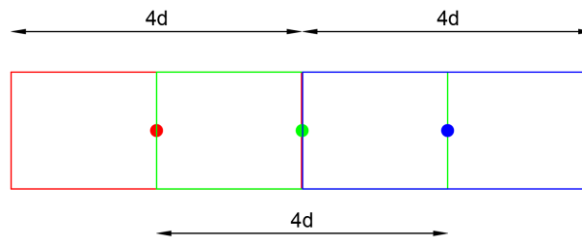
Figure 116 Schematic overlap of SIR sections, with section width $4d$ and overlap $2d$.

Suppressing warnings:

CTRL WARN 28 $No results found in the database for loadcases which are not defined
CTRL WARN 10989 $No results found in the database for loadcases which are not defined

The number of LC is variable and SIR needs to know which load cases are relevant, load cases 100 to 1000 with step size 1 are added, which means that some are empty.

Maxima: Superpositioning

In the program MAXIMA: Superpositioning the maxima and minima per section series are searched for the shear force due to TS. The input are the load case series 400, 500 and 600 which contain all positions of the TSs with load distribution to the top of the deck for the determination of the shear force. The maxima and minima per section series are then added to QTSV with load case series 1000, an overview is given in Table 59. To create the combinations, use is made of the function COMB which has the relevant ACT as primary input. The superposition is performed by the SUPP function which only searches for the maxima and minima (MAMI), this saves significantly time.

COMB	ACT	SUPP	SECTIONS (ETYP BSCT)	LC series
1	QV1, QV2, QV3	1	SIR Sections 100-series (face of the wall)	1100
2	QV1, QV2, QV3	2	SIR Sections 200-series (end of the haunch)	1200
3	QV1, QV2, QV3	3	SIR Sections 300-series (midspan)	1300

Table 59 Overview of defined combinations and superposition for the determination of the maxima and minima for shear force due to TS.

Maxima: Combinations

In the program MAXIMA: Combinations the combinations for ULS verification are made. Two different groups of combinations are made for the purpose of determining the maximum bending moment and the maximum shear force. An overview of the ULS minimum and maximum combinations made is given in Table 60.

COMB	ACT	SUPP	SECTIONS (ETYP BSCT)	LC series
101	G, QUDM, QTSM	101	SIR Sections 100-series (face of the wall)	11000
102	G, QUDV, QTSV	102	SIR Sections 100-series (face of the wall)	21000
201	G, QUDM, QTSM	201	SIR Sections 200-series (end of the haunch)	12000
202	G, QUDV, QTSV	202	SIR Sections 200-series (end of the haunch)	22000
301	G, QUDM, QTSM	301	SIR Sections 300-series (midspan)	13000
302	G, QUDV, QTSV	302	SIR Sections 300-series (midspan)	23000

Table 60 Overview of ULS combinations for 3D FEM plate model

The following warning is suppressed:

CTRL WARN 83 $No linear or superposed Load Case found for Action G_1/G_2 (Not used)

Maxima: Combinations for Mxy and redistribution

In reinforced concrete, the reinforcement must not only absorb the moments in the main directions, but also the torsional moment, for which purpose the torsion moment M_{xy} must be added to the corresponding maximum occurring moment. In formula form:

$$M_{XX,ULS,max} = m_{xx} + |m_{xy}| \tag{D.1}$$

$$M_{XX,ULS,min} = m_{xx} - |m_{xy}| \tag{D.2}$$

If in a section the occurring bending moment reaches the moment capacity of that section, the bending moment can be redistributed if the section with an opposite moment has excess capacity. For the redistribution of bending moments, it is therefore important to know the corresponding moment at the support for the maximum moment in the span and vice versa. This may also apply to moments in the haunch, both hogging and possibly sagging bending moment.

The problem, however, is that SOFiSTiK the information about which load cases are in the governing combination is not stored, and so cannot be recalled requesting bending moments in other sections for that specific combination. To avoid absolute brute force, where everything is combined, a more intelligent solution is used.

Redistribution from span to face of the wall
For the maximum sagging moment in the span it can be assumed that the TSs are halfway through the span, which results in just one combination shown in Table 61.

COMB	LC	SUPP	SECTIONS (ETYP BSCT)	LC series
111	LC 100 LC 110 LC 111 LC 120 LC 220 LC 300+#steps	111	SIR Sections 300-series (midspan) for corresponding M_{xy}	13100
			SIR Sections 100-series (face of the wall) for redistribution	11900
			SIR Sections 100-series (face of the wall) for corresponding M_{xy}	11100

Table 61 Overview of combinations for M_{xy} and redistribution of bending moment from span to support for 3D FEM plate model.

Redistribution from face of the wall to span
The exact location of the TSs for the maximum hogging moment is not known in advance, but it is known where this approximately should be. A set of locations, based on the earlier defined steps, is selected and checked afterwards in the Excel results file. If one of the selected locations corresponds than that location is taken, otherwise the conservative assumption is made to take the maximum sagging moment in the span.

It is assumed that the maximum hogging moment in the section at the face of the wall is obtained when the TSs are placed at 20% of the span. Depending on the number of steps calculated several steps before and after the assumed position are also selected. By default with 10 steps, one step before and after the TSs location of 20% of the span is taken, with every 10 steps, one step before and one step after the estimated critical location is added.

An overview of the combinations made, the system behind them, and the associated load cases created is shown for the default number of 10 steps in Table 62.

COMB	LC	SUPP	SECTIONS (ETYP BSCT)	LC series
311	LC 100 LC 110 LC 111 LC 120 LC 220 LC 303	311	SIR Sections 100-series (face of the wall) for lookup	13500
		311	SIR Sections 300-series (midspan) for redistribution	13900
		311	SIR Sections 100-series (face of the wall) for corresponding M_{xy}	13300
		311	SIR Sections 300-series (midspan) for corresponding M_{xy}	13400
312	LC 100 LC 110 LC 111 LC 120 LC 220 LC 304 (predicted)	312	SIR Sections 100-series (face of the wall) for lookup	13510
		312	SIR Sections 300-series (midspan) for redistribution	13910
		312	SIR Sections 100-series (face of the wall) for corresponding M_{xy}	13310
		312	SIR Sections 300-series (midspan) for corresponding M_{xy}	13410
313	LC 100 LC 110 LC 111 LC 120 LC 220 LC 305	313	SIR Sections 100-series (face of the wall) for lookup	13520
		313	SIR Sections 300-series (midspan) for redistribution	13920
		313	SIR Sections 100-series (face of the wall) for corresponding M_{xy}	13320
		313	SIR Sections 300-series (midspan) for corresponding M_{xy}	13420

Table 62 Overview of combinations for redistribution of bending moment from support to span for 3D FEM plate model.

The checks of the results obtained with structures from the database show that for medium to large spans the estimate is correct, and that the correct corresponding moment is found. For small spans, with culverts, the corresponding moment is often not found, the deviation can be significant with such structures given the short span. If the exact corresponding moment is not found, the maximum is used and is therefore always conservative.

Redistribution from haunch to face of the wall
It may occur that the bending moment must be redistributed from a sagging moment at the end of the haunch to a hogging moment at the face of the wall. The exact critical location of the TSs for a sagging moment in the section at the end of the haunch is unknown, it is expected to be the first step of TS which is the closest to the wall. A set of locations, based on the earlier defined steps, is selected and checked afterwards in the Excel results file. If one of the selected locations corresponds than that location is taken, otherwise the conservative assumption is made to take the maximum hogging moment in the section at the face of the wall. Depending on the number of total steps, additional load cases, steps, are added for the check. By default, with 10 steps, 2 extra steps are added further from the face of the wall.

An overview of the combinations made, the system behind them, and the associated load cases created is shown for the default number of 10 steps in Table 63.

COMB	LC	SUPP	SECTIONS (ETYP BSCT)	LC series
211	LC 100 LC 110 LC 111 LC 120 LC 220 LC 301 (predicted)	211	SIR Sections 200-series (end of the haunch) for lookup	12800
		211	SIR Sections 100-series (face of the wall) for redistribution	12900
		211	SIR Sections 200-series (end of the haunch) for corresponding M_{xy}	12100
		211	SIR Sections 100-series (face of the wall) for corresponding M_{xy}	12200
212	LC 100 LC 110 LC 111 LC 120 LC 220 LC 302	212	SIR Sections 200-series (end of the haunch) for lookup	12810
		212	SIR Sections 100-series (face of the wall) for redistribution	12910
		212	SIR Sections 200-series (end of the haunch) for corresponding M_{xy}	12110
		212	SIR Sections 100-series (face of the wall) for corresponding M_{xy}	12210
213	LC 100 LC 110 LC 111 LC 120 LC 220 LC 303	213	SIR Sections 200-series (end of the haunch) for lookup	12820
		213	SIR Sections 100-series (face of the wall) for redistribution	12920
		213	SIR Sections 200-series (end of the haunch) for corresponding M_{xy}	12120
		213	SIR Sections 100-series (face of the wall) for corresponding M_{xy}	12220

Table 63 Overview of combinations for redistribution of bending moment from support to span for 3D FEM plate model.

It should be noted that the 3D FEM plate model often does not calculate a sagging moment in the cut at the end of the haunch.

Redistribution from haunch to span
If the section at the end of the haunch does not have sufficient moment capacity for the maximum occurring hogging moment, if there is still residual capacity in the span, it can be redistributed from the hogging moment in the haunch to a sagging moment in the span. The exact critical location of the TSs for a hogging moment in the section at the end of the haunch is unknown, but it is expected to be the first step of TS which is the closest to the wall. A set of locations, based on the earlier defined steps, is selected and checked afterwards in the Excel results file. If one of the selected locations corresponds than that location is taken, otherwise the conservative assumption is made to take the maximum sagging moment in the span. Depending on the number of total steps, additional load cases, steps, are added for the check. By default, with 10 steps, 2 extra steps are added further from the face of the wall.

An overview of the combinations made, the system behind them, and the associated load cases created is shown for the default number of 10 steps in Table 64.

COMB	LC	SUPP	SECTIONS (ETYP BSCT)	LC series
221	LC 100 LC 110 LC 111 LC 120 LC 220 LC 301 (predicted)	221	SIR Sections 200-series (end of the haunch) for lookup	12500
		221	SIR Sections 300-series (midspan) for redistribution	12600
		221	SIR Sections 200-series (end of the haunch) for corresponding M_{xy}	12300
		221	SIR Sections 300-series (midspan) for corresponding M_{xy}	12400
222	LC 100 LC 110 LC 111 LC 120 LC 220 LC 302	222	SIR Sections 200-series (end of the haunch) for lookup	12510
		222	SIR Sections 300-series (midspan) for redistribution	12610
		222	SIR Sections 200-series (end of the haunch) for corresponding M_{xy}	12310
		222	SIR Sections 300-series (midspan) for corresponding M_{xy}	12410
223	LC 100 LC 110 LC 111 LC 120 LC 220 LC 303	223	SIR Sections 200-series (end of the haunch) for lookup	12520
		223	SIR Sections 300-series (midspan) for redistribution	12620
		223	SIR Sections 200-series (end of the haunch) for corresponding M_{xy}	12320
		223	SIR Sections 300-series (midspan) for corresponding M_{xy}	12420

Table 64 Overview of combinations for redistribution of bending moment from haunch to span for 3D FEM plate model.

Results: Excel output

The results of SOFiSTiK are exported to the fixed Excel file *"results.xlsx"*, this file may not be modified or deleted. For each main section, the correct set of sections is selected for each mechanism, bending moment or shear force, using the FILT function. The results are exported per section force and per main section, midspan, end of the haunch or face of the wall, to a separate worksheet by the XLSX function. In Excel, the calculated section forces are averaged over the width of the integration section, standard sections $4d$ and edge section $2d$, and presented at the *"OVERVIEW"* worksheet. An overview of the SOFiSTiK export is shown in Table 65. By requesting the bending moment in the span at section midspan for the load case of maximum or minimum bending moment in the other sections there is an error in the redistribution, this error is limited for most underpasses and culverts due to the relatively small span. The error becomes significant for structures with a span from about 10m.

Table 65 is shown on the next page.

Main section	Section force	SIR section series	Load Case	Export WorkSheet
Face of the wall	My – MAMI	100 – series	11000; 11001	Face-M
	My – recreate MIN	100 – series	13500 – series	Face-Mcheck
	My – corresponding at midspan	300 – series	13900 – series	Face-Mred
	Mxy – corresponding at face of the wall	100 – series	13300 – series	Face-Face-Mxy
	Mxy – corresponding at midspan	300 – series	13400 – series	Face-Span-Mxy
	Vz – MAMI	100 – series	21000; 21001	Face-V
End of the haunch	My – MAMI	200 – series	12000; 12001	Haunch-M
	My – recreate MIN	200 – series	12500 – series	Haunch--Mcheck
	My – corresponding at midspan	300 – series	12600 – series	Haunch--Mred
	Mxy – corresponding at end of the haunch	200 – series	12300 – series	Haunch—Haunch-Mxy
	Mxy – corresponding at midspan	300 – series	12400 – series	Haunch—Span-Mxy
	My – recreate MAX	200 – series	12800 – series	Haunch+-Mcheck
	My – corresponding at face of the wall	100 – series	12900 – series	Haunch+-Mred
	Mxy – corresponding at end of the haunch	200 – series	12100 – series	Haunch+-Haunch-Mxy
	Mxy – corresponding at face of the wall	100 – series	12200 – series	Haunch+-Face-Mxy
	Vz – MAMI	200 – series	22000; 22001	Haunch-V
Midspan	My – MAMI	300 – series	13000; 13001	Span-M
	My – corresponding at face of the wall	100 – series	11901	Span-Mred
	Mxy – corresponding at midspan	300 – series	13001	Span-Span-Mxy
	Mxy – corresponding at face of the wall	100 – series	11001	Span-Face-Mxy
	Vz – MAMI	300 – series	23000; 23001	Span-V

Table 65 Overview of Excel results output for 3D FEM plate model.

An example of the Excel output to Auto_SOFiSTiK is shown on the next page.

Royal HaskoningDHV *Enhancing Society Together*	**Project**	XX9999	-	**Naam Project**	
	Omschrijving	**Validatieberekening**			
	Status	**SO**			
	Versie				
	Opgezet door			**Datum**	**30-12-2020**
	Gecontroleerd			**Datum**	**dd-mm-yyyy**

SOFiSTiK OUTPUT

3D Model 2D QUAD plaatelementen v.2020

Effectieve hoogte dek

Effectieve hoogte dek dag	d_{clear}	294 mm
Effectieve hoogte dek voute	d_{haunch}	298 mm
Effectieve hoogte dek midspan	$d_{midspan}$	294 mm

Breedte integratie strook (SECTION)

Section dag	$4\ d_{clear}$	1,18 m
Section voute	$4\ d_{haunch}$	1,192 m
Section midspan	$4\ d_{midspan}$	1,176 m

Snede in de dag van de wand

MEd,clear,min = My - |Mxy| = -89.25 - 2.31	$M_{Ed,clear,min}$	-91,56 kNm
MEd,clear,max = My - |Mxy| = -5.95 - 2.31	$M_{Ed,clear,max}$	-8,26 kNm
MIN-VZ ULS	$V_{Ed,clear,min}$	-239,51 kN
MAX-VZ ULS	$V_{Ed,clear,max}$	-13,49 kN
Bijbehorend veldmoment voor $M_{Ed,clear,min}$	$M_{Ed,midspan}$	159,79 kNm

Snede aan het einde van de voute

MEd,haunch,min = My - |Mxy| = -89.26 - 2.32	$M_{Ed,haunch,min}$	-91,58 kNm
MEd,haunch,max = My - |Mxy| = -5.95 - 2.02	$M_{Ed,haunch,max}$	-7,97 kNm
MIN-VZ ULS	$V_{Ed,haunch,min}$	-240,01 kN
MAX-VZ ULS	$V_{Ed,haunch,max}$	-13,53 kN
Bijbehorend veldmoment voor $M_{Ed,haunch,min}$	$M_{Ed,span}$	154,67 kNm
Bijbehorend moment in de dag voor $M_{Ed,haunch,max}$	$M_{Ed,clear}$	-82,73 kNm

Snede in het veldmidden

MEd,span,min = My + |Mxy| = 11.11 + 0.09	$M_{Ed,midspan,mi}$	11,20 kNm
MEd,span,max = My + |Mxy| = 152.88 + 0.09	$M_{Ed,midspan,ma}$	152,97 kNm
MIN-VZ ULS	$V_{Ed,midspan,min}$	-19,30 kN
MAX-VZ ULS	$V_{Ed,midspan,ma}$	92,29 kN
Bijbehorend moment in de dag van de wand voor $M_{Ed,midspan,max}$	$M_{Ed,clear}$	-111,41 kNm

Common running errors

To keep Auto_SOFiSTiK working, **the following files should never be deleted**:

- *"Execute_teddy.bat"*
- *"Execute_teddy.vbs"*
- *"results.xlsx"*

It is possible that an error occurs while running the TEDDY script, these errors cannot be explained but are automatically resolved when using the ASA Tool by rerunning the TEDDY script. If only Auto_SOFiSTiK is used, the user must do this himself.

It has happened when using the ASA Tool that corrupt SOFiSTiK database (.cdb) files arise. In this case the TEDDY script does not even pass the TEMPLATE: Input parameters, in that case you can delete the files in the folder "run" **except for the files mentioned above**.

D2   In-plane load distribution of TS

DATA-028 INTER – 0,0m edge distance – Ratio 1,36

Analytical

$V_{Ed;dag}$	$V_{Rd;c;EC}$	$U.C._{EC}$	Combi	$V_{Rd;c;RBK}$	$U.C._{RBK}$
187,189042	129,0142538	1,45091753	6.10b	168,9049038	1,108251081

135,3 kN as a result of TS (all 3, incl. load factors)

	Tandemstel 1		Tandemstel 2		Tandemstel 3	
Effectieve breedte 1^e as	**4,09**	m	**5,17**	m	**6,93**	m
Effectieve breedte 2^e as	**5,29**	m	**7,57**	m	**6,93**	m

Visualisatie effectieve breedtes per as per tandemstel

Tandemstel 1

Belasting per as		$Q_k * \alpha_{Q1}$	289 kN
Effectieve breedte TS1 as 1		$b_{eff;11}$	4,09 m
Dwarskracht t.g.v. TS1 as 1	$((Q_k * \alpha_{Q1}) / b_{eff;11}) * ((L_{span} - L_{11;achter})/L_{span})$	$V_{Ek;TS1;1}$	50,1 kN/m
Effectieve breedte TS1 as 2		$b_{eff;12}$	5,29 m
Dwarskracht t.g.v. TS1 as 2	$((Q_k * \alpha_{Q1}) / b_{eff;12}) * ((L_{span} - L_{12;achter})/L_{span})$	$V_{Ek;TS1;2}$	25,6 kN/m
Dwarskracht t.g.v. TS1		$V_{Ek;TS1}$	75,7 kN/m

3D FEM-INTER

$V_{Ed;dag}$	$V_{Rd;c;RBK}$	$U.C._{RBK}$
-254,997	168,9049	1,509709
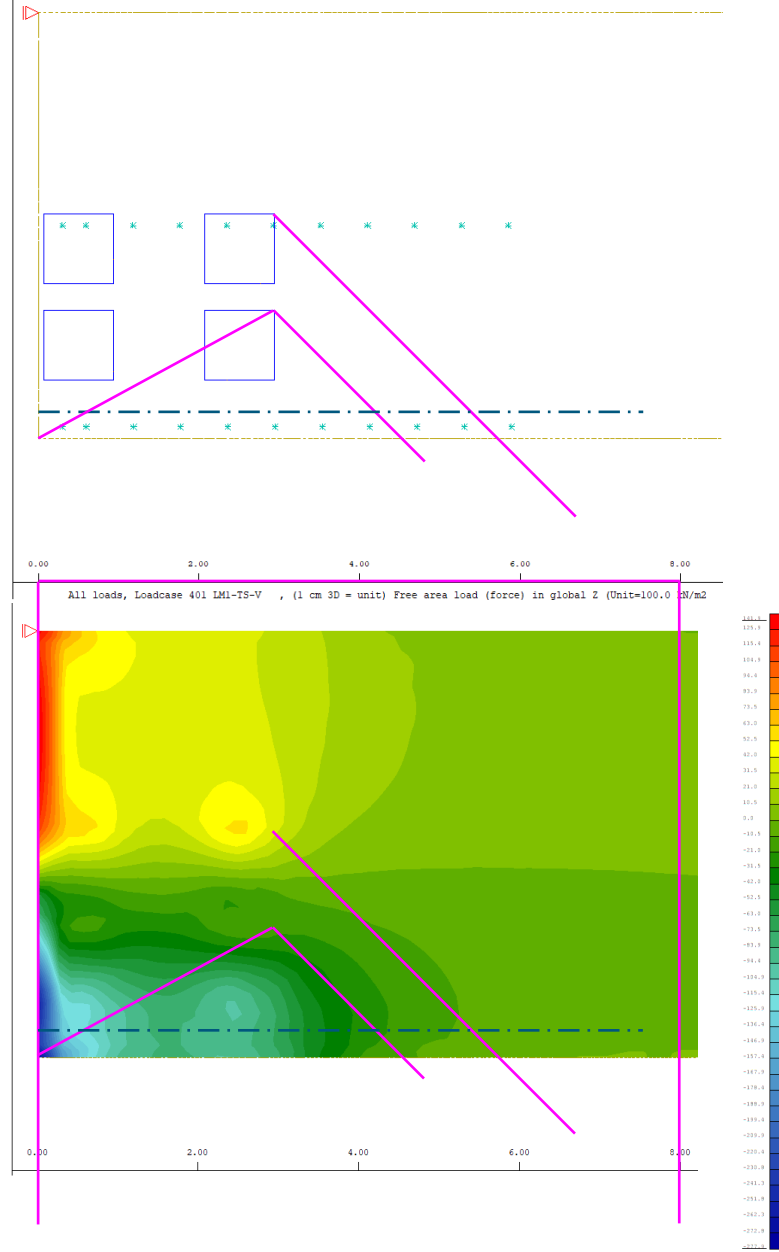
Critical section at edge.

DATA-028 INTER – 0,5m edge distance – Ratio 1,20

Analytical

$V_{Ed;dag}$	$V_{Rd;c;EC}$	U.C.,EC	Combi	$V_{Rd;c;RBK}$	U.C.,RBK	Combi
174,692793	129,0142538	1,35405808	6.10b	168,9049038	1,034267148	6.10b

126,3 kN as a result of TS (all 3, incl. load factors)

	Tandemstel 1		Tandemstel 2		Tandemstel 3	
Effectieve breedte 1ᵉ as	4,59	m	5,17	m	6,93	m
Effectieve breedte 2ᵉ as	5,79	m	7,57	m	6,93	m

Visualisatie effectieve breedtes per as per tandemstel

Tandemstel 1

Belasting per as		$Q_k * \alpha_{Q1}$	289 kN
Effectieve breedte TS1 as 1		$b_{eff;11}$	4,59 m
Dwarskracht t.g.v. TS1 as 1	$((Q_k * \alpha_{Q1}) / b_{eff;11}) * ((L_{span} - L_{11;achter})/L_{span})$	$V_{Ek;TS1;1}$	44,6 kN/m
Effectieve breedte TS1 as 2		$b_{eff;12}$	5,79 m
Dwarskracht t.g.v. TS1 as 2	$((Q_k * \alpha_{Q1}) / b_{eff;12}) * ((L_{span} - L_{12;achter})/L_{span})$	$V_{Ek;TS1;2}$	23,4 kN/m
Dwarskracht t.g.v. TS1		$V_{Ek;TS1}$	68,0 kN/m

3D FEM-INTER

$V_{Ed;dag}$	$V_{Rd;c;RBK}$	$U.C._{RBK}$
-209,991	168,9049	1,243249
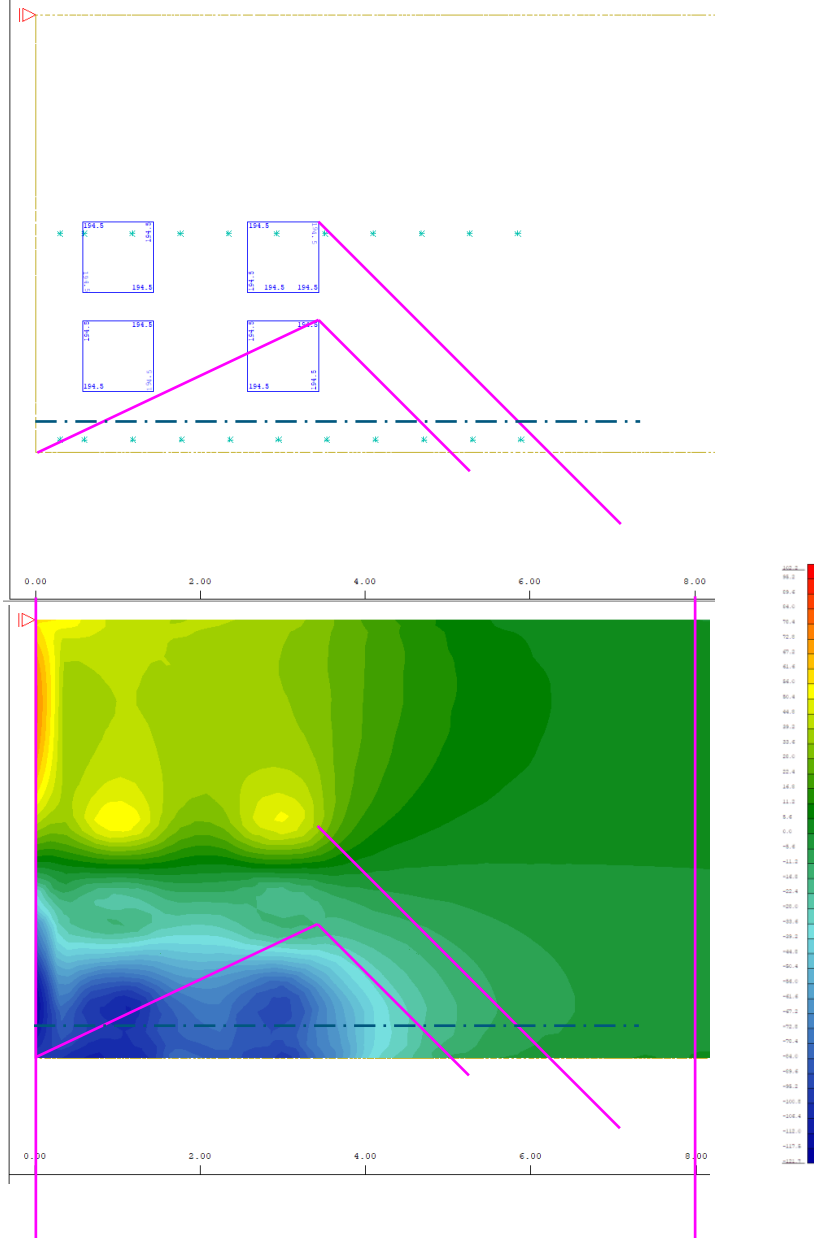
Critical section between TS1 and TS2.

3D FEM-FULL
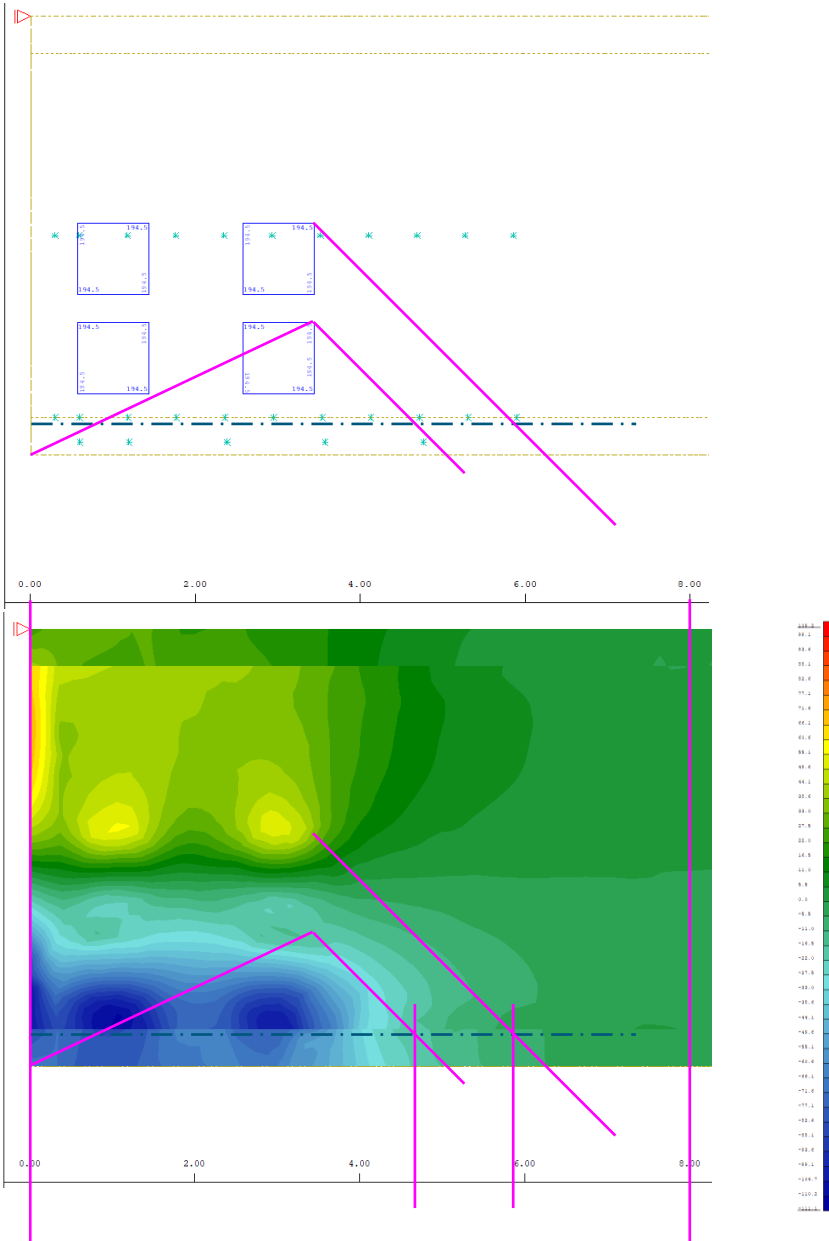
Critical section between TS1 and TS2.
Part of shear force transferred as normal force in haunch due to inclined model line.

DATA-002 INTER – 0,0m edge distance – Ratio 1,30

Analytical

$V_{Ed;dag}$	$V_{Rd;c;EC}$	$U.C._{EC}$	Combi	$V_{Rd;c;RBK}$	$U.C._{RBK}$	Combi
223,825902	212,5089483	1,05325401	6.10b	254,0004518	0,881202771	6.10b

171,6 kN as a result of TS (all 3, incl. load factors)

	Tandemstel 1		Tandemstel 2		Tandemstel 3	
Effectieve breedte 1^e as	3,76	m	4,51	m	6,49	m
Effectieve breedte 2^e as	4,96	m	6,91	m	6,49	m

Visualisatie effectieve breedtes per as per tandemstel

Tandemstel 1

Belasting per as		$Q_k * \alpha_{Q1}$	300 kN
Effectieve breedte TS1 as 1		$b_{eff;11}$	3,76 m
Dwarskracht t.g.v. TS1 as 1	$((Q_k * \alpha_{Q1}) / b_{eff;11}) * ((L_{span} - L_{11;achter})/L_{span})$	$V_{Ek;TS1;1}$	60,1 kN/m
Effectieve breedte TS1 as 2		$b_{eff;12}$	4,96 m
Dwarskracht t.g.v. TS1 as 2	$((Q_k * \alpha_{Q1}) / b_{eff;12}) * ((L_{span} - L_{12;achter})/L_{span})$	$V_{Ek;TS1;2}$	31,1 kN/m
Dwarskracht t.g.v. TS1		$V_{Ek;TS1}$	91,2 kN/m

3D FEM-INTER

$V_{Ed;dag}$	$V_{Rd;c;RBK}$	$U.C._{RBK}$
-282,13	254,0005	1,110745
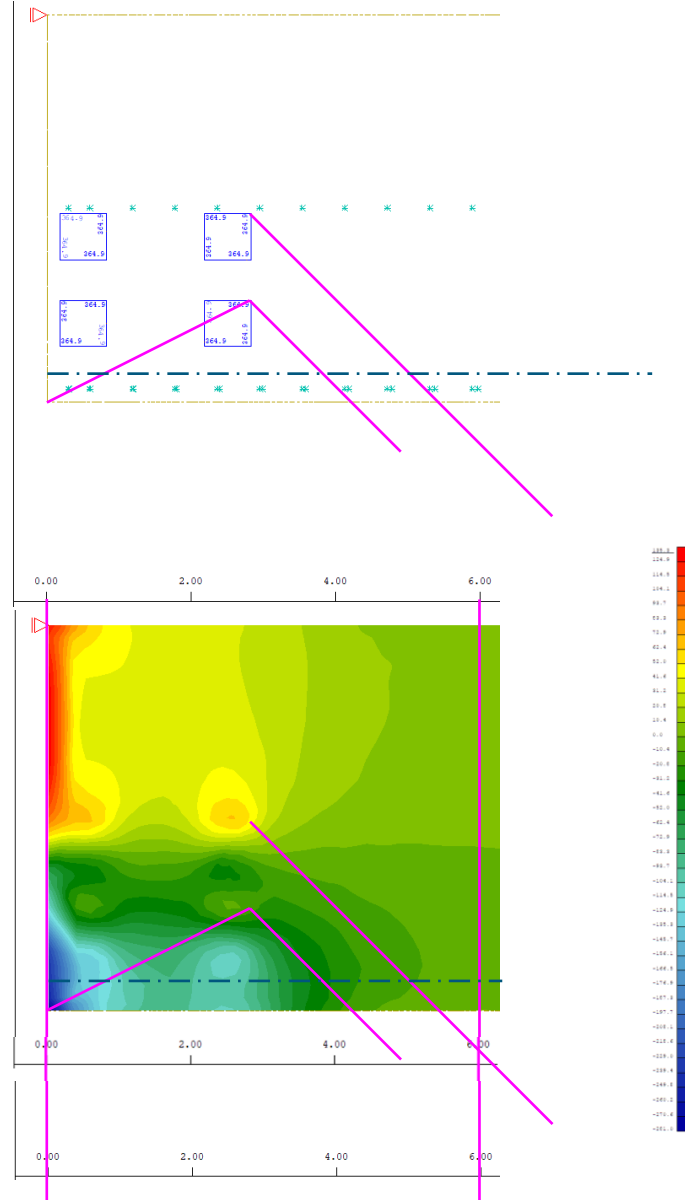
Critical section at edge

DATA-002 INTER – 0,5m edge distance – Ratio 1,16

Analytical

$V_{Ed;dag}$	$V_{Rd;c;EC}$	$U.C._{EC}$	Combi	$V_{Rd;c;RBK}$	$U.C._{RBK}$	Combi
207,317568	212,5089483	0,975571	6.10b	254,0004518	0,816209446	6.10b

159,4 kN as a result of TS (all 3, incl. load factors)

	Tandemstel 1		Tandemstel 2		Tandemstel 3	
Effectieve breedte 1^e as	**4,26**	m	**4,51**	m	**6,49**	m
Effectieve breedte 2^e as	**5,46**	m	**6,91**	m	**6,49**	m
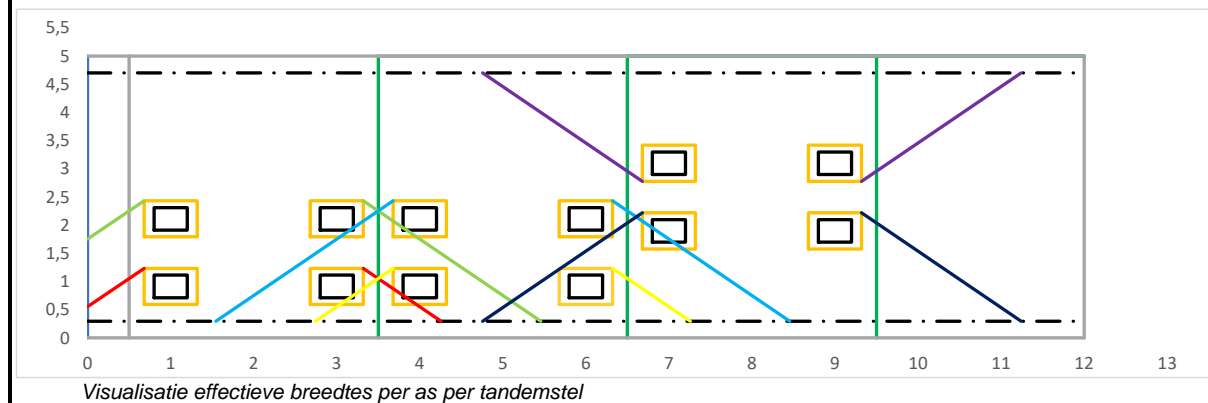
Visualisatie effectieve breedtes per as per tandemstel

Tandemstel 1

Belasting per as		$Q_k * \alpha_{Q1}$	300 kN
Effectieve breedte TS1 as 1		$b_{eff;11}$	4,26 m
Dwarskracht t.g.v. TS1 as 1	$((Q_k * \alpha_{Q1}) / b_{eff;11}) * ((L_{span} - L_{11;achter})/L_{span})$	$V_{Ek;TS1;1}$	53,1 kN/m
Effectieve breedte TS1 as 2		$b_{eff;12}$	5,46 m
Dwarskracht t.g.v. TS1 as 2	$((Q_k * \alpha_{Q1}) / b_{eff;12}) * ((L_{span} - L_{12;achter})/L_{span})$	$V_{Ek;TS1;2}$	28,2 kN/m
Dwarskracht t.g.v. TS1		$V_{Ek;TS1}$	81,3 kN/m

3D FEM-INTER

$V_{Ed;dag}$	$V_{Rd;c;RBK}$	$U.C._{RBK}$
-239,714	254,000	-0,94376
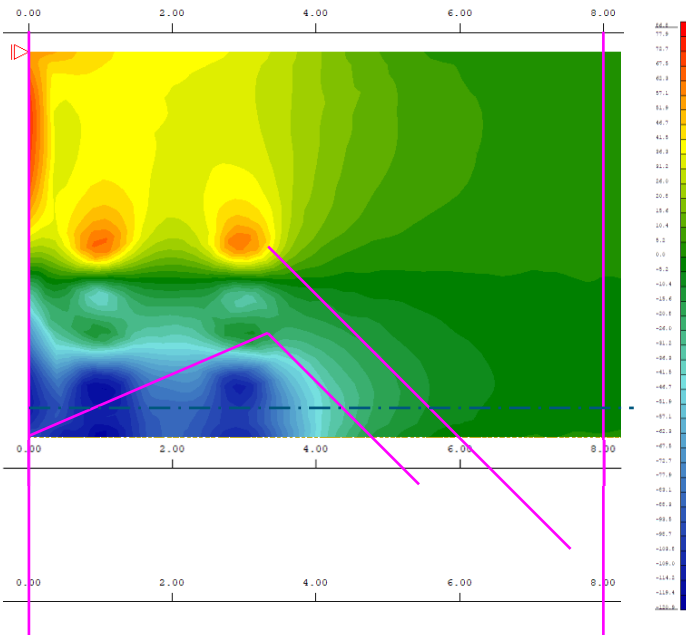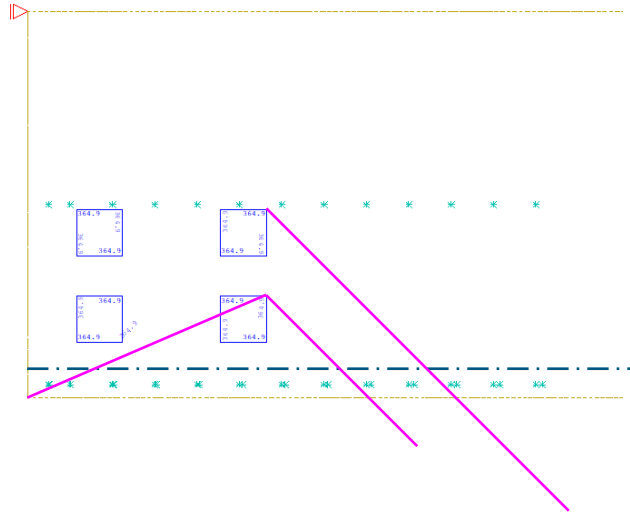
Critical section between TS1 and TS2.

3D FEM – FULL
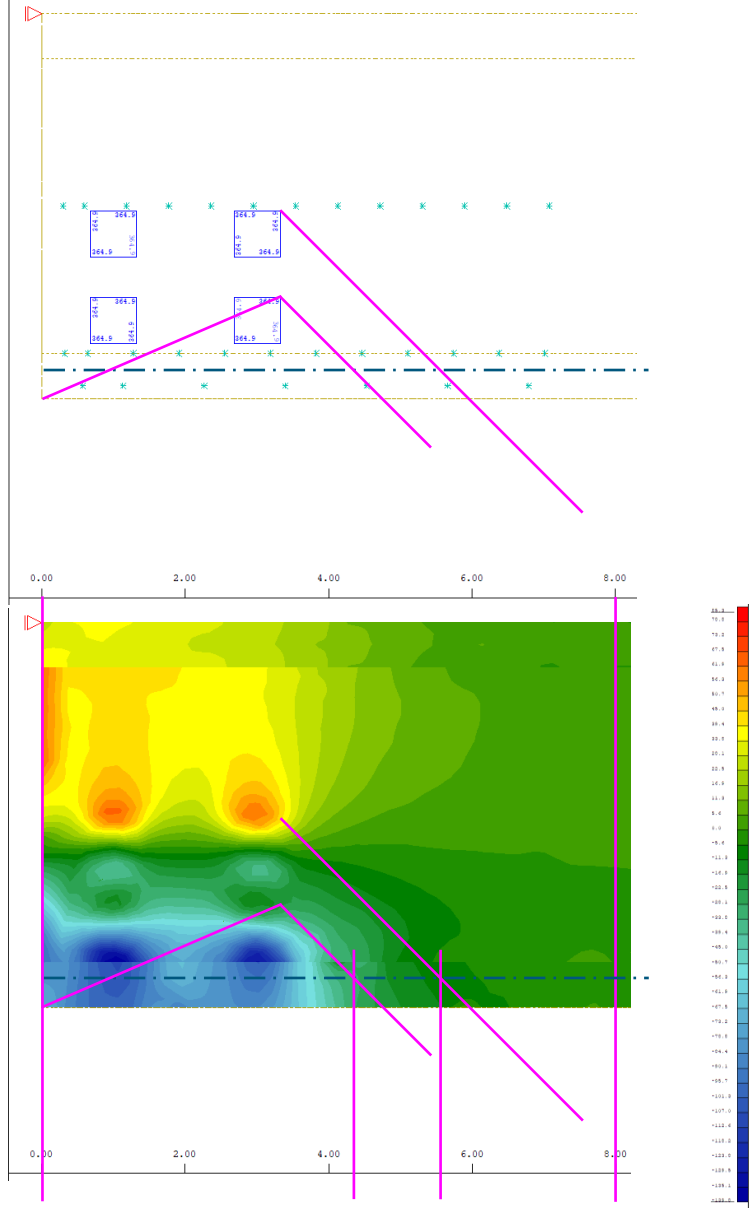
Critical section between TS1 and TS2.
Part of shear force

E

Appendix – Chapter 6: Automated Structural Assessment Tool

E1   Impressions of the ASA Tool

See next page for images.

Input   (Single, non-database)

Royal HaskoningDHV — Enhancing Society Together

Project	DATA-039-FA - De Stoepert A79 62A 113
Omschrijving	Validatieberekening
Status	SO
Versie	0.5
Opgezet door	D.Jilissen	Datum	10-12-2020
Gecontroleerd	V.Achternaam	Datum	dd-mm-yyyy

ALGEMENE INFORMATIE

Update links   Start calculation

Naam van de constructie	DATA-039-FA - De Stoepert A79 62A 113
Object in beheer van	Rijkswaterstaat
Stichtingsjaar	1973
Liggend in een	RW
Kruist een	ETW
Kruisingshoek	56,6 graden 62,89 gon

Analytisch model wordt overgeslagen voor kruisingshoek kleiner dan 80gon

Beoordeling conform R.B.K. 1.1

Beoordelingsniveau	Gebruik
Gevolgklasse	CC3
Referentieperiode	30 jaar
Restlevensduur	30 jaar

GEOMETRIE

Dagmaat wand-wand	L_{dag}	9480 mm
Dek breedte	b_{dek}	61810 mm
Dekdikte veld	$h_{dek;veld}$	570 mm
Lengte voute	L_{voute}	1200 mm
Hoogte voute	h_{voute}	300 mm
Dekdikte aansluiting voute	$h_{dek;voute}$	570 mm
Dekdikte dag wand	$h_{dek;dag}$	870 mm
Inwendige hoogte doos	h_{intern}	5000 mm
Wanddikte	h_{wand}	570 mm
Vloerdikte	h_{vloer}	650 mm

MATERIALEN

BETON

Betonkwaliteit — Eigenschappen — RWS b.j. vóór 1976

Materiaalstijfheid (E-modulus) dek	E_{dek}	10000 N/mm^2
Materiaalstijfheid (E-modulus) wanden	E_{wand}	10000 N/mm^2
Materiaalstijfheid (E-modulus) vloer	E_{vloer}	10000 N/mm^2

WAPENING

Dek - Onderzijde veldmidden

Gebruikt wapeningsstaal — Eigenschappen — VB 74 + VB 74/84 FeB 400 HW, HWL
Wapening aan de onderzijde van het dek in overspanningsrichting t.p.v. veldmidden

Trekwapening laag 1	ø25 -	250 mm
Trekwapening laag 2	ø22 -	250 mm
Betondekking	c_{veld}	30 mm

Verankering — Volledig verankerd

Dek - Onderzijde voute

Gebruikt wapeningsstaal — Eigenschappen — VB 74 + VB 74/84 FeB 400 HW, HWL
Wapening aan de onderzijde van het dek in overspanningsrichting t.p.v. voute

Trekwapening laag 1	ø25 -	250 mm
Trekwapening laag 2	ø22 -	250 mm
Betondekking	c_{voute+}	30 mm

Verankering — Berekend
Trekwapening laag 1
Type verankering — Recht
Randafstand beschouwde wapening — 105 mm
Trekwapening laag 2
Type verankering — Recht
Randafstand beschouwde wapening — 102 mm

Dek - Bovenzijde voute

Gebruikt wapeningsstaal — Eigenschappen — VB 74 + VB 74/84 FeB 400 HW, HWL
Wapening aan de bovenzijde van het dek in overspanningsrichting t.p.v. voute

Trekwapening laag 1	ø25 -	250 mm
Trekwapening laag 2	ø25 -	250 mm
Betondekking	c_{voute-}	30 mm

Verankering — Berekend
Trekwapening laag 1
Type verankering - start — 0
Type verankering - eind — Recht
Start - omgebogen staaf in wand beschouwd als volledig verankerd
Eind - lengte beschouwde wapening voorbij de dag van de wand — $L_{p,clear}$ — 0 mm
Trekwapening laag 2
Type verankering - start — 0
Type verankering - eind — Recht
Start - omgebogen staaf in wand beschouwd als volledig verankerd
Eind - lengte beschouwde wapening voorbij de dag van de wand — $L_{p,clear}$ — 2000 mm

Dek - Dag van de wand

Gebruikt wapeningsstaal — Eigenschappen — VB 74 + VB 74/84 FeB 400 HW, HWL
Wapening aan de bovenzijde van het dek in overspanningsrichting t.p.v. dag bij de wand

Trekwapening laag 1	ø25 -	250 mm
Trekwapening laag 2	ø25 -	250 mm
Betondekking	c_{dag-}	30 mm

Verankering — Berekend
Trekwapening laag 1
Type verankering - start — 0
Type verankering - eind — Recht
Start - omgebogen staaf in wand beschouwd als volledig verankerd
Eind - lengte beschouwde wapening voorbij de dag van de wand — $L_{p,clear}$ — 0 mm
Trekwapening laag 2
Type verankering - start — 0
Type verankering - eind — Recht
Start - omgebogen staaf in wand beschouwd als volledig verankerd
Eind - lengte beschouwde wapening voorbij de dag van de wand — $L_{p,clear}$ — 0 mm

GROND

Referentieniveau bovenkant kunstwerk t.o.v. NAP		+ 10,00 m NAP
Grondwaterstand		+ 0,00 m NAP
Aantal grondlagen bovenop kunstwerk	1	

Grondlaag 1 — Advanced settings

Grondsoort	Zand, zanderig
Dikte grondlaag 1	$h_{grond;1}$ — 0 mm

Grond naast kunstwerk — Advanced settings

Grondsoort	Zand, zanderig

ASFALT

Dikte asfaltlaag op kunstwerk	h_{asfalt}	220 mm

Advanced settings

OVERIG

Minimale randafstand verkeersbelasting op beschouwd onderdeel	$e_{rand;min}$	0,00 m
Maximale randafstand verkeersbelasting op beschouwd onderdeel	$e_{rand;max}$	0,00 m
Aantal vrachtwagens per jaar per rijstrook	N_{obs}	2000000 stuks

Output (Database)

Processing